Imperial College London

Impact of Phosphorus Ligand Modification on Transition Metal Coordination and Homogeneous Carbonylation Catalysis

by

Dillon Tay Wei Peng

A thesis submitted for the degree of Doctor of Philosophy

Imperial College London

Department of Chemistry

May 2020

Examiners:

Prof. Paul G. Pringle

Dr. Philip W. Miller

Declaration of Originality

I declare that this thesis is entirely work of my own unless otherwise stated and appropriately referenced. Experiments of which the results are presented in this thesis have been carried out by me at Imperial College London and the Agency of Science, Technology and Research (A*STAR) – Institute of Chemical and Engineering Sciences (ICES) between October 2015 and December 2019. None of the work contained herein has, to the best of my knowledge, been previously submitted for a degree at this or any other institution.

Copyright Declaration

Publications

Chapter 2 (excluding sections 2.5 and 2.6) has been adapted from '*gem-Dialkyl Effect in Diphosphine Ligands: Synthesis, Coordination Behavior, and Application in Pd-Catalyzed Hydroformylation*', Dillon W. P. Tay, James D. Nobbs, Charles Romain, Andrew J. P. White, Srinivasulu Aitipamula, Martin van Meurs and George J. P. Britovsek. *ACS Catalysis*, **2020**, *10* (1), 663-671.

Conference Contributions

Poster Presentations

9 – 13 Jul 2017	*The European Association for Chemical and Molecular Sciences (EuCheMS) 22nd Conference on Organometallic Chemistry (EuCOMC XXII)*, Amsterdam, Netherlands
25 May 2018	*Singapore Catalysis Society (SCS) Forum*, Biopolis, Singapore
4 Jul 2018	*Postgraduate Symposium*, Imperial College London, UK
19 – 21 Nov 2018	*7th Asia-Oceania Conference on Green and Sustainable Chemistry (AOC-GSC7)*, Biopolis, Singapore

Oral Presentations

23 – 24 June 2019	*Southeast Asia Catalysis Conference (SACC2019)*, NUS, Singapore

Acknowledgements

A PhD thesis is a work of more than just the candidate, but an amalgam of the vested efforts, innovations and thoughts of many that have had some influence in shaping the journey and thus, been part of the story. It has been a humbling experience and a pleasure to have had the privilege of so many who have helped, encouraged, critiqued and overall made it worthwhile. My heartfelt gratitude to George, for your patient guidance, amiable discussions, practical wisdom and warmth. I did not realise how important a role the supervisor plays, but I could not have asked for a better one. Thank you. In that same vein, my utmost respect and thanks to Martin and James as well, essentially the ones who taught me everything I know from day one when I first wandered onto the remote island of Jurong as a fresh graduate. Thanks to Martin for advising me not only in how best to proceed with research direction but also in enjoying durian. Thanks to James, for first teaching me Schlenk techniques, for guiding me day-to-day when I first arrived and for your steadfast friendship through the years which I treasure. I also would like to thank so many others who have been an integral part of this PhD, without you, I would never have made it this far. From my time at Imperial, Atanas, Dom and Charles, for your guidance and sharing your experience, Craig, for helping us all when we were fresh year ones, Sarah and Sara, for your friendship and fun times in and out of the lab, and most especially to Richard, Richy my brother and comrade-in-arms, who everyday and through the seasons has been a steadfast friend, a confidant and who was always up for a drink, I could not have made it without you. To those in ICES, Sigit (no.1 nice guy), Don (thank you senior), Boonying (helpful big sis), Junhui (favourite labmate), Ludger (best eggnog), Wendy (badminton kaki), Anueshree (the queen), Lindy (friendliest LO), Ayu (kindest LO), Eddie (best project mate), Fiona (best admin), Jozel (no im not sure), Suming (undefeatable), Wang Cun (most hardworking), Mr Lee (very helpful), Ritchie (super-mechanic) and so many others, thank you for being part of the journey.

Finally, thanks to my family, Mum who encouraged me to pursue this, Dad, for your unwavering support in your own way. Sis, who is always so encouraging and buys me bread, Kor, who always believed I could make Legend and recommended me the best web novels, Clar, who is the most fun to talk to, joke around with and drives me home from gym, Auntie, who taught me how to cook and keeps us all alive. *To God be the Glory, The Best is Yet to Be.*

Abstract

Subtle changes in phosphorus ligand structure have been known to lead to significant changes in metal-ligand coordination behaviour and subsequent catalytic performance. A combination of both experimental and computational techniques has been employed to study the influence of phosphorus ligand modification on its coordination behaviour and performance in homogeneous olefin carbonylation.

The *gem*-dialkyl effect (also known as the Thorpe-Ingold effect) can be applied to C_3-bridged bis(diphenylphosphine) ligands via geminal substitution of two alkyl groups (R) on the central carbon of the C_3-bridge. Structurally, the *gem*-dialkyl effect has been observed to distort 6-membereded chelates formed in diphosphine-palladium(II) chloride complexes from a chair (R = H) to a half-chair (R = Me, Et, iPr) and eventually to a twist-boat (R = tBu) conformation. In terms of catalytic performance, the *gem*-dialkyl effect favours reductive hydroformylation to directly produce alcohols from olefins during palladium catalysed hydroformylation. The *gem*-dialkyl effect has also been observed to hinder isomerisation and promote reaction rate in palladium catalysed methoxycarbonylation of terminal olefins.

Modification of the C_2-linker from ethylene to phenyl in diphobane ligands has resulted in a dramatic shift in chemoselectivity from alcohols to aldehydes in palladium catalysed olefin hydroformylation. The competition between hydroformylation and alkoxycarbonylation in palladium catalysed olefin carbonylation has also been tuned by introducing substituents (X) on phenyl-bridged diphobanes to favour aldehyde (X = H), alcohol (X = OMe, OMe) or ester (X = CF_3) products respectively.

The testing of a series of ligands in ruthenium catalysed tandem reverse Water-Gas Shift-hydroformylation-reduction of olefins to alcohols has shown that bidentate ligands and higher monodentate ligand-to-metal ratios favour olefin hydrogenation. The choice of solvent has also been found to play a crucial role as high CO_2 pressures at reaction conditions can expand the solvent, alter its physical properties and thus influence catalytic activity.

Abbreviations

%V_Bur – Ligand buried volume

(+)-NMDPP – 2-isopropyl-5-methylcyclohexyl)diphenylphosphane

(S,S)-DIOP – (((4S,5S)-2,2-Dimethyl-1,3-dioxolane-4,5-diyl)bis(methylene))bis(diphenylphosphane)

2-EH – 2-Ethylhexanol

2PA – 2-Pentenoic acid

3PA – 3-Pentenoic acid

4PA – 4-Pentenoic acid

a-BCOPP – 1,2-Di(9-phosphabicyclo[4.2.1]nonan-9-yl)benzene

ADA – Adipic acid

BCOPA – 9,9'-(4-Methoxy-1,2-phenylene)bis(9-phosphabicyclo[3.3.1]nonane)

BCOPE – 1,2-Di(9-phosphabicyclo[3.3.1]nonan-9-yl)ethane

BCOPF – 9,9'-(4-(Trifluoromethyl)-1,2-phenylene)bis(9-phosphabicyclo[3.3.1]nonane)

BCOPP – 1,2-Di(9-phosphabicyclo[3.3.1]nonan-9-yl)benzene

BCOPT – 9,9'-(4-(Tert-butyl)-1,2-phenylene)bis(9-phosphabicyclo[3.3.1]nonane)

BCOPV – 9,9'-(4,5-Dimethoxy-1,2-phenylene)bis(9-phosphabicyclo[3.3.1]nonane)

BINAPHOS – 6-((2'-(Diphenylphosphaneyl)-[1,1'-binaphthalen]-2-yl)oxy)-2-methyl-1-vinylbenzo[d]naphtho[1,2-f][1,3,2]dioxaphosphepine

BIPHEPHOS – 2,2'-Bis[(1,1'-biphenyl-2,2'-diyl)phosphite]-3,3'-di-tert-butyl-5,5'-dimethoxy-1,1'-biphenyl

BISBI – 2,2'-Bis(diphenylphosphinomethyl)-1,1'-biphenyl

BMIM – 1-Butyl-3-methyl-1H-imidazol-3-ium

BOBPHOS – 1,2,10,11-Tetramethyl-4,8-bis(t-butyl)-6-[[2,5-diphenyl-1-phospholanyl) methoxy]-dibenzo[d,f][1,3,2]dioxaphosphepin]

BPX – 1,1'-(1,2-Phenylenebis(methylene))bis(2,2,6,6-tetramethylphosphinan-4-one)

Ca. – Circa (approximately)

CAM – Ceric ammonium molybdate

COD – 1,5-Cyclooctadiene

$CyPPh_2$ – Cyclohexyldiphenylphosphane

CYTOP – 1,3,5,7-Tetramethyl-8-phenyl-2,4,6-trioxa-8-phosphaadamantane

DME – dimethoxyethane

DMSO – Dimethylsulfoxide

DnBPP – 1,3-Bis(dibutylphosphaneyl)propane

DPPB – 1,4-Bis(diphenylphosphaneyl)butane

DPPBz – 1,2-Bis(diphenylphosphaneyl)benzene

DPPDIPP – (2,2-Diisopropylpropane-1,3-diyl)bis(diphenylphosphane)

DPPDMP – (2,2-Dimethylpropane-1,3-diyl)bis(diphenylphosphane)

DPPE – 1,2-Bis(diphenylphosphaneyl)ethane

DPPF – 1,1'-Bis(diphenylphosphino)ferrocene

DPPIPIPP – (2-Isopentyl-2-isopropylpropane-1,3-diyl)bis(diphenylphosphane)

DPPP – 1,3-Bis(diphenylphosphaneyl)propane

DsBPE – 1,2-Bis(di-sec-butylphosphaneyl)ethane

DsBPP – 1,3-Bis(di-sec-butylphosphaneyl)propane

DTBPDMP – (2,2-Dimethylpropane-1,3-diyl)bis(di-tert-butylphosphane)

DTBPIPIPP – (2-Isopentyl-2-isopropylpropane-1,3-diyl)bis(diphenylphosphane)

DtBPP – 1,3-Bis(di-tert-butylphosphaneyl)propane

DTBPP – 1,3-Bis(di-tert-butylphosphaneyl)propane

DTBPX – 1,2-Bis((di-tert-butylphosphaneyl)methyl)benzene

ESA – Ethylsuccinic acid

EI – Electron ionisation

ESI-MS – Electrospray ionisation mass spectrometry

Ferrocene-P_2 – Bis((tert-butyl(pyridin-2-yl)phosphanyl)methyl)ferrocene

Ferrocene-Phosphetane – (2,4-Dimethylphosphetane)ferrocene

FID – Flame ionisation detector

GC – Gas chromatography

GCMS – Tandem gas chromatography-mass spectrometry

GVL – γ-Valerolactone

HOMO – Highest occupied molecular orbital

M2P – Methyl 2-pentenoate

M3P – Methyl 3-pentenoate

M4P – Methyl 4-pentenoate

Me_2Phospholane-Ph – 2,5-Dimethyl-1-phenylphospholane

Me_2POPh – 5,5-Dimethyl-2-phenoxy-1,3,2-dioxaphosphinane

Me-BISBI – 2,2'-Bis((dimethylphosphaneyl)methyl)-1,1'-biphenyl

MeO-BINAP-PCy_2 – Dicyclohexyl(2'-methoxy-[1,1'-binaphthalen]-2-yl)phosphane

Meso-bis-PAd_2 – 1-(1,3,5,7-Tetramethyl-2,4,6-trioxa-8-phosphaadamantan-8-yl)-3-(1,3,5,7-tetramethyl-2,4,6-trioxa-8-phosphaadamantan-8-yl)propane

MGA – 2-Methylglutaric acid

MSA – Methanesulfonic acid

MSD – Mass selective detector

MTBE – Methyl tertiary butyl ether

MV – Methyl valerate

NMP – N-Methyl-2-pyrrolidone

NMR – Nuclear magnetic resonance spectroscopy

NSAID – Non-steroidal anti-infammatory drugs

P(o-tolyl) or $P(o\text{-}tol)_3$ – Tri-o-tolylphosphane

Phobane – 9-Phosphabicyclo[3.3.1]nonane

pKa – Negative base-10 logarithm of acid dissociation constant

PMA – Propylmalonic acid

P-M-P – Phosphorus-metal-Phosphorus

POPh – 2-Phenoxy-1,3,2-dioxaphosphinane

Psig – Pounds per square inch in gauge

PTFE – Polytetrafluoroethylene

PyCl – 1,3-Dimesityl-1H-imidazol-3-ium chloride

rWGS – Reverse water-gas shift

Syngas – Synthesis gas (a gaseous mixture of CO and H2)

TFA – 2,2,2-Trifluoroacetic acid

TfOH – Trifluoromethanesulfonic acid

THF – Tetrahydrofuran

TLC – Thin layer chromatography

TON – Turnover number

TPPTS – 3,3′,3″-Phosphanetriyltris(benzenesulfonic acid) trisodium salt

TsOH – 4-Methylbenzenesulfonic acid

ν – Wavenumber

XRD – X-ray diffraction

Table of Contents

List of Figures

List of Tables

Chapter 1 – Introduction

1.1 Carbonylation Background

Carbonylation is the process of introducing carbon monoxide (CO) into organic or inorganic substrates. The catalytic introduction of CO via carbonylation is a key step in several large-scale industrial processes that produce valuable products or chemical intermediates that serve as precursors to valuable products (**Figure 1.1**).

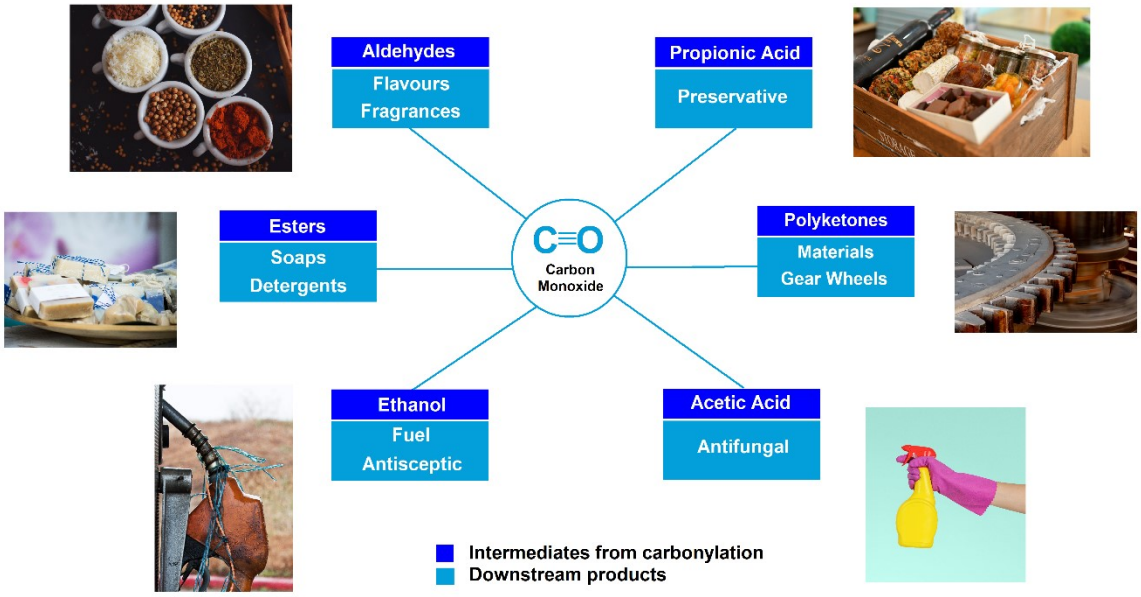

Figure 1.1[a] Carbonylation products.

Carbonylation may be catalysed heterogeneously or homogeneously and typically involves Group 8, 9 or 10 transition metals such as cobalt, iridium, iron, nickel, palladium, platinum, rhodium or ruthenium,[1] although some other transition metals have also shown activity.[2] The identity of the transition metal used is typically of importance for carbonylation reactions but it may also differ within the same carbonylation process. Acetic acid for example, is a homogeneously catalysed carbonylation product with a global production of about 20 million metric tonnes per annum in 2016[3] and has been experiencing fast growing demand in China.[4] Acetic acid has been employed mainly as a solvent[5] and as a precursor for the production of vinyl acetate monomer[6] and ethyl acetate.[7] Acetic acid also has minor applications as an antifungal, an antiseptic and has been used for food preservation, agricultural, chemical and water treatment processes. In 1916, BASF began manufacturing acetic acid in Germany on an industrial scale via the hydration of acetylene to acetaldehyde followed by manganese catalysed oxidation in air (**Figure 1.2**).[8]

[a] Images reproduced with the permission of the rights holder, Unsplash.

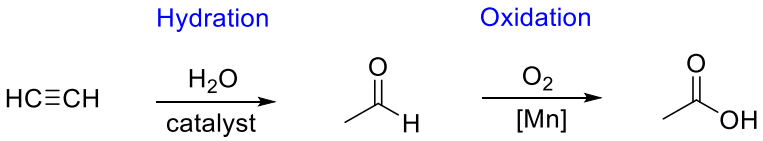

Figure 1.2 Synthetic route to acetic acid from acetylene.

By the mid-1900s however, industrial production of acetic acid mostly transitioned to catalytic carbonylation of methanol, the process by which it is still manufactured today.[6] Research into methanol carbonylation catalysts at BASF progressed from iodide promoted cobalt catalysts[9] to methyl iodide promoted rhodium catalysts.[10] These rhodium systems were later picked up by Monsanto, who in 1966, established the Monsanto process[11] using rhodium/iodide anion co-catalysts that allowed operation under milder conditions. The Monsanto process was itself largely supplanted in 1996 by the greener and more efficient Cativa process,[12] based on an iridium catalyst developed by BP Chemicals. The catalytic carbonylation of methanol alone has been catalysed on an industrial scale by cobalt, rhodium and iridium, suggesting that the carbonylation process is amenable to a range of transition metals. The ideal choice of transition metal, however, is a more involved matter that requires a deeper understanding of the reaction mechanism in question. In this case, the replacement of rhodium with iridium in the Cativa process enabled methanol carbonylation to run in a more cost-efficient manner due to drier conditions, suppression of the water-gas shift reaction and a decrease in by-product formation.[13]

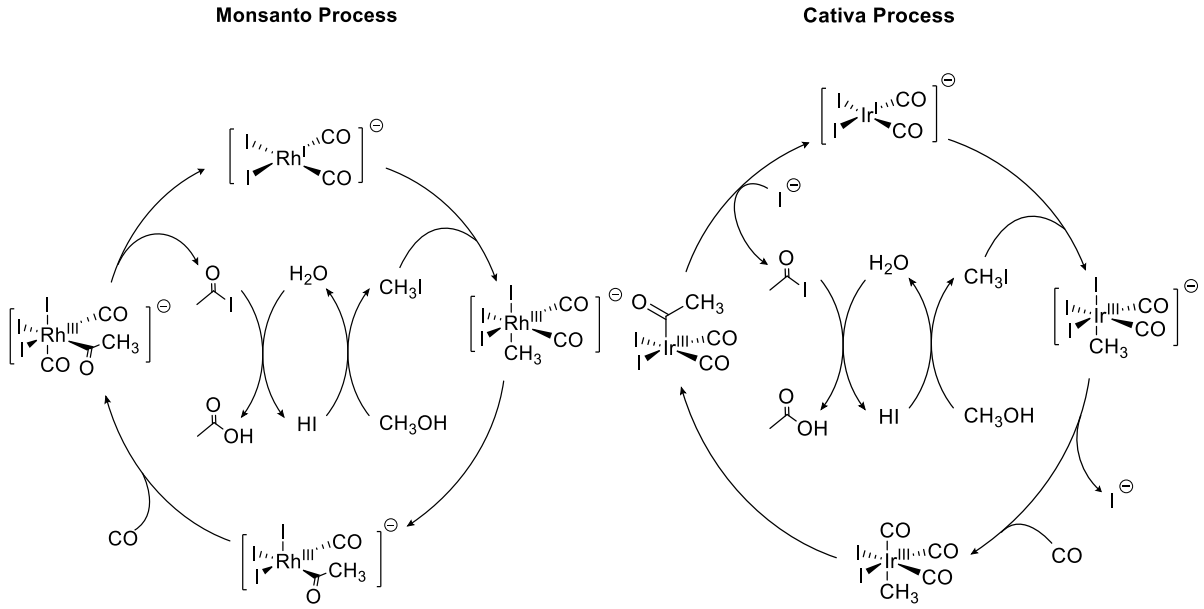

Figure 1.3 Catalytic cycles for the Monsanto[14] and Cativa[15] processes.

The Monsanto and Cativa processes share largely similar reaction mechanisms (**Figure 1.3**), starting with Group 9 transition metals that form square planar d^8 *cis*-coordinated metal(I) dicarbonyl diiodide

complexes. Oxidative addition of methyl iodide occurs to form a metal(III) alkyl complex that undergoes migratory insertion of CO to form a metal(III) acyl complex that then reductively eliminates acetyl iodide. Nucleophilic attack of H_2O on acetyl iodide produces the desired acetic acid product as well as HI that can convert more MeOH to methyl iodide via an acid-catalysed nucleophilic substitution. Methyl iodide then re-enters the catalytic cycle via oxidative addition to the metal(I) dicarbonyl diiodide complex.

Despite these similarities however, there are subtle differences between the two systems that result in significant advantages for the Cativa process. The Monsanto process is 1st order with respect to H_2O up to 8 wt.% and is independent thereafter while the Cativa process achieves its maximum reaction rate at 5 wt.% H_2O and decreases in rate with more or less H_2O content.[16] The H_2O content of the reaction mixture is an important parameter as it determines the extent of the metal-catalysed water-gas shift as a side reaction (**Equation 1.1**).

Equation 1.1 Metal-catalysed water-gas shift reaction.[16] M = Rh or Ir.

$$[M(CO)_2I_2]^{\ominus} + 2\,HI \longrightarrow [M(CO)_2I_4]^{\ominus} + H_2$$

$$[M(CO)_2I_4]^{\ominus} + H_2O + CO \longrightarrow [M(CO)_2I_2]^{\ominus} + CO_2 + 2\,HI$$

$$H_2O + CO \longrightarrow CO_2 + H_2$$

The water-gas shift reaction represents a significant loss of CO as the gaseous by-products (CO_2 and H_2) dilute the CO present in the reactor and eventually starve the system of CO, resulting in an increased need for venting. This limits the efficiency of CO utilisation to about 85% in the Monsanto process.[16] Lowering H_2O content to circumvent this issue introduces its own set of problems. Aside from a reduction in reaction rate due to lower H_2O content, there is also an accumulation of the water-gas shift intermediate, $[Rh(CO)_2I_4]^-$, which is a precursor to catalyst decomposition forming insoluble RhI_3. On the other hand, iridium catalysts have been found to remain robust even at 0.5 wt.% H_2O, allowing them to operate under low H_2O conditions that suppress gaseous by-products from the water-gas shift reaction and increase CO utilisation to about 94%.[16]

The major liquid by-product from the catalytic carbonylation of methanol is propionic acid, produced from the carbonylation of ethanol present as an impurity within the methanol feed.[16] There is however, more propionic acid detected in the Monsanto process than accounted for by ethanol impurities. The rhodium system employed in the Monsanto process is also known for hydroformylation,[17] and instead of reductively eliminating acetyl iodide, hydrogenolysis of the rhodium(III) acyl intermediate may occur instead to give acetaldehyde. Acetaldehyde can then be

reduced by H_2 present in the system (generated from the water-gas shift reaction) to give ethanol, which is then subsequently carbonylated to give propionic acid by-products (**Equation 1.2**).

Equation 1.2 Rhodium-catalysed production of propionic acid.

$$[Rh(CO)(COCH_3)I_3]^{\ominus} + HI \longrightarrow [Rh(CO)I_4]^{\ominus} + CH_3CHO$$

$$CH_3CHO + H_2 \xrightarrow{[Rh]} CH_3CH_2OH$$

$$CH_3CH_2OH + CO \xrightarrow{[Rh]} CH_3CH_3CO_2H$$

In the conventional high H_2O content Monsanto process, the amount of acetaldehyde present in the reactor often reaches several hundred ppm, in contrast to the Cativa process which typically sees no more than 30 ppm of acetaldehyde impurity.[16] As a result, the Monsanto process usually requires more purification, leading to higher production costs.

It has also been shown that the oxidative addition of MeI, the rate-determining step for the conventional high H_2O content Monsanto process, occurs about 150 times faster in the Cativa process for $[Ir(CO)_2I_2]^-$ than for the Monsanto process' $[Rh(CO)_2I_2]^-$.[15] As a result, the rate determining step for the Cativa process is not the oxidative addition of MeI, but is instead the formation of $[Ir(CH_3)(CO)_3I_2]$ from $[Ir(CH_3)(CO)_2I_3]^-$ via ligand exchange of I^- for CO. Initial studies by Monsanto showed iridium to be less active than rhodium for methanol carbonylation. However, the addition of a ruthenium carbonyl iodide complex as a promoter to facilitate the loss of I^- speeds up the rate-determining ligand exchange step to give an iridium-based methanol carbonylation system superior to its rhodium counterpart.[18]

On the whole, the robust iridium catalyst in the Cativa process allows for lower H_2O conditions that suppress the water-gas shift reaction, run at a lower vent rate, increase CO utilisation from 85% to 94% and cut about 30% of CO_2 emissions per metric tonne of acetic acid compared to the analogous Monsanto rhodium process.[16] The reduced amount of propionic acid and H_2O impurities in the Cativa process also lower purification and drying costs, making it the preferred method of acetic acid production today. Despite the progress made over many years of research on methanol carbonylation catalysts however, there are still challenges that have yet to be addressed fully. For example, one of the major drawbacks of both the Monsanto and Cativa processes is the highly acidic reaction media (HI) which causes corrosion problems and requires the reactors to be made of expensive corrosion-resistant alloys. Research into iodide-free methanol carbonylation is ongoing.[19-20]

The diverse range of industrially important carbonylation products and the subtle differences between carbonylation catalysts make homogeneous carbonylation catalysis an immense field of study. As seen above with the example of acetic acid, there can be several interdependent variables in the catalytic cycle that complicate reaction optimisation. For the purposes of this thesis, the following sections will

focus on giving a brief overview on the topics of homogeneously catalysed hydroformylation and alkoxycarbonylation of olefins. This will be followed by a discussion on CO surrogates for olefin carbonylation before the scope and objectives of this thesis are defined.

1.2 Olefin Hydroformylation

Hydroformylation is a carbonylation reaction where CO and H_2, typically employed as a gaseous mix known as synthesis gas (or syngas), are added to a substrate to make a formyl group (H-C=O). Olefin hydroformylation is an atom-economical reaction that converts olefins to terminal and branched aldehyde products except in the case of ethylene, from which only terminal aldehydes are possible (**Figure 1.4**).

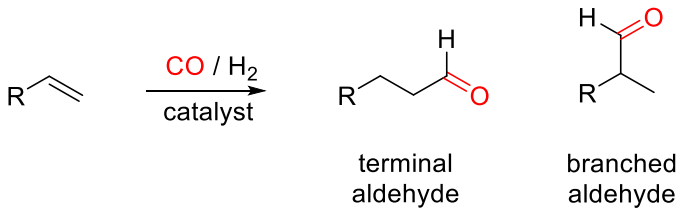

Figure 1.4 Hydroformylation of olefins.

Hydroformylation was serendipitously discovered by Otto Roelen in 1938 at the Ruhrchemie plant in Oberhausen while performing research on Fischer-Tropsch catalysts.[21] He observed that ethylene reacted with CO and H_2 in the presence of a mixture of cobalt, thorium and magnesium oxide to yield "oxo products" such as diethyl ketones and propionaldehyde and hence dubbed it the "oxo process".[22] Since then, hydroformylation has become one of the largest and arguably, one of the most important homogeneously catalysed industrial reactions.[23] In 2008, global production of oxo chemicals reached nearly 10.4 million metric tonnes. Quantitatively, the most important oxo chemical is n-butyraldehyde which accounts for about 75% of global aldehyde use. This is followed by C_6-C_{13} aldehydes for plasticizer alcohols, isobutyraldehyde, valeraldehyde then C_{12}-C_{18} aldehydes for detergent alcohols.[24] Hydroformylation can also be employed as the first step in converting olefins to a wide range of bulk chemicals such as alcohols, carboxylic acids, esters, amines and heavier olefins (**Figure 1.5**).

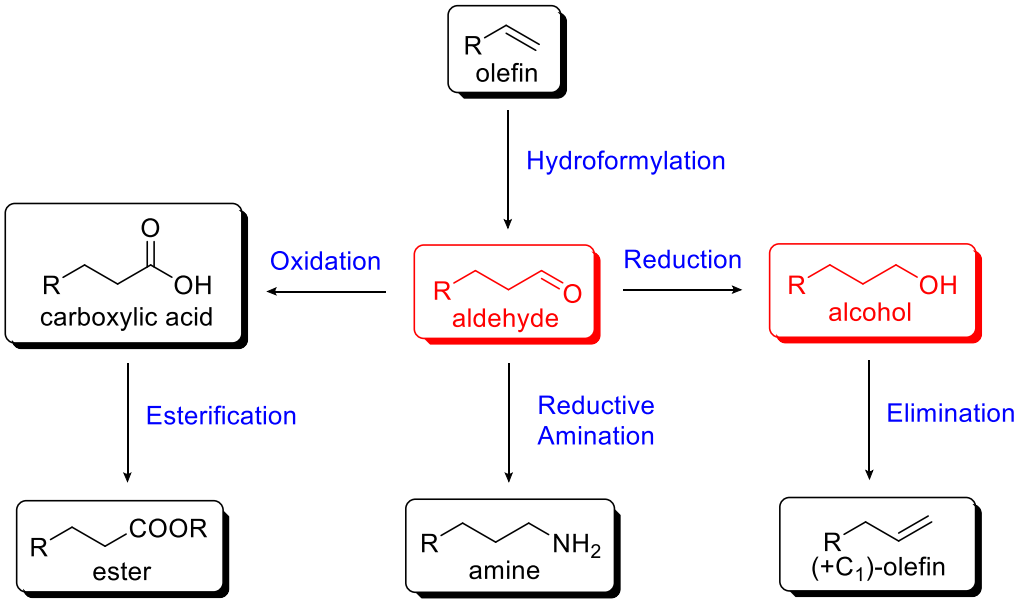

Figure 1.5 Products derived from olefin hydroformylation.

Amongst the various products (**Figure 1.5**) that can be derived from olefin hydroformylation however, the focus for the following sub-sections will be narrowed to the two highlighted in red, namely aldehydes and alcohols.

1.2.1 Cobalt-catalysed Hydroformylation

The earliest hydroformylation systems followed the original procedure of Roelen or were based on cobalt carbonyl complexes.[25-26] The majority of hydroformylation then was catalysed by cobalt and just 15 years after Roelen's discovery, the first production plant running Co-catalysed hydroformylation of propylene was commissioned at Ruhrchemie in Germany. By the end of the 1960s, most hydroformylation plants employed [$HCo(CO)_4$] at high temperatures (140 to 180 °C) and high pressures (200 to 450 bar) for their processes despite the harsh conditions required.[27] Aside from the forcing reaction conditions however, another pressing issue encountered by unmodified cobalt hydroformylation catalysts at that time was its poor linear selectivity (60 – 70%) for the more valuable n-aldehyde product.[28] To overcome this deficiency, cobalt was modified with monodentate phosphine ligands to increase its linear selectivity to as high as 90%.[28] Electron-donating phosphine ligands increase electron density at the cobalt centre and make the Co-H bond more hydridic compared to the unmodified [$HCo(CO)_4$] catalyst, hindering double bond migration and promoting terminal functionalisation of 1-olefins.[29-30] However, this modification also brought about lower activities[31] and increased hydrogenation activity that facilitated low-value paraffin formation and the reduction of aldehydes to alcohols, the latter of which has been considered desirable for certain applications.[32] The basicity of tertiary monodentate phosphines has been found to correlate inversely with

hydroformylation activity but directly with linear selectivity in Co-catalysed olefin hydroformylation (**Figure 1.6**).[33]

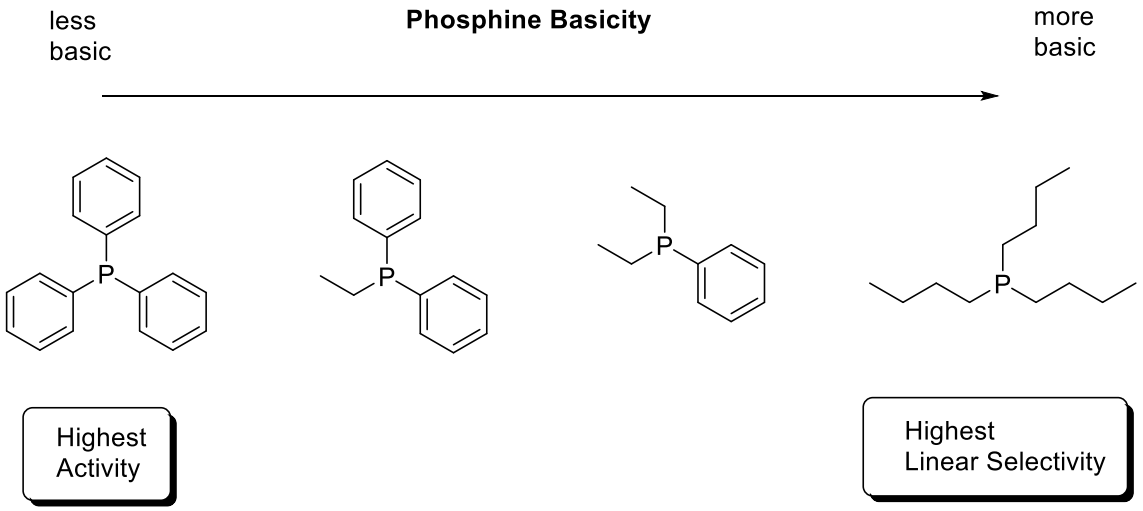

Figure 1.6 Dependence of activity and linear selectivity of monodentate phosphine modified Co-catalysed hydroformylation on phosphine basicity.[33]

Trialkyl phosphine ligands have stronger σ-donor and poorer π-acceptor properties than CO, resulting in an electron-rich cobalt centre that exhibits increased π-back donation of electron density to the CO ligands, binding them more strongly and thus increasing the thermal stability of the catalyst.[34] This increased thermal stability enables the reaction to be run at higher temperatures to combat the lower activity accompanying linear-selective basic phosphines. In this respect, P^nBu_3 emerged as one of the preferred ligands to be applied on an industrial scale (Shell process).[28] Other tertiary phosphines, such as those based on 9-phosphabicyclononane (phobane, **Figure 1.7**), were subsequently developed and have also been successfully applied in Co-catalysed hydroformylation of olefins to alcohols by Shell.[35-36] An overview of the mechanistic aspects of Co-catalysed hydroformylation has been given by Hebrard and Kalck.[37]

1.2.2 Rhodium-catalysed Hydroformylation

Aside from cobalt, rhodium is the only other transition metal that has been employed in industrial hydroformylation.[33] In the 1960s, researchers at Union Carbide Corporation (now Dow Chemical Company) and a research group at Imperial College London led by Sir Geoffrey Wilkinson,[38] independently found that rhodium catalysts modified with organophosphines could catalyse hydroformylation with superior performance to existing cobalt systems.[27] Rhodium is about 3 to 4 orders of magnitude more active for hydroformylation,[39] exhibits superior linear selectivity in the presence of excess ligand,[27] suppresses hydrogenation to low-value paraffins and operates under milder conditions (**Table 1.1**).

Table 1.1 Comparison between commercial cobalt and rhodium hydroformylation processes.[40]

	Cobalt	**Modified Cobalt**	**Modified Rhodium**
Catalyst	$[HCo(CO)_4]$	$[HCo(CO)_3(PBu_3)]$	$[HRh(CO)(PPh_3)_3]$
Temperature / °C	110 – 180	160 – 200	100
Pressure / bar	200 – 300	50 – 100	<20
Major Product	Aldehydes	Alcohols	Aldehydes
***n / iso* Ratio**	2 – 4	7	>10
Hydroformylation Yield / %	90	80*	98
Paraffin Yield / %	1	15	0.9
Other By-Products / %	9	5	1.0

* Inclusive of aldehydes and alcohols.

Increasing *n*:*iso* ratio from 3:1 to 10:1 translates to manufacturing *n*-butyraldehyde using approximately 30% less propylene. This meant savings of about USD$6 million per year on propylene and synthesis gas feedstocks for large commercial plants.[34] It was not long before the first rhodium-based hydroformylation plants were commissioned by Ruhrchemie (1974), Union Carbide Corporation (1976) and Mitsubishi Chemical Corporation (1978). Due to the substantial advantages afforded by rhodium catalysed hydroformylation, the rest of the chemicals industry were quick to convert their hydroformylation processes from cobalt to rhodium systems. Initially in the 1980s, more than 90% of commercial hydroformylation was conducted using cobalt. By 1995 however, nearly 80% was done using rhodium instead, mostly due to rhodium's superior hydroformylation activity for lighter olefins and the large global production of n-butyraldehyde.[41] Recently however, there has been renewed interest in cobalt hydroformylation catalysts due to cationic cobalt(II) bisphosphine hydrido-carbonyl catalysts exhibiting hydroformylation activities far superior to traditional neutral cobalt(I) catalysts.[42] Unlike rhodium, cobalt-based systems are known to reduce the intermediate aldehydes to alcohols, and the direct production of alcohols from olefins may be desirable for certain applications.[43]

Organic ligands play a pivotal role in altering the catalytic properties of transition metals for hydroformylation. The design and development of hydroformylation ligands through the years can also be viewed as a description of the progress made in the field of hydroformylation, where successive ligands show improved catalytic profiles or optimise the reaction for specific applications (**Figure 1.7**).

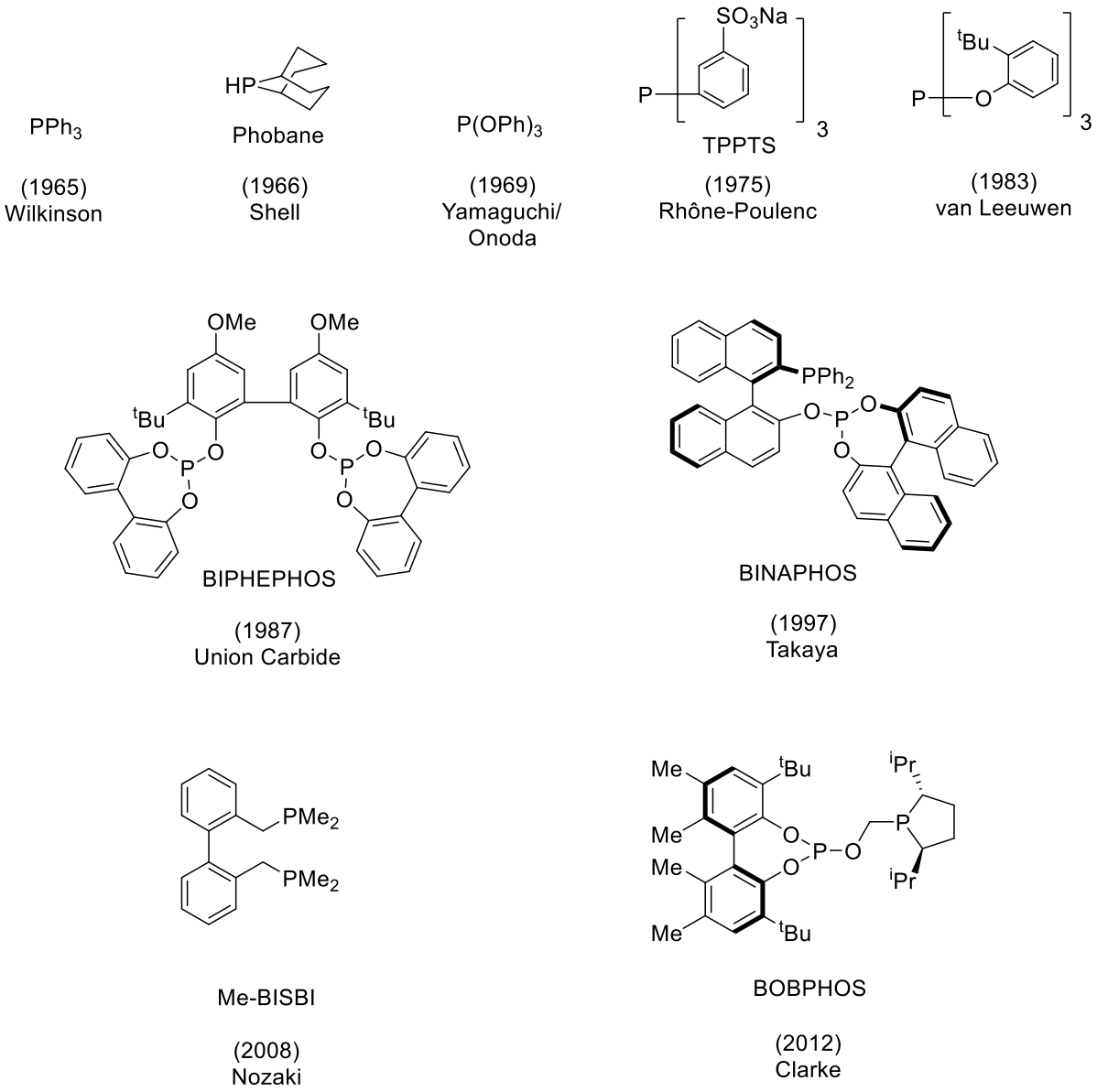

Figure 1.7 Ligands developed for rhodium-catalysed hydroformylation applications.[33, 44-50]

A paradigm shift was initiated by Wilkinson, who first employed PPh_3 to modify rhodium complexes[44] for propylene hydroformylation.[34] Subsequently, phosphites such as $P(OPh)_3$ were found to afford superior hydroformylation rates that allowed them to be considered for hydroformylation of higher (C_4 and above) olefin feedstocks.[51] However, these simple phosphite ligands are susceptible to hydrolysis under hydroformylation conditions (**Figure 1.8**).[52]

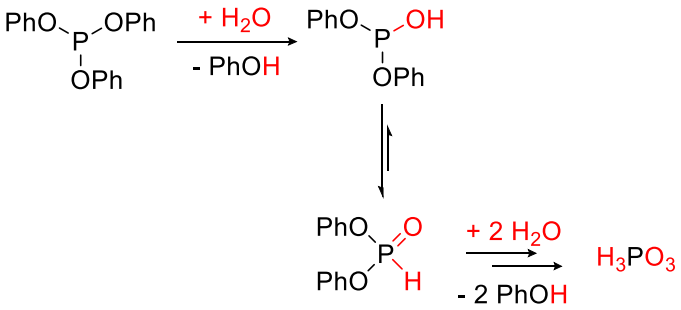

Figure 1.8 Hydrolysis of $P(OPh)_3$ to H_3PO_3.

To bolster catalyst stability, bulky groups were introduced to control reactivity via kinetic inhibition.[33] For example, the introduction of ortho-positioned tert-butyl substituents on $P(OPh)_3$ as described by van Leeuwen.[46, 53] In 1981, these types of bulky monodentate phosphites were claimed for hydroformylation by Shell[54] and Union Carbide.[55]

In an alternative avenue of research, Rhône-Polenc developed a water-soluble sulphonated phosphine, TPPTS (**Figure 1.7**), that enabled an aqueous biphasic hydroformylation process with more efficient catalyst recycling. The catalyst could be removed to the aqueous phase before distillation of the product, avoiding thermal stress on the catalyst and decreasing rhodium loss to the parts per billion range.[56] The high cost of rhodium at that time meant that millions of euros per year could be saved via catalyst preservation this way.[57]

In the following years, researchers at Davy Process Technology and Union Carbide reached a milestone in the development of hydroformylation ligands with the advent of bidentate ligands such as the bulky bisphosphite, BIPHEPHOS (**Figure 1.7**).[47] Sterically hindered, chelating bisphosphites like BIPHEPHOS create favourable steric environments around the rhodium centre that give excellent regioselectivities (*n*:*iso* ≥40:1) under mild conditions (70 psig 1:1 CO/H_2, 60 °C).[58-59] Since its introduction in 1987, BIPHEPHOS has garnered the interest of various research groups who have investigated it for various applications. Some notable achievements include:

(1) TOFs of 44,000 h^{-1} in the hydroformylation of 1-dodecene[60]
(2) 94% conversion with 95% selectivity to *n*-nonanal in the tandem isomerisation-hydroformylation of *trans*-4-octene[61]
(3) 89% aldehyde yield with *n*:*iso* ratio of 89:11 in the tandem isomerisation-hydroformylation of oleonitrile[62]

Subsequent modification of the bulky chelating bidentate ligand template enabled its application to enantioselective rhodium-catalysed hydroformylation processes. For example, a barrier to rotation can be created by leveraging on the rigidity and steric bulk of certain substituents like naphthalene to

form atropisomers. An example of this can be seen in the mixed phosphite-phosphine bidentate ligands, BINAPHOS and BOBPHOS (**Figure 1.7**). Atropisomerism present in the ligand architecture confers enhanced stereo- and regioselective discriminating properties on rhodium systems modified with these ligands. The use of BINAPHOS can reverse the high linear selectivities typical for bulky chelating bidentate ligands to instead yield 90% of the branched aldehyde product from styrene with 94% ee of the (*S*)-isomer.[48] Alternatively, BOBPHOS may also be used to perform a similar enantioselective hydroformylation of vinyl acetate to give >99% branched aldehyde yield with 83% ee of the (*R*)-isomer.[50] Another innovative effort by Nozaki and co-workers brought together the high *n*:*iso* ratios afforded by BISBI[63] with the hydrogenation activity of trialkylphosphines to create a mixed phosphine ligand, Me-BISBI (**Figure 1.9**), in order to facilitate tandem hydroformylation-reduction of olefins to alcohols.

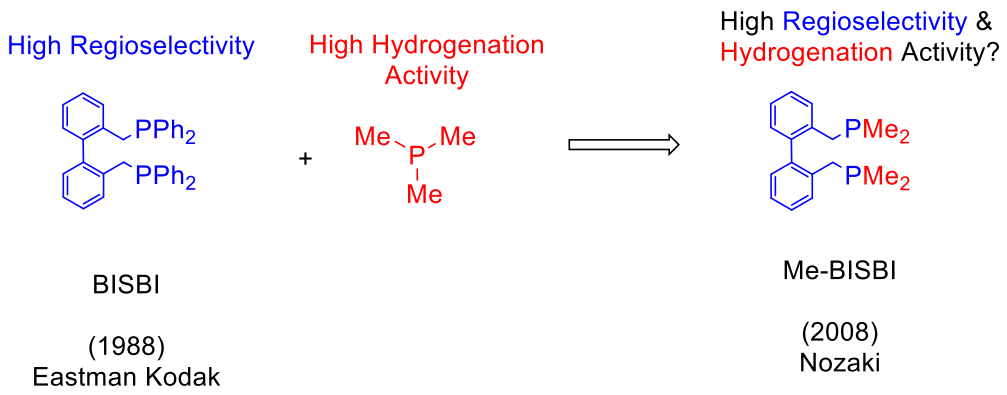

Figure 1.9 Combination of structural elements in BISBI[63] and PMe_3 to make Me-BISBI.[49]

They were able to achieve 97% alcohol yield with a *n*:*iso* ratio of about 4:1 in the tandem hydroformylation-reduction of 1-decene to 1-undecanol.[49]

Due to the large success of rhodium in its technical application, there has been considerable industrial and academic interest in rhodium-catalysed hydroformylation.[33] This has generated extensive literature on the subject, out of which, only a limited selection has been presented above to introduce the area.

1.2.3 Ruthenium-catalysed Hydroformylation

The large demand for rhodium in chemical processes and its high price at that time motivated the search for alternative transition metal catalysts.[2] Wilkinson and co-workers pioneered the application of ruthenium catalysts in homogeneous olefin hydroformylation with the use of $[Ru(CO)_3(PPh_3)_2]$ complexes to convert 1-pentene to hexanal.[64] Their investigations into propylene hydroformylation with unmodified ruthenium carbonyl complexes revealed that its linear selectivity was lower than unmodified cobalt but higher than unmodified rhodium catalysts. Unmodified ruthenium catalysts

also exhibit higher hydrogenation activity than that of rhodium catalysts, resulting in increased alcohol and paraffin yields.[65]

Ruthenium could also be used synergistically to improve existing hydroformylation systems.[66] For example, the bimetallic $Co_2(CO)_8/Ru_3(CO)_{12}$ system has been shown to give initial cyclohexene hydroformylation rates about 27 times that of the monometallic $CO_2(CO)_8$ catalyst.[67] The superior hydrogenation activity of ruthenium has also been combined with the excellent hydroformylation properties of rhodium to create a tandem hydroformylation-hydrogenation catalyst to directly produce alcohols from olefins.[68-70]

Wilkinson and co-workers observed that polynuclear ruthenium complexes such as $Ru_3(CO)_{12}$ were less active for hydroformylation than mononuclear complexes, and subsequently proposed a mechanism involving $[Ru(H)_2(CO)_2(PPh_3)_2]$ as the active species.[71] On the basis of observations from spectroscopic analysis, Süss-Fink and co-workers have also proposed an alternative mechanism for polynuclear ruthenium complexes such as $[HRu_3(CO)_{11}]^-$ that proceeded via an intermediary intact trinuclear metal cluster.[72-75]

More recently, Beller and co-workers have developed an electron-rich imidazole-substituted dialkylphosphine that assists in the Ru-catalysed hydroformylation of 1-octene to yield 79% nonanal with 95% linear selectivity.[76] They also surveyed a series of monodentate and bidentate ligands to eventually find 2-phosphino-substituted imidazoles as suitable ligands in Ru-catalysed tandem hydroformylation-reduction of 1-octene to give up to 90% nonanol and 91% linear selectivity.[77-78]

1.2.4 Palladium-catalysed Hydroformylation

As opposed to cobalt and rhodium, far fewer studies have been conducted on palladium catalysed hydroformylation.[2] Interest in the area was stimulated after discoveries by Drent and co-workers at Shell showed that cationic palladium diphosphine complexes could function as valuable hydroformylation catalysts.[79-81] In 2000, Drent and Budzelaar investigated various bidentate phosphine ligands and acid co-catalysts for palladium catalysed olefin hydroformylation (**Figure 1.10**).[82-83]

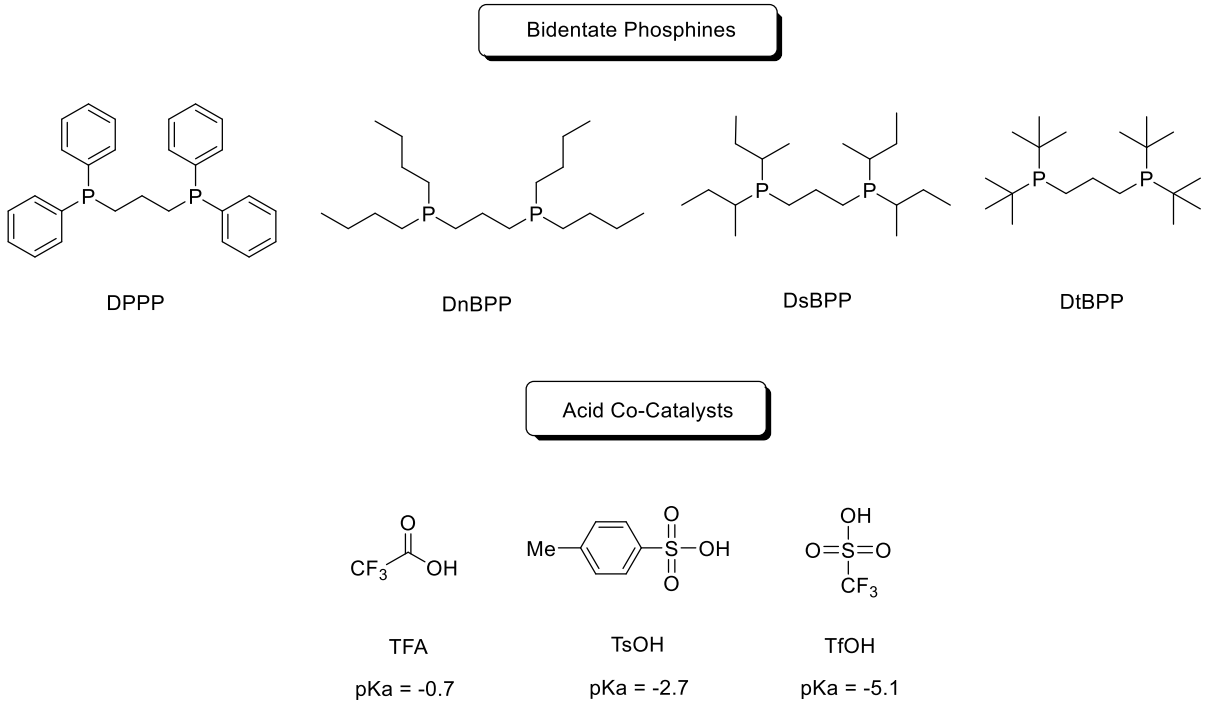

Figure 1.10 Some bidentate phosphines and acid co-catalysts (with their associated pK_a values)[84] investigated by Drent and Budzelaar.[83]

They observed that linear selectivity improved by about 15% when DnBPP was replaced with its sterically bulkier sec-butyl analogue, DsBPP (**Figure 1.10**), in palladium catalysed hydroformylation of propylene.[83] This suggests that restriction of coordination space at the coordination centre by sterically bulky ligands favour 1,2-(*n*) olefin insertion (generating *n*-alkyl intermediates) over 2,1-(*iso*) insertion (generating sterically demanding *iso*-alkyl intermediates), resulting in improved linear selectivities (**Figure 1.11**).

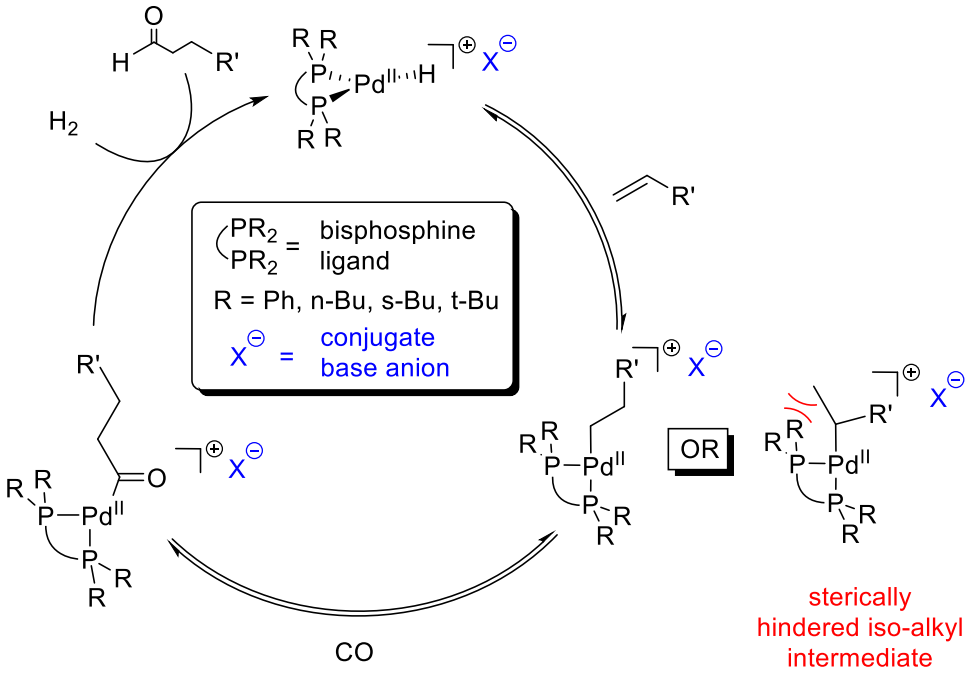

Figure 1.11 Proposed catalytic cycle for palladium catalysed olefin hydroformylation.[83]

The active catalyst is believed to be a palladium(II) hydride complex with a neutral cis-chelating diphosphine ligand. Subsequent coordination and migratory insertion of olefin produces a Pd-alkyl intermediate that then yields a Pd-acyl complex upon coordination and insertion of CO. Hydrogenolysis of the Pd-acyl bond releases aldehyde and regenerates the active palladium(II) hydride species to close the catalytic cycle.

Replacing TsOH (pK_a = -2.7) with less acidic TFA (pK_a = -0.7) in DPPP (**Figure 1.10**) modified palladium catalysed hydroformylation of propylene also increases aldehyde product linearity by 10%.[83] The influence of the acid co-catalyst was linked with the basicity of its associated conjugate base anion (X^-), and two hypotheses for the observed improved linear selectivity were proposed by Drent:[83]

(1) Stronger coordination and hence closer proximity between the conjugate base anion and cationic palladium complex resulting in greater congestion at the palladium centre and thus a preference for sterically less demanding Pd-*n*-alkyl intermediates that lead to linear aldehydes.

(2) More strongly coordinating conjugate base anions that discriminate for Pd-*n*-acyl intermediates over Pd-*iso*-acyl intermediates when assisting in electrophilic activation of H_2 during hydrogenolysis. Since hydrogenolysis is thought to be the only irreversible step in the catalytic cycle (**Figure 1.11**),[83] this leads to the formation of more linear aldehydes.

However, it should be noted that extent of cation-anion coordination is also affected by reaction solvent.[83] Cation-anion dissociation is facilitated by solvation in polar protic solvents that minimise anion coordinating effects, while in non-polar solvents, such ion pairs stay in closer proximity. In fact, when polar aprotic diglyme is replaced by polar protic methanol as the reaction solvent, the major product obtained switches from aldehydes (80% yield) to ketones (95% yield) when using DnBPP and TsOH (**Figure 1.10**).[83] This suggests that the conjugate base anion plays an active role in the reaction mechanism, and that cation-anion coordination has significant influence on chemoselectivity.

Beller et al. also noted in a separate study that the amount of acid used in palladium catalysed hydroformylation of 1-octene is inversely related with linear selectivity.[85] However, they attributed this phenomenon to increased isomerisation at higher acid concentrations instead of any direct involvement by the acid co-catalyst.

The interplay between ligand basicity and acid co-catalyst pK_a determining chemoselectivity for palladium catalysed olefin hydroformylation may also be represented visually (**Figure 1.12**).[83]

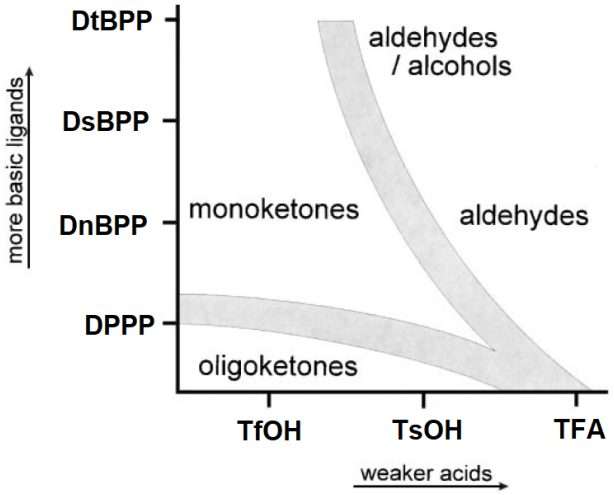

Figure 1.12[b] Scheme of chemoselectivity as a function of ligand basicity and acid strength.[83]

At the palladium(II) acyl intermediate of the catalytic cycle (**Figure 1.11**), discrimination between olefin insertion (to yield ketones) and hydrogenolysis (to yield aldehydes) occurs. The olefin insertion product has been reported to be stabilised via internal coordination of the β-carbonyl oxygen atom to the palladium(II) centre to form a 5-membered chelate (**Figure 1.13**).[86-87]

[b] Adapted from ref. 84 with the permission of the rights holder, Elsevier.

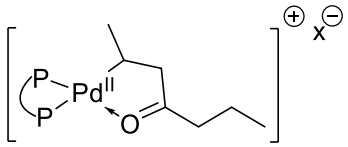

Figure 1.13 Coordination of the oxygen atom from the β-carbonyl group to palladium(II) centre. X^- = non-coordination anion. P⌢P = bidentate diphosphine ligand.

A more electrophilic palladium(II) centre should favour such coordination, lower the energy barrier for olefin insertion and thus favour olefin insertion over hydrogenolysis to give more ketone products. Conversely, more basic ligands or weaker acids with conjugate bases that are associated with stronger coordination to the palladium(II) centre decrease the electrophilicity of the palladium(II) centre and should favour hydrogenolysis to aldehydes instead. The combination of these two competing effects of ligand basicity and acid strength demarcate the boundaries in **Figure 1.12** separating ketone and aldehyde formation. More basic and coordinating anions have been proposed to influence chemoselective discrimination in the following two ways:[83]

(1) Basic anion-assisted heterolytic cleavage of H_2 to facilitate hydrogenolysis, hence favouring hydrogenolysis over olefin insertion.
(2) Coordinating anions remain in close proximity to the palladium(II) centre and block the coordination site from olefin coordination but not from smaller H_2 molecules, hence favouring hydrogenolysis.

In 2006, Drent and co-workers reported further findings on the influence of ligand and anion properties on palladium catalysed olefin hydroformylation,[88] this time based around a C_2-bridged diphosphine, BCOPE (**Figure 1.14**).

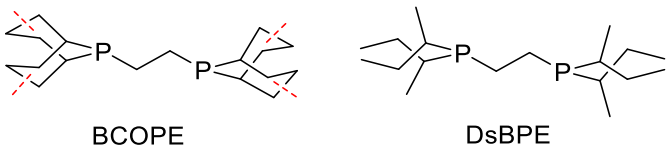

Figure 1.14 Structural comparison between BCOPE and DsBPE. Dotted lines indicate bonds that have been formally "cut" for ring opening of BCOPE to give DsBPE.

BCOPE has a C_2-bridge linking two 9-phosphabicyclo[3.3.1]nonyl or "phobane" moieties (**Figure 1.14**). Phobane belongs to the class of phosphacycles exhibiting a strained C-P-C bridgehead of approximately 90°, down from the typical 107° in trigonal pyramidals.[89] This restricted geometry alters p-character in its lone pair orbital, the energy of its HOMO as well as its σ-donor and π-acceptor properties.[90] Extensive studies on the unique characteristics of phobanes and their derivatives have been reported by Pringle and co-workers.[91-93] Phobane can be formally ring-opened by "cutting" a

single bond, as indicated by the dotted lines in **Figure 1.14**, to give two *sec*-butyl groups. This simple disconnection, however, has significant implications on catalytic performance (**Table 1.2**).

Table 1.2 Comparison of BCOPE and DsBPE in palladium catalysed olefin hydroformylation.[88]

Ligand	Substrate	Additive	TOF / h^{-1}	Alcohol Yield (Linear) / %	Ketone Yield / %	Paraffin Yield / %
BCOPE	1-Octene	-	130	88 (68)	10	2
DsBPE	1-Octene	-	40	4 (51)	88	7
BCOPE	*i*-C_8-C_{10}	-	150	89 (65)	3	8
DsBPE	*i*-C_8-C_{10}	-	<10	-	-	-
BCOPE	1-Octene	Cl^-	1000	95 (79)	4	1
DsBPE	1-Octene	Cl^-	40	7 (55)	86	7
BCOPE	*i*-C_8-C_{10}	Cl^-	1000	99 (72)	<1	<1
DsBPE	*i*-C_8-C_{10}	Cl^-	<10	-	-	-

Conditions: 105 °C, CO:H_2 (1:2) 60 bar, substrate = 0.13 mol, $Pd(OAc)_2$ = 0.25 mmol, TfOH = 0.5 mmol, L/Pd = 1.4, Cl/Pd = 0.4, solvent = sulfolane/H_2O (20:1) 10 mL. *i*-C_8-C_{10} is an equilibrated mixture of internal C_8-C_{10} alkenes (12% C_8, 44% C_9 and 44% C_{10}). Linear = 1-alcohol/total alcohol product.

There is a switch in chemoselectivity from 88% alcohol yield (BCOPE) to 88% ketone yield (DsBPE) along with a roughly threefold reduction in rate for 1-octene substrates (see **Table 1.2**, entries 1 and 2). BCOPE also retains its activity for internal olefin substrates to give 89% alcohol yield while DsBPE is nearly inactive for internal olefin substrates. The difference in activity for internal olefin substrates is thought to be linked to ligand steric bulk as defined by their Tolman cone angles.[88] The Tolman cone angle,[94] a classical measure of ligand steric bulk, takes the angle (θ) from a cone formed from the metal centre at the vertex and the van der Waals spheres of the ligand substituents as the outermost edges (**Figure 1.15**).

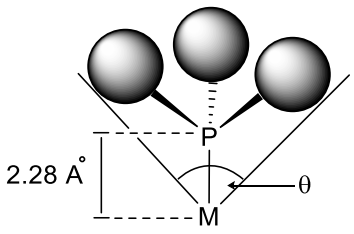

Figure 1.15 Tolman cone angle,[95] θ. M = metal centre.

The more flexible and dynamic *sec*-butyl groups on DsBPE have a Tolman cone angle of about 130 - 170° while the more rigid cyclic phobanes on BCOPE have a relatively smaller cone angle of about 120 - 130°.[96] The greater congestion of the coordination sphere by DsBPE is expected to hinder the

formation of sterically demanding Pd-*iso*-alkyl intermediates resulting from olefin insertion of internal olefins (**Figure 1.16**) and thus hinder isomerisation.

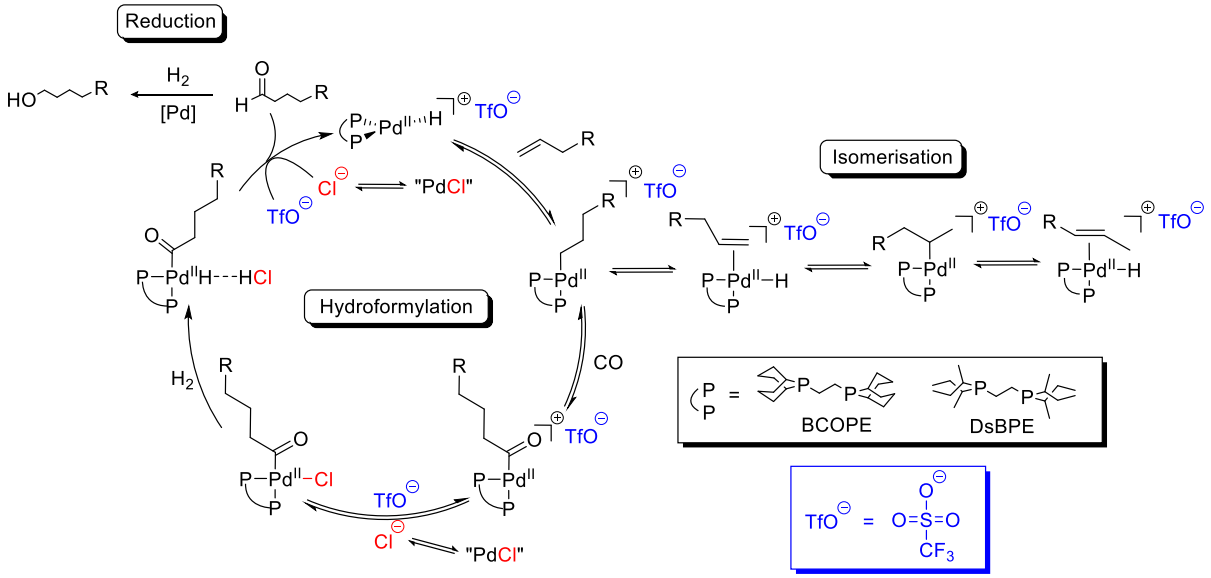

Figure 1.16 Proposed catalytic cycle for anion promoted palladium catalysed olefin hydroformylation.[88]

In addition, low energy transition states involving agostic interactions between β-hydrogens of the *iso*-alkyl moiety and the cationic palladium(II) centre (**Figure 1.17**) can facilitate the isomerisation process. These are also expected to be less favourable for DsBPE due to its more hindered coordination sphere.

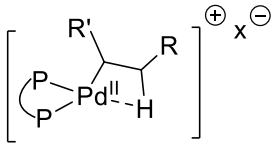

Figure 1.17 Agostic interaction of β-hydrogen. R/R' = alkyl. X^- = non-coordinating anion. P⌢P = bidentate diphosphine ligand.

Unlike DsBPE, BCOPE exhibits facile isomerisation to yield similar amounts of alcohol product (88 – 89%) with similar linear selectivity (65 – 68%) and rate (130 – 150 h^{-1}) regardless of whether the starting substrate is a terminal or internal olefin (see **Table 1.2**, entries 1 and 3).

Finally, with the addition of substoichiometric amounts of Cl^-, there is a boost in reaction rate, chemo- and regioselectivity to linear alcohols for BCOPE while DsBPE shows no significant change (**Table 1.2**). This promoting effect was only observed at substoichiometric amounts of Cl^- (with respect to palladium) while inhibition of catalytic activity was observed at higher Cl^- concentrations.[88] This suggests that only a relatively small fraction of palladium coordinated to Cl^- facilitates the rate-determining hydrogenolysis step, too much and the increased concentration of Cl^- is expected to block

coordination sites and inhibit catalytic activity (**Figure 1.16**). Chloride ions are likely be found within the system bound to palladium as several potential Pd-Cl species, which have been grouped as "PdCl" (**Figure 1.16**).[88] Halogens are known catalyst poisons,[97] and although the exact mechanism through which Cl^- promotes palladium catalysed hydroformylation has yet to be determined, Drent has proposed that the close proximity of Cl^- to the cationic palladium(II) centre enables a Cl^- assisted heterolytic cleavage of H_2 that facilitates the rate-determining hydrogenolysis step (**Figure 1.16**). The greater steric bulk of DsBPE is believed to hinder the penetration of Cl^- into the coordination sphere and prevents it from assisting in hydrogenolysis, blocking any such promoting effects.[88]

The improvement in linear selectivity (ca. 10%) observed after addition of Cl^- was attributed to the greater amount of space available at the palladium(II) centre of Pd-*n*-acyl intermediates that allow Cl^- to better approach and promote hydrogenolysis. Furthermore, the decrease in paraffin formation observed with addition of Cl^- (**Table 1.2**) seems to support that Cl^- selectively interacts with Pd-acyl intermediates to promote hydrogenolysis, as the hydrogenolysis of Pd-alkyl intermediates is suppressed instead of being promoted to give less paraffins (see **Table 1.2**, entries 3 and 7).

Several palladium-based hydroformylation systems have since been patented by Shell for different applications, including:

(1) Tandem hydroformylation-reduction of terminal and internal olefins to linear alcohols.[98-99]
(2) Tandem hydroformylation-reduction of olefin feeds containing dienes.[100]
(3) Homologation of secondary C_n alcohols to linear C_{n+1} alcohols via a dehydration-isomerisation-hydroformylation-reduction cascade.[101]

The recent developments demonstrating the versatility of palladium-based hydroformylation catalysts to produce different oxo products from olefins and the unique catalytic aspects of phobane ligands in cationic palladium complexes hint at the potential of palladium-based systems within the field of hydroformylation.

1.3 Olefin Alkoxycarbonylation

Olefin alkoxycarbonylation or sometimes also referred to as hydroesterification, is the addition of CO and alcohol (ROH) to an olefin to form terminal or branched esters except in the case of ethylene where only terminal esters are possible (**Figure 1.18**).

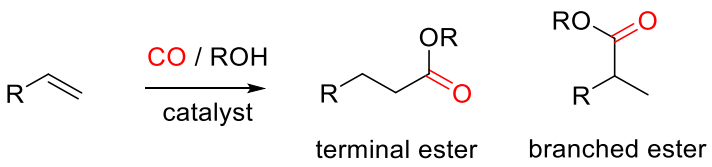

Figure 1.18 Alkoxycarbonylation of olefins.

This process is related to the Reppe carbonylation of Walter Reppe, whose pioneering work at BASF in the early 1900s involved the alkoxycarbonylation of alkynes such as acetylene to yield unsaturated esters.[102] Although Reppe initially used nickel complexes for this process,[103] during the ensuing years of catalyst development, cobalt[104-106] and palladium[107] catalysts came to the fore due to their superior activities. Palladium complexes, in particular, are well-known to catalyse alkoxycarbonylation for a broad range of olefinic substrates under mild conditions and are still considered state-of-the-art for the industrial production of esters.[108] For example, the commercial production of methyl propanoate, an important intermediate for methyl methacrylate polymers (acrylic), is presently made via the palladium catalysed methoxycarbonylation of ethylene (Lucite Alpha Process) on a more than 300,000 metric tonne per annum scale.[109] The following sub-sections will focus on giving a brief overview of such palladium-based alkoxycarbonylation systems.[107]

1.3.1 Mechanistic Aspects

Studies on the mechanism of palladium catalysed ethylene methoxycarbonylation[110-111] have led to the proposal of two different catalytic cycles for the reaction – a hydride cycle and a methoxy cycle (**Figure 1.19**).

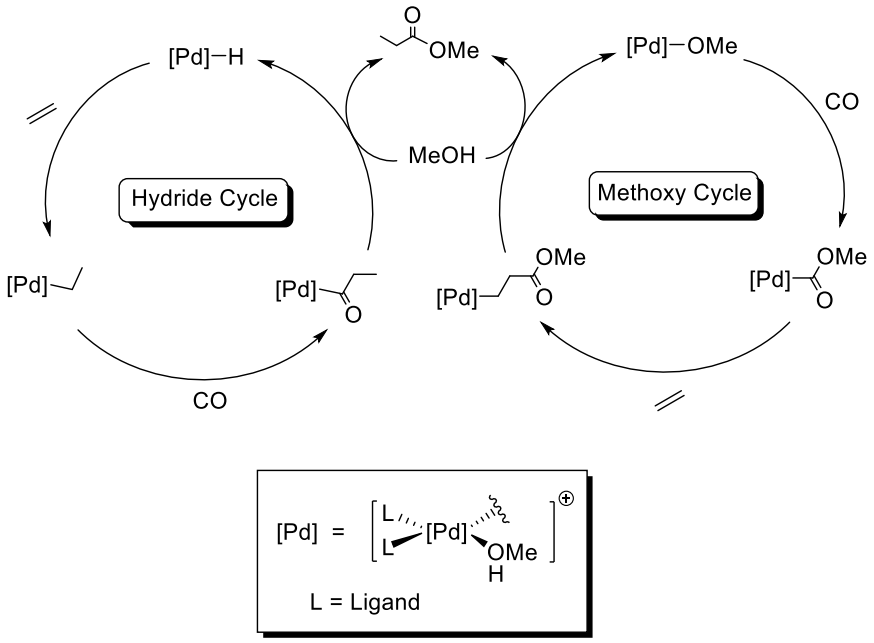

Figure 1.19 Hydride and methoxy cycles for palladium catalysed methoxycarbonylation of ethylene.

In the hydride cycle, ethylene inserts into Pd-H to form a Pd-alkyl intermediate. Subsequent coordination and migratory insertion of CO yields a Pd-acyl that then undergoes nucleophilic attack by methanol to give methyl propanoate and regenerates the starting Pd-H complex. In the methoxy cycle, CO insertion into Pd-methoxy occurs instead to give a Pd-carbomethoxy intermediate. Subsequent coordination and migratory insertion of ethylene yields a Pd-alkyl intermediate that undergoes alcoholysis to give the desired ester and regenerates the Pd-methoxy complex.

Ethylene-CO copolymerisation is closely related to ethylene methoxycarbonylation[112] where instead of terminating at a single fragment, multiple alternating insertions of ethylene and CO lead to the formation of valuable high-melting polyketone products.[113] Polymer end group analysis[114] showing the presence of both diester- and diketone-terminated copolymer necessitates that both hydride and methoxy mechanisms must be active in ethylene-CO copolymerisation.[115] However, multinuclear NMR spectroscopy and ^{13}C-labelling studies support that ethylene methoxycarbonylation operates exclusively via the hydride cycle.[116] This mechanistic proposal has also been extended to the alkoxycarbonylation of styrene,[117-119] suggesting that olefin alkoxycarbonylation in general follows the hydride mechanism.

Further mechanistic studies on the hydride and methoxy cycles have revealed that this difference can be traced to discrimination at the termination step that yields the ester product.[111] For the hydride cycle, termination via nucleophilic attack of methanol on the Pd-acyl intermediate has been shown to proceed on the timescale of tens of minutes at -30 °C.[111] For the methoxy cycle however, termination via methanolysis of the Pd-alkyl intermediate takes several days even at 20 °C.[111] The significant difference in reaction rates may be related to the formation of stable palladium β-ester chelates (**Figure 1.20**) in the methoxy cycle.

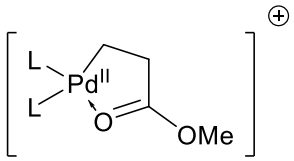

Figure 1.20 Palladium β-ester chelate. L = Ligand.

Although methanolysis of palladium β-ester chelates (**Figure 1.20**) to give esters is slow, CO insertion into its Pd-alkyl bond is relatively fast.[111] Subsequent insertion of ethylene to the resulting Pd-acyl intermediate brings it back to a similar β-ester chelate which again favours ethylene insertion over methanolysis. The continued alternating insertions of CO and ethylene eventually yield a polyketone, which may explain why the methoxy cycle is absent in ethylene methoxycarbonylation but is still observed for ethylene-CO copolymerisation. It then follows that any catalyst system favouring the

methoxy cycle also favours copolymerisation while catalyst systems that favour the hydride cycle can be considered as potential candidates to be employed for alkoxycarbonylation.

1.3.2 Monodentate Phosphine Ligands

Olefin alkoxycarbonylation was initially carried out using ligand-free systems such as the $PdCl_2$/HCl system employed by Tsuji et al.[120] requiring high pressures (100 bar) of CO at 80 °C.[120] However, James and Stille were able improve upon this by using a bimetallic $PdCl_2/CuCl_2$ catalyst to methoxycarbonylate olefins at room temperature and low CO pressure (3 bar).[121-122] Stoichiometric quantities of $CuCl_2$ were used to re-oxidise palladium(0) that precipitated from the reaction mixture to facilitate this reaction. Alper and co-workers went on to use the $PdCl_2/CuCl_2$ catalyst to alkoxycarbonylate terminal and internal olefins with diols under oxidative and acidic conditions.[123]

The influence of ligands on catalytic performance was taken advantage of by Yun and co-workers, who took the $PdCl_2/CuCl_2$ system established by Alper et al. and modified it with a 2:1 (with respect to palladium) excess of PPh_3 to achieve 97% branched selectivity when methoxycarbonylating 4-methylstyrene.[124] Cavinato and Toniolo also noted that a 4:1 (with respect to palladium) excess of PPh_3 preserved their $[PdCl_2(PPh_3)_2]$ catalysts from decomposing to metallic palladium.[125-126] Alper and co-workers observed that P(o-tolyl)$_3$ (**Figure 1.21**) performed a similar function to prevent formation of palladium black.[127] Since then, monodentate phosphine ligands (**Figure 1.21**) with varying steric and electronic properties have been employed for several applications of palladium catalysed alkoxycarbonylation.[128]

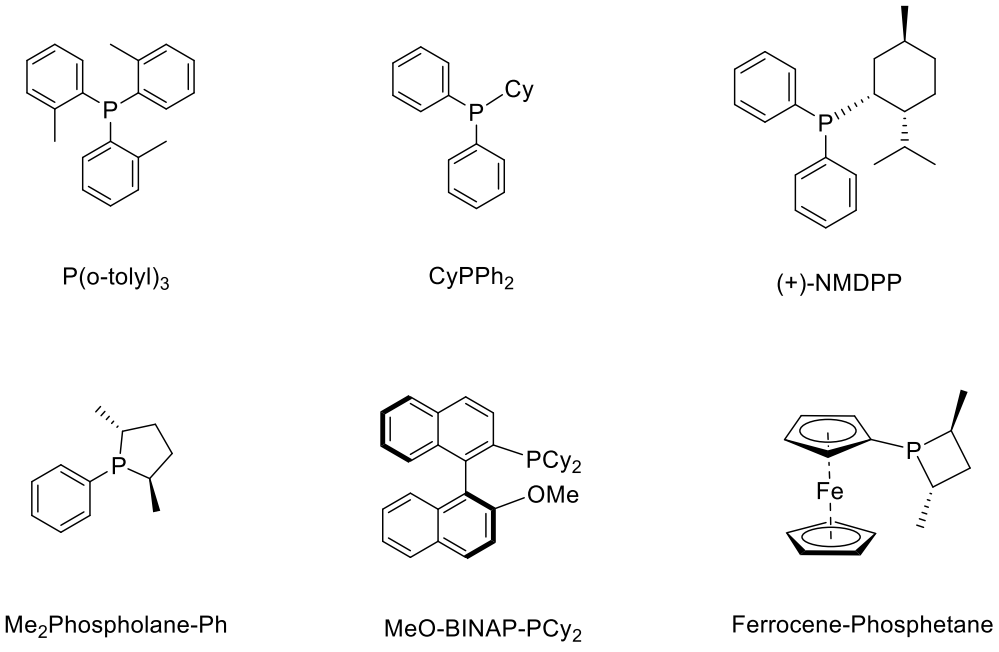

Figure 1.21 Monodentate phosphine ligands for palladium-catalysed olefin alkoxycarbonylation. Cy = cyclohexyl.

For example, monodentate phosphine ligands have been applied in palladium catalysed alkoxycarbonylation for the synthesis of α-arylpropionic acids such as ketoprofen and naproxen. Ketoprofen and naproxen are non-steroidal anti-inflammatory drugs (NSAIDs) that possess analgesic properties and are commonly prescribed for pain relief. The precursor to these types of drugs is often the corresponding branched ester that can be synthesized via branched selective alkoxycarbonylation of an appropriate α-olefin (**Figure 1.22**).

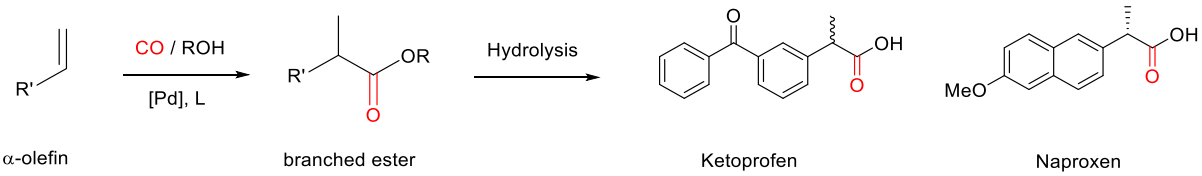

Figure 1.22 Alkoxycarbonylation route to α-arylpropionic acids. R = alkyl or aryl.

Hydrolysis of the branched ester intermediate then yields the desired α-arylpropionic acid drug (**Figure 1.22**). The preparation of the corresponding branched esters of ketoprofen[129] and naproxen[130] have been achieved with remarkable regioselectivity (>99%) by employing $CyPPh_2$ and (+)-NMDPP (**Figure 1.21**) respectively.

In the area of regio- and enantioselective styrene methoxycarbonylation, Nozaki et al. have used Me_2Phospholane-Ph (**Figure 1.22**) to achieve 98% branched selectivity with 2.4% ee of the (*R*)-isomer[131] and MeO-BINAP-PCy_2 (**Figure 1.22**) to achieve 100% branched selectivity with 53% ee of the (*S*)-isomer.[132] Additionally, Claver and co-workers demonstrated that chiral phosphetanes such as ferrocene-phosphetane (**Figure 1.22**) could give 97% branched selectivity and 29% ee of the (*R*)-isomer when methoxycarbonylating styrene.[133]

1.3.3 Bidentate Diphosphine Ligands

Alongside the high activities and selectivities of monodentate phosphine ligands in palladium catalysed olefin alkoxycarbonylation,[134-136] bulky chelating diphosphine ligands (**Figure 1.23**) were developed to improve linear selectivity and to enable tandem isomerisation-alkoxycarbonylation of internal olefins to linear esters.

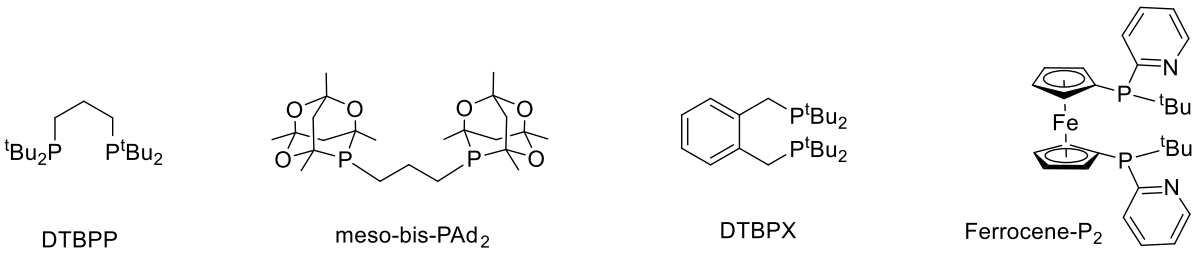

Figure 1.23 Bulky chelating diphosphine ligands for palladium-catalysed alkoxycarbonylation.

Palladium complexes modified with DTBPP (**Figure 1.23**) afford ester products in 75% linear selectivity when methoxycarbonylating a thermodynamic mix of internal C_{14} olefins. Changing ligand from DTBPP to meso-bis-PAd_2 increases rate by two orders of magnitude with no loss in linear selectivity (78%).[137] Palladium complexes modified with meso-bis-PAd_2 also methoxycarbonylate terminal C_{14} olefins about 2.5 times faster than it does internal C_{14} olefins with similar linear selectivity (80%), suggesting that isomerisation is rate-limiting in this case. Pringle and co-workers proposed that the difference in catalytic performance between DTBPP and meso-bis-PAd_2 may be associated with the unique stereoelectronic characteristics of the phosphatrioxaadamantane cage found in meso-bis-PAd_2.[137] Ligand electronic characteristics have been assessed from the ν(CO) of the A_1 band for $[Ni(CO)_2(Ligand)]$ complexes of DTBPP and meso-bis-PAd_2. The CO stretching frequency for $[Ni(CO)_2(DTBPP)]$ (1976 cm^{-1}) was found to be much lower than for the corresponding meso-bis-PAd_2 complex (ν(CO) = 2002 cm^{-1}), indicating that the P atoms in meso-bis-PAd_2 have low σ-basicity/high π-acidity that bear more of a resemblance to $P(aryl)_2R$ ligands such as the phenyl analogue of DTBPP, $Ph_2P(CH_2)_3PPh_2$ (ν(CO) = 1997 cm^{-1}). The combination of electronegative oxygen atoms alpha to the phosphorus and the constrained acute (ca. 90°) C-P-C angle[138] found in the cage contribute to the unique stereoelectronic characteristics and catalytic performance of meso-bis-PAd_2.

The application of DTBPP (**Figure 1.23**) in palladium catalysed methoxycarbonylation of ethylene affords TOFs of 15,000 h^{-1} with 98% selectivity for the desired ester product.[139] Replacing the C_3 backbone in DTBPP with a xylyl group (DTBPX, **Figure 1.23**) more than triples activity to 50,000 h^{-1} with 99.98% selectivity for the desired ester product.[139] Due to its high activity and excellent selectivity, Pd-DTBPX complexes are still considered state-of-the-art for selective alkoxycarbonylation of ethylene,[140] and are also favoured for tandem isomerisation-alkoxycarbonylation[141] of higher olefins. Pd-DTBPX is used industrially by Mitsubishi-Lucite for ethylene methoxycarbonylation in their 2-step Alpha process to produce methyl methacrylate polymers.[142] Pringle and co-workers have also demonstrated that different substituents on the P atom in the DTBPX framework (heterodiphosphines) made excellent ligands for palladium catalysed olefin alkoxycarbonylation.[143-144]

Further modification from a xylyl to a ferrocene backbone and substituting one of the *tert*-butyl substituents on the P atoms for 2-pyridyl (Ferrocene-P_2, **Figure 1.23**) results in a further threefold increase in rate for ethylene methoxycarbonylation.[145] A number of bulky chelating diphosphines with metallocene backbones have since been reported for palladium catalysed alkoxycarbonylation,[146-149] although none as active as the mixed *tert*-butyl/2-pyridyl diphosphines. The high alkoxycarbonylation activity of mixed *tert*-butyl/2-pyridyl diphosphine modified palladium catalysts stems from the installation of a basic pyridine moiety in close proximity to the reaction centre that is able to facilitate the rate-determining alcoholysis step.[150] Mixed phosphines that include a 2-pyridyl moiety were

originally developed by Drent and co-workers at Shell for the methoxycarbonylation of propyne.[151] These mixed phosphines were found to be highly active (TOFs of 40,000 h^{-1}) and selective (99.95%) for producing methyl methacrylate and have since been leveraged for other applications. For example, the *tert*-butyl/2-pyridyl analogues of DTBPP[152] and DTBPX,[150] show activity for the methoxycarbonylation of sterically hindered tetra-substituted olefins (**Figure 1.24**) to linear esters with 99% selectivity despite DTBPX being inactive.

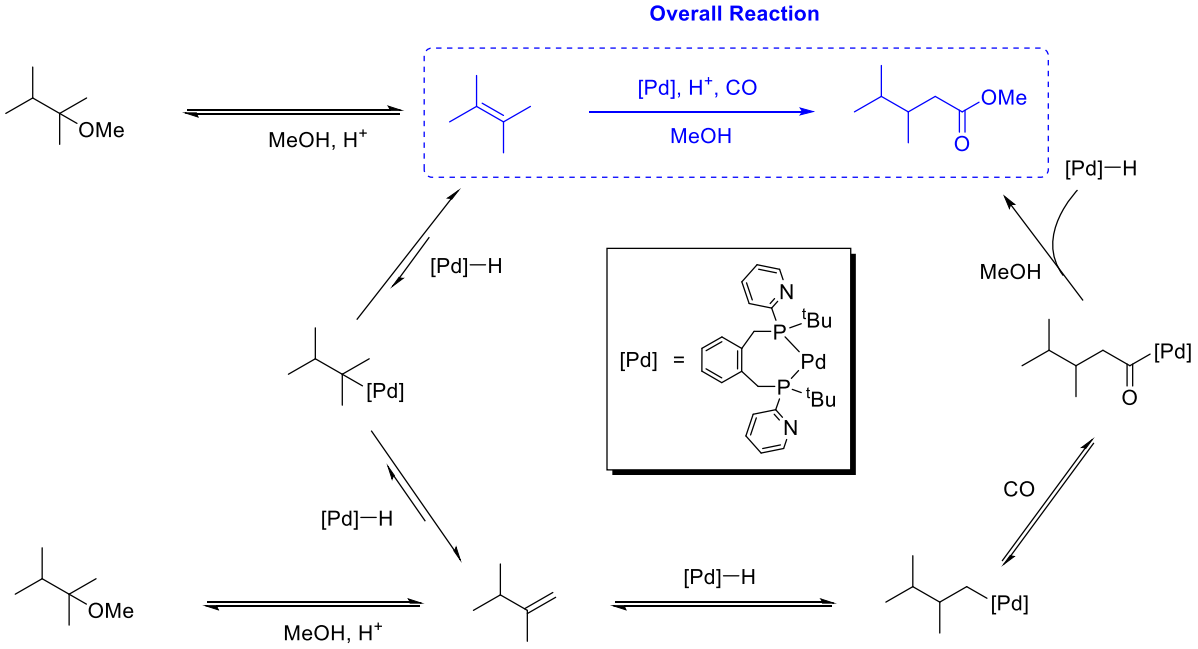

Figure 1.24 Palladium-catalysed isomerisation-methoxycarbonylation of tetramethylethylene.[150]

Following the hydride mechanism, coordination and migratory insertion of tetramethylethylene into Pd-H gives the corresponding Pd-alkyl complex that then must first undergo β-hydride elimination in order to give the terminal olefin required to form terminal esters. This terminal olefin can then re-insert into Pd-H to give a terminal Pd-alkyl complex that is transformed to a Pd-acyl intermediate via migratory insertion of CO. Finally, nucleophilic attack of methanol on the Pd-acyl complex yields the desired terminal ester and regenerates the Pd-H species (**Figure 1.24**). For DTBPX modified palladium complexes however, no carbonylated products are observed. Instead, only the acid-promoted electrophilic addition of methanol to form methoxy ethers in 50% yield occurs.[150] Given the inactivity of Pd-DTBPX for alkoxycarbonylation of hindered tetra-substituted olefins and the catalytic cycle proposed in **Figure 1.24**, two key problems can be identified:

(1) Difficult formation of tertiary Pd-alkyl intermediates required for the isomerisation of tetra-substituted olefins to terminal olefins necessary for terminal ester formation.
(2) Need to shift the equilibrium from methyl ethers to terminal ester products.

The mixed *tert*-butyl/pyridine ligands overcome these issues by accelerating the alcoholysis of the terminal Pd-acyl species. Given that alcoholysis the only irreversible step in the catalytic cycle (**Figure 1.24**),[150] facilitating alcoholysis of the terminal Pd-acyl intermediate biases the equilibrium to favour formation of the terminal ester product. Indeed, palladium complexes modified with the mixed *tert*-butyl/2-pyridyl analogue of DTBPX give excellent terminal ester yields (98%) in the methoxycarbonylation of tetramethylethylene.[150] Tertiary methoxy ethers can also undergo acid-promoted elimination of methanol to give a suitable olefin substrate (**Figure 1.24**), enabling ethers such as methyl *tert*-butyl ether (MTBE) to be used in the production of methyl 3-methylbutanoate via palladium catalysed methoxycarbonylation through an olefin intermediate.[152]

Nobbs et al. described another variation on DTBPX (**Figure 1.25**) that formally connects two methyl groups located on adjacent *tert*-butyl substituents with a carbonyl bridge to form a 6-membereded phosphorinone ring (BPX, **Figure 1.25**).[153]

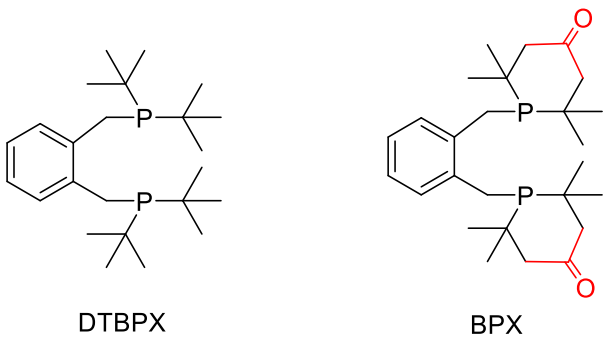

DTBPX BPX

Figure 1.25 Structures of DTBPX and BPX.

Palladium complexes modified with ring-closed BPX (**Figure 1.25**), matched or surpassed the activity and selectivity of DTBPX when applied in palladium catalysed isomerising methoxycarbonylation of a broad range of terminal, internal, branched and functionalised olefins.[153] BPX exhibits poorer σ-donor properties than DTBPX, and shows a *v*(CO) of 1956.8 cm^{-1} versus the 1948.3 cm^{-1} found in DTBPX for their respective [(Ligand)Rh(CO)Cl] complexes. The reduced ability of BPX to donate electron density to the rhodium centre results in less π-back donation from rhodium to the π* CO anti-bonding orbital, resulting in a stronger CO bond and hence a higher wavenumber observed for the CO stretch. Competitive protonation experiments between DTBPX and BPX in the presence of CH_3SO_3H yielded only $[DTBPX(H)_2]^{2+}$, corroborating that BPX is indeed a weaker base than DTBPX. The improvement in alkoxycarbonylation activity observed from palladium complexes modified with BPX instead of DTBPX has been attributed to BPX's poorer σ-donor properties, resulting in a more electrophilic palladium centre that facilitates the rate-determining methanolysis step of the catalytic cycle.

1.3.4 Tandem Isomerisation-Alkoxycarbonylation of Functionalised Olefins

Tandem isomerisation-alkoxycarbonylation of functionalised olefins to produce α,ω-functionalised compounds has been garnering interest due to its utility in transforming renewable resources such as plant oils into polymeric products.[154] Fatty acids from plant oils are attractive monomers for polymerisation due to their long-chain methylene sequences that enable polymer crystallisation and render them hydrophobic.[155-156] For example, the transformation of fatty acids found in sunflower oil to polyesters (**Figure 1.26**).

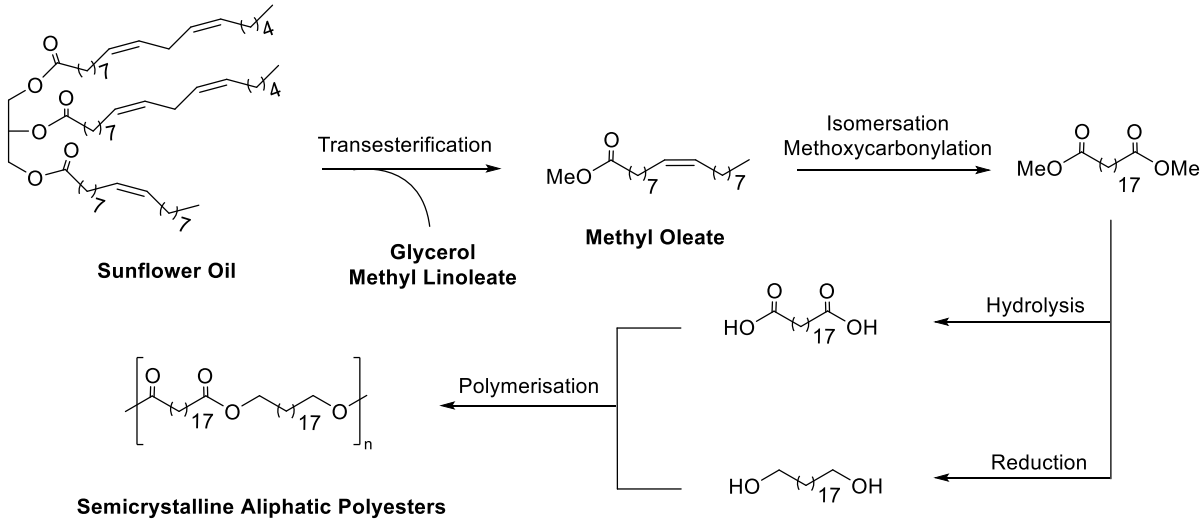

Figure 1.26 Transformation of triglycerides to polyesters.

One of the primary components of sunflower oil is a triglyceride formed from glycerol and several different fatty acids, about a third of which are mono-unsaturated omega-9 C_{18}-oleic acid. Transesterification of the triglyceride with methanol releases methyl oleate, that can then be transformed to a 1,19-diester via tandem isomerisation-methoxycarbonylation of the internal double bond. The 1,19-diester can either be hydrolysed to a dicarboxylic acid or reduced to a diol, and the two then polymerised together to produce polyesters (**Figure 1.26**). These types of long-chain aliphatic polyesters possess melting points and crystallization temperatures suitable for thermoplastic processing.[157-158]

The Pd-DTBPX system described by Cole-Hamilton and co-workers[140] has been applied to tandem isomerisation-alkoxycarbonylation of simple internal olefins,[140] unsaturated esters and unsaturated carboxylic acids.[141] Pd-DTBPX has also been employed for the direct conversion of triglycerides to α,ω-diesters via a metathesis-isomerisation-methoxycarbonylation-transesterification reaction sequence.[159] Pd-DTBPX demonstrates excellent selectivity (90.6%)[160] for the linear 1,19-diester when performing tandem isomerisation-methoxycarbonylation of methyl oleate and was patented by BASF in 2011 for the production of polymers from renewable resources.[161] The remarkable selectivity of Pd-

DTBPX for linear α,ω-diester products has been traced to the nature of DTBPX as a chelating diphosphine that prefers linear insertion products and exhibits a relatively slower methanolysis of branched Pd-acyl intermediates.[162] Comprehensive studies on the mechanistic features of palladium-catalysed tandem isomerisation-methoxycarbonylation have been reported by Mecking and co-workers.[162-163] Cationic palladium complexes modified with BPX (**Figure 1.25**) have also been patented by the Agency for Science, Technology and Research (A*STAR) in 2017 for similar applications such as the tandem isomerisation-methoxycarbonylation of methyl 2-pentenoate to dimethyl adipate, a precursor to a 6,6-nylon monomer (adipic acid). BPX was reported to exhibit similar linear selectivity (97%) as DTBPX but at 1.5 times the rate.[164]

In summary, palladium catalysed olefin alkoxycarbonylation has seen major progress due to ligand development and advances in mechanistic understanding that have led to the establishment of several industrial processes. There has been striking differences in catalytic performance arising from seemingly simple modifications to ligand backbone or phosphorus substituents. Significant improvements arising from subtle structural changes indicate the importance of systematic ligand variation in probing structure-activity relationships for unexpected and unprecedented properties.

1.4 CO Surrogates

Carbon monoxide (CO) is a toxic gas that has been known to poison about 50,000 people annually in the United States alone.[165] The effects of CO poisoning range from headaches and dizziness to coma and death. In addition to its toxicity, CO is also a colourless, odourless and flammable gas. The difficulty in handling, storing and transporting toxic CO represents a major health concern for those involved in its use, especially when working with it on large-scale industrial carbonylation processes.[23] To address this, much effort has been directed toward developing alternative carbonylation methodologies.[166-168] This section will briefly cover a selection of CO surrogates and their associated olefin carbonylation methodologies before focusing on carbon dioxide (CO_2) as a CO surrogate, especially on its use via the ruthenium catalysed reverse Water-Gas Shift (rWGS) reaction.

1.4.1 Formaldehyde

A common strategy to circumvent the use of CO is through its substitution with a precursor that can produce CO in situ under reaction conditions. The simplest aldehyde, formaldehyde, can operate as a CO surrogate this way through formation of a metal-formyl complex that decarbonylates to give syngas (CO/H_2). However, this metal-formyl complex may also undergo olefin insertion to yield aldehydes (**Figure 1.27**).[167]

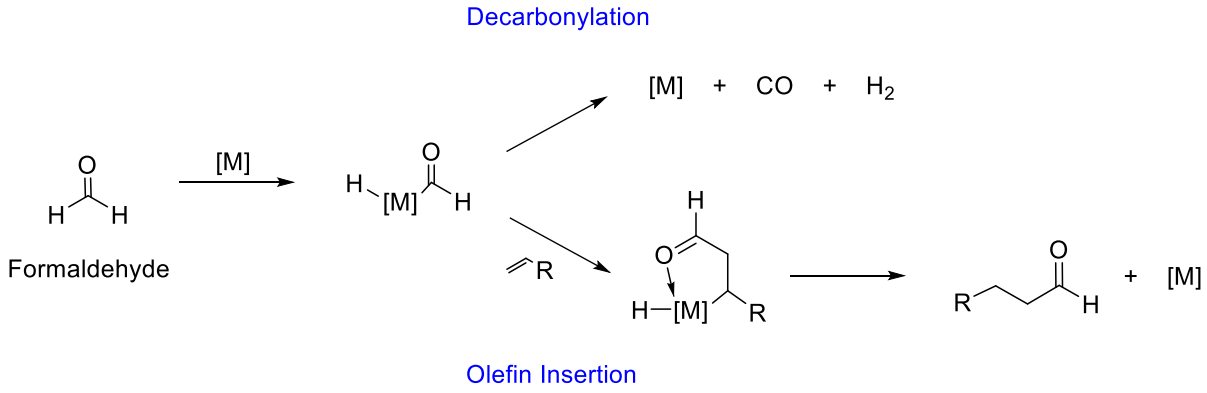

Figure 1.27 Reaction pathways for formaldehyde as a CO surrogate in olefin carbonylation. [M] = transition metal complex.

Formaldehyde can be employed in an aqueous solution, as formalin, or in its polymeric solid form, as paraformaldehyde. There have been reports from as early as 1982 noting the use of paraformaldehyde as a CO surrogate in Rh-catalysed hydroformylation of 1-hexene to give moderate yields of heptanal (67%).[169] Since then, the application of formaldehyde as a CO surrogate has been expanding to include branched selective hydroformylation of allyl alcohols,[170] linear selective hydroformylation of α-olefins,[171] olefin methoxycarbonylation[172] and microwave-assisted hydroformylation of β,γ-unsaturated amides.[173]

1.4.2 Methanol

Methanol is an abundant potential source of CO that has a global production of about 35 million metric tonnes annually.[167] The use of methanol as a CO surrogate is slightly more demanding than formaldehyde, requiring the removal of an additional molecule of H_2 (**Figure 1.28**).

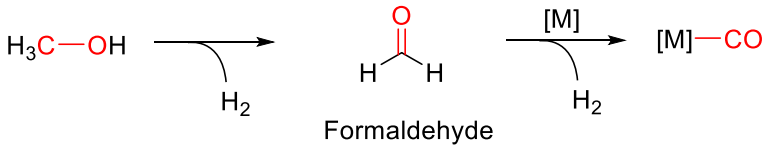

Figure 1.28 Decarbonylation of methanol. [M] = transition metal complex.

The presence of methanol and an additional equivalent of H_2 enable methanolysis or hydrogenation that consequently allow methanol surrogates to give a more diverse range of products. In 1986, Keim and co-workers reported the use of methanol both as a CO and an alcohol source for the methoxycarbonylation of short chain (C_2 – C_5) olefins.[174] Methanol has also been used in conjunction with paraformaldehyde as a CO surrogate for linear selective methoxycarbonylation of olefins.[172]

1.4.3 Formic Acid

Formic acid is most commonly derived from hydrolysis of methyl formate or as a by-product from the catalytic carbonylation of methanol. It had a global capacity of about 720,000 metric tonnes in 2013.[175] Formic acid has been noted to decompose to CO and H_2O at elevated temperatures and under acidic conditions.[176] It has been regarded as an attractive CO surrogate option due to its liquid nature and low toxicity[177] that simplifies transportation, storage and handling processes. Formic acid has been used as CO surrogate in olefin hydroxycarbonylation,[178] linear selective tandem hydroformylation-reduction of olefins[179] and linear selective alkoxycarbonylation of hindered olefins.[180]

1.4.4 Formates

Formates serve as CO surrogates for olefin carbonylation via a mechanism analogous to that for formaldehyde. Taking the simplest formate, methyl formate, as an example, there is first an oxidative addition of the formyl group to a metal centre[181] before diverging to two pathways, decomposition to CO and methanol or olefin insertion (**Figure 1.29**).[182]

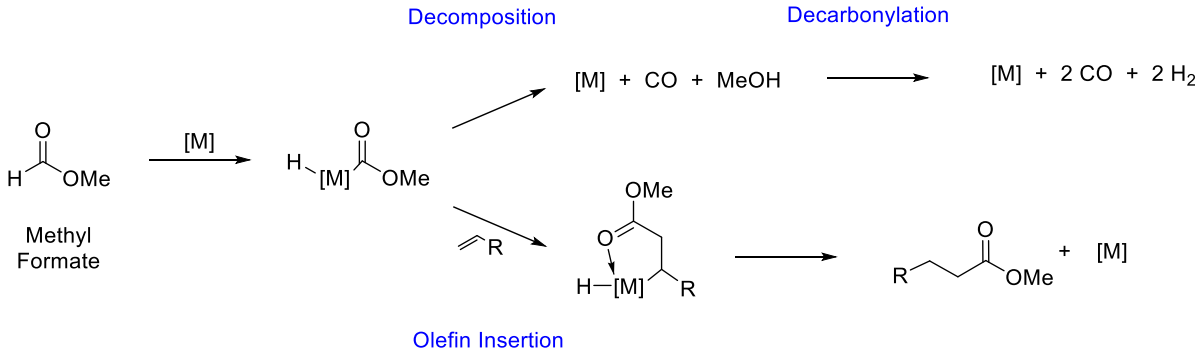

Figure 1.29 Reaction pathways for methyl formate as a CO surrogate in olefin carbonylation. [M] = transition metal complex.

CO and methanol generated via decomposition of the acyl complex can subsequently undergo methanol decarbonylation (**Figure 1.28**) to eventually give two equivalents of CO and H_2 per equivalent of methyl formate. In this respect, methyl formate has been reported as a source of syngas (CO/H_2) in the tandem hydroformylation-reduction of cycloalkenes to alcohols.[183] Aside from methyl formate, many other formates[184-185] including simple *n*-alkyl formates[186] and phenyl formate[187] have also been employed as CO surrogates in olefin alkoxycarbonylation.

1.4.5 Carbon Dioxide (CO_2)

Amongst the many CO surrogate options, CO_2 has arguably drawn the most interest.[188-192] The widespread use of fossil fuels across many fields of human activity have resulted in exponentially increasing anthropogenic CO_2 emissions over the past century.[193] The gradual accumulation of CO_2 has

recently reached critical levels, surpassing 400 ppm in March 2015.[194] Exceedingly high concentrations of CO_2 has led to a string of negative consequences for the ecosystem, such as global warming, rising sea levels and ocean acidification.[193] In order to mitigate the high concentration of atmospheric CO_2, much effort has been devoted to the development of technologies for the efficient capture, storage and utilisation of CO_2.[195-196] CO_2 can be used as a C_1 feedstock in the production of value-added products,[197-199] and a number of strategies have emerged that employ CO_2 as a CO surrogate in olefin carbonylation catalysis. Some examples include Ru-mediated transfer hydrogenation,[200-201] hydrosilylation,[202-204] electroreduction[205] and the reverse Water-Gas Shift (rWGS) reaction.[206-208]

In 1914, Bosch and Wild first observed the rWGS reaction (**Equation 1.3**) while attempting to produce H_2 from steam and CO over an iron oxide catalyst.[209]

Equation 1.3 The reverse Water-Gas Shift reaction.

$$CO_2 + H_2 \rightleftharpoons CO + H_2O \qquad \Delta H^0_{298K} = +42.1 \text{ kJ mol}^{-1}$$

Due to the endothermic nature of the forward reaction, high temperatures are required to shift the equilibrium in favour of CO production.[210-211] Indeed, when starting from a stoichiometric composition of CO_2/H_2, temperatures of more than 700 °C are required to achieve just 50% conversion to CO/H_2O.[212] In this respect, thermally robust heterogeneous catalysts that promote the rWGS reaction have been widely investigated, and a comprehensive review of over 100 different metal-based heterogeneous catalysts immobilised on metal oxide supports (such as ZnO, TiO_2, SiO_2 or Al_2O_3) has recently been given by Kattel et al.[213] One downside of these catalysts however, is the elevated temperatures (450 – 600 °C) required that complicate the coupling of these methodologies for subsequent carbonylation chemistry with the CO produced.[191] Homogeneous catalysts with ancillary ligands are also often unstable at high temperatures, resulting in ligand dissociation and catalyst decomposition.

In 2000 however, Tominaga and Sasaki were able to couple CO produced in situ from a homogeneous ruthenium catalysed rWGS reaction to the ruthenium catalysed tandem hydroformylation-reduction of olefins at 140 °C.[208] The addition of LiCl salt proved critical for the activation of ruthenium cluster complexes to facilitate rWGS of CO_2 to CO and enabled the reaction to be run at milder temperatures.[208] A survey of different salt additives by Tominaga and Sasaki revealed a trend of decreasing activity down the group for both the alkali metal cation (Li > Na > K) and halide anion (Cl > Br > I).[214] They proposed that increasing cation size decreases activity due to the poorer solubility of the salt while increasing halide size decreases activity due to weaker basic properties that are less able

to perform the key step in the catalytic cycle involving deprotonation of the ruthenium hydride complex (**Figure 1.30**).[214]

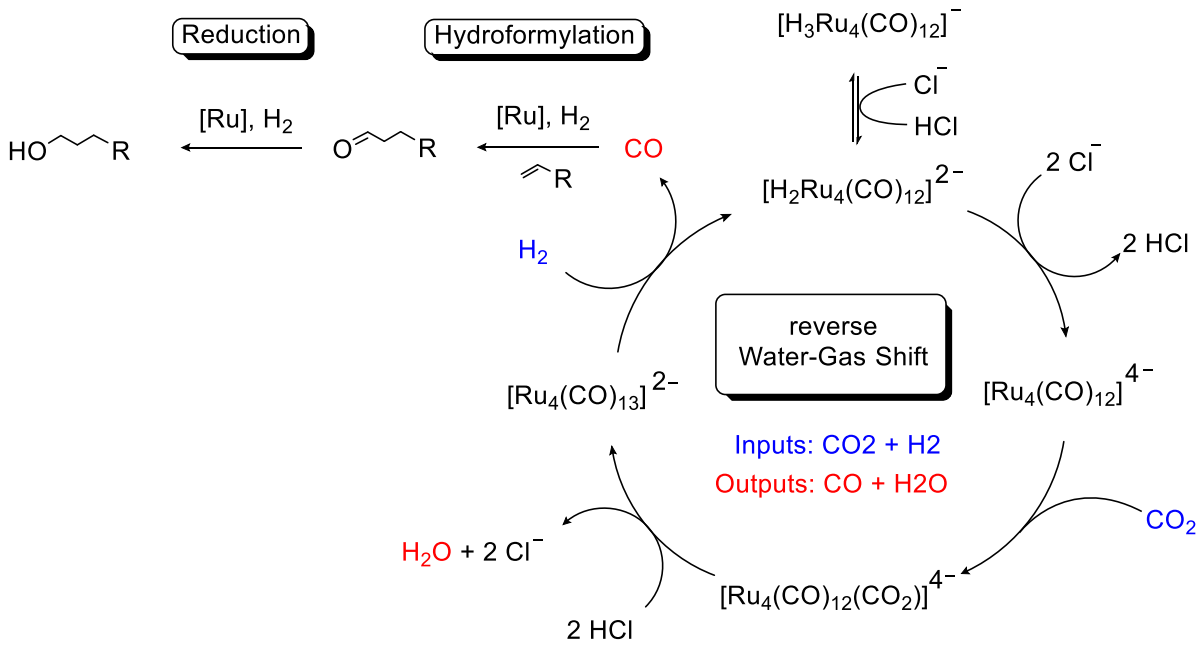

Figure 1.30 Proposed mechanism of ruthenium-catalysed reverse Water-Gas Shift (rWGS) reaction coupled to tandem hydroformylation-reduction of olefins.[214] [Ru] = ruthenium cluster complex.

Further investigation into the reaction mechanism via electrospray-ionisation (ESI) mass spectrometry of the reaction mixture revealed the presence of $[H_3Ru_4(CO)_{12}]^-$.[214] $[H_3Ru_4(CO)_{12}]^-$ can be generated from $Ru_3(CO)_{12}$ (the ruthenium precatalyst) under reaction conditions via the following equilibria (**Equation 1.4**).[215-216]

Equation 1.4 Equilibria generating $[H_3Ru_4(CO)_{12}]^-$ from $Ru_3(CO)_{12}$.[215-216]

$$\frac{7}{3}\ Ru_3(CO)_{12} + 3\ Cl^- + H_2 \rightleftharpoons 2\ [HRu_3(CO)_{11}]^- + [RuCl_3(CO)_3]^- + 3\ CO$$

$$3\ [HRu_3(CO)_{11}]^- + Ru_3(CO)_{12} + 3\ H_2 \rightleftharpoons 3\ [H_3Ru_4(CO)_{12}]^- + 9\ CO$$

Three equivalents of halide anion from the salt additive acts as a base to deprotonate $[H_3Ru_4(CO)_{12}]^-$ to yield the key tetranuclear anionic species, $[Ru_4(CO)_{12}]^{4-}$, that is known to coordinate CO_2.[217] Subsequent coordination of CO_2 and electrophilic attack of two equivalents of HCl converts CO_2 to CO before H_2 displaces CO to close the cycle and return the $[H_2Ru_4(CO)_{12}]^{2-}$ complex.[214] The released CO can then be used for ruthenium catalysed tandem hydroformylation-reduction of olefins in situ.[74]

In 2014, Beller and co-workers extended this work by developing phosphite ligands (**Figure 1.31**) with the aim of suppressing olefin hydrogenation and improving reaction efficiency while operating under milder conditions and at lower catalyst loadings.[218]

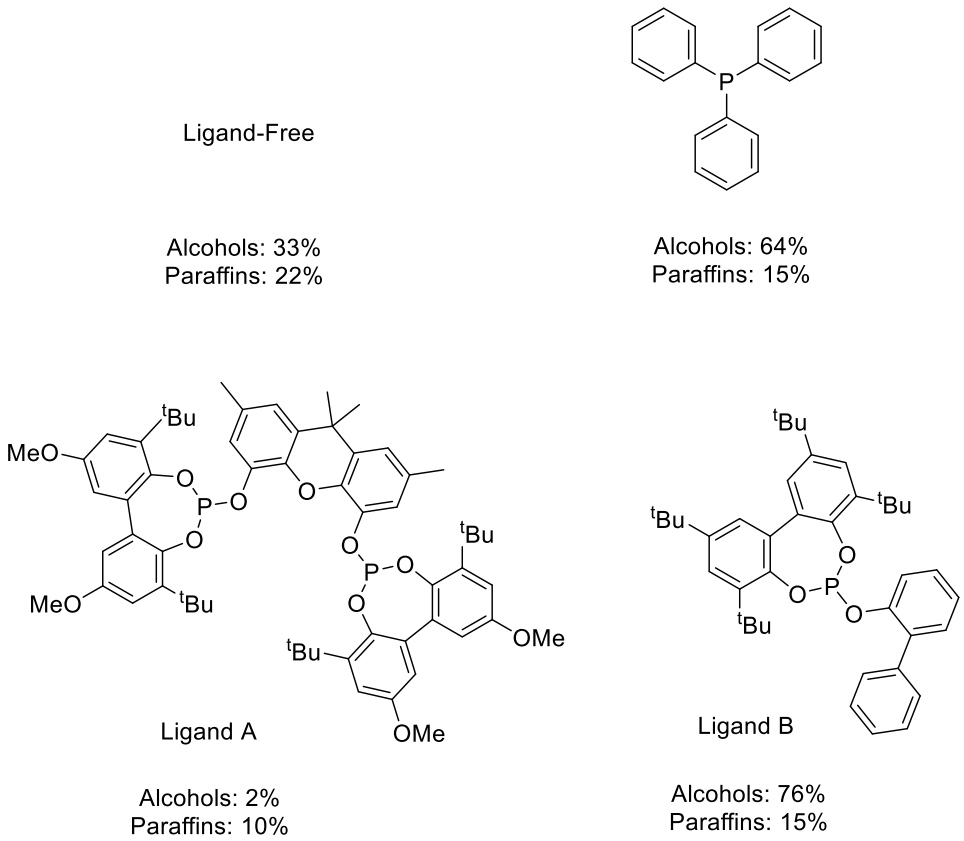

Figure 1.31 Phosphite ligands and product yields from ruthenium catalysed tandem hydroformylation-reduction of 1-octene using CO_2 as a CO surrogate.[218]

The phosphite ligands were evaluated for ruthenium catalysed tandem hydroformylation-reduction of 1-octene using CO_2/H_2 and compared against the ligand-free system (**Figure 1.31**). Bulky chelating bisphosphites favoured for rhodium hydroformylation systems such as the Xantphos-like[219] Ligand A were found to be nearly inactive, yielding mostly paraffins. Simple PPh_3 however, showed a minor improvement in alcohol yield and a slight decrease in paraffin yield over the ligand-free system, albeit with the formation of unidentified high-boiling side products. The use of monophosphite Ligand B though, gave both desirable outcomes of improved alcohol yield as well as suppressed hydrogenation to low-value paraffins with good mole balance (95%).

In order to investigate the impact of Ligand B on the reaction mechanism, the following steps were studied individually by Beller and co-workers:[218]

(1) Reverse Water-Gas Shift (rWGS) reaction
(2) Hydroformylation
(3) Aldehyde reduction

Ligand B (**Figure 1.31**) was found to have no impact on the rWGS reaction but LiCl was essential, corroborating the findings of Tominaga and Sasaki.[214] Under low CO pressure (5 bar) that mimicked

the low concentration of CO under rWGS conditions, Ligand B was found to have significant influence on the hydroformylation step, producing predominantly alcohols while the ligand-free system mainly gave paraffins. This suggests that it is at this step that Ligand B has its primary impact, facilitating olefin carbonylation to favour oxo products over paraffins. Interestingly, LiCl was found to facilitate the aldehyde reduction step, and in its absence most of the starting aldehyde remained unconverted. The effects of LiCl on aldehyde reduction may be related to Drent's proposal of anion-assisted electrophilic activation of H_2 to facilitate the generation of metal hydrides performing the hydrogenation (**Figure 1.16**).[88]

The ruthenium-based rWGS system pioneered by Tominaga and Sasaki[207] has since been studied extensively[220-227] and been employed for various applications, including the production of cyclic carbonates from epoxides,[228-229] olefin hydroaminomethylation[230-231] and methanol homologation.[232] Few of these however, have taken advantage of the influence phosphorus ligands can have on catalyst activity and selectivity like Beller and co-workers have.[218] Ligand σ-donor/π-acceptor properties and steric congestion can have significant impact on catalytic activity,[233] and it would be valuable to explore the potential ligands have to facilitate CO_2 utilisation as a CO surrogate via the homogeneous ruthenium catalysed rWGS reaction for commercially valuable applications such as olefin carbonylation.

1.5 Scope and Objectives

The preceding sections have given a brief introduction on the impact ligands have on catalytic performance in the fields of hydroformylation and alkoxycarbonylation. In reference to these fields, this thesis will focus on three discrete but related areas:

(1) Exploration of the *gem*-dialkyl effect, also known as the Thorpe-Ingold effect[234-235] in bidentate diphosphine ligands (**Figure 1.32**).

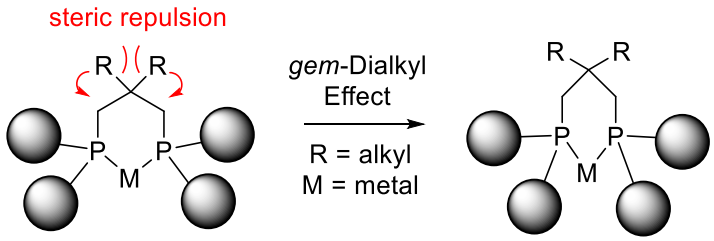

Figure 1.32 The *gem*-dialkyl effect, also known as the Thorpe-Ingold effect,[235] acting on C_3-bridged diphosphine ligands.

The *gem*-dialkyl effect, also known as the "Thorpe-Ingold Effect", was first proposed by Thorpe and Ingold in 1915.[234] They postulated that mutual repulsion between two geminally substituted alkyl

groups on an open carbon chain altered bond angles, promoted cyclisation and stabilised small ring structures.[235] The Thorpe-Ingold effect[235] is a well-established phenomenon in organic synthesis that accelerates cyclisation reactions, but is less well known for organometallic applications.[236-237] The *gem*-dialkyl effect can be tuned by varying the steric bulk of the geminal alkyl groups, allowing for systematic variation of ligand structure to probe structure-activity relationships.

One of the objectives of this thesis is to study the impact of the *gem*-dialkyl effect on bidentate diphosphine ligands in terms of its ligand properties, transition metal coordination behaviour and catalytic performance in palladium catalysed hydroformylation and alkoxycarbonylation of olefins. Compared to the wealth of literature published on cobalt and rhodium hydroformylation systems, palladium still stands to benefit from further study on its use as a hydroformylation catalyst. This investigation into the *gem*-dialkyl effect on ligands may also serve as a basis for future work on its application to ligands for other catalytic processes.

(2) Backbone modification of diphobane ligands (**Figure 1.33**).

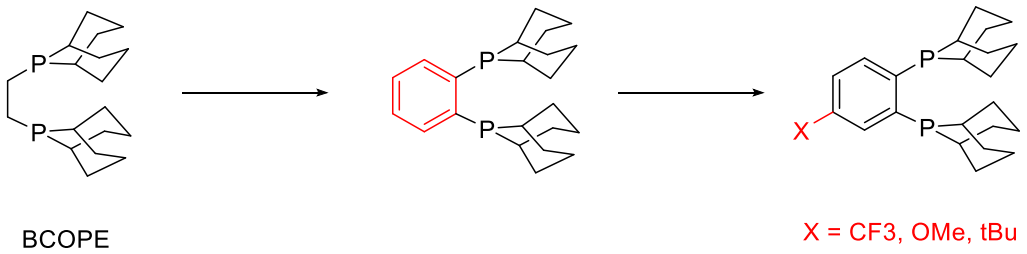

Figure 1.33 Backbone modification of diphobane ligands.

The unique characteristics of the phobane moiety in BCOPE (**Figure 1.33**) result in a highly active and selective palladium-based hydroformylation catalyst.[88] The striking differences in catalytic performance observed from backbone modification of bidentate ligands for palladium-based alkoxycarbonylation catalysts suggest that applying similar variation to the unique diphobane scaffold may result in unprecedented activities and selectivities.

One of the objectives of this thesis is to study the effect of backbone modification on diphobane ligands in palladium catalysed olefin carbonylation. In this respect, the scope for backbone modification is limited to two areas. Firstly, comparison of the performance of phenylene-bridged diphobane against C_2-bridged BCOPE (**Figure 1.33**) in palladium catalysed olefin hydroformylation. Secondly and finally, substitution of phenylene-bridged diphobane with various groups (**Figure 1.33**) and comparison of their catalytic performance in palladium catalysed olefin carbonylation.

(3) Investigation into ligands that facilitate the production of oxo products from olefins using CO_2 as a CO surrogate via the ruthenium catalysed reverse Water-Gas Shift (rWGS) reaction.

The ruthenium cluster catalyst pioneered by Tominaga and Sasaki has shown much promise in utilising CO_2 as a CO surrogate to convert olefins to alcohols in a single pot.[207] Despite the large amount of research interest it has attracted,[220-227] there have been few reports on the use of ligands to optimise the process.[218] The third and final objective of this thesis is to build upon existing knowledge by investigating alternative ligand structures that can be applied in conjunction with the known ruthenium cluster catalyst to use CO_2 as a CO surrogate in tandem rWGS-carbonylation catalysis.

1.6 Chapter 1 References

1. Bertleff, W.; Roeper, M.; Sava, X., Carbonylation. In *Ullmann's Encyclopedia of Industrial Chemistry*, Elvers, B., Ed. Wiley-VCH Verlag GmbH & Co. KGaA: 2007; Vol. 7, p 75.
2. Pospech, J.; Fleischer, I.; Franke, R.; Buchholz, S.; Beller, M., *Angew. Chem. Int. Ed.* **2013,** *52*, 2852-2872.
3. Asaro, M. *On-Purpose Acetic Acid*; IHS Chemical: 2016; pp 12-313.
4. Tremblay, J.-F., *C&EN* **2009,** *87*, 22-23.
5. Sell, C. S., Ingredients for the Modern Perfumery Industry. In *The Chemistry of Fragrances: From Perfumer to Consumer*, Sell, C. S., Ed. Royal Society of Chemistry: 2006; Vol. 38, pp 52-131.
6. Berre, C. L.; Serp, P.; Kalck, P.; Torrence, G. P., Acetic Acid. In *Ullmann's Encyclopedia of Industrial Chemistry*, Elvers, B., Ed. Wiley-VCH Verlag GmbH & Co. KGaA: 2014; pp 4-12.
7. Riemenscheider, W.; Bolt, H. M., Esters, Organic. In *Ullmann's Encyclopedia of Industrial Chemistry*, Elvers, B., Ed. Wiley-VCH Verlag GmbH & Co. KGaA: 2012; pp 252-259.
8. Neumann, B.; Schneider, H., *Angew. Chem.* **1920,** *33*, 189-192.
9. Eby, R. T.; Singleton, T. C., *Applied Industrial Catalysts*. 1st ed.; Academic Press: 1983; p 316.
10. Roth, J. F., *Platinum Met. Rev.* **1975,** *19*, 12-14.
11. Paulik, F. E.; Roth, J. F., *Chem. Commun. (London)* **1968**, 1578a-1578a.
12. Lancaster, M., *Green Chemistry : An Introductory Text*. 2nd ed.; Royal Society of Chemistry: Cambridge, 2002.
13. Sunley, G. J.; Watson, D. J., *Catal. Today* **2000,** *58*, 293-307.
14. Dekleva, T. W.; Forster, D., Mechanistic Aspects of Transition-Metal-Catalyzed Alcohol Carbonylations. In *Advances in Catalysis*, Eley, D. D.; Pines, H.; Weisz, P. B., Eds. Academic Press: 1986; Vol. 34, pp 81-130.
15. Maitlis, P. M.; Haynes, A.; Sunley, G. J.; Howard, M. J., *J. Chem. Soc., Dalton Trans.* **1996**, 2187-2196.
16. Jones, J. H., *Platinum Met. Rev.* **2000,** *44*, 94-105.

17. Dawes, J. L.; Devon, T. J. Eastman Kodak Company, Hydroformylation Process Utilizing an Unmodified Rhodium Catalyst and the Stabilization and Regeneration Thereof. US4400547A, 1983.

18. Garland, C. S.; Giles, M. F.; Sunley, J. G. BP Chemicals Limited, Process for the Production of Acetic Acid. US5672743A, 1994.

19. Dingwall, L. D.; Lee, A. F.; Lynam, J. M.; Wilson, K.; Olivi, L.; Deeley, J. M. S.; Gaemers, S.; Sunley, G. J., *ACS Catal.* **2012,** *2*, 1368-1376.

20. Ren, Z.; Lyu, Y.; Song, X.; Liu, Y.; Jiang, Z.; Lin, R.; Ding, Y., *Adv. Mater.* **2019,** *31*, 1904976.

21. Cornils, B.; Herrmann, W. A.; Rasch, M., *Angew. Chem. Int. Ed. Engl.* **1994,** *33*, 2144-2163.

22. Roelen, O. Otto Roelen, Production of Oxygenated Carbon Compounds. US2327066A, 1943.

23. Franke, R.; Selent, D.; Börner, A., *Chem. Rev.* **2012,** *112*, 5675-5732.

24. Dave, D. *Oxo Alcohols*; IHS Chemical: 2016; pp 14-353.

25. Heck, R. F.; Breslow, D. S., *J. Am. Chem. Soc.* **1961,** *83*, 4023-4027.

26. Ungváry, F., *J. Organomet. Chem.* **1972,** *36*, 363-370.

27. Tudor, R.; Shah, A., *Johnson Matthey Technol. Rev.* **2017,** *61*, 246-256.

28. Cornils, B.; Börner, A.; Franke, R.; Zhang, B.; Wiebus, E.; Schmid, K., *Applied Homogeneous Catalysis with Organometallic Compounds*. 3rd ed.; Wiley-VCH Verlag GmbH & Co. KGaA: Weinheim, Germany, 2017.

29. Tucci, E. R., *Ind. Eng. Chem. Prod. Res. Dev.* **1968,** *7*, 125-128.

30. Tucci, E. R., *Ind. Eng. Chem. Prod. Res. Dev.* **1968,** *7*, 32-38.

31. Tucci, E. R., *Ind. Eng. Chem. Prod. Res. Dev.* **1970,** *9*, 516-521.

32. Drent, E.; Van Ginkel, R.; Jager, W. W. Shell Internationale Research Maatschappij B.V., Process for Producing Olefins. WO2008034894 A1, 2008.

33. Börner, A.; Franke, R., *Hydroformylation: Fundamentals, Processes, and Applications in Organic Synthesis*. 1st ed.; Wiley-VCH Verlag GmbH & Co. KGaA: Weinheim, Germany, 2016; Vol. 1, p 283.

34. Smith, F. J., *Platinum Met. Rev.* **1975,** *19*, 93-95.

35. Mason, R. F.; Valley, M.; Van Winkle, J. L. Shell Oil Company, Oxo Alcohols using Catalysts Comprising Ditertiary Phosphines. US3527818, 1970.

36. Winkle, J. L. V.; Morris, R. C.; Mason, R. F. Shell Oil Company, Single Stage Hydroformylation of Olefins to Alcohols. US3420898A, 1969.

37. Hebrard, F.; Kalck, P., *Chem. Rev.* **2009,** *109*, 4272-4282.

38. Geoffrey, W., *Science* **1974,** *185*, 109-112.

39. Siegel, H.; Himmele, W., *Angew. Chem. Int. Ed. Engl.* **1980,** *19*, 178-183.

40. Russell, M. J. H., *Platinum Met. Rev.* **1988,** *32*, 179-186.

41. Beller, M.; Cornils, B.; Frohning, C. D.; Kohlpaintner, C. W., *J. Mol. Catal. A: Chem.* **1995,** *104*, 17-85.

42. Hood, D. M.; Johnson, R. A.; Carpenter, A. E.; Younker, J. M.; Vinyard, D. J.; Stanley, G. G., *Science* **2020,** *367*, 542-548.

43. Torres, G. M.; Frauenlob, R.; Franke, R.; Borner, A., *Catal. Sci. Technol.* **2015,** *5*, 34-54.

44. D. E, W., *Platinum Met. Rev.* **1968,** *12*, 135-135.

45. Kuntz, E. G. Rhone-Poulenc Industries, Aldehyde Preparation by Olefin Hydroformylation in Liquid Phase - Using Catalyst System Containing Sulphonated Aryl Phosphine and Rhodium FR2314910A1, 1975.

46. van Leeuwen, P. W. N. M.; Roobeek, C. F., *J. Organomet. Chem.* **1983,** *258*, 343-350.

47. Billig, E.; Abatjoglou, A. G.; Bryant, D. R. Union Carbide Corp, Transition Metal Complex Catalyzed Processes. US4668651A, 1987.

48. Nozaki, K.; Sakai, N.; Nanno, T.; Higashijima, T.; Mano, S.; Horiuchi, T.; Takaya, H., *J. Am. Chem. Soc.* **1997,** *119*, 4413-4423.

49. Ichihara, T.; Nakano, K.; Katayama, M.; Nozaki, K., *Chem. - Asian J.* **2008,** *3*, 1722-1728.

50. Noonan, G. M.; Fuentes, J. A.; Cobley, C. J.; Clarke, M. L., *Angew. Chem. Int. Ed.* **2012,** *51*, 2477-2480.

51. Barnard, C. F. J., *Platinum Met. Rev.* **1990,** *34*, 207-214.

52. Gerrard, W.; Hudson, H. R., *Organic Phosphorus Compounds*. Wiley-Interscience: New York, 1973; Vol. 5.

53. Jongsma, T.; Challa, G.; van Leeuwen, P. W. N. M., *J. Organomet. Chem.* **1991,** *421*, 121-128.

54. Van Leeuwen, P. W. N.; Roobeek, C. F. Shell Internationale Research Maatschappij B.V., A Process for the Hydroformylation of Olefins. EP0054986A1, 1981.

55. Abatjoglou, A. G.; Robert, B. D.; Michael, M. J. Union Carbide Chem Plastic, Stabilization of Phosphite Ligands in Hydroformylation Process. EP0697391B1, 1995.

56. Cornils, B.; Kuntz, E. G., *J. Organomet. Chem.* **1995,** *502*, 177-186.

57. Wiese, K.-D.; Obst, D., Hydroformylation. In *Catalytic Carbonylation Reactions*, Beller, M., Ed. Springer Berlin Heidelberg: Berlin, Heidelberg, 2006; pp 1-33.

58. Cuny, G. D.; Buchwald, S. L., *J. Am. Chem. Soc.* **1993,** *115*, 2066-2068.

59. Tudor, R.; Ashley, M., *Platinum Met. Rev.* **2007,** *51*, 164-171.

60. Vogl, C.; Paetzold, E.; Fischer, C.; Kragl, U., *J. Mol. Catal. A: Chem.* **2005,** *232*, 41-44.

61. Behr, A.; Obst, D.; Schulte, C.; Schosser, T., *J. Mol. Catal. A: Chem.* **2003,** *206*, 179-184.

62. Le Goanvic, L.; Ternel, J.; Couturier, J.-L.; Dubois, J.-L.; Carpentier, J.-F., *Catalysts* **2018,** *8*, 21.

63. Devon, T. J.; Phillips, G. W.; Puckette, T. A.; Stavinoha, J. L.; Vanderbilt, J. J. Eastman Kodak Company, Chelate Ligands for Low Pressure Hydroformylation Catalyst and Process Employing Same. US4694109A, 1988.

64. Evans, D.; Osborn, J. A.; Jardine, F. H.; Wilkinson, G., *Nature* **1965,** *208*, 1203-1204.

65. Schulz, H. F.; Bellstedt, F., *Ind. Eng. Chem. Prod. Res. Dev.* **1973,** *12*, 176-183.

66. Zhang, Y.; Shinoda, M.; Shiki, Y.; Tsubaki, N., *Fuel* **2006,** *85*, 1194-1200.

67. Hidai, M.; Fukuoka, A.; Koyasu, Y.; Uchida, Y., *J. Mol. Catal.* **1986,** *35*, 29-37.

68. Takahashi, K.; Yamashita, M.; Ichihara, T.; Nakano, K.; Nozaki, K., *Angew. Chem. Int. Ed.* **2010,** *49*, 4488-4490.

69. Takahashi, K.; Yamashita, M.; Nozaki, K., *J. Am. Chem. Soc.* **2012,** *134*, 18746-18757.

70. Takahashi, K.; Yamashita, M.; Tanaka, Y.; Nozaki, K., *Angew. Chem. Int. Ed.* **2012,** *51*, 4383-4387.

71. Sanchez-Delgado, R. A.; Bradley, J. S.; Wilkinson, G., *J. Chem. Soc., Dalton Trans.* **1976**, 399-404.

72. Süss-Fink, G., *J. Organomet. Chem.* **1980,** *193*, C20-C22.

73. Süss-Fink, G.; Herrmann, G., *J. Chem. Soc., Chem. Commun.* **1985**, 735-737.

74. Süss-Fink, G.; Schmidt, G. F., *J. Mol. Catal.* **1987,** *42*, 361-366.

75. Johnson, B. F. G.; Lewis, J.; Raithby, P. R.; Süss, G., *J. Chem. Soc., Dalton Trans.* **1979**, 1356-1361.

76. Fleischer, I.; Wu, L.; Profir, I.; Jackstell, R.; Franke, R.; Beller, M., *Chem. Eur. J.* **2013,** *19*, 10589-10594.

77. Fleischer, I.; Dyballa, K. M.; Jennerjahn, R.; Jackstell, R.; Franke, R.; Spannenberg, A.; Beller, M., *Angew. Chem. Int. Ed.* **2013,** *52*, 2949-2953.

78. Wu, L.; Fleischer, I.; Jackstell, R.; Profir, I.; Franke, R.; Beller, M., *J. Am. Chem. Soc.* **2013,** *135*, 14306-14312.

79. Drent, E.; Mul, W. P.; Budzelaar, P. H. M., *Comments Inorg. Chem.* **2002,** *23*, 127-147.

80. Drent, E. Shell Oil Company, Process for the Preparation of Alcohols. US5214220, 1992.

81. Drent, E.; Pello, D. H. L.; Suykerbuyk, J. C. L. J. Shell Oil Company, Hydroformylation Process. US5488174, 1994.

82. Drent, E. Shell Internationale Research Maatschappij B.V., Process for the Preparation of Aldehydes. EP0220767B1, 1987.

83. Drent, E.; Budzelaar, P. H. M., *J. Organomet. Chem.* **2000,** *593–594*, 211-225.

84. Stewart, R., *The Proton, Applications to Organic Chemistry*. Academic Press: Orlando, 1985.

85. Jennerjahn, R.; Piras, I.; Jackstell, R.; Franke, R.; Wiese, K.-D.; Beller, M., *Chem. Eur. J.* **2009,** *15*, 6383-6388.

86. Dekker, G. P. C. M.; Elsevier, C. J.; Vrieze, K.; van Leeuwen, P. W. N. M.; Roobeek, C. F., *J. Organomet. Chem.* **1992,** *430*, 357-372.

87. Low, C. H.; Nobbs, J. D.; van Meurs, M.; Stubbs, L. P.; Drent, E.; Aitipamula, S.; Pung, M. H. L., *Organometallics* **2015,** *34*, 4281-4292.

88. Konya, D.; Almeida Leñero, K. Q.; Drent, E., *Organometallics* **2006,** *25*, 3166-3174.

89. Carreira, M.; Charernsuk, M.; Eberhard, M.; Fey, N.; Ginkel, R. v.; Hamilton, A.; Mul, W. P.; Orpen, A. G.; Phetmung, H.; Pringle, P. G., *J. Am. Chem. Soc.* **2009,** *131*, 3078-3092.

90. Dodds, D. L.; Floure, J.; Garland, M.; Haddow, M. F.; Leonard, T. R.; McMullin, C. L.; Orpen, A. G.; Pringle, P. G., *Dalton Trans.* **2011,** *40*, 7137-7146.

91. Downing, J. H.; Gee, V.; G. Pringle, P., *Chem. Commun.* **1997**, 1527-1528.

92. Eberhard, M. R. New Strategies In 9-Phosphabicyclononane Chemistry. Ph.D. Thesis, University of Bristol, United Kingdom, 2001.

93. Lister, J. M.; Carreira, M.; Haddow, M. F.; Hamilton, A.; McMullin, C. L.; Orpen, A. G.; Pringle, P. G.; Stennett, T. E., *Organometallics* **2014,** *33*, 702-714.

94. Tolman, C. A., *Chem. Rev.* **1977,** *77*, 313-348.

95. Tolman, C. A., *J. Am. Chem. Soc.* **1970,** *92*, 2956-2965.

96. Marsh, P. S. Synthesis, Characterisation and Precious Metal Chemistry of Symmetrical and Unsymmetrical Diphosphines Based on 9-Phosphabicyclononanes. Ph.D. Thesis, University of Bristol, United Kingdom, 2003.

97. Simone, D. O.; Kennelly, T.; Brungard, N. L.; Farrauto, R. J., *Appl. Catal.* **1991,** *70*, 87-100.

98. Drent, E.; Van Ginkel, R.; Jager, W. W. Shell Oil Company, Process for the Hydroformylation of an Ethylenically Unsaturated Compound. US7414155B2, 2008.

99. Drent, E.; Van Ginkel, R.; Jager, W. W. Shell Internationale Research Maatschappij B.V., Process for the Hydroformylation of an Ethylenically Unsaturated Compound. WO2004028689A2, 2004.

100. Drent, E.; Van Der Steen, H.; Moene, R. Shell Oil Company, Hydroformylation of Olefin Feeds Containing Dienes. US6156936, 2000.

101. Drent, E.; Jager, W. W. Shell Oil Company, Hydroformylation Reactions. US5780684, 1997.

102. Kiss, G., *Chem. Rev.* **2001,** *101*, 3435-3456.

103. Walter, R.; Walter, S.; Herbert, F. BASF SE, Production of Acrylic Acid Esters. US2738364A, 1952.

104. Akio, M., *Bull. Chem. Soc. Jpn.* **1973,** *46*, 524-530.

105. Milstein, D.; Huckaby, J. L., *J. Am. Chem. Soc.* **1982,** *104*, 6150-6152.

106. Hofmann, P. Huels AG, Process for Alkoxycarbonylating Alpha-Olefins Having a Single Branch. US4460510A, 1982.

107. Brennführer, A.; Neumann, H.; Beller, M., *ChemCatChem* **2009,** *1*, 28-41.

108. Kalck, P.; Urrutigoïty, M., *Inorg. Chim. Acta* **2015,** *431*, 110-121.

109. Eastham, G. R.; Cameron, P. A.; Tooze, R. P.; Cavell, K. J.; Edwards, P. G.; Coleman, D. L. Lucite International Uk Limited, A Phospha-Adamantane (S) Catalytic System. WO2004014552A1, 2003.

110. Clegg, W.; Eastham, G. R.; Elsegood, M. R. J.; Heaton, B. T.; Iggo, J. A.; Tooze, R. P.; Whyman, R.; Zacchini, S., *Organometallics* **2002,** *21*, 1832-1840.

111. Liu, J.; Heaton, B. T.; Iggo, J. A.; Whyman, R.; Bickley, J. F.; Steiner, A., *Chem. Eur. J.* **2006,** *12*, 4417-4430.

112. Pugh, R. I.; Drent, E., *Adv. Synth. Catal.* **2002,** *344*, 837-840.

113. Drent, E.; Budzelaar, P. H. M., *Chem. Rev.* **1996,** *96*, 663-682.

114. Mul, W. P.; Drent, E.; Jansens, P. J.; Kramer, A. H.; Sonnemans, M. H. W., *J. Am. Chem. Soc.* **2001,** *123*, 5350-5351.

115. Drent, E.; Van Broekhoven, J. A. M.; Doyle, M. J., *J. Organomet. Chem.* **1991,** *417*, 235-251.

116. Eastham, G. R.; Heaton, B. T.; Iggo, J. A.; Tooze, R. P.; Whyman, R.; Zacchini, S., *Chem. Commun.* **2000**, 609-610.

117. del Río, I.; Claver, C.; van Leeuwen, Piet W. N. M., *Eur. J. Inorg. Chem.* **2001,** *2001*, 2719-2738.

118. Cavinato, G.; Vavasori, A.; Toniolo, L.; Benetollo, F., *Inorg. Chim. Acta* **2003,** *343*, 183-188.

119. Seayad, A.; Jayasree, S.; Damodaran, K.; Toniolo, L.; Chaudhari, R. V., *J. Organomet. Chem.* **2000,** *601*, 100-107.

120. Tsuji, J.; Morikawa, M.; Kiji, J., *Tetrahedron Lett.* **1963,** *4*, 1437-1440.

121. James, D. E.; Hines, L. F.; Stille, J. K., *J. Am. Chem. Soc.* **1976,** *98*, 1806-1809.

122. James, D. E.; Stille, J. K., *J. Am. Chem. Soc.* **1976,** *98*, 1810-1823.

123. Fergusson, S. B.; Alper, H., *J. Chem. Soc., Chem. Commun.* **1984**, 1349-1351.

124. Yun, H. S.; Lee, K. H.; Lee, J. S., *J. Mol. Catal. A: Chem.* **1995,** *95*, 11-17.

125. Cavinato, G.; Toniolo, L., *J. Mol. Catal.* **1981,** *10*, 161-170.

126. Cavinato, G.; Toniolo, L.; Botteghi, C., *J. Mol. Catal.* **1985,** *32*, 211-218.

127. Vieira, T. O.; Green, M. J.; Alper, H., *Org. Lett.* **2006,** *8*, 6143-6145.

128. Keglevich, G.; Kégl, T.; Odinets, I. L.; Vinogradova, N. M.; Kollár, L., *C. R. Chim.* **2004,** *7*, 779-784.

129. Ramminger, C.; Zim, D.; Lando, V. R.; Fassina, V.; Monteiro, A. L., *J. Braz. Chem. Soc.* **2000,** *11*, 105-111.

130. Hiyama, T.; Wakasa, N.; Kusumoto, T., *Synlett* **1991,** *1991*, 569-570.

131. Nozaki, K.; Kantam, M. L.; Horiuchi, T.; Takaya, H., *J. Mol. Catal. A: Chem.* **1997,** *118*, 247-253.

132. Kawashima, Y.; Okano, K.; Nozaki, K.; Hiyama, T., *Bull. Chem. Soc. Jpn.* **2004,** *77*, 347-355.

133. Muñoz, B.; Marinetti, A.; Ruiz, A.; Castillon, S.; Claver, C., *Inorg. Chem. Commun.* **2005,** *8*, 1113-1115.

134. Seayad, A.; Kelkar, A. A.; Toniolo, L.; Chaudhari, R. V., *J. Mol. Catal. A: Chem.* **2000,** *151*, 47-59.

135. de Pater, J. J. M.; Tromp, D. S.; Tooke, D. M.; Spek, A. L.; Deelman, B.-J.; van Koten, G.; Elsevier, C. J., *Organometallics* **2005,** *24*, 6411-6419.

136. Yoshihiro, S.; Ken-ichiro, B., *Chem. Lett.* **1976,** *5*, 727-730.

137. Pugh, R. I.; Drent, E.; Pringle, P. G., *Chem. Commun.* **2001**, 1476-1477.

138. Dunne, B. J.; Morris, R. B.; Orpen, A. G., *J. Chem. Soc., Dalton Trans.* **1991**, 653-661.

139. Clegg, W.; R. J. Elsegood, M.; R. Eastham, G.; P. Tooze, R.; Lan Wang, X.; Whiston, K., *Chem. Commun.* **1999**, 1877-1878.

140. Jimenez Rodriguez, C.; Foster, D. F.; Eastham, G. R.; Cole-Hamilton, D. J., *Chem. Commun.* **2004**, 1720-1721.

141. Jiménez-Rodriguez, C.; Eastham, G. R.; Cole-Hamilton, D. J., *Inorg. Chem. Commun.* **2005,** *8*, 878-881.

142. Pearson, J. M.; Hadden, R. A. Lucite International UK Limited, Process for the Palladium and Phosphine Ligand Catalyzed Carbonylation of Ethylene. US6489506B2, 2001.

143. Fanjul, T.; Eastham, G.; Fey, N.; Hamilton, A.; Orpen, A. G.; Pringle, P. G.; Waugh, M., *Organometallics* **2010,** *29*, 2292-2305.

144. Fanjul, T.; Eastham, G.; Haddow, M. F.; Hamilton, A.; Pringle, P. G.; Orpen, A. G.; Turner, T. P. W.; Waugh, M., *Catal. Sci. Technol.* **2012,** *2*, 937-950.

145. Dong, K.; Sang, R.; Fang, X.; Franke, R.; Spannenberg, A.; Neumann, H.; Jackstell, R.; Beller, M., *Angew. Chem. Int. Ed.* **2017,** *56*, 5267-5271.

146. Bianchini, C.; Meli, A.; Oberhauser, W.; Parisel, S.; Gusev, O. V.; Kal'sin, A. M.; Vologdin, N. V.; Dolgushin, F. M., *J. Mol. Catal. A: Chem.* **2004,** *224*, 35-49.

147. Bianchini, C.; Meli, A.; Oberhauser, W.; Van Leeuwen, P. W. N.; Zuideveld, M. A.; Freixa, Z.; Kamer, P. C. J.; Spek, A. L.; Gusev, O. V.; Kal'sin, A. M., *Organometallics* **2003,** *22*, 2409-2421.

148. Gusev, O. V.; Kalsin, A. M.; Peterleitner, M. G.; Petrovskii, P. V.; Lyssenko, K. A.; Akhmedov, N. G.; Bianchini, C.; Meli, A.; Oberhauser, W., *Organometallics* **2002,** *21*, 3637-3649.

149. Butler, I. R.; Baker, P. K.; Eastham, G. R.; Fortune, K. M.; Horton, P. N.; Hursthouse, M. B., *Inorg. Chem. Commun.* **2004,** *7*, 1049-1052.

150. Dong, K.; Fang, X.; Gülak, S.; Franke, R.; Spannenberg, A.; Neumann, H.; Jackstell, R.; Beller, M., *Nat. Commun.* **2017,** *8*, 14117.

151. Drent, E.; Arnoldy, P.; Budzelaar, P. H. M., *J. Organomet. Chem.* **1993,** *455*, 247-253.

152. Liu, J.; Dong, K.; Franke, R.; Neumann, H.; Jackstell, R.; Beller, M., *Chem. Commun.* **2018**.

153. Nobbs, J. D.; Low, C. H.; Stubbs, L. P.; Wang, C.; Drent, E.; van Meurs, M., *Organometallics* **2017,** *36*, 391-398.

154. Biermann, U.; Bornscheuer, U.; Meier, M. A. R.; Metzger, J. O.; Schäfer, H. J., *Angew. Chem. Int. Ed.* **2011,** *50*, 3854-3871.

155. Chikkali, S.; Mecking, S., *Angew. Chem. Int. Ed.* **2012,** *51*, 5802-5808.

156. Stempfle, F.; Ritter, B. S.; Mülhaupt, R.; Mecking, S., *Green Chem.* **2014,** *16*, 2008-2014.

157. Stempfle, F.; Quinzler, D.; Heckler, I.; Mecking, S., *Macromolecules* **2011,** *44*, 4159-4166.

158. Quinzler, D.; Mecking, S., *Angew. Chem. Int. Ed.* **2010,** *49*, 4306-4308.

159. Zhu, Y.; Patel, J.; Mujcinovic, S.; Jackson, W. R.; Robinson, A. J., *Green Chem.* **2006,** *8*, 746-749.

160. Christl, J. T.; Roesle, P.; Stempfle, F.; Wucher, P.; Göttker-Schnetmann, I.; Müller, G.; Mecking, S., *Chem. Eur. J.* **2013,** *19*, 17131-17140.

161. Mecking, S.; Quinzler, D. BASF SE, Polymers Made of Renewable Resources. US9096715B2, 2011.

162. Roesle, P.; Dürr, C. J.; Möller, H. M.; Cavallo, L.; Caporaso, L.; Mecking, S., *J. Am. Chem. Soc.* **2012,** *134*, 17696-17703.

163. Roesle, P.; Caporaso, L.; Schnitte, M.; Goldbach, V.; Cavallo, L.; Mecking, S., *J. Am. Chem. Soc.* **2014,** *136*, 16871-16881.

164. Van Meurs, M.; Nobbs, J. D.; Low, C. H.; Stubbs, L. P.; Drent, E. Agency for Science, Technology and Research, A Catalyst for the Carbonylation of Alkenes. WO2017135897A1, 2017.

165. Rose, J. J.; Wang, L.; Xu, Q.; McTiernan, C. F.; Shiva, S.; Tejero, J.; Gladwin, M. T., *Am. J. Respir. Crit. Care Med.* **2017,** *195*, 596-606.

166. Morimoto, T.; Kakiuchi, K., *Angew. Chem. Int. Ed.* **2004,** *43*, 5580-5588.

167. Wu, L.; Liu, Q.; Jackstell, R.; Beller, M., *Angew. Chem. Int. Ed.* **2014,** *53*, 6310-6320.

168. Peng, J.-B.; Qi, X.; Wu, X.-F., *Synlett* **2017,** *28*, 175-194.

169. Okano, T.; Kobayashi, T.; Konishi, H.; Kiji, J., *Tetrahedron Lett.* **1982,** *23*, 4967-4968.

170. Rosales, M.; González, A.; González, B.; Moratinos, C.; Pérez, H.; Urdaneta, J.; Sánchez-Delgado, R. A., *J. Organomet. Chem.* **2005,** *690*, 3095-3098.

171. Makado, G.; Morimoto, T.; Sugimoto, Y.; Tsutsumi, K.; Kagawa, N.; Kakiuchi, K., *Adv. Synth. Catal.* **2010,** *352*, 299-304.

172. Liu, Q.; Yuan, K.; Arockiam, P.-B.; Franke, R.; Doucet, H.; Jackstell, R.; Beller, M., *Angew. Chem. Int. Ed.* **2015,** *54*, 4493-4497.

173. Cini, E.; Airiau, E.; Girard, N.; Mann, A.; Salvadori, J.; Taddei, M., *Synlett* **2011,** *2011*, 199-202.

174. Behr, A.; Kanne, U.; Keim, W., *J. Mol. Catal.* **1986,** *35*, 19-28.

175. Drury, D. J., Formic Acid. In *Kirk-Othmer Encyclopedia of Chemical Technology*, John Wiley & Sons, Inc.: New York, 2013; pp 1-9.

176. Sordakis, K.; Tang, C.; Vogt, L. K.; Junge, H.; Dyson, P. J.; Beller, M.; Laurenczy, G., *Chem. Rev.* **2018,** *118*, 372-433.

177. Gibson, H. W., *Chem. Rev.* **1969,** *69*, 673-692.

178. Simonato, J.-P.; Walter, T.; Métivier, P., *J. Mol. Catal. A: Chem.* **2001,** *171*, 91-94.

179. Mura, M. G.; Luca, L. D.; Giacomelli, G.; Porcheddu, A., *Adv. Synth. Catal.* **2012,** *354*, 3180-3186.

180. Sang, R.; Kucmierczyk, P.; Dong, K.; Franke, R.; Neumann, H.; Jackstell, R.; Beller, M., *J. Am. Chem. Soc.* **2018,** *140*, 5217-5223.

181. Legrand, C.; Castanet, Y.; Mortreux, A.; Petit, F., *J. Chem. Soc., Chem. Commun.* **1994**, 1173-1174.

182. Keim, W.; Becker, J., *J. Mol. Catal.* **1989,** *54*, 95-101.

183. Jenner, G., *Tetrahedron Lett.* **1991,** *32*, 505-508.

184. Konishi, H.; Manabe, K., *Synlett* **2014,** *25*, 1971-1986.

185. Fleischer, I.; Jennerjahn, R.; Cozzula, D.; Jackstell, R.; Franke , R.; Beller, M., *ChemSusChem* **2013,** *6*, 417-420.

186. Nahmed, E. M.; Jenner, G., *J. Mol. Catal.* **1990,** *59*, L15-L19.

187. Wang, H.; Dong, B.; Wang, Y.; Li, J.; Shi, Y., *Org. Lett.* **2014,** *16*, 186-189.

188. Artz, J.; Müller, T. E.; Thenert, K.; Kleinekorte, J.; Meys, R.; Sternberg, A.; Bardow, A.; Leitner, W., *Chem. Rev.* **2017**.

189. Wang, L.; Sun, W.; Liu, C., *Chin. J. Chem.* **2018**, *36*, 353-362.

190. Dong, K.; Wu, X.-F., *Angew. Chem. Int. Ed.* **2017,** *56*, 5399-5401.

191. Nielsen, D. U.; Hu, X.-M.; Daasbjerg, K.; Skrydstrup, T., *Nat. Catal.* **2018,** *1*, 244-254.

192. Wu, L.; Liu, Q.; Jackstell, R.; Beller, M., Recent Progress in Carbon Dioxide Reduction Using Homogeneous Catalysts. In *Carbon Dioxide and Organometallics*, Lu, X.-B., Ed. Springer International Publishing: Cham, 2016; pp 279-304.

193. Intergovernmental Panel on Climate Change (IPCC) *Climate Change 2014 - Synthesis Report - Summary for Policymakers*; 2014.

194. Ritter, S. K., *C&EN* **2015,** *93*, 28.

195. D'Alessandro, D. M.; Smit, B.; Long, J. R., *Angew. Chem. Int. Ed.* **2010,** *49*, 6058-6082.

196. Xiaoding, X.; Moulijn, J. A., *Energy Fuels* **1996,** *10*, 305-325.

197. Leitner, W., *Angew. Chem. Int. Ed. Engl.* **1995,** *34*, 2207-2221.

198. Dibenedetto, A.; Angelini, A.; Stufano, P., *J. Chem. Technol. Biotechnol.* **2014,** *89*, 334-353.

199. Kaiser, P.; Unde, R. B.; Kern, C.; Jess, A., *Chem. Ing. Tech.* **2013,** *85*, 489-499.

200. Wu, L.; Liu, Q.; Fleischer, I.; Jackstell, R.; Beller, M., *Nat. Commun.* **2014,** *5*, 3091.

201. Dibenedetto, A.; Stufano, P.; Nocito, F.; Aresta, M., *ChemSusChem* **2011,** *4*, 1311-1315.

202. Ren, X.; Zheng, Z.; Zhang, L.; Wang, Z.; Xia, C.; Ding, K., *Angew. Chem. Int. Ed.* **2017,** *56*, 310-313.

203. Lang, X.-D.; He, L.-N., *ChemSusChem* **2018,** *11*, 2062-2067.

204. Gehrtz, P. H.; Hirschbeck, V.; Fleischer, I., *Chem. Commun.* **2015,** *51*, 12574-12577.

205. Jensen, M. T.; Rønne, M. H.; Ravn, A. K.; Juhl, R. W.; Nielsen, D. U.; Hu, X.-M.; Pedersen, S. U.; Daasbjerg, K.; Skrydstrup, T., *Nat. Commun.* **2017,** *8*, 489.

206. Daza, Y. A.; Kuhn, J. N., *RSC Adv.* **2016,** *6*, 49675-49691.

207. Ken-ichi, T.; Yoshiyuki, S.; Kohnosuke, H.; Taiki, W.; Masahiro, S., *Chem. Lett.* **1994,** *23*, 1391-1394.

208. Tominaga, K.-i.; Sasaki, Y., *Catal. Commun.* **2000,** *1*, 1-3.

209. Bosch, C.; Wild, W. BASF SE, Producing Hydrogen. US1115776A, 1914.

210. Bustamante, F.; Enick, R. M.; Cugini, A. V.; Killmeyer, R. P.; Howard, B. H.; Rothenberger, K. S.; Ciocco, M. V.; Morreale, B. D.; Chattopadhyay, S.; Shi, S., *AlChE J.* **2004,** *50*, 1028-1041.

211. Moe, J. M., *Chem. Eng. Prog.* **1962,** *58*, 33-36.

212. Oshima, K.; Shinagawa, T.; Nogami, Y.; Manabe, R.; Ogo, S.; Sekine, Y., *Catal. Today* **2014,** *232*, 27-32.

213. Kattel, S.; Liu, P.; Chen, J. G., *J. Am. Chem. Soc.* **2017,** *139*, 9739-9754.

214. Tominaga, K.-i.; Sasaki, Y., *J. Mol. Catal. A: Chem.* **2004,** *220*, 159-165.

215. Dombek, B. D., *J. Organomet. Chem.* **1983,** *250*, 467-483.

216. Bricker, J. C.; Nagel, C. C.; Shore, S. G., *J. Am. Chem. Soc.* **1982,** *104*, 1444-1445.

217. Chang, B.-H., *J. Organomet. Chem.* **1985,** *291*, c31-c33.

218. Liu, Q.; Wu, L.; Fleischer, I.; Selent, D.; Franke, R.; Jackstell, R.; Beller, M., *Chem. Eur. J.* **2014,** *20*, 6888-6894.

219. van Leeuwen, P. W. N. M.; Kamer, P. C. J., *Catal. Sci. Technol.* **2018,** *8*, 26-113.

220. Jääskeläinen, S.; Haukka, M., *Appl. Catal., A* **2003,** *247*, 95-100.

221. Kontkanen, M.-L.; Oresmaa, L.; Moreno, M. A.; Jänis, J.; Laurila, E.; Haukka, M., *Appl. Catal., A* **2009,** *365*, 130-134.

222. Tominaga, K.-i.; Yoshiyuki, S., *Chem. Lett.* **2004,** *33*, 14-15.

223. Tominaga, K.-i., *Catal. Today* **2006,** *115*, 70-72.

224. Tsuchiya, K.; Huang, J.-D.; Tominaga, K.-i., *ACS Catal.* **2013,** *3*, 2865-2868.

225. Li, W.; Guo, L.; Zheng, X.; Cao, Z.; Liu, N., *Prot. Met. Phys. Chem. Surf.* **2017,** *53*, 602-611.

226. Fujita, S.-i.; Okamura, S.; Akiyama, Y.; Arai, M., *Int. J. Mol. Sci.* **2007,** *8*, 749-759.

227. Ali, M.; Gual, A.; Ebeling, G.; Dupont, J., *ChemCatChem* **2014,** *6*, 2224-2228.

228. Tominaga, K.-i.; Sasaki, Y.; Watanabe, T.; Saito, M., *J. Chem. Soc., Chem. Commun.* **1995**, 1489-1490.

229. Tominaga, K.-I.; Sasaki, Y.; Watanabe, T.; Saito, M., *Energy* **1997,** *22*, 169-176.

230. Ali, M.; Gual, A.; Ebeling, G.; Dupont, J., *ChemSusChem* **2016,** *9*, 2129-2134.

231. Srivastava, V. K.; Eilbracht, P., *Catal. Commun.* **2009,** *10*, 1791-1795.

232. Asare Bediako, B. B.; Qian, Q.; Zhang, J.; Wang, Y.; Shen, X.; Shi, J.; Cui, M.; Yang, G.; Wang, Z.; Tong, S.; Han, B., *Green Chem.* **2019,** *21*, 4152-4158.

233. Kamer, P. C. J.; van Leeuwen, P. W. N. M., *Phosphorus(III) Ligands in Homogeneous Catalysis: Design and Synthesis*. Wiley: 2012.

234. Beesley, R. M.; Ingold, C. K.; Thorpe, J. F., *J. Chem. Soc., Trans.* **1915,** *107*, 1080-1106.

235. Jung, M. E.; Piizzi, G., *Chem. Rev.* **2005,** *105*, 1735-1766.

236. van Rijn, J. A.; Siegler, M. A.; Spek, A. L.; Bouwman, E.; Drent, E., *Organometallics* **2009,** *28*, 7006-7014.

237. van Rijn, J. A.; Gouré, E.; Siegler, M. A.; Spek, A. L.; Drent, E.; Bouwman, E., *J. Organomet. Chem.* **2011,** *696*, 1899-1903.

Chapter 2 – The *gem*-Dialkyl Effect in Diphosphine Ligands

2.1 Introduction on the *gem*-Dialkyl Effect

The *gem*-dialkyl effect,[1] also known as the Thorpe-Ingold effect, was first proposed by Thorpe and Ingold in 1915.[2] They postulated that mutual repulsion between two geminally substituted alkyl groups on an open carbon chain simultaneously widens bond angle α and compresses bond angle β (**Figure 2.1**).[3]

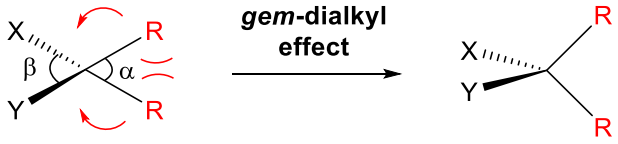

Figure 2.1 The *gem*-dialkyl effect. X and Y = reactive groups.

The decrease in β brings the reactive groups, X and Y, closer together and promotes cyclisation (Thorpe-Ingold effect).[4] Bruice and Pandit attributed the acceleration in cyclisation by the *gem*-dialkyl effect to an increase in rotamer population possessing the right orientation for reaction to occur.[5] The geminally substituted alkyl groups increase the number of gauche interactions, hinder rotation in the open chain substrate and entropically favours ring closure to the cyclised product.[6] If β happened to be part of a small ring, the *gem*-dialkyl effect also aided in ring stabilisation.[1] Following its discovery, the *gem*-dialkyl effect has found many applications in synthetic organic chemistry, including Diels-Alder cycloadditions,[7] dipolar cycloadditions,[8] ene reactions[9] and Claisen rearrangements.[10-11]

In the context of organometallic chemistry, bond angle modifications effected via the *gem*-dialkyl effect (**Figure 2.1**) can be applied to bidentate diphosphine ligands. These modifications may have additional implications for catalyst conformation and geometry (**Figure 2.2**), that in turn, could influence catalytic activity and selectivity.

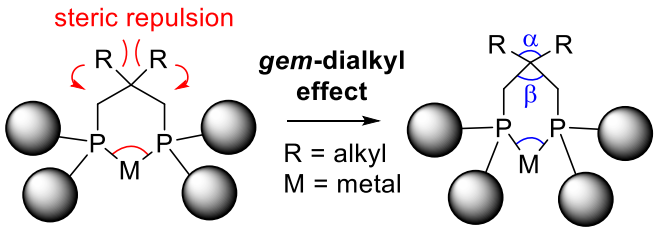

Figure 2.2 The *gem*-dialkyl effect in metal-diphosphine complexes.

The *gem*-dialkyl effect is expected to expand and compress the α and β angles respectively, and may also modify the P-M-P ligand bite angle and influence catalytic performance via steric or electronic bite angle effects. Steric bite angle effects involve an overall change in the steric environment of the catalyst that modifies catalytic activity or selectivity due to changes in the energies of intermediates and transition states in the catalytic cycle.[12] Electronic bite angle effects on the other hand, are orbital

effects that stabilise or destabilise initial, transition or final reaction states due to changes in metal hybridisation and metal orbital energies.[13] Another consequence of the *gem*-dialkyl effect on metal-diphosphine complexes is an increase in the kinetic stability of the chelate (**Figure 2.3**).

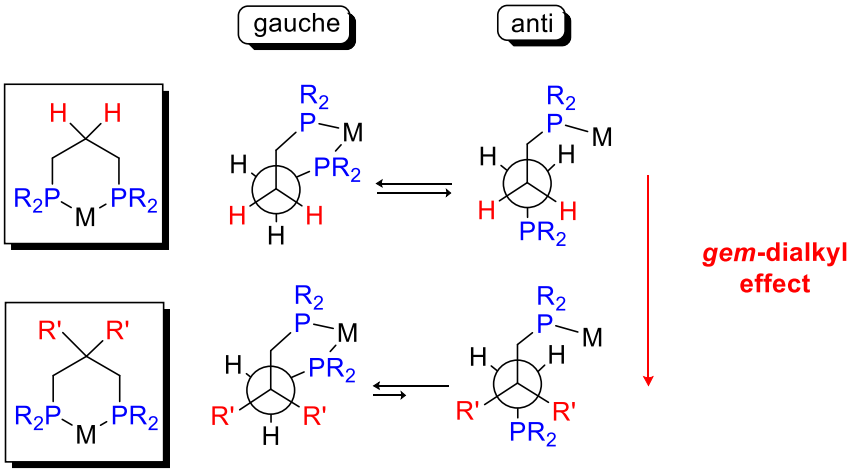

Figure 2.3 Improved chelate kinetic stability due to the *gem*-dialkyl effect. R = alkyl, M = metal.

The presence of geminally substituted alkyl groups restricts rotational freedom by increasing torsional energy barriers. Moreover, additional gauche interactions present in its "anti" conformation raise the energy of the unchelated "anti" conformation and biases the equilibrium in favour of the "gauche" conformation where chelation occurs.[14] The increase in chelate stability has been leveraged as a mechanistic tool to probe for phosphine dissociation as an elementary step in reactions involving chelating diphosphine ligands.[15-16] The *gem*-dialkyl effect has also been reported to alter CO substitution behaviour,[17] improve Pd-catalysed allylation yield,[18-19] modulate polyketone formation[20] and favour branched selectivity in Ni-catalysed alkylation.[21]

This chapter investigates the application of the *gem*-dialkyl effect on C_3-bridged diphosphines as ligands for Pd-catalysed hydroformylation and methoxycarbonylation of olefins. A series of diphosphines (**Figure 2.4**) bearing various *gem*-dialkyl groups substituted on the central carbon of their C_3-bridges have been synthesised and characterised.

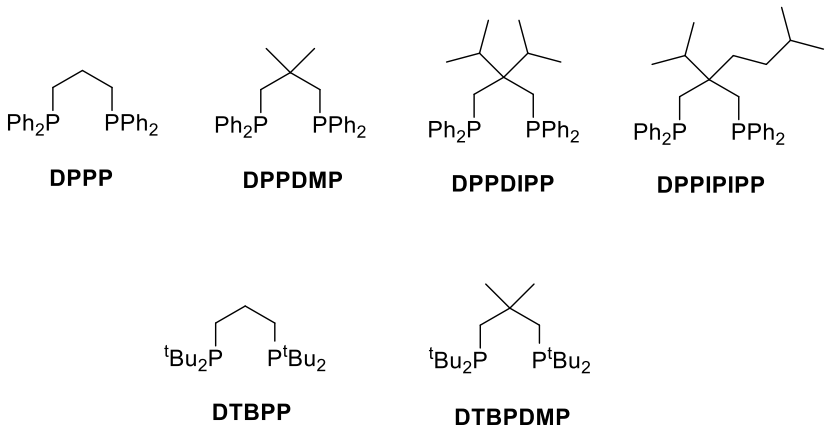

Figure 2.4 Series of *gem*-dialkyl diphosphine ligands studied.

Crystals of the corresponding [Pd(diphosphine)Cl_2] complexes have been synthesised and studied via XRD. The XRD data obtained has been modelled and extrapolated in a DFT study to investigate the relationship between the *gem*-dialkyl effect and geometry in Pd-diphosphine complexes. Finally, the ligand series has been evaluated in Pd-catalysed hydroformylation and methoxycarbonylation to study the *gem*-dialkyl effect on catalytic performance.

2.2 Synthesis and Characterisation

Synthesis of *gem*-dialkyl ligands may proceed via a S_N2 reaction between two equivalents of phosphine nucleophile and an electrophilic precursor possessing two leaving groups connected by the C_3-bridge desired (**Figure 2.5**).[22-23]

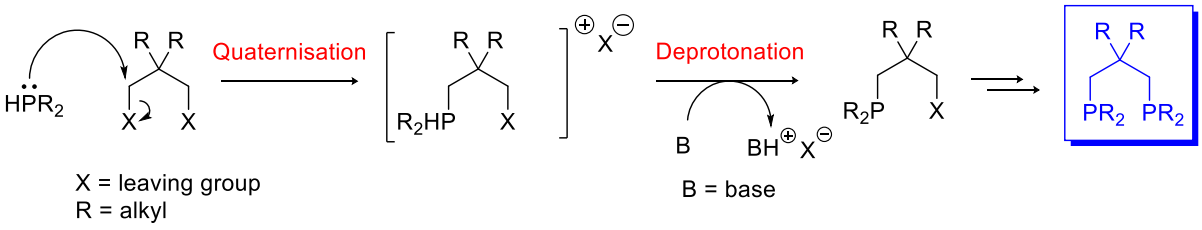

Figure 2.5 Synthesis of *gem*-dialkyl diphosphine ligands.

A S_N2 reaction between secondary phosphine and a C_3-bridged precursor with two leaving groups affords a positively charged intermediate that can be deprotonated and the cycle repeated to yield the desired *gem*-dialkyl ligand. However, treatment of the secondary phosphine with a suitably strong base to first form a phosphide should simultaneously enhance its nucleophilicity and promote the desired S_N2 reaction. The absence of β-hydrogens on the electrophile also excludes competing elimination reactions, favouring the use of stronger nucleophiles. Moreover, employing phosphide nucleophiles should boost yields by eliminating the need for deprotonation as an intermediate step.

In the following sub-sections, the synthesis and characterisation of a series of C_3-bridged *gem*-dialkyl diphosphine ligands (**Figure 2.4**) is discussed.

2.2.1 Electrophile Precursors for *gem*-Dialkyl Ligand Synthesis

Three classes of electrophilic precursors for the synthesis of *gem*-dialkyl ligands were investigated (**Figure 2.6**) – tosylates (**Type I**), halides (**Type II**) and cyclic sulfates (**Type III**). These functionalities were selected for their weak conjugate basicity which imply good leaving group ability. In particular, cyclic sulfates have been favoured for their synthetic utility in activating 1,3-diols toward nucleophilic attack.[24-25]

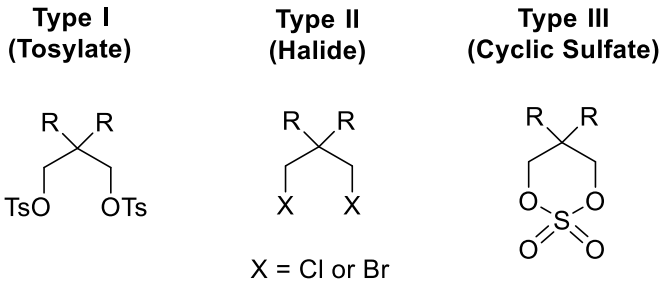

Figure 2.6 Three types of electrophilic precursors to *gem*-dialkyl diphosphine ligands.

The targeted series of *gem*-dialkyl backbones included three symmetrically substituted analogues of varying steric bulk (R = H, Me and *i*Pr) and an asymmetric *iso*-propyl/*iso*-pentyl (*i*Pr/*i*Pent) analogue (**Figure 2.7**).

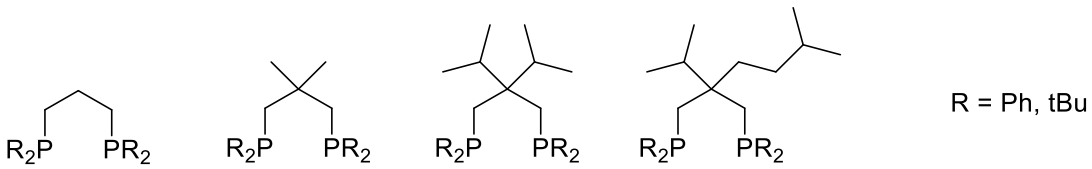

Figure 2.7 Synthetic targets for C_3-bridged *gem*-dialkyl diphosphine ligands.

Type I tosylate and **Type III** cyclic sulfate precursors were synthesised from their corresponding diols following literature procedures[26-27] while **Type II** bromide precursors were prepared via Appel reaction[28] likewise from their corresponding diols. The asymmetric *iso*-propyl/*iso*-pentyl bridged diol was synthesised from commercially available 2-isopropyl-5-methyl-2-hexenal via Aldol reaction with formaldehyde followed by a crossed Cannizzaro[29] reaction (**Figure 2.8**).

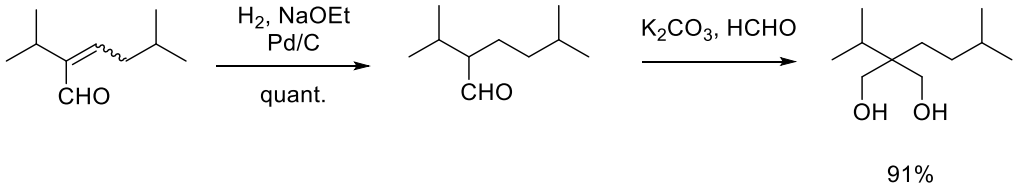

Figure 2.8 Synthesis of asymmetric geminally substituted *iso*-propyl/*iso*-pentyl diol.

Synthesis of di-*iso*-propyl C_3-bridged diol was achieved via malonate chemistry. Excess isopropyl bromide was required as competing elimination of HBr by deprotonated malonate acting as a base (E2 mechanism) instead of a nucleophile (S_N2 mechanism) also consumed isopropyl bromide to give propene as a by-product. However, repeated additions of excess isopropyl bromide eventually yielded diethyl bis(*iso*-propyl)malonate that was then reduced to give the desired di-*iso*-propyl C_3-bridged diol (**Figure 2.9**).

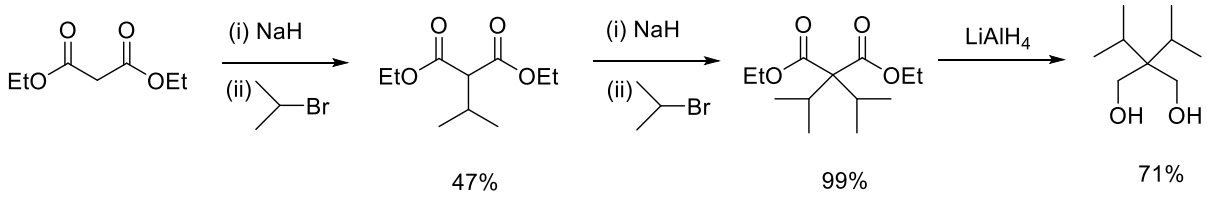

Figure 2.9 Synthesis of di-*iso*-propyl C_3-bridged diol.

Conversion of diol to cyclic sulfate proceeded via the formation of an intermediate cyclic sulfite through treatment with $SOCl_2$ followed by Ru-catalysed oxidation in air (**Figure 2.10**).[27]

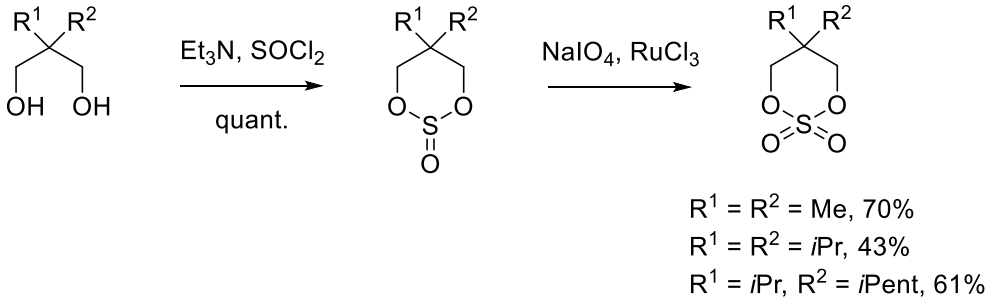

Figure 2.10 General synthetic route to cyclic sulfate.[27]

^{1}H NMR of the intermediate cyclic sulfite revealed asymmetric chemical environments for its two geminal R groups and α-hydrogens, as illustrated below in **Figure 2.11**.

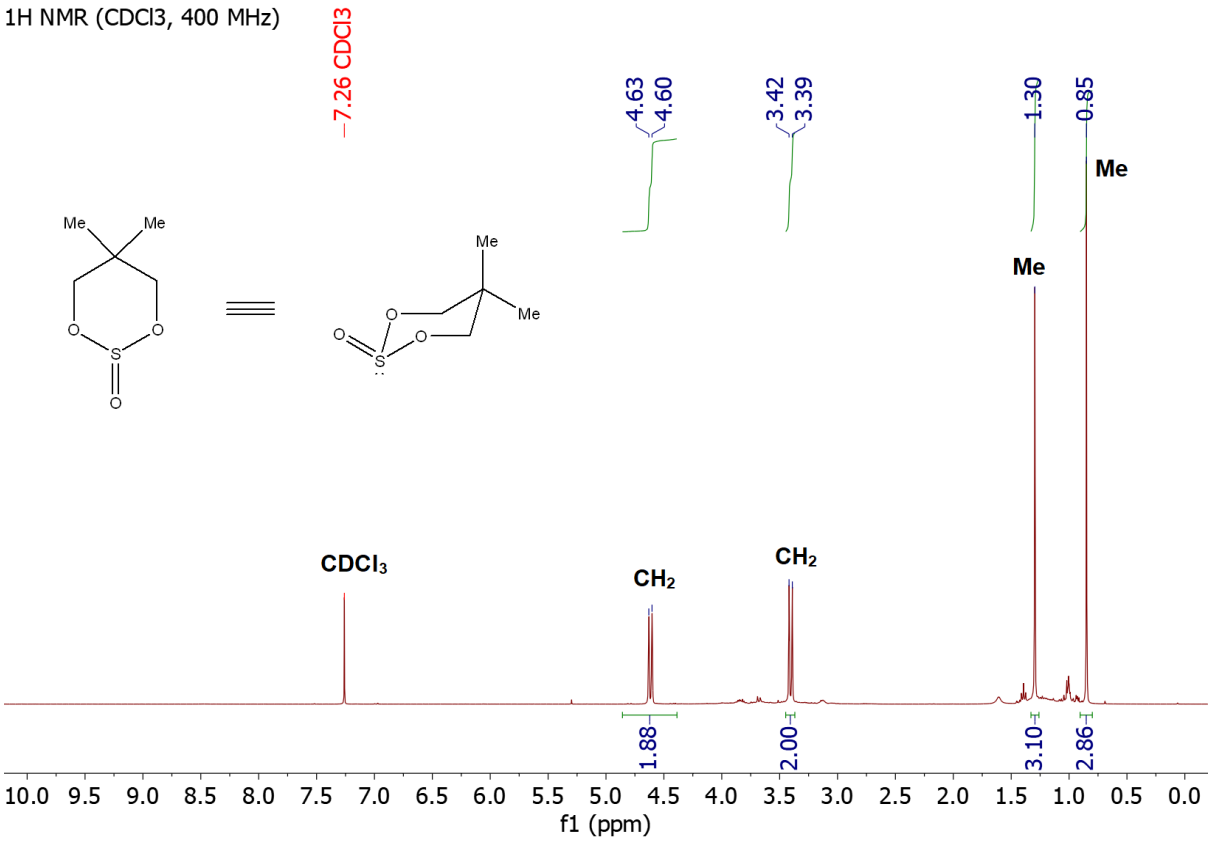

Figure 2.11 ^{1}H NMR (400 MHz, $CDCl_3$, 25 °C) of dimethyl cyclic sulfite.

Due to the trigonal pyramidal geometry of the sulfite group in its 6-membereded chair conformer, the O atom is displaced toward a given orientation. As a result, the chemical environments of Me and α-H are affected by their relative position (cis/trans) to the O atom. Subsequent Ru-catalysed oxidation symmetrises the molecule by replacing the lone pair on the S atom with a second O atom, resulting in the convergence of the geminal chemical shifts.

2.2.2 Synthesis of *gem*-Dialkyl Ligands

The desired series of *gem*-dialkyl diphosphine ligands was generated via the two-step process of first, treatment of secondary phosphine in THF with n-butyl lithium to form lithium phosphide, followed by addition of electrophile precursor to the freshly prepared lithium phosphide solution with gentle heating (65 °C) to encourage S_N2 substitution (**Table 2.1**). It should be noted that lithium phosphides such as LiP^tBu_2 precipitated as a white solid in non-polar solvents like hexane, giving emulsions that resulted in no reaction. The use of polar THF however, gave homogeneous coloured solutions that yielded desired product and allowed for convenient work-up via removal of the low-boiling solvent under vacuum.

Table 2.1 Synthesis of *gem*-dialkyl diphosphine ligands.[a]

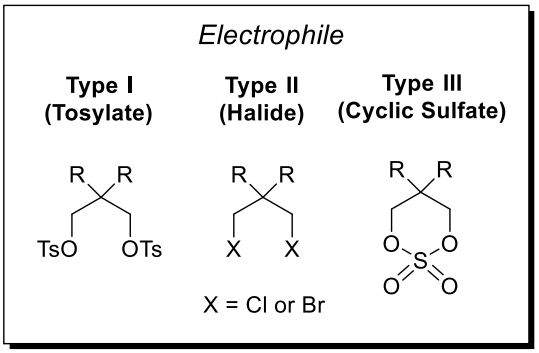

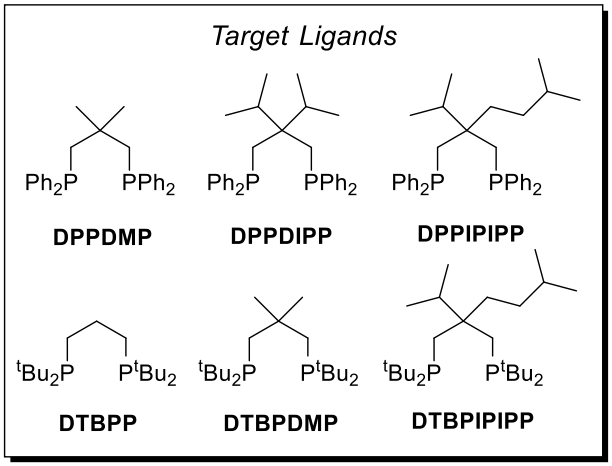

Entry	Target Ligand	H-PR_2	Electrophile	R^1	R^2	Time / h	Isolated Yield / %
1	**DPPDMP**	H-PPh_2	**Type I**	Me	Me	24	0
2	**DPPDMP**	H-PPh_2	**Type II** (Cl)	Me	Me	24	96
3	**DPPIPIPP**	H-PPh_2	**Type II** (Br)	*i*Pr	*i*Pent	72	16
4	**DPPIPIPP**	H-PPh_2	**Type III**	*i*Pr	*i*Pent	96	14
5	**DPPDIPP**	H-PPh_2	**Type III**	*i*Pr	*i*Pr	168	11
6	**DTBPP**	H-P^tBu_2	**Type II** (Br)	H	H	24	63
7	**DTBPDMP**	H-P^tBu_2	**Type II** (Cl)	Me	Me	24	<1
8	**DTBPDMP**	H-P^tBu_2	**Type III**	Me	Me	72	20
9	**DTBPIPIPP**	H-P^tBu_2	**Type III**	*i*Pr	*i*Pent	120	0

[a]Conditions: H-PR_2 (2.1 eq), electrophile (1 eq), ^{n}BuLi (2.1 eq), THF, 65 °C.

No desired product was observed in the $^{31}P\{^1H\}$ NMR of the product mixture from entry 1. Instead, the major phosphorus by-product (ca. 48% of all integrated P signals) was a singlet at -15.0 ppm, a chemical shift suggesting its identity as Ph_2P-PPh_2 (literature value[30] = -15.2 ppm). A similarly suspected ^{t}Bu$_2$P-P^{t}Bu$_2$ species at 40.7 ppm (literature value[31] = 40.6 ppm) was observed as the major product (ca. 58% of all integrated P signals) for entry 7. This is consistent with an earlier report by Eberhard that described the formation of P-P bonded species as the major product from treatment of decorated C_3-bridged di-tosylates with lithium phosphide.[23] Eberhard also noted that exchanging tosylate for a better leaving group such as triflate did not resolve this issue.

$LiPPh_2$ successfully substituted **Type II** (Cl) dimethyl electrophile to give **DPPDMP** in 96% yield (entry 2, **Table 2.1**), but reacting **Type II** (Cl) dimethyl electrophile with LiP^tBu_2 instead gave $^tBu_2P\text{-}P^tBu_2$ as the major product.

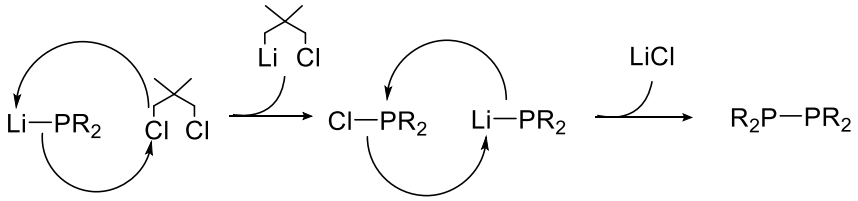

Figure 2.12 Proposed mechanism for formation of P-P bonded species, adapted from literature.[32]

Earlier work by Harris and Pretzer on the synthesis of P-P bonded diphosphines from alkyl halides described a mechanism for the formation of these species.[32] An adapted version is illustrated in **Figure 2.12** above. The dihalide electrophile possesses β-methyl groups that hinder the approach of nucleophiles, especially bulky ones such as LiP^tBu_2. LiP^tBu_2 nucleophiles should thus preferentially attack the less hindered ClP^tBu_2, resulting in the formation of $^tBu_2P\text{-}P^tBu_2$ instead. The use of **Type III** cyclic sulfate precursors however, excludes halogens in the reaction mixture and should prevent the formation of $R_2P\text{-}PR_2$ species via such a mechanism. A possible mechanism for the formation of P-P species is proposed in **Figure 2.13** below.

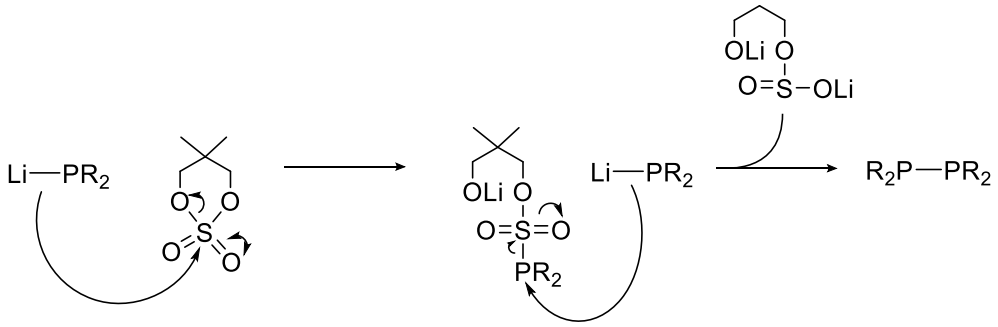

Figure 2.13 Proposed mechanism for the formation of P-P bonded species.

There are two factors that may contribute to the suppression of P-P bonded by-products by cyclic sulfates. Firstly, entropy. For dihalides, a single halide anion is eliminated after each nucleophilic substitution by lithium phosphide to maintain the same total number of species. However, in the case of cyclic sulfates, the total number of species is reduced as the sulfate fragment remains attached to the substrate at a secondary point after nucleophilic substitution, resulting in a greater loss of entropy. Secondly, in order to form the P-P bonded species from the singly substituted sulfate intermediate via the proposed mechanism above, an unfavourable nucleophilic attack must occur to eliminate a doubly charged anionic species.

Starting from cyclic sulfates instead of dihalides appeared to favour the desired reaction, and **DTBPDMP** was eventually synthesised from its corresponding **Type III** cyclic sulfate electrophile in 20% yield (entry 8, **Table 2.1**). Treating asymmetric *iso*-propyl/*iso*-pentyl **Type III** cyclic sulfate (entry 4, **Table 2.1**) with $LiPPh_2$ however, gave a crude product with a $^{31}P\{^1H\}$ NMR spectrum showing desired **DPPIPIPP** (ca. 60% of all integrated P signals) together with a single major by-product that appeared as a singlet at -16.3 ppm (ca. 36% of all integrated P signals). The mixture was protected with BH_3 to prevent phosphine oxidation upon exposure to air and purified via column chromatography. Deprotection with refluxing EtOH[33] yielded the desired asymmetric *iso*-propyl/*iso*-pentyl ligand, **DPPIPIPP**, in significantly reduced yield (14% isolated vs 60% by $^{31}P\{^1H\}$ NMR in the crude). A similar procedure gave the di-*iso*-propyl analogue **DPPDIPP** (entry 5, **Table 2.1**) in modest yield (11%).

Treating *iso*-propyl/*iso*-pentyl **Type III** cyclic sulfate with LiP^tBu_2 gave no desired ligand product despite extended reaction times (entry 9, **Table 2.1**). The lack of desired product may be due to the increase in steric bulk of both the lithium phosphide and the geminal alkyl groups in the β-position that hindered the approach of the nucleophile and prevented any significant S_N2 reaction from occurring.

Subsequent attempts to improve the yield of **DPPIPIPP** using $LiPPh_2$ with **Type II** (Br) *iso*-propyl/*iso*-pentyl electrophiles resulted in a product mixture with similar by-products as that from **Type III** cyclic sulfate. The crude product mixture required further purification to give a similarly modest yield of **DPPIPIPP** (16%, entry 3, **Table 2.1**). This suggests that the identity of the leaving group does not play a significant role in the occurring side reaction and that it may be an issue with the synthetic strategy of using lithium phosphides in general. A possible alternative to circumvent this issue could be a reversal of polarities (Umpolung),[34] by generating di-Grignard reagents from 1,3-dihalides to act as nucleophiles on chlorophosphine electrophiles instead.[35]

2.2.3 Chelation Competition Between DPPP and DPPDMP

Competitive chelation experiments between unmodified **DPPP** and *gem*-dimethylated **DPPDMP** ligands were carried out to study the impact of the *gem*-dialkyl effect on formation of [Pd(diphosphine)Cl_2] complexes. Equimolar amounts of **DPPP**, **DPPDMP** and Pd(1,5-cyclooctadiene)Cl_2] were mixed in CH_2Cl_2 and analysed via $^{31}P\{^1H\}$ NMR (**Figure 2.14**). An insert containing PPh_3 (-5.4 ppm) as an internal standard in $C_2D_2Cl_4$ was also placed into the NMR tube to act as a reference and for the deuterium lock. A small amount of $POPh_3$, likely from the atmospheric oxidation of PPh_3 was also detected at 29.7 ppm.

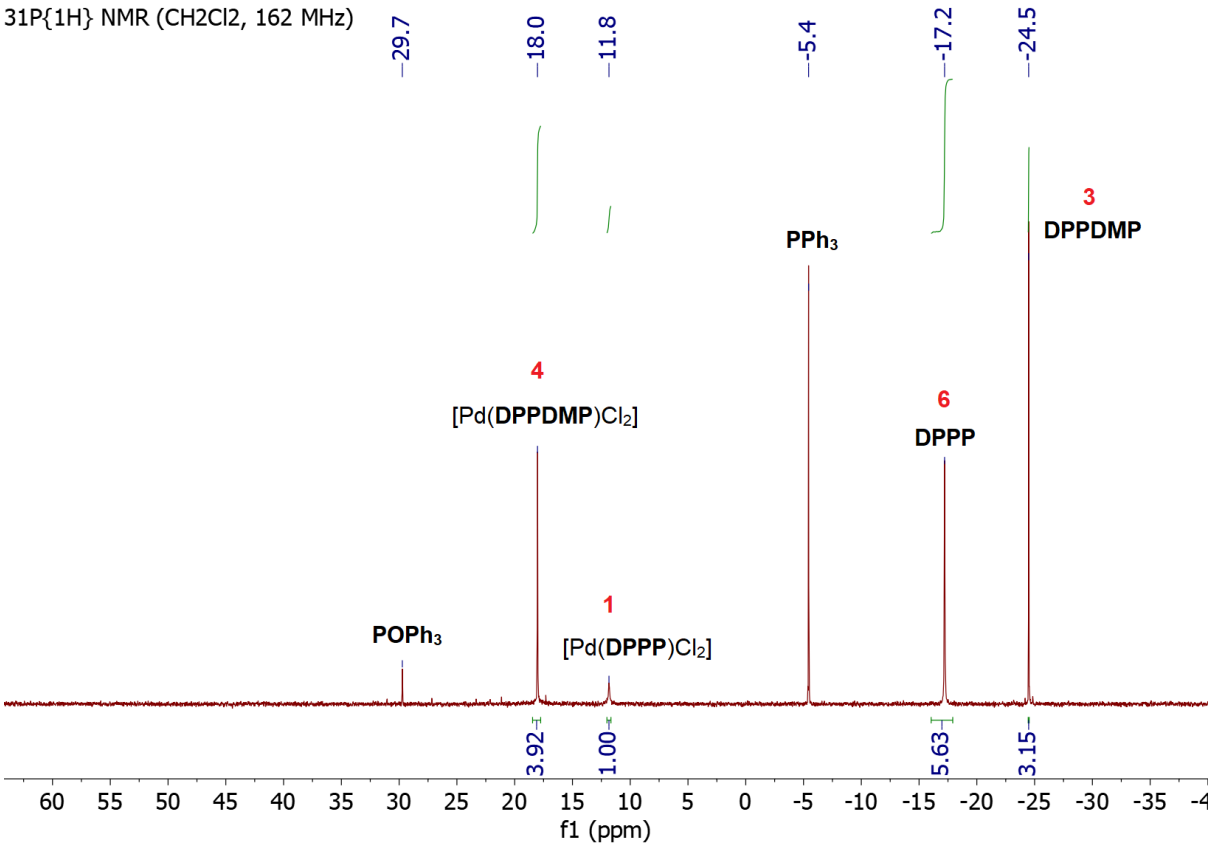

Figure 2.14 $^{31}P\{^{1}H\}$ NMR (162 MHz, CH_2Cl_2, 25 °C) of the competitive chelation experiment between **DPPP** and **DPPDMP** to form their palladium(II) chloride complex. NMR insert of $C_2D_2Cl_4$ with PPh_3 present for reference.

The formation of [Pd(**DPPDMP**)Cl_2] was favoured over [Pd(**DPPP**)Cl_2] in a 4:1 ratio. The equilibrium favouring the formation of [Pd(**DPPDMP**)Cl_2] suggests that application of the *gem*-dialkyl effect results in a more stable chelate complex. After standing under argon atmosphere for more than a month at 25 °C, the ratio of the components in the mixture remained unchanged (**Figure 2.14**), suggesting that the mixture was at equilibrium. It should be noted however, that even at a 4:1 ratio the energy difference between the two complexes is estimated to be around 3.4 kJ mol^{-1}, such a difference can be brought about by solvent effects and caution should be exercised with regards to generalising this result to other solvents.

2.2.4 [Pd(Diphosphine)Cl_2] Complexes

Palladium(II) chloride complexes of the *gem*-dialkyl diphosphine ligands were obtained by mixing equimolar amounts of the corresponding ligand with [Pd(1,5-cyclooctadiene)Cl_2] in CH_2Cl_2 (**Figure 2.15**).

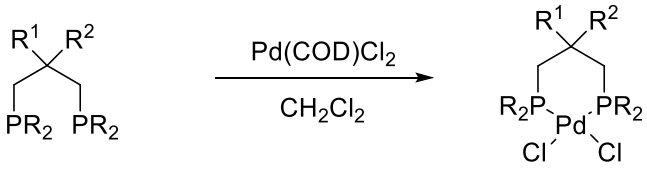

$R^1 = R^2$ = Me, R = Ph, [Pd(**DPPDMP**)Cl_2]: 97% yield
R^1 = *i*Pr, R^2 = *i*Pent, R = Ph, [Pd(**DPPIPIPP**)Cl_2]: 96% yield
$R^1 = R^2$ = *i*Pr, R = Ph, [Pd(**DPPDIPP**)Cl_2]: 99% yield
$R^1 = R^2$ = Me, R = ^{t}Bu, [Pd(**DTBPDMP**)Cl_2]: 98% yield

Figure 2.15 Synthesis of [Pd(diphosphine)Cl_2] complexes. COD = 1,5-cyclooctadiene.

Crystals suitable for single crystal x-ray diffraction (XRD) were grown either by layering pentane on CH_2Cl_2 solutions of the complexes or via slow vapour diffusion of cyclohexane into CH_2Cl_2 solutions of the complexes. Their molecular structures along with selected bond angles and lengths are shown below in **Figure 2.16** and **Table 2.2** respectively.

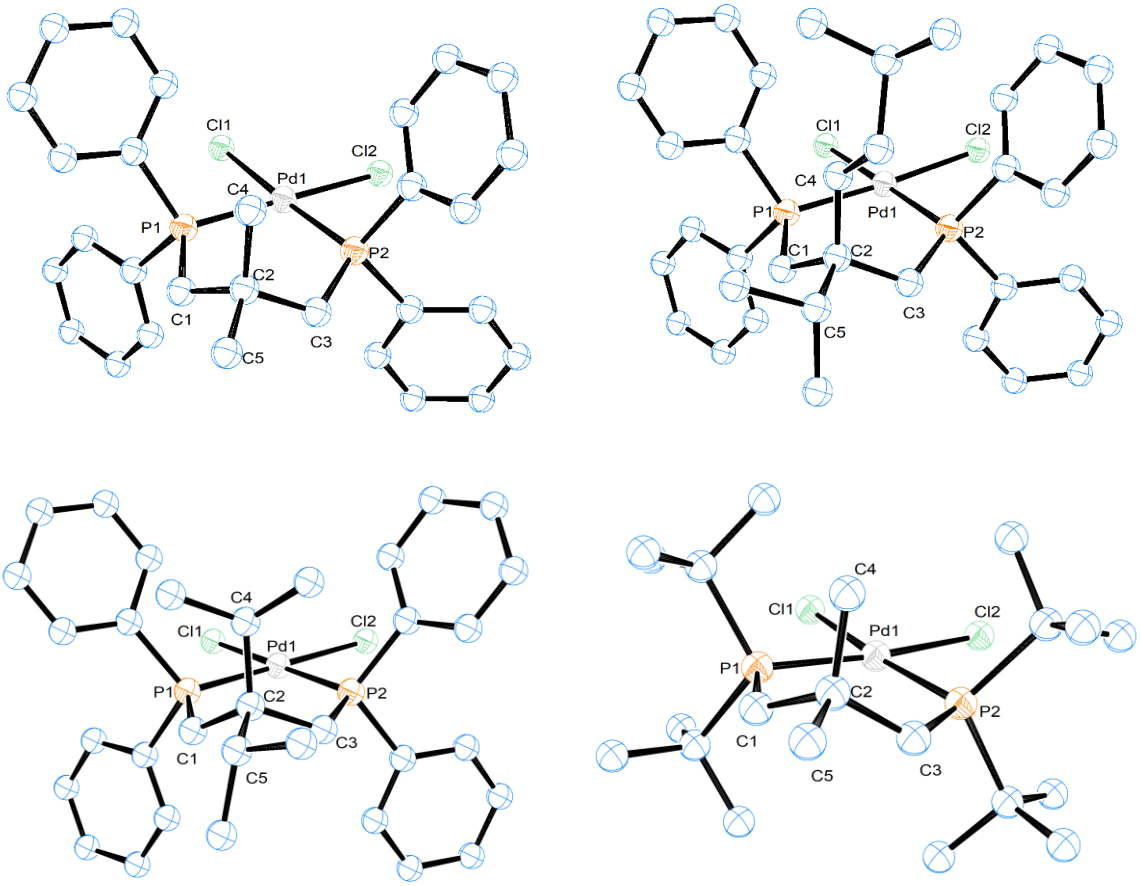

Figure 2.16 Molecular structures of [Pd(diphosphine)Cl_2] complexes for **DPPDMP** (top left), **DPPIPIPP** (top right), **DPPDIPP** (bottom left) and **DTBPDMP** (bottom right). Structures refined by Dr. Andrew White.

Table 2.2 Selected bond angles (°) and bond lengths (Å) of [Pd(diphosphine)Cl_2] complexes.

	[Pd(**DPPP**)Cl_2]*	[Pd(**DPPDMP**)Cl_2]	[Pd(**DPPIPIPP**)Cl_2]	[Pd(**DPPDIPP**)Cl_2]	[Pd(**DTBPP**)Cl_2]*	[Pd(**DTBPDMP**)Cl_2]
C^4-C^2-C^5 (external)	-	109.5 (3)	109.5 (3)	111.74 (19)	-	106.7 (4)
C^1-C^2-C^3 (internal)	117.0 (5)	110.1 (3)	108.2 (3)	107.27 (19)	111.8 (7)	110.9 (4)
P^1-Pd^1-P^2	90.58 (5)	95.84 (3)	96.29 (4)	94.69 (2)	97.73 (8)	98.03 (5)
Cl^1-Pd^1-Cl^2	90.78 (5)	91.59 (3)	91.85 (4)	90.95 (3)	86.17 (8)	84.80 (5)
P^2-Pd^1-Cl^2	91.10 (5)	84.49 (3)	86.37 (4)	86.66 (2)	89.89 (8)	88.64 (5)
P^1-Pd^1-Cl^1	87.74 (5)	88.09 (3)	85.59 (4)	87.69 (3)	91.60 (8)	88.51 (5)
P^1-Pd^1	2.249 (2)	2.2371 (9)	2.2452 (11)	2.2386 (7)	2.309 (2)	2.3041 (13)
P^2-Pd^1	2.244 (1)	2.2423 (9)	2.2449 (11)	2.2433 (6)	2.296 (2)	2.2966 (14)
Pd^1-Cl^2	2.351 (1)	2.3391 (9)	2.3480 (10)	2.3586 (7)	2.377 (2)	2.3686 (13)
Pd^1-Cl^1	2.358 (2)	2.3570 (9)	2.3381 (12)	2.3435 (7)	2.368 (2)	2.3548 (13)

*Values taken from literature.[36-37]

2.2.5 Changes in Bond Angles

Application of the *gem*-dialkyl effect to diphosphine ligands should result in the simultaneous expansion of the external angle (C^4-C^2-C^5) and compression of the internal angle (C^1-C^2-C^3) due to mutual repulsion between the geminal alkyl groups.[1] Comparison of the C^1-C^2-C^3 internal angle across the PPh_2 series show a decreasing trend in the order **DPPP** (117°) > **DPPDMP** (110°) > **DPPIPIPP** (108°) ≈ **DPPDIPP** (107°) where bulkier geminal alkyl groups exhibit greater internal angle compression as expected from the *gem*-dialkyl effect. Taking a confidence interval of 99.7% (or 3-sigma) some differences are not statistically significant. It should also be noted that packing effects may also influence bond angles to a certain extent, which may account for some of the variation observed. Interestingly, there is no increase in external C^4-C^2-C^5 angle going from **DPPDMP** (two primary alkyl groups) to **DPPIPIPP** (one primary, one secondary alkyl group) despite the increase in steric bulk. Their external C^4-C^2-C^5 angles remain around the ideal tetrahedral value of 109.5° despite a 2° compression of the C^1-C^2-C^3 internal angle going from **DPPDMP** to **DPPIPIPP**. Instead, a distortion is observed in the 6-membereded chelate comprised of the C_3 backbone, both P donor atoms and the Pd metal centre. The original chair-like conformation adopted by the **DPPDMP** complex (cyan, **Figure 2.17**) distorts towards a half-chair for **DPPIPIPP** (red, **Figure 2.17**) with the Pd metal atom moving up about 2° toward planarity with the P-C-C-P plane while maintaining the square planar geometry expected of d^8 complexes.

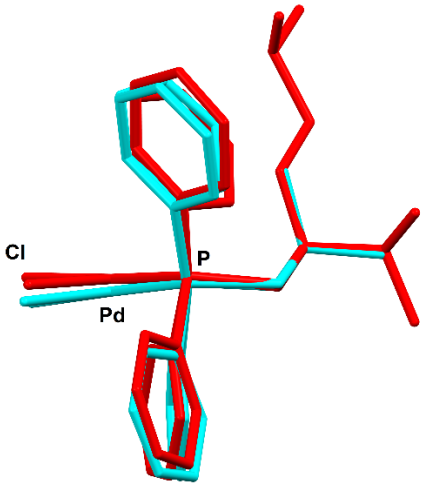

Figure 2.17 Overlapped molecular structures of [Pd(**DPPDMP**)Cl_2] (cyan) and [Pd(**DPPIPIPP**)Cl_2] (red).

Transitioning from **DPPIPIPP** (one primary, one secondary alkyl group) to **DPPDIPP** (two secondary alkyl groups) however, gave the expected C^4-C^2-C^5 external angle expansion of about 1°.

In contrast to the significant C^1-C^2-C^3 internal angle compression of 7° observed going from **DPPP** to **DPPDMP** however, the P^{t}Bu$_2$ analogues **DTBPP** and **DTBPDMP** show nearly similar C^1-C^2-C^3 internal angles (**Table 2.2**) despite undergoing the same *gem*-dimethylation transformation on the central carbon of its C_3-bridge.

2.2.6 P-Pd-P Ligand Bite Angle

Another parameter of interest that can be modified by the *gem*-dialkyl effect is P-Pd-P ligand bite angle.[38] The introduction of geminal alkyl groups of increasing steric bulk results in an initial increase in P-Pd-P ligand bite angle from 91° (**DPPP**) to 96° (**DPPDMP**/**DPPIPIPP**) before going back down to 95° (**DPPDIPP**). This non-linear trend suggests that a complicated relationship between the *gem*-dialkyl effect and P-Pd-P ligand bite angle, likely due in part to distortions in the 6-membered chelate ring. Unlike the changes observed for the PPh$_2$ series however, the P^{t}Bu$_2$ analogues **DTBPP** and **DTBPDMP** exhibit similar P-Pd-P ligand bite angles despite *gem*-dimethylation of the backbone (**Table 2.2**).

2.2.7 Overall Spatial Arrangement

Unlike other complexes in the series, [Pd(**DPPP**)Cl_2] (orange, **Figure 2.18**) exhibits an asymmetrical spatial arrangement. The introduction of *gem*-dimethyl groups to give [Pd(**DPPDMP**)Cl_2] (red, **Figure 2.18**) appears to impose a more regular pattern and brings about a widening of the P-Pd-P bite angle by 5°. This perturbation of the P-Pd-P ligand bite angle is accommodated without altering the Cl-Pd-Cl bond angle which remains around 91°. Instead, a distortion of the square planar geometry occurs. This can be seen in **Figure 2.18** as a twisting of the Cl atoms out of the P-Pd-P plane.

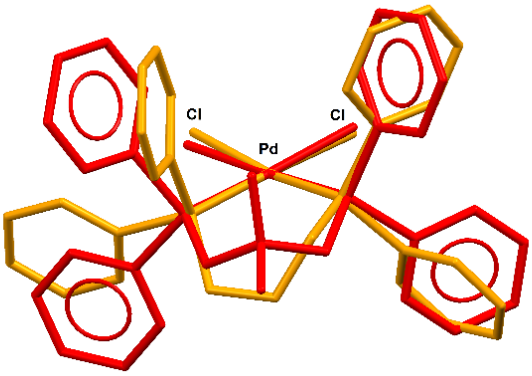

Figure 2.18 Overlaid molecular structures of [Pd(**DPPP**)Cl_2] (orange) and [Pd(**DPPDMP**)Cl_2] (red).

2.2.8 Ligand Buried Volume (%V_Bur)

The *gem*-dialkyl effect may cause subtle changes in the overall spatial orientation of the complex that may also alter coordination space around the Pd centre. Regretfully, classical methods of quantifying ligand steric bulk such as the Tolman cone angle[39] are insufficient to probe these nuanced changes as they reference the substituents directly connected to the P donor atom that, in this case, are identical throughout the series of ligands. The *gem*-dialkyl effect instead acts via remote modification of the ligand backbone to indirectly influence coordination space via conformational changes. In an attempt to provide a more comprehensive measure of ligand steric bulk, Falivene and co-workers have introduced a computational tool that describes the coordination sphere around the metal centre via a parameter they term ligand buried volume (%V_Bur).[40-41] Ligand buried volume (%V_Bur) is defined as the amount of space occupied by the ligand of interest in a sphere of a specified radius around a given coordination centre (see section **5.4.5** for details). Comparison of the %V_Bur values across the PPh_2 ligand series reveals a trend of increasing steric congestion in order of *gem*-dialkyl steric bulk – **DPPP** (38.9%) < **DPPDMP** (41.1%) < **DPPIPIPP** (41.8%) < **DPPDIPP** (42.2%). A similar trend is observed for the P^tBu_2 analogues where the %V_Bur is less for **DTBPP** (45.2%) than for **DTBPDMP** (46.5%).

2.3 Density Functional Theory (DFT) Modelling

Unless specified otherwise, density functional calculations were performed on all systems using the Gaussian 16 (revision A03) set of programs.[42] Geometry optimisations were carried out using the B3LYP hybrid functional[43-44] in the gas phase. The electronic configuration of the molecular systems were described by the triple-ζ basis set with polarisation functions of Ahlrichs and co-workers (DEF2TZVPP basis set in Gaussian 16).[45-46] London dispersion corrections with Becke-Johnson damping (GD3BJ in Gaussian 16) were taken from the work of Grimme, Becke and Johnson.[47-49]

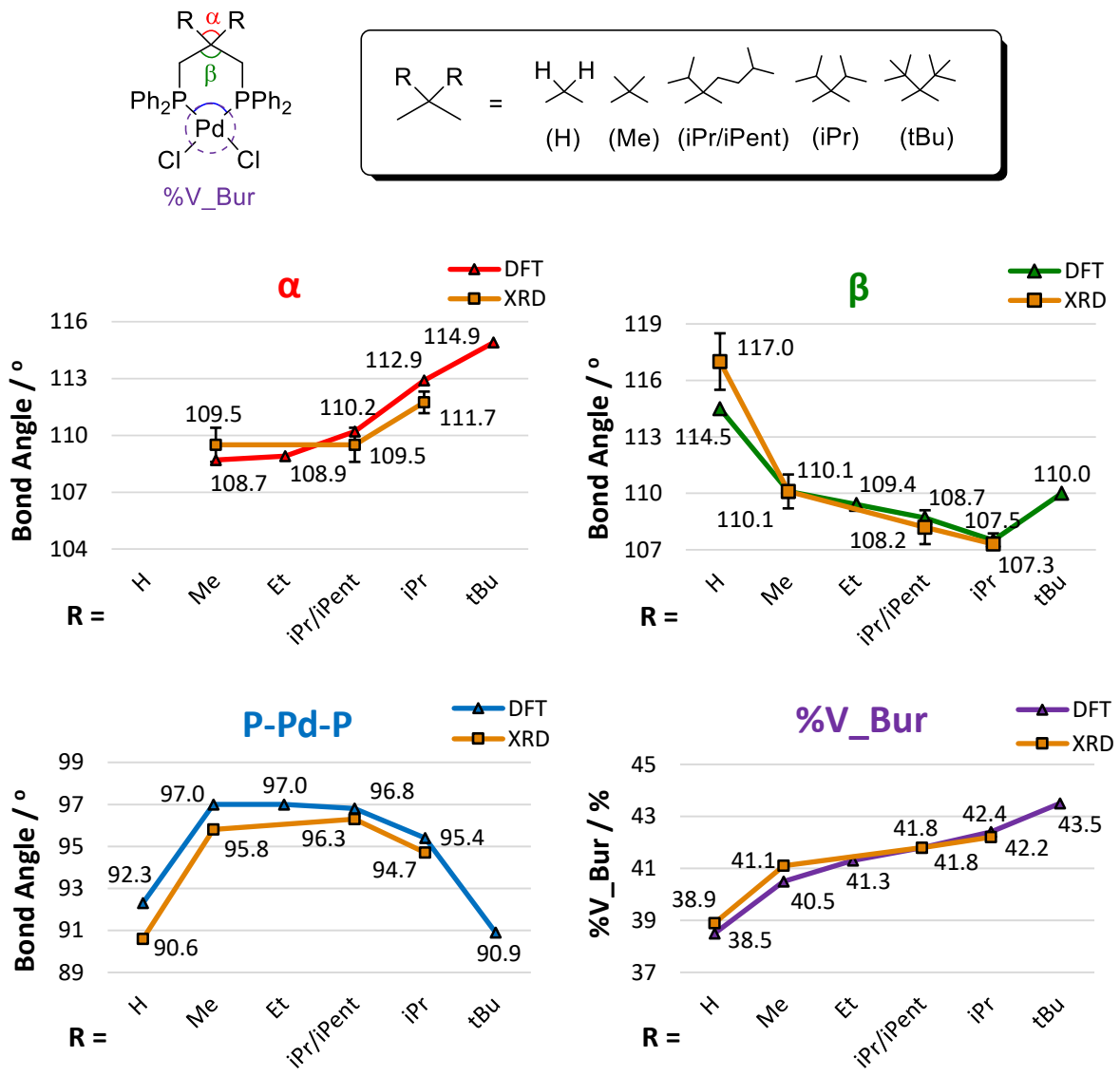

Figure 2.19 Graphs of the [Pd(diphosphine)Cl_2] parameters with error bars at 99.7% confidence. *Top Left*: α angle vs. R group. *Top Right*: β angle vs. R group. *Bottom Left*: P-Pd-P angle vs. R group. *Bottom Right*: %V_Bur vs. R group.

2.3.1 Bond Angle Expansion and Compression

The external angle (α) increases with increasing R group size, from 109° in the dimethyl analogue (**DPPDMP**) to 115° in the di-*tert*-butyl analogue (**Figure 2.19**, top left). As R group size increases, the internal β angle also shows a corresponding decrease from 115° for the di-hydrogen analogue (**DPPP**) to 107° for the di-*iso*-propyl analogue (**DPPDIPP**) (**Figure 2.19**, top right). The simultaneous angle expansion and compression is in line with expectations of the *gem*-dialkyl effect on geometry. In contrast to the continual increase in external α angle with increasing R group size however, the internal β angles appear to taper off asymptotically when approaching the ideal tetrahedral angle of

109.5°. Moreover, there is a trend reversal for the bulkiest di-*tert*-butyl analogue, which shows an increase in β to 110° from 107° in the di-*iso*-propyl analogue (**DPPDIPP**) (**Figure 2.19**, top right).

2.3.2 6-membered Chelate Distortion

Closer inspection of the molecular structures reveals that not all the tension generated from steric repulsion between the increasingly bulky *gem*-dialkyl groups goes toward compressing the internal bond angle (β). There instead is a portion of it that appears to be released via distortion of the complex, resulting in conformational changes in its 6-membereded chelate. This is illustrated in **Figure 2.20** below as a distortion of the initial chair conformation (R = H, Me) towards a half-chair (R = Et, iPr/iPent) and ultimately to a twist-boat conformation (R = iPr and tBu).

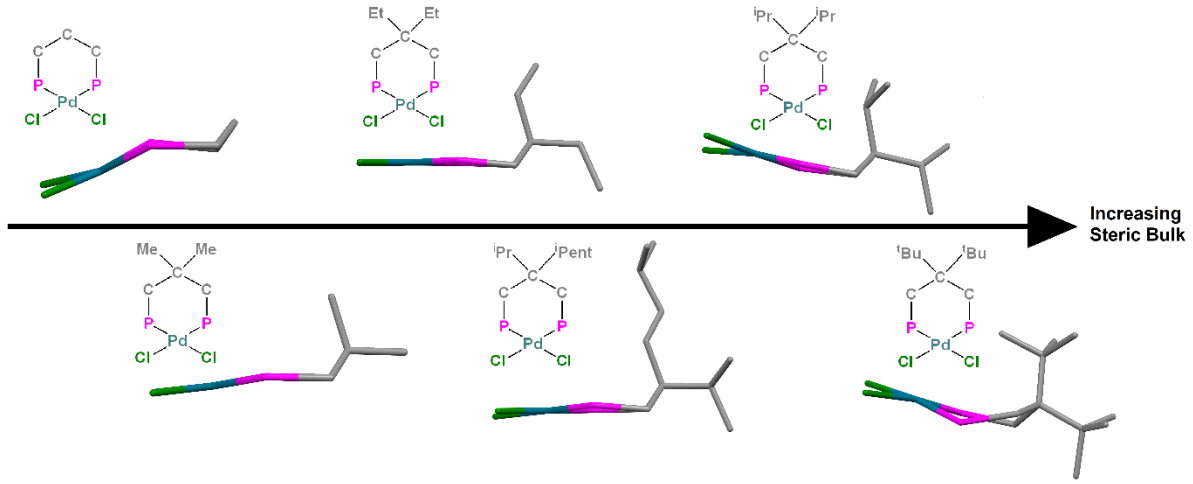

Figure 2.20 Calculated [Pd(diphosphine)Cl_2] structures arranged by increasing steric bulk of *gem*-dialkyl groups showing 6-membered chelate conformations (side view across P–C bonds). Phenyl groups and hydrogen atoms removed for clarity.

2.3.3 P-Pd-P Ligand Bite Angle Trend

The P-Pd-P ligand bite angles follow an up-and-down trend, reaching a maximum of 97° (R = Me, Et) before returning to 91° (R = ^{t}Bu), a value like that of the unmodified analogue (R = H, 92°). For smaller R groups such as Me or Et, the *gem*-dialkyl effect widens the P-Pd-P ligand bite angle. However, for larger R groups such as *i*Pr or ^{t}Bu, there is an accompanying distortion in the 6-membereded chelate that overall, results in a decrease in P-Pd-P ligand bite angle instead. The compounding of these 4 factors: α angle expansion, β angle compression, chelate distortion and altered spatial arrangement, results in a complicated relationship between the *gem*-dialkyl effect and P-Pd-P ligand bite angle. A more direct relationship between P-Pd-P bite angle and the *gem*-dialkyl effect may perhaps be achieved with C_1-bridged diphosphines,[50] where bond angle compression from the *gem*-dialkyl effect may directly translate to bringing the P atoms closer together and thus result in smaller P-Pd-P ligand bite angles.

2.3.4 Trend in Coordination Space

Ligand buried volume (%V_Bur) calculations indicate that there is a general trend toward greater restriction of coordination space around the Pd centre as the steric bulk of the geminal R groups increases. This is represented by the positive relationship between %V_Bur and R group steric bulk in the order: 38.5% (**H**) < 40.5% (**Me**) < 41.3% (**Et**) < 41.8% (**iPr/iPent**) < 42.4% (**iPr**) < 43.5% (**tBu**). This suggests a trend of increasing hindrance of the coordination sphere due to the *gem*-dialkyl effect.

2.4 Hydroformylation

2.4.1 Pd-DPPP Catalysed Hydroformylation of 1-Octene

Commercially available **DPPP** has been employed to test various reaction conditions for palladium catalysed hydroformylation of 1-octene and the results are summarized in **Table 2.3**. The catalyst was formed in situ by mixing $Pd(OAc)_2$ with **DPPP** in diglyme followed by addition of CF_3CO_2H (see section **5.4.6** for details). The choice of CF_3CO_2H as acid co-catalyst was advised from a previous study conducted by Drent and Budzelaar.[51-52]

Table 2.3 DPPP modified palladium catalysed hydroformylation of 1-octene.[a]

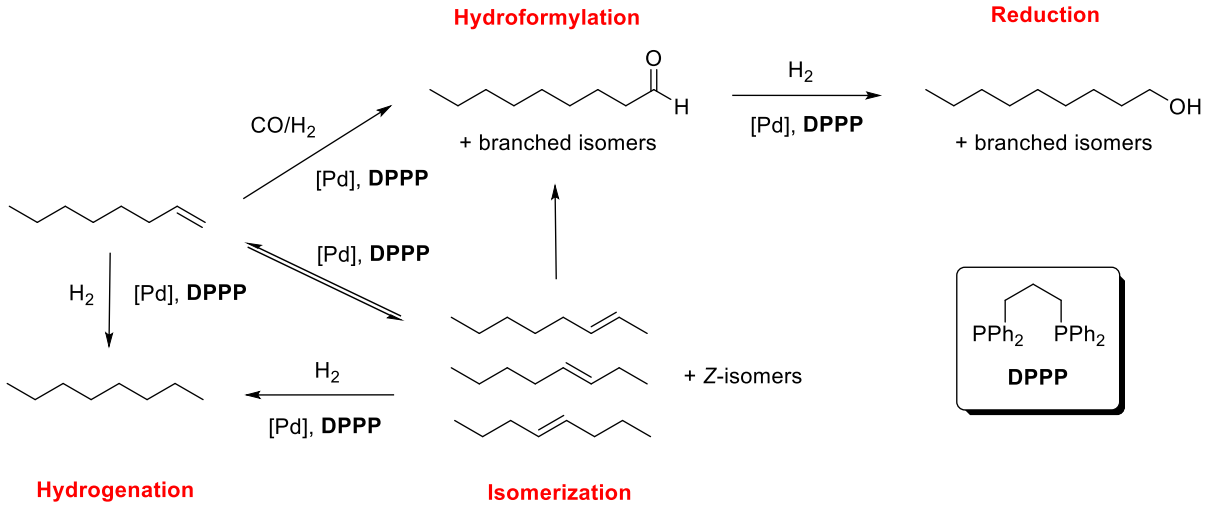

#	L/ Pd	Acid/ Pd	Temp / °C	Conv / %	Internal Octenes (Isom.)[b] / %	Octane / %	Nonanal (lin.)[c] / %	Nonanol (lin.)[c] / %	TON[d]
1	2.4	4	125	72	36 (56)	4	25 (84)	0 (n.a.)	120
2[e]	2.4	4	125	54	43 (48)	6	0 (n.a.)	0 (n.a.)	0
3	0	4	125	9	3 (3)	0	0 (n.a.)	0 (n.a.)	0
4	2.4	0	125	9	3 (3)	0	0 (n.a.)	0 (n.a.)	0

5	2.4	50	125	99	46 (98)	4	46 (73)	2 (90)	230
6	1.1	50	125	99	50 (98)	6	42 (72)	1 (91)	210
7	1.1	4	110	6	3 (4)	0	3 (84)	0 (n.a.)	10
8	1.1	4	125	63	29 (47)	5	27 (83)	0 (n.a.)	130
9	1.1	4	150	53	34 (42)	3	10 (86)	0 (n.a.)	50

[a]Conditions: 1-octene (2 mL), **DPPP**, $Pd(OAc)_2$ (0.21 mol%), CF_3CO_2H, 60 bar CO/H_2 (1:1), diglyme (15 mL), 5 h. n.a. = not applicable. [b]Isomerisation = sum of internal octenes/sum of all octenes. [c]Linearity = 1-isomer/sum of all regioisomers. [d]TON = sum of moles of nonanal and nonanol/moles of the catalyst. [e]no CO/H_2. Note: all single runs.

The initial experiment (run 1) duplicating the reaction conditions by Drent and Budzelaar[51] gave moderate conversion (72%) to a mixture containing internal octenes, nonanal and octane. Some olefin hydrogenation to paraffins is expected due to the affinity palladium has for hydrogenation.[53] In the experiments using Acid/Pd = 4 (runs 1 – 3 and 7 – 9), the product mixture also contained black solid that is suspected to be palladium black from catalyst decomposition. Palladium black has been reported to catalyse the hydrogenation of octene,[54] and may also be involved in the production of octane observed. Unexpectedly, even in the absence of syngas (run 2), there is still olefin hydrogenation to octane observed (6%). Acids have been known to act as alternative hydrogen sources for palladium catalysed transfer hydrogenation of olefins.[55-56] However, in run 2 there is an insufficient amount of acid (0.8 mol%) to account for the amount of octane produced (6%). Alternatively, octene may be disproportionating to give octadiene and octane. The palladium catalysed disproportionation of cyclohexene to cyclohexane and benzene as well as the palladium catalysed transfer hydrogenation of olefins using cyclohexene as a hydrogen donor has been described in the literature.[57-58]

2.4.2 Octene Isomerisation

In the absence of syngas (run 2, **Table 2.3**), olefin isomerisation is still observed (43% internal octenes). A survey of the literature reveals at least two possible mechanisms of olefin isomerisation, a π-allyl mechanism[59] and an addition-elimination mechanism[60-61] (**Figure 2.21**).

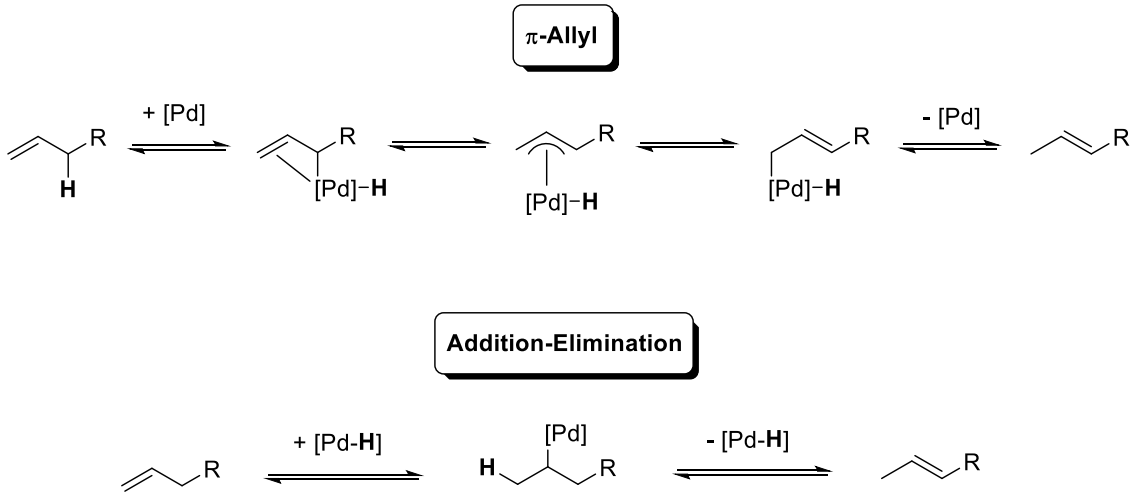

Figure 2.21 Two mechanisms of metal catalysed olefin isomerisation.

The π-allyl mechanism proceeds via the oxidative addition of C-H to a Pd(0) complex to generate a Pd-alkyl species. The Pd-alkyl species shifts the double bond via a π-allyl intermediate before reductively eliminating the isomerised olefin. The addition-elimination mechanism on the other hand, proceeds via addition of a Pd-hydride complex across the double bond to give a Pd-alkyl intermediate. The Pd-alkyl intermediate then performs a β-hydride elimination to generate the isomerised olefin.

At first glance, run 2 (**Table 2.3**) showing olefin isomerisation in the absence of H_2 appears to favour the π-allyl mechanism. However, the required Pd-hydride for the addition-elimination mechanism may also be generated through reaction with an acid (**Figure 2.22**).

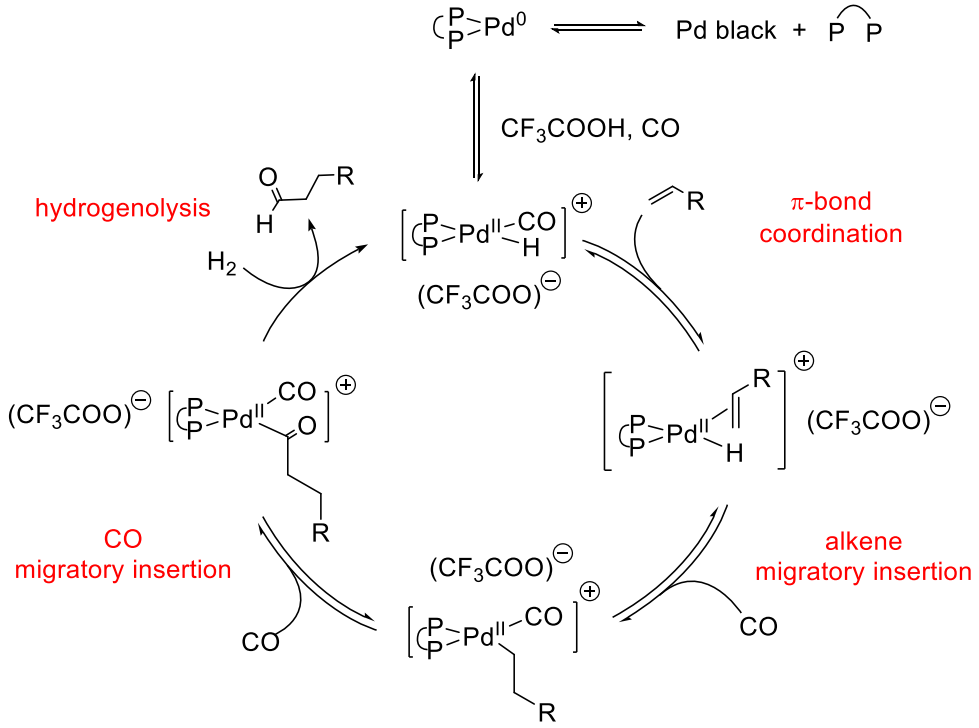

Figure 2.22 Proposed mechanism for palladium catalysed hydroformylation of olefins, adapted from literature.[51, 62] P⌒P = diphosphine ligand. R = alkyl group.

In the catalytic cycle proposed above (**Figure 2.22**) adapted from Drent and co-workers,[51, 62] CF_3CO_2H protonates a cis-chelated diphosphine-Pd complex to generate the active Pd hydride intermediate. Subsequent coordination and insertion of olefin generates a Pd-alkyl intermediate that can perform β-hydride elimination to generate isomerised olefins via the addition-elimination mechanism (**Figure 2.21**). The slight excess of acid relative to Pd (Acid/Pd = 4) in run 2 (**Table 2.3**) suggests that the equilibrium should favour the formation of Pd-hydride species and hence, should also favour the addition-elimination mechanism of olefin isomerisation.

2.4.3 Importance of Ligand and Acid Co-Catalyst

The lack of catalytic activity in the absence of diphosphine ligand **DPPP** (run 3, **Table 2.3**) indicates that an active catalyst cannot be generated from unmodified palladium even in the presence of acid. The lack of catalytic activity in the absence of acid (run 4, **Table 2.3**) shows that the acid co-catalyst is also essential for catalytic activity. The combination of these results shows that both ligand and acid are essential for this palladium based hydroformylation system.

2.4.4 Effect of Excess Acid

Increasing the equivalents of acid with respect to palladium to 50 (run 5, **Table 2.3**), boosts both isomerisation and hydroformylation activity, matching similar reports in the literature.[63]

Visual inspection of the product mixtures from run 5 and run 1 (**Table 2.3**) show that addition of excess acid preserves the original yellow colour of the reaction mixture with no deposition of black solid at the conclusion of the reaction. The absence of black solid in run 5 (**Table 2.3**) suggests that a robust catalyst is formed in the presence of a large excess of acid, possibly by altering the position of equilibrium (**Figure 2.22**) to decrease the concentration of Pd(0) diphosphine complex that can agglomerate to palladium black. Preservation of active catalyst by addition of a large excess of acid may also explain the increases in activity.

At Acid/Pd = 4 the resulting octene composition was 56% internal octenes with respect to all octenes (run 1, **Table 2.3**), but increasing to Acid/Pd = 50 gave a nearly thermodynamic octene composition[64] with 98% of the remaining octenes as internal octenes (run 5, **Table 2.3**), indicating that olefin isomerisation was more facile in the presence of a large excess of acid. The increase in octene isomerisation is accompanied by a corresponding decrease in linear selectivity (84% to 73%), which is likely due to an increase in internal octene concentration throughout the reaction period.

Despite the increases in hydroformylation and isomerisation activity due to the large excess of acid, olefin hydrogenation activity stays constant (4% octane yield). The unaffected paraffin yield suggests that acid plays an active role in hydroformylation instead of merely preserving the active catalyst by

preventing agglomeration to palladium black. Drent and Budzelaar have proposed that acid co-catalysts are involved in palladium catalysed hydroformylation of olefins via their conjugate base anion assisting the heterolytic cleavage of H_2 to facilitate the rate-determining hydrogenolysis step.[51] If this were the case, run 5 (**Table 2.3**) showing an increase in hydroformylation but not in olefin hydrogenation also suggests that the anions also discriminate for the Pd-acyl intermediate over the Pd-alkyl intermediate (**Figure 2.22**) when promoting hydrogenolysis, in order to increase nonanal yield without changing octane yield.

Finally, when a large excess of acid (Acid/Pd = 50) is used, reductive hydroformylation to nonanol (2%) is also observed (run 5, **Table 2.3**). A mechanism of homogeneous palladium catalysed reduction of aldehydes to alcohols has been proposed by Zhou and co-workers[65] involving Pd-hydride as the active catalyst (**Figure 2.23**).

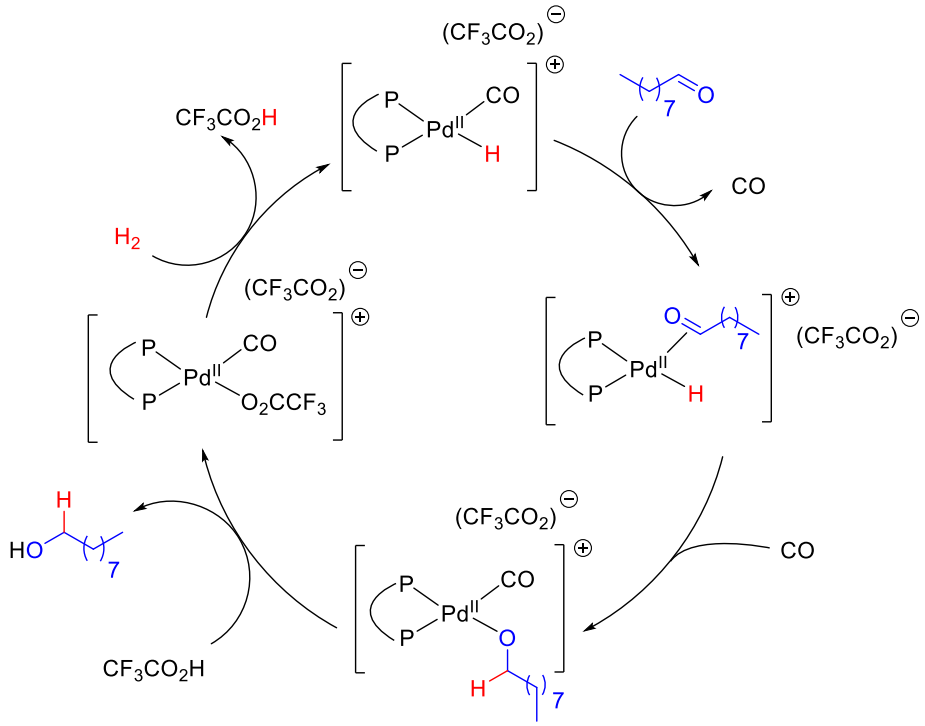

Figure 2.23 Proposed reaction mechanism for homogeneous palladium catalysed reduction of aldehydes to alcohols, adapted from Zhou and co-workers.[65]

The large excess of acid preserving the active Pd-hydride intermediate may have a two-fold effect: firstly, increasing aldehyde concentration by increasing overall hydroformylation activity and secondly, the Pd-hydride itself may be involved in reducing aldehyde to alcohol. Alternatively, assuming the insertion of aldehyde into Pd-hydride is fast and reversible, increases in acid concentration may also facilitate trapping of the Pd-alkoxide intermediate by protonation to give the alcohol product.

2.4.5 Effect of Ligand/Pd Ratio

Generally, an excess of ligand is employed in rhodium catalysed hydroformylation to stabilise the catalyst complex, prevent loss of expensive rhodium catalyst to decomposition and obtain high linear selectivities.[66] In the case of this palladium system however, hydroformylation activity and linear selectivity was maintained despite a reduction in Ligand/Pd ratio from 2.4 (run 5, **Table 2.3**) to 1.1 (run 6, **Table 2.3**), possibly due in part to catalyst stabilisation from the large excess of acid.

2.4.6 Effect of Temperature

Experiments at 110 °C, 125 °C and 150 °C (runs 7 – 9, **Table 2.3**) were conducted to investigate the relationship between temperature and catalytic performance (**Figure 2.24**).

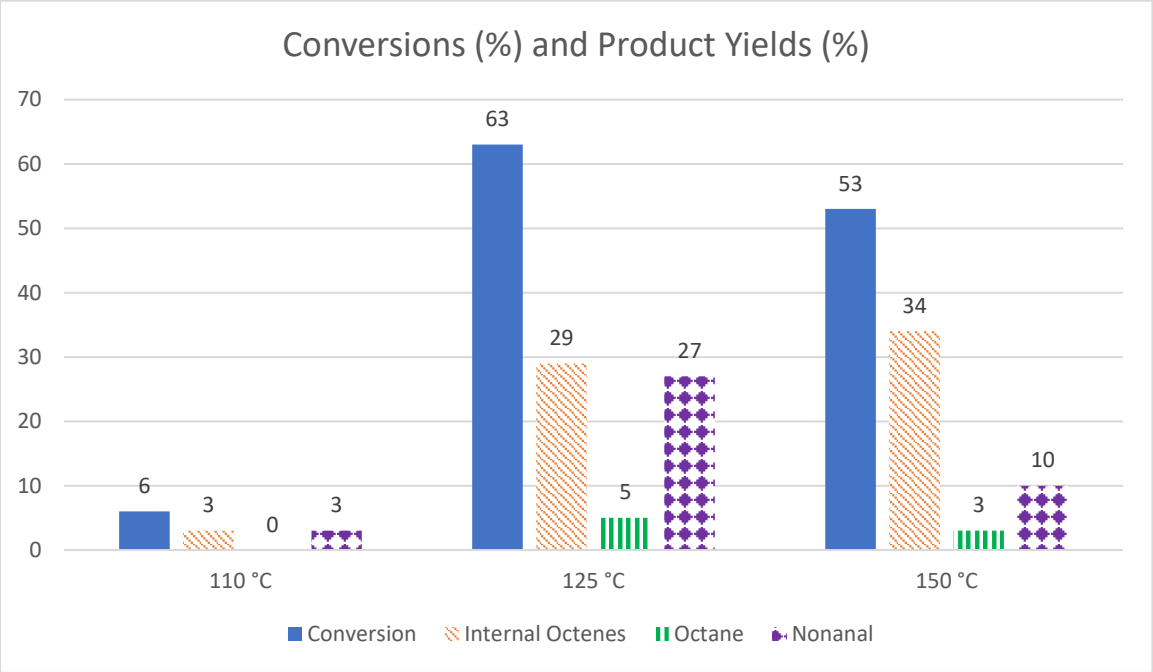

Figure 2.24 Bar graph showing product yields from **DPPP** modified palladium catalysed hydroformylation of 1-octene at 110 °C, 125 °C and 150 °C (runs 7 – 9, **Table 2.3**).

At 110 °C, there is low conversion (6%), poor isomerisation to internal octenes (3%) and low aldehyde yield (3%) likely overall poor catalytic activity at low temperature. Conversely at 150 °C, catalytic activity appears to instead be limited by catalyst thermal stability. Rapid catalyst degradation at elevated temperatures can give an initially high rate of reaction that quickly decreases to result in less productivity than if the catalyst had a sustained but lower activity. The balance between reaction temperature encouraging catalytic activity and catalyst thermal stability appears to find an optimum at 125 °C, where the highest conversion (63%) and aldehyde yield (27%) was achieved (**Figure 2.24**). It should be noted however, that the three temperatures tested are separated by a significant range that may contain yet more optimal conditions.

2.4.7 Pd-Catalysed Hydroformylation of Olefins

The PPh_2 ligand series consisting of **DPPP**, **DPPDMP**, **DPPIPIPP** and **DPPDIPP** has been evaluated in palladium catalysed hydroformylation of olefins and the results are summarised in **Table 2.4**. The catalyst was formed in situ by mixing $Pd(OAc)_2$ with diphosphine ligand in diglyme followed by addition of CF_3CO_2H (see section **5.4.6** for details).

Table 2.4 Palladium catalysed hydroformylation of olefins.[a]

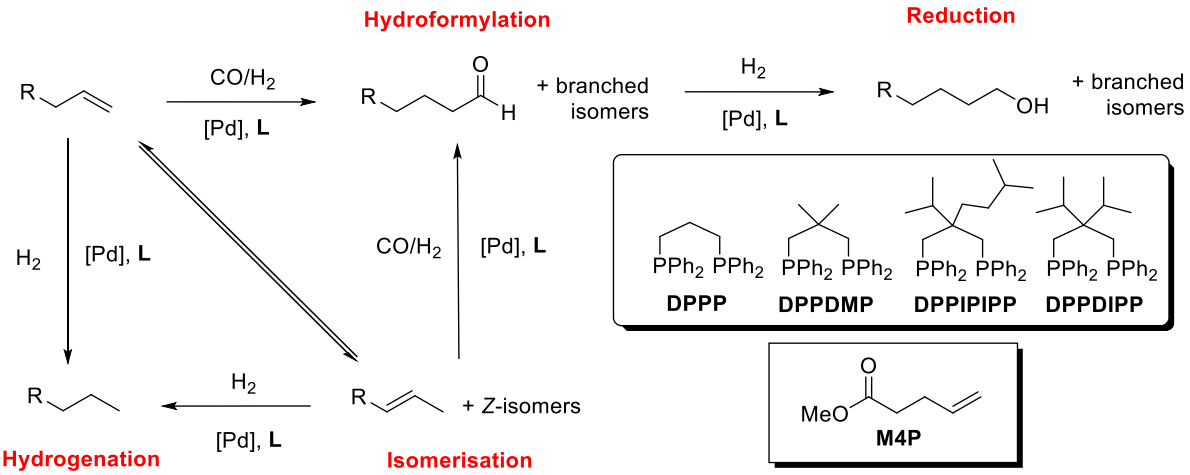

#	Olefin	Ligand	L/ Pd	Conv / %	Internal Olefins (Isom.)[b] / %	Alkane / %	Aldehyde (lin.)[c] / %	Alcohol[d] (lin.)[c] / %	TON[e]
1[f]	1-octene	**DPPP**	2.4	72	36 (56)	4	25 (84)	0 (n.a.)	120
2[f]	1-octene	**DPPDMP**	2.4	75	40 (61)	5	24 (84)	0 (n.a.)	110
3	1-octene	**DPPP**	2.4	99	46 (98)	4	46 (73)	2 (90)	230
4	1-octene	**DPPDMP**	2.4	99	55 (98)	7	36 (72)	1 (91)	180
5	1-octene	**DPPIPIPP**	2.4	98	66 (97)	8	16 (67)	6 (91)	100
6	1-octene	**DPPIPIPP**	1.1	97	69 (96)	9	18 (70)	2 (94)	100
7[g]	1-octene	**DPPIPIPP**	1.1	99	46 (98)	4	13 (50)	24 (89)	180
8[h]	1-octene	**DPPP**	1.1	99	28 (98)	0	67 (70)	2 (88)	410
9[h]	1-octene	**DPPDMP**	1.1	99	41 (98)	0	51 (70)	2 (89)	310
10[h]	1-octene	**DPPIPIPP**	1.1	99	51 (98)	1	34 (67)	9 (91)	250
11[h]	1-octene	**DPPDIPP**	1.1	99	53 (98)	0	30 (67)	9 (90)	230
12	*trans*-2-octene	**DPPP**	2.4	37	78 (99)	4	18 (71)	<1 (n.d.)	90

13	*trans*-2-octene	**DPPDMP**	2.4	27	86 (99)	4	7 (69)	<1 (n.d.)	30
14[h]	*trans*-4-octene	**DPPP**	1.1	58	66 (99)	0	27 (66)	1 (83)	170
15[h]	*trans*-4-octene	**DPPDMP**	1.1	48	75 (99)	0	14 (65)	1 (82)	90
16[f,h]	M4P	**DPPP**	2.0	63	15 (29)	1	38 (84)	0 (n.a.)	230
17[f,h]	M4P	**DPPDMP**	2.0	65	18 (34)	1	38 (86)	0 (n.a.)	230

[a]Conditions: olefin (12.7 mmol), Pd(OAc)2 (0.21 mol%), ligand (L/Pd = 2.4), CF_3CO_2H (Acid/Pd = 50), 60 bar CO/H_2 (1:1), diglyme (15 mL), 125 °C, 5 h. n.d. = not determined. n.a. = not applicable. [b]Isomerisation = sum of internal olefins/sum of all olefins. [c]Linearity = 1-isomer/sum of all regioisomers. [d]Derivatives of alcohol products (i.e., esters/ethers) included. [e]TON = sum of moles of aldehyde and alcohol/moles of the catalyst. [f]Acid/Pd = 4. [g]72 h. [h]Olefin (32.2 mmol), $Pd(OAc)_2$ (0.17 mol%), diglyme (30 mL), 24 h. Note: all single runs.

Product mixtures from runs using Acid/Pd = 4 (runs 1 & 2, **Table 2.4**) contained significant amounts of black solid that was assumed to be palladium black from catalyst decomposition. The similar results despite using different ligands (**DPPP** and **DPPDMP**) under these conditions may be due to rapid catalyst degradation that occurred before any appreciable difference in catalytic performance emerged. Isolation of the spent catalyst after the hydroformylation reaction revealed the formation of a bis(ligand) complex [Pd(**DPPP**)$_2$]$(CF_3CO_2)_2$ (**Figure 2.25**).

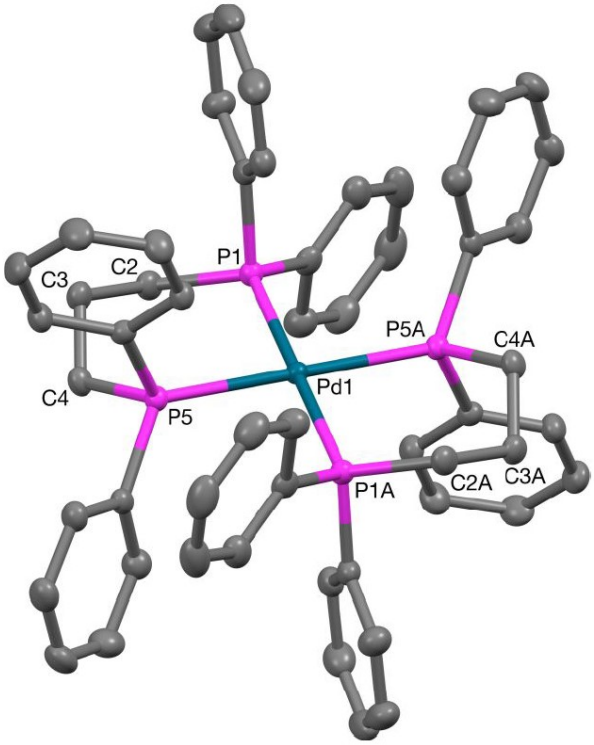

Figure 2.25 The structure of the cis-symmetric di-cationic complex present in the crystal of [Pd(**DPPP**)$_2$]$(CF_3CO_2)_2$ (50% probability ellipsoids). Structure refined by Dr. Andrew White.

Subsequent experiments were run at 125 °C to maximise conversion and at Acid/Pd = 50 for catalyst stability.

To contextualise these results, a comparison against other Pd-based hydroformylation systems is presented below (**Table 2.5**).

Table 2.5 Comparison between *gem*-dialkyl ligand **DPPIPIPP** of this work against contemporary bidentate ligands for Pd-based hydroformylation systems.

Origin	**Commercial**	**This work**	**Beller[63]**	**Drent[62]**
Ligand	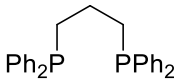	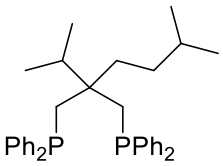	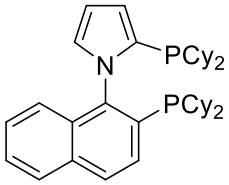	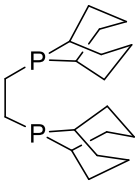
Temperature / °C	125	125	100	105
Substrate	1-Octene	1-Octene	1-Octene	1-Octene
Major Product	Nonanal	Nonanal	Nonanal	Nonanol
Yield / %	67[a]	34	42	95
***n / iso* Ratio**	2.3	2.0	2.8	3.8
TON	410	250[b]	210	480
By-products / %	-	1 (Octane)	15 (Aldol)	4 (Ketones)

Ph = Phenyl. Cy = Cyclohexyl. [a]Unable to replicate 98% yield reported by Drent[51] despite similar reaction conditions. [b]TON inclusive of nonanol product.

Despite the poorer aldehyde yield obtained with the *gem*-dialkyl ligand (**DPPIPIPP**) there is a slight shift in chemoselectivity to give a mixture of nonanal and nonanol hydroformylation products, suggesting that the *gem*-dialkyl effect can tune chemoselectivity in the reaction.

2.4.8 *gem*-Dialkyl Effects on Activity and Chemoselectivity

At Ligand/Pd = 2.4 (runs 3 – 5, **Table 2.4**), there are high conversions (98 – 99%) across the series but a trend of decreasing hydroformylation activity as steric bulk at the ligand backbone increases. Linear selectivity is hardly affected by the *gem*-dialkyl effect, remaining around 70%. In the case of **DPPIPIPP** however, there is more aldehyde reduction to nonanol observed (6%). The higher reductive hydroformylation activity of **DPPIPIPP** suggests that reductive hydroformylation of 1-octene to 1-nonanol can be favoured by increasing *gem*-dialkyl substituent size. Alcohol product linearity is generally higher than aldehyde linearity, indicating that the hydrogenation step favours primary over secondary aldehyde substrates.

2.4.9 Extended Reaction Time

Following the earlier results (runs 7 & 8, **Table 2.3**) that gave similar yields despite decreasing Ligand/Pd ratio from 2.4 to 1.1, **DPPIPIPP**/Pd ratio was decreased from 2.4 to 1.1 (runs 5 & 6, **Table 2.4**). In this case however, a decrease in reductive hydroformylation to nonanol (6% to 2%) was observed. To encourage higher yields, reaction time was extended from 5 h to 72 h (run 7, **Table 2.4**). After 72 h, nonanol yield did indeed increase to 24%, but only 14% of it existed as free alcohol in solution. During the extended reaction time, the nonanol product reacts with diglyme and CF_3CO_2H present, forming alcohol derivatives (**Figure 2.26**).

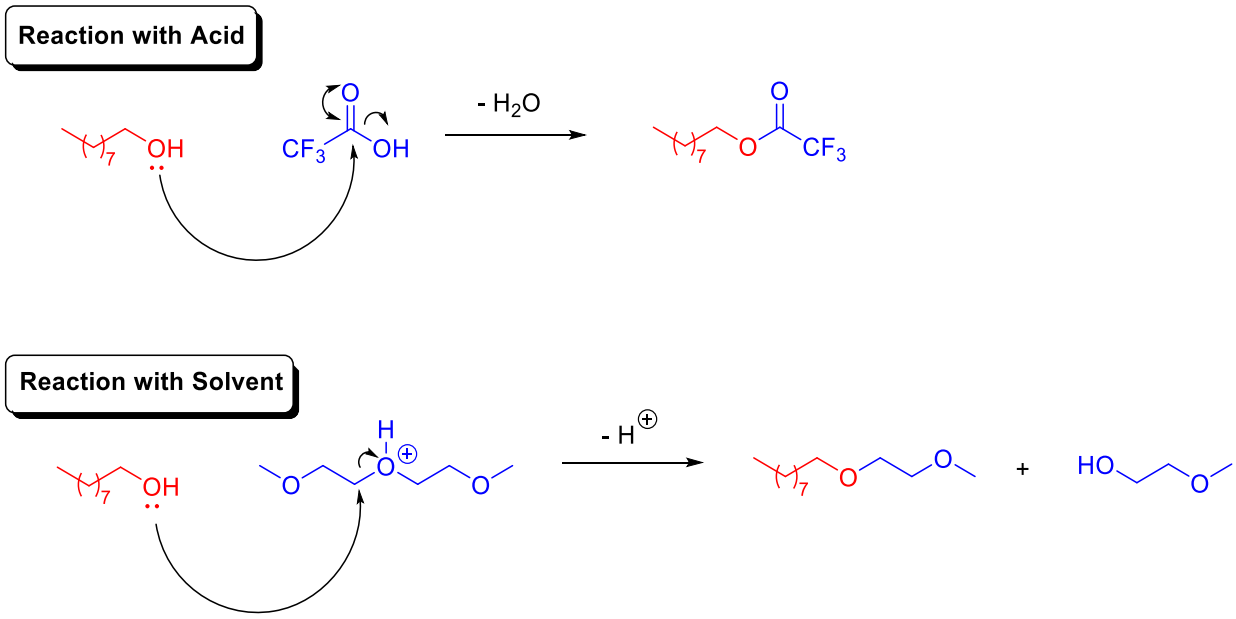

Figure 2.26 Reaction of nonanol with acid and solvent.

The nonanol (24%) obtained in run 7 (**Table 2.4**) consisted of a mixture of 14% free nonanol, 9% trifluoroacetic acid ester and 1% of glycol ether from reaction with diglyme. When reaction time was restricted to 5 hours however, alcohol derivatives are minimised (<1%) due to the low concentration of alcohol and shorter reaction time.

When reaction conditions were set to Ligand/Pd = 1.1 and 24 h (runs 8 – 11, **Table 2.4**), a trend like that for Ligand/Pd = 2.4 and 5 h was observed. Increases in geminal alkyl group steric bulk reduce nonanal formation and increase reductive hydroformylation to nonanol.

2.4.10 Gas Uptake and Kinetics

Monitoring reactor pressures showed that the rate of syngas uptake decreases over time as expected, and that most syngas uptake occurs within the first 5 h (**Figure 2.27**). Initial rates determined from the tangents to the gas uptake curves for the first 12 min gave the relative initial rates for the ligand series as 2.5 (**DPPP**) > 2.0 (**DPPDMP**) > 1.6 (**DPPIPIPP**) > 1.0 (**DPPDIPP**).

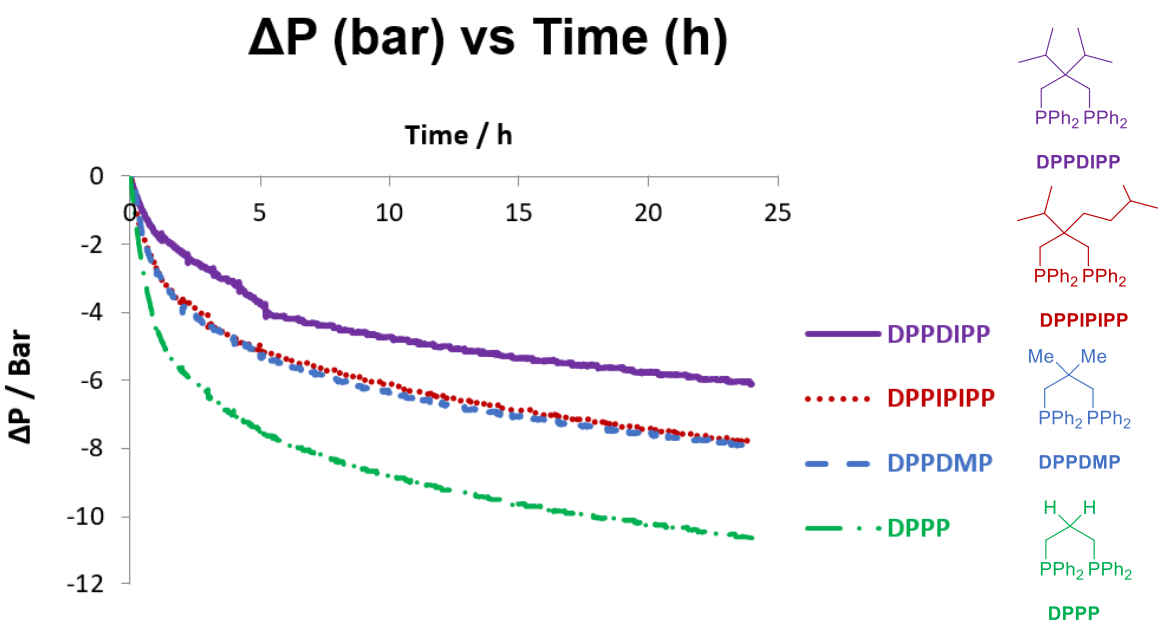

Figure 2.27 Pressure profile for hydroformylation runs 8 – 11 (**Table 2.4**).

The *gem*-dialkyl effect appears to reduce the rate of hydroformylation, possibly due to the increasingly restricted coordination space (as indicated by %V_Bur, see sub-section **2.2.8**) which may hinder the approach of reactants.

2.4.11 Pd-Catalysed Hydroformylation of Internal Alkenes

Internal alkenes (*trans*-2-octene and *trans*-4-octene) could also be hydroformylated using catalysts formed from **DPPP** and **DPPDMP** (runs 12 – 15, **Table 2.4**), indicating that isomerising hydroformylation is possible with these ligands, albeit with lower conversion compared to that of 1-octene. Comparison of the experiments run under similar conditions revealed a roughly 60% reduction in TON compared to 1-octene when using either *trans*-2-octene (runs 3 vs 12, **Table 2.4**) or *trans*-4-octene (runs 8 vs 14, **Table 2.4**) as substrate. Hydroformylation of internal alkenes was observed to be slower than for terminal alkenes, suggesting that olefin isomerisation is rate-determining in this case.[67-68]

2.4.12 Pd-Catalysed Hydroformylation of Methyl 4-Pentenoate (M4P)

The alkenoate ester, methyl 4-pentenoate (M4P), has also been investigated as a substrate for catalysts formed from **DPPP** and **DPPDMP** (runs 16 & 17, **Table 2.4**). Competing olefin hydrogenation to low value methyl esters[69-70] is an undesired side reaction that is often exacerbated for functionalised olefin substrates such as alkenoate esters.[71-72] Both **DPPP** and **DPPDMP** gave similar conversions (63 – 65%) with moderate aldehyde yield (38%) and low olefin hydrogenation (1%), indicating that these ligands are suitable to be applied for the hydroformylation of terminal alkenoate esters. The poor isomerisation activity also suggests that hydroformylation is fast relative to isomerisation, hindering

significant formation of the thermodynamically favoured α,β-unsaturated methyl 2-pentenoate ester that has been reported to be more prone to hydrogenation.[73-74]

2.4.13 Mechanistic Aspects of Pd-Catalysed Hydroformylation

The mechanism for the palladium catalysed hydroformylation reaction has been little studied in contrast to rhodium catalysed hydroformylation.[66, 75] Based on currently available information, the formation of $[Pd(ligand)(CO)H]^+$ (**I**, **Figure 2.28**) under reaction conditions ($p(CO/H_2)$ = 60 bar) is assumed as the starting point in the catalytic cycle, formed from $[Pd(ligand)X_2]$ through the heterolytic activation of H_2 and CO coordination.[76-77] An associative substitution with the olefin substrate will give $[Pd(ligand)(olefin)H]^+$ (**III**, **Figure 2.28**), which undergoes migratory insertion to yield a Pd-alkyl complex (**VII**, **Figure 2.28**). Preliminary DFT calculations of these initial steps in the catalytic hydroformylation cycle for the complexes with three symmetrically substituted *gem*-dialkyl ligands (R = H, Me and ^{t}Bu) have shown that the *gem*-dialkyl effect does not affect the overall energy barriers for olefin coordination and insertion (+25.3, +25.7 and +24.7 kcal/mol for H, Me and ^{t}Bu, respectively).

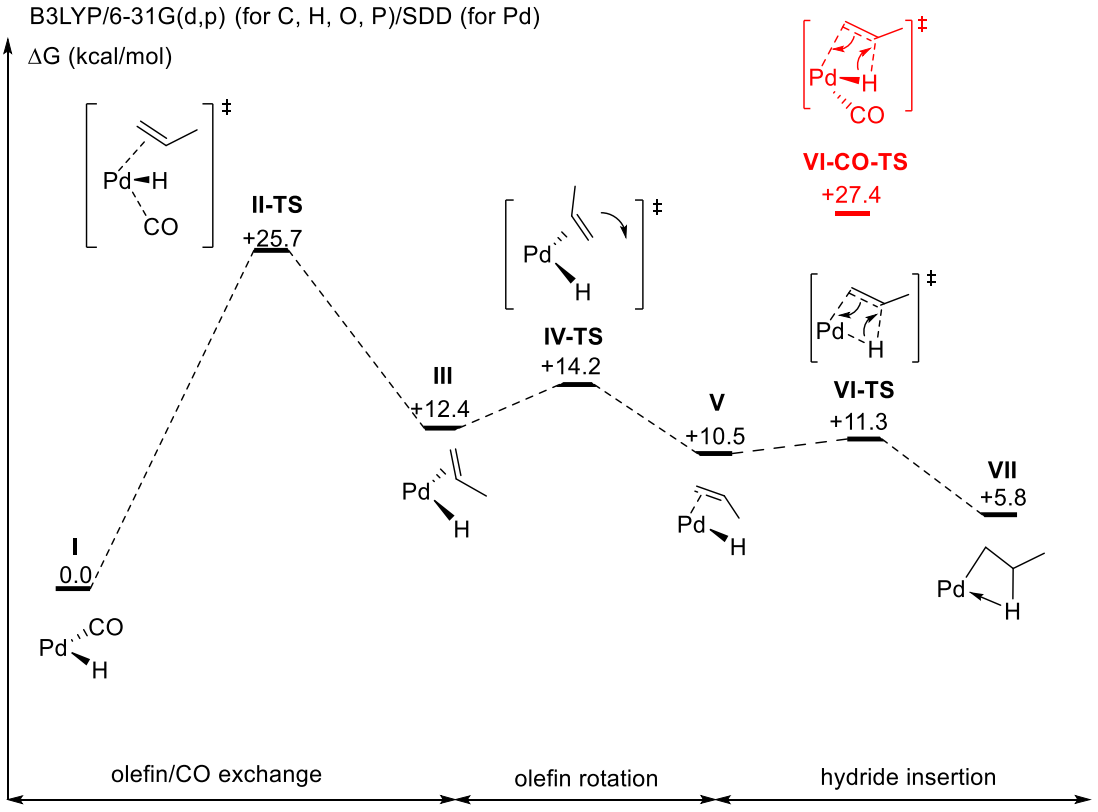

Figure 2.28 Potential energy surface (PES) showing olefin insertion pathway for [Pd(**DPPDMP**)(H)(CO)]$^+$. **DPPDMP** ligand and positive charges removed for clarity. DFT calculations carried out in collaboration with Dr. Charles Romain.[78]

This agrees with the fast olefin isomerisation observed with all catalysts. The resting state is most likely a palladium(II) acyl complex, $[Pd(ligand)(acyl)(CO)]^+$, as seen in other palladium catalysed carbonylation reactions such as alternating CO-olefin copolymerization[79] and olefin

methoxycarbonylation.[80] The final hydrogenolysis step is presumed to be rate-determining in this case, similar to methanolysis and hydrolysis reactions in methoxy- and hydroxycarbonylations.[81-82]

2.5 Pd-Catalysed Olefin Methoxycarbonylation

DTBPP and **DTBPDMP** have been evaluated in methoxycarbonylation of terminal and internal olefins and the results are summarised in **Table 2.6**. Results from **DTBPX** (industrially employed by Lucite)[83] have been included for comparison. The catalyst was formed in situ by mixing $Pd(OAc)_2$ with two equivalents of ligand in MeOH followed by the addition of CH_3SO_3H.[84]

Table 2.6 Palladium catalysed methoxycarbonylation of olefins.[a]

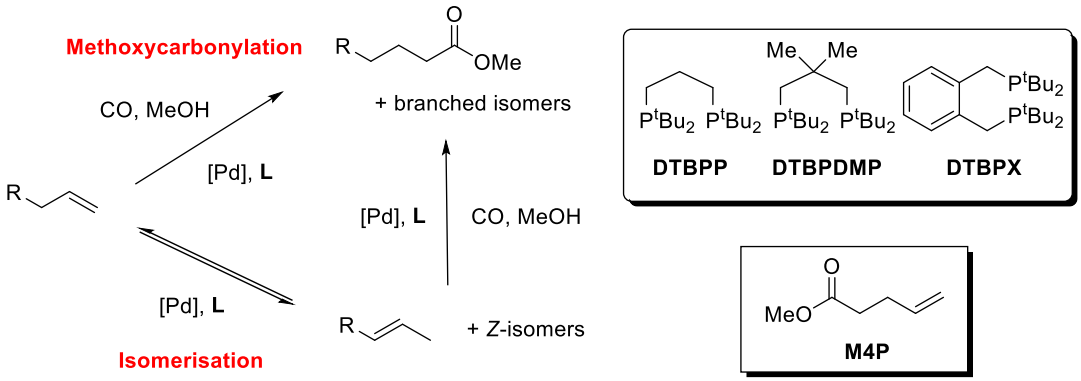

#	Olefin	Ligand	Temp / °C	Conv / %	Ester (lin)[b] / %	Olefin Yield (Relative to all Olefins) / % 1-iso	2-iso	3-iso	4-iso	TON[c]
1	1-hexene	**DTBPP**	105	98	21 (86)	2 (3)	48 (75)	14 (22)	n.a.	500
2	1-hexene	**DTBPDMP**	105	99	50 (83)	1 (3)	28 (75)	8 (22)	n.a.	1200
3	1-hexene	**DTBPX**	105	100	82 (94)	<1 (4)	8 (74)	2 (22)	n.a.	2000
4[d]	1-hexene	**DTBPDMP**	105	98	36 (86)	2 (3)	34 (77)	9 (20)	n.a.	850
5[d]	1-hexene	**DTBPX**	105	100	75 (94)	<1 (2)	10 (76)	3 (22)	n.a.	1800
6[e]	1-hexene	**DTBPDMP**	100	99	23 (86)	2 (2)	57 (75)	17 (23)	n.a.	550

Thermodynamic Distribution of Hexene Isomers[85]						(1)	(78)	(21)	n.a.	
7	1-octene	**DTBPP**	60	44	31 (89)	56 (81)	6 (9)	5 (7)	2 (3)	750
8	1-octene	**DTBPDMP**	60	13	9 (87)	87 (96)	3 (3)	1 (1)	<1 (<1)	200
9	1-octene	**DTBPP**	75	80	32 (90)	20 (29)	22 (32)	19 (28)	15 (21)	750
10	1-octene	**DTBPP**	90	98	25 (90)	2 (3)	30 (40)	28 (37)	15 (20)	600
11[e]	1-octene	**DTBPDMP**	100	99	8 (87)	1 (1)	36 (40)	33 (35)	22 (24)	200
12	1-octene	**DTBPP**	105	98	16 (87)	2 (2)	33 (39)	30 (36)	19 (23)	400
13	1-octene	**DTBPDMP**	105	94	24 (84)	6 (8)	37 (49)	24 (32)	9 (11)	600
14	1-octene	**DTBPP**	150	97	10 (89)	3 (3)	34 (38)	34 (38)	19 (21)	250
15	1-octene	**DTBPDMP**	150	98	15 (85)	2 (2)	33 (39)	32 (38)	18 (21)	350
16	*trans*-4-octene	**DTBPP**	75	3	1 (86)	<1 (<1)	1 (1)	1 (1)	97 (98)	0
17	*trans*-4-octene	**DTBPP**	105	80	17 (84)	1 (1)	32 (39)	30 (36)	20 (24)	400
18	*trans*-4-octene	**DTBPDMP**	105	21	2 (74)	<1 (<1)	11 (11)	8 (8)	79 (81)	50
Thermodynamic Distribution of Octene Isomers[64]						(1)	(39)	(33)	(27)	
19	M4P	**DTBPP**	105	98	19 (92)	n.a.	51 (65)	26 (33)	2 (2)	450
20	M4P	**DTBPDMP**	105	74	2 (91)	n.a.	26 (27)	42 (45)	26 (28)	50

[a]Conditions: olefin (80.6 mmol), $Pd(OAc)_2$ (0.04 mol%), CH_3SO_3H (Acid/Pd = 10), ligand (L/Pd = 2), 50 bar CO, MeOH (20 mL), 4 h. n.a. = not applicable. [b]Linearity = 1-isomer/sum of all regioisomers. [c]TON = moles of ester/moles of the catalyst. [d]anisole internal standard added after catalysis. [e]100 °C, heat under argon then pressurise to 50 bar CO after heating. Note: all single runs.

Initial methoxycarbonylation experiments (runs 1 – 6) were carried out with 1-hexene as the substrate. Comparison of the ester yields from the runs employing **DTBPP** (run 1) and **DTBPDMP** (run 2) show a roughly 2.5-fold increase in methoxycarbonylation activity due to the *gem*-dialkyl effect. A similar effect is observed for 1-octene (runs 12 & 13) albeit to a lesser extent of about 1.5-fold.

2.5.1 Catalyst Stability

Parallel experiments were also set-up mimicking runs 12 and 13 (**Table 2.6**) but with samples drawn at regular intervals throughout the reaction period. Regular sampling revealed that the initially amber coloured solution from the run employing **DTBPP** was decolourised after 20 min while the run employing **DTBPDMP** maintained its starting light grey colour until 1 h. This suggests that a more robust catalyst was formed from **DTBPDMP** than from **DTBPP**. Kinetic stabilisation of Pd-diphosphine chelates via the *gem*-dialkyl effect has been reported in the literature,[15] and in this case, may be the cause of the observed increase in methoxycarbonylation activity. A similar phenomenon was observed in chelation competition experiments (sub-section **2.2.3**) where the *gem*-dialkyl effect promoted the formation of chelated palladium(II) chloride complexes.

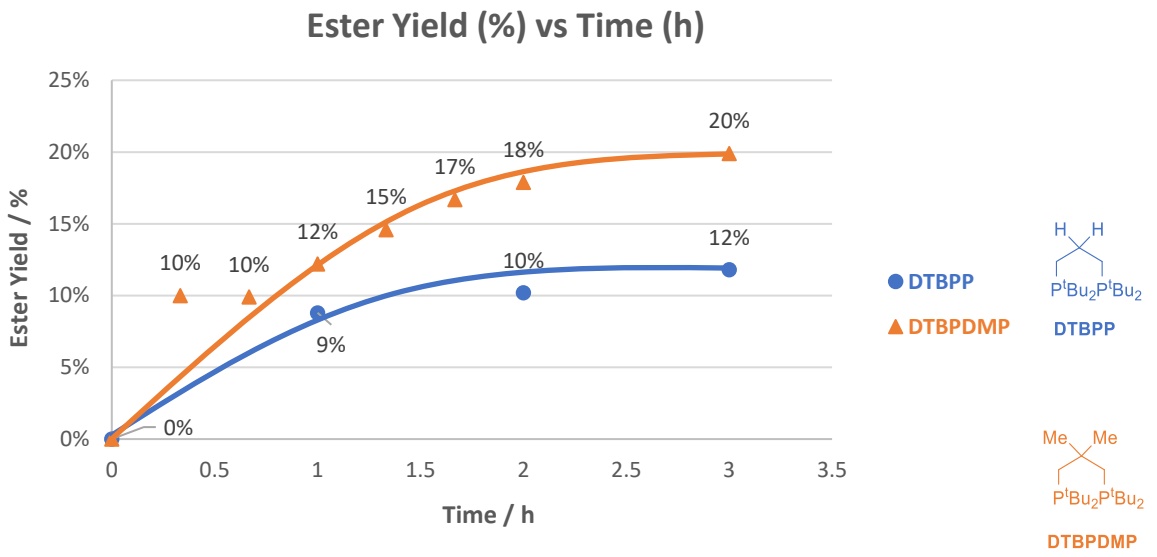

Figure 2.29 Graph of ester yield (%) vs time (h) for parallel runs mimicking runs 12 & 13 (**Table 2.6**).

Despite decolourisation of the reaction mixtures after 1 h, some methoxycarbonylation activity persisted, indicating that despite the decolourisation, the active catalyst was not entirely decomposed after 1 h. The overall ester yields were slightly decreased compared to the batch reactor runs (runs 12 & 13, **Table 2.6**) likely due losses in CO pressure during sampling.

2.5.2 *gem*-Dialkyl Effects on Octene Isomerisation

Monitoring the parallel runs mimicking runs 12 & 13 (**Table 2.6**) also revealed a divergence in the olefin isomerisation abilities of the catalysts formed from **DTBPP** and **DTBPDMP** (**Figure 2.30**).

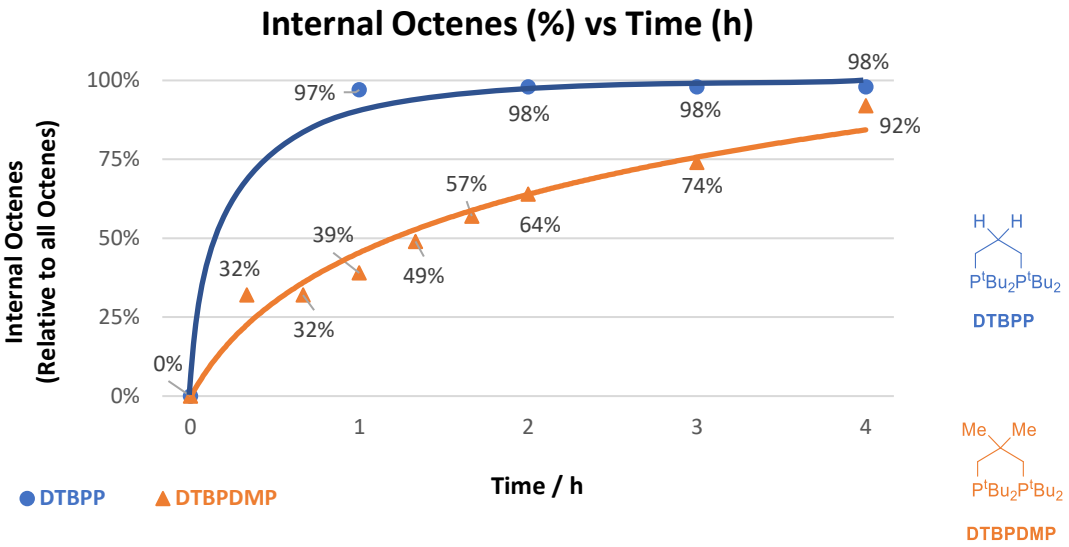

Figure 2.30 Graph of internal octenes (relative to all octenes, %) vs time (h) for parallel runs mimicking runs 12 & 13 (**Table 2.6**).

The run employing **DTBPP** exhibited facile olefin isomerisation to give a thermodynamic composition of octenes[64] quickly while the run employing **DTBPDMP** showed a gentler curve (**Figure 2.30**) indicating a slower rate of olefin isomerisation. It should be noted that as significant catalyst decomposition is observed, caution should be exercised in drawing conclusions as palladium black has also been known to catalyst olefin isomerisation.[86] The initial divergence in olefin isomerisation however, may possibly be linked to ligand flexibility. Introduction of steric bulk on the ligand backbone in **DTBPDMP** creates additional steric interactions that limit flexibility. Ligand flexibility has been noted to enable the stabilisation of a wider variety of transition states, resulting in the reduction of activation energies for multiple reaction pathways.[77] In this case, the rigidity imposed by the *gem*-dialkyl effect may restrict isomerisation ability by disfavouring the transition state leading to olefin isomerisation. Alternatively, the *gem*-dialkyl effect may instead be imposing a conformation that favours the transition state leading to methoxycarbonylation. The "facilitated transition state" phenomenon has been hypothesised as one of the possible explanations for the rate acceleration observed resulting from the *gem*-dialkyl effect.[87]

2.5.3 Effect of Anisole

The internal standard, anisole, is typically injected prior to pressurising with CO gas and heating to reaction temperature. However, runs 4 and 5 (**Table 2.6**) were carried out without any anisole in the reaction mixture. Comparison of the results from the runs revealed a promoting effect on methoxycarbonylation activity with the presence of anisole. An increase of nearly 50% in TON is observed for **DTBPDMP** upon addition of anisole (run 2 vs run 4, **Table 2.6**), while **DTBPX** shows a moderate increase of about 10% (run 3 vs. run 5, **Table 2.6**). Gusevskaya and co-workers observed a

similar promoting effect by anisole in rhodium catalysed hydroformylation, and proposed that hydrogen bonding between anisole and hydroxyl groups present on the substrate prevented their coordination and deactivation of the active catalyst.[88] In the presence of an excess of MeOH during methoxycarbonylation however, the relatively minute amount of anisole added as an internal standard might not have such an impact. Alternatively, anisole could be facilitating the rate-determining methanolysis step in the catalytic cycle by weakening the O-H bond in MeOH through hydrogen bonding, thus promoting methoxycarbonylation activity.

2.5.4 Heating under Argon

Preparation of methoxycarbonylation experiments typically followed the order of sealing the Parr reactor, charging with the prepared reaction mixture, pressurising to 50 bar with CO gas then heating to 105 °C (runs 2 and 13, **Table 2.6**). However, runs 6 and 11 (**Table 2.6**) had the prepared reaction mixture sealed in the Parr reactor under argon and heated to 100 °C prior to being pressurised with CO gas. This change resulted in a significant decrease in TON (ca. 50% for 1-hexene, run 6, **Table 2.6** and ca. 33% for 1-octene, run 11, **Table 2.6**) compared to the standard procedure (runs 2 and 13, **Table 2.6**). Aside from the 5 °C difference in temperature, pressurising before heating also results in a higher than 50 bar final pressure due to Charles's law, and pressurising after heating results in slightly less total CO added since the initial argon atmosphere expands under heat and before being topped up to 50 bar with CO. Higher CO pressures have been shown to have an inhibiting effect on olefin isomerisation,[89] but differences of up to 25 bar CO pressure are reported to have only minor effects on ester yield (± 4%) for Pd-catalysed methoxycarbonylation of 1-decene.[89] An excess of CO relative to olefin present in both cases renders the decrease in total CO added trivial and unlikely to have such an impact. It is more probable that CO pressure increases the thermal stability of the **DTBPDMP** modified palladium catalyst, possibly through favouring the formation of a [Pd(**DTBPDMP**)$(CO)_2$] complex and preventing its decomposition during heating. Ligand loss such as the loss of CO has been noted as one of the pathways for the decomposition of homogeneous catalysts.[90-91]

2.5.5 Effect of Temperature

At 105 °C, reaction mixtures from runs 12 and 13 (**Table 2.6**) decolourised with deposition of black solid observed at the end of 4 h. Samples drawn at regular intervals show that decolourisation is complete after 1 h, suggesting that at 105 °C, it is within the first hour that the difference in catalytic performance due to the *gem*-dialkyl effect occurs. Conducting the experiments at lower temperatures may preserve the active catalyst and allow for sustained catalytic activity to better identify the impact of the *gem*-dialkyl effect. Conversely, if the kinetic stability of the chelate complex is indeed improved by the *gem*-dialkyl effect,[15] higher temperatures may instead highlight the difference in catalyst

robustness. The ester yields obtained from running the reaction at different temperatures using **DTBPP** and **DTBPDMP** have been plotted below (**Figure 2.31**).

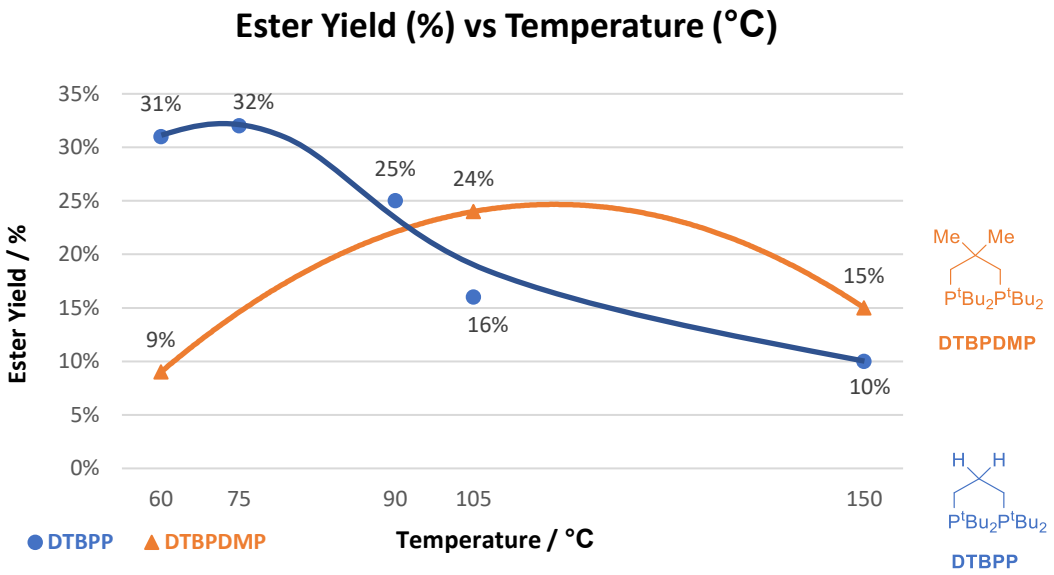

Figure 2.31 Graph of Ester Yield (%) vs Temperature (°C) for palladium-catalysed methoxycarbonylation of 1-octene (runs 7 – 10 and 12 – 15, **Table 2.6**).

At 60 °C, both **DTBPP** (run 7, **Table 2.6**) and **DTBPDMP** (run 8, **Table 2.6**) retained their original colours of yellow and grey respectively over 4 h with no deposition of black solid observed. The run using **DTBPP** almost doubles in ester yield (from 16% to 31%), likely benefiting from sustained catalytic activity from preserved active catalyst. On the other hand, the run using **DTBPDMP** shows a decrease in ester yield (from 24% to 9%) instead. In the latter case, the loss of thermal energy slowing down reaction rate or decreasing the population of complexes meeting the activation energy requirements may instead outweigh the positive effects of catalyst preservation. There is also likely to be a higher activation energy barrier for **DTBPDMP** due to its more hindered coordination sphere as indicated by its greater ligand buried volume (%V_Bur) of 46.5% as compared to the 45.2% of **DTBPP**.

Ester yields from the runs using **DTBPP** generally decrease as reaction temperature increases from 60 °C to 150 °C (**Figure 2.31**), likely due to increasingly rapid catalyst decomposition. The runs using **DTBPDMP** show an initial increase in ester yield, reaching a maximum near 105 °C before decreasing with increasing reaction temperature over the same range (**Figure 2.31**). The maximum ester yield for runs using **DTBPDMP** was obtained at a higher temperature (105 °C) than **DTBPP** (75 °C), suggesting that the *gem*-dialkyl effect results in a more thermally robust active catalyst.

Employing **DTBPP** at 60 °C results in hardly any olefin isomerisation observed, leaving most of the starting octene untouched in a composition of 81:9:7:3 for 1-, 2-, 3- and 4-octenes in the product mixture (run 7, **Table 2.6**). An ester yield of 31% was still obtained at this temperature despite the lack

of isomerisation activity, suggesting that the activation energy barrier for methoxycarbonylation is lower than that for isomerisation in this case.

2.5.6 Pd-Catalysed Methoxycarbonylation of *Trans*-4-Octene

The internal alkene, *trans*-4-octene, has been investigated as substrate using catalysts formed from **DTBPP** and **DTBPDMP** (runs 16 – 18, **Table 2.6**). At 105 °C, the catalyst formed from **DTBPDMP** was nearly inactive (2% ester yield), with most of the starting substrate (79%) left untouched at the end of 4 h (run 18, **Table 2.6**). The loss of isomerisation ability prompted by the *gem*-dialkyl effect coupled with the high linear selectivity of bulky di-*tert*-butyl phosphine ligands prevents any significant methoxycarbonylation of internal olefins. On the other hand, the superior isomerisation ability of the catalyst formed from **DTBPP** enables it to methoxycarbonylate both *trans*-4-octene and 1-octene with similar performance (16 – 17% ester yield, runs 12 and 17, **Table 2.6**). However, when reaction temperature was reduced to 75 °C, catalysts formed from **DTBPP** showed negligible catalytic activity with 97% of the starting *trans*-4-octene found in the product mixture after 4 h (run 16, **Table 2.6**), reinforcing the earlier hypothesis that the activation energy for methoxycarbonylation is lower than that for isomerisation.

2.5.7 Pd-Catalysed Methoxycarbonylation of Methyl 4-Pentenoate (M4P)

The alkenoate ester, methyl 4-pentenoate (M4P), has also been investigated as substrate using catalysts formed from **DTBPP** and **DTBPDMP** (runs 19 and 20, **Table 2.6**). The run employing **DTBPP** gave similar yields compared to internal or terminal olefin substrates, yielding 19% of the diester product and a methyl pentenoate composition of 65:33:2 for the 2-, 3- and 4-isomers (run 19, **Table 2.6**). The 2% M4P remaining indicates facile isomerisation, suggesting that **DTBPP** may also be applied in the methoxycarbonylation of internal methyl pentenoate substrates. **DTBPDMP** on the other hand showed little methoxycarbonylation activity, yielding only 2% of the diester product (run 20, **Table 2.6**). Surprisingly, the *gem*-dialkyl effect appears to have the opposite effect when methoxycarbonylating terminal alkenoate esters instead of the promoting effect observed for unfunctionalised terminal olefins (runs 12 and 13, **Table 2.6**). The presence of a carbonyl group in alkenoate esters however, enables the formation of stable 4-,[81] 5-[92] and 6-membered[93] chelates as described in the literature (**Figure 2.32**).

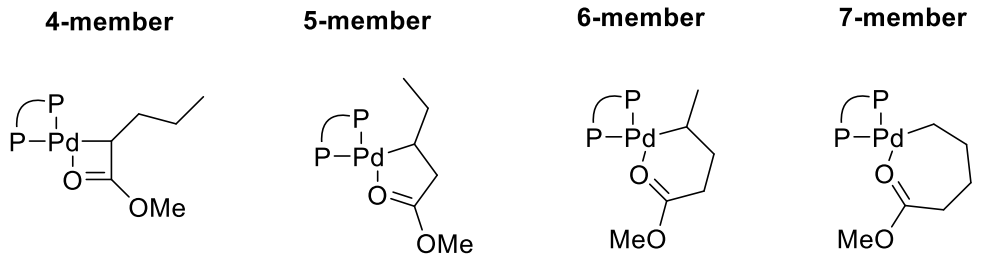

Figure 2.32 Proposed palladium chelate intermediates from reaction with methyl pentenoates. P⌢P = diphosphine ligand.

If the carbonyl group from the methyl pentenoate substrate does strongly coordinate to the Pd centre in the Pd-alkyl complex, it may require one arm of the diphosphine ligand to dissociate so that CO may coordinate and insert for methoxycarbonylation to occur. The increase in stability of the chelate complex by the *gem*-dialkyl effect in **DTBPDMP** in this case may then be counterproductive, as it would hinder phosphine dissociation and give a decrease in methoxycarbonylation activity while maintaining isomerisation activity as observed in run 13 (**Table 2.6**).

2.6 Pd-Catalysed Cyclocarbonylation of 2-Allylphenol

The synthesis of heterocycles via palladium catalysed cyclocarbonylation has been garnering interest[94-95] as a method for the preparation of pharmacological compounds.[96] In particular, 3,4-dihydrocoumarins exhibit interesting therapeutic properties that include immunomodulatory and estrogenic activity.[97-98] 3-Methyl-3,4-dihydrocoumarins (**6**, **Table 2.7**) and other lactones of similar structure may be synthesised via cyclocarbonylation of 2-allylphenol (**Table 2.7**). **DPPP**, its *gem*-dimethylated analogue **DPPDMP**, and a selection of diphosphine ligands have been evaluated in the palladium catalysed cyclocarbonylation of 2-allylphenol and the results are summarised in **Table 2.7**. The reaction conditions were adapted from a previous study by Alper and co-workers.[99]

Table 2.7 Palladium catalysed cyclocarbonylation of 2-allylphenol.[a]

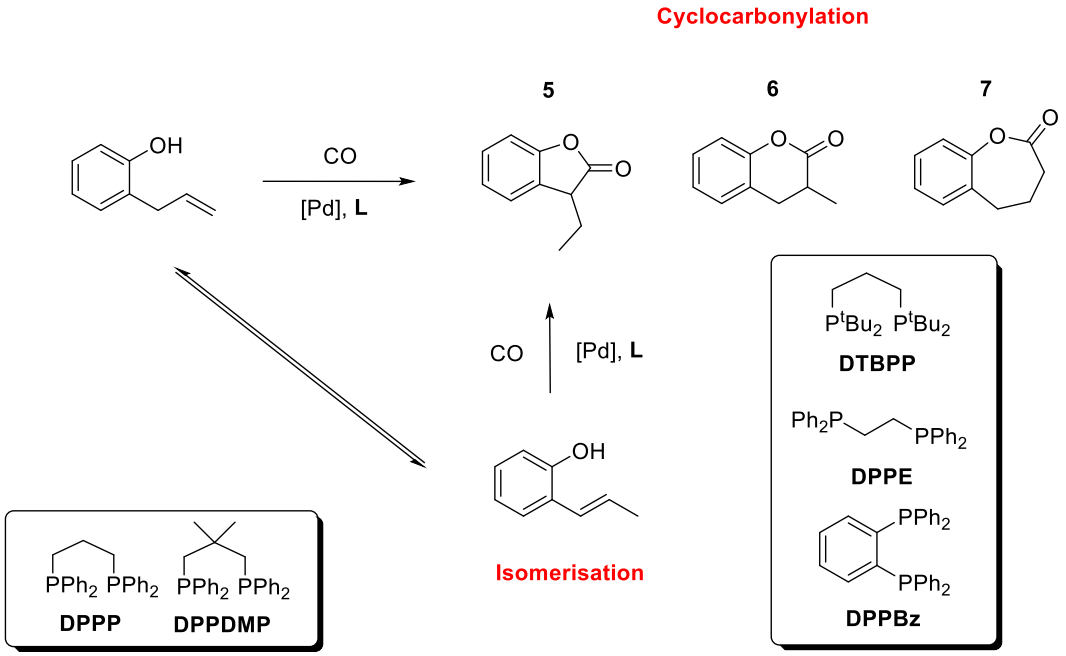

#	Ligand	Time / h	Conv. / %	Isom. / %	5 / %	6 / %	7 / %	TON[b]
1	**DTBPP**	5	30	27	2	0	1	<10
2	**DPPBz**	5	12	5	1	1	5	<10
3	**DPPE**	5	11	5	1	1	5	<10
4	**DPPP**	5	66	6	1	8	50	30
5	**DPPDMP**	5	79	7	2	8	62	40
6	**DPPP**	24	100	3	3	15	79	50
7[c]	**DPPDMP**	72	100	<1	15	12	72	200

[a]Conditions: 2-allylphenol (3.8 mmol), $Pd(OAc)_2$ (2 mol%), ligand (L/Pd = 2), 40 bar CO/H_2 (1:1), Toluene (15 mL), 90 °C. Yields were determined via ^1H NMR spectroscopy using 1,4-dioxane as an internal standard. [b]TON = sum of moles of 5-, 6- and 7-membered cyclocarbonylation products/moles of catalyst. [c]2-allylphenol (15.2 mmol), $Pd(OAc)_2$ (0.5 mol%). Note: all single runs.

The catalyst formed from **DTBPP** was inactive for Pd-catalysed cyclocarbonylation of 2-allylphenol but showed some olefin isomerisation (27%) to the thermodynamically favoured internal olefin (run 1, **Table 2.7**).

Amongst the bis(diphenylphosphine) ligands, only **DPPP** and **DPPDMP** showed significant cyclocarbonylation activity to favour formation of the 7-membered lactone product (runs 4 and 5, **Table 2.7**). Alper and co-workers previously employed **CYTOP** (**Figure 2.33**) under similar reaction conditions to obtain the 6-membereded lactone as the major product.[99] However, other palladium-based cyclocarbonylation systems using **DPPB** (**Figure 2.33**) in ionic liquid **BMIM PF_6** (**Figure 2.33**) or

(S,S)-DIOP (**Figure 2.33**) with HCl as an acid co-catalyst have also been reported to yield the 7-membered lactone as the major product from 2-allylphenol.[100-101]

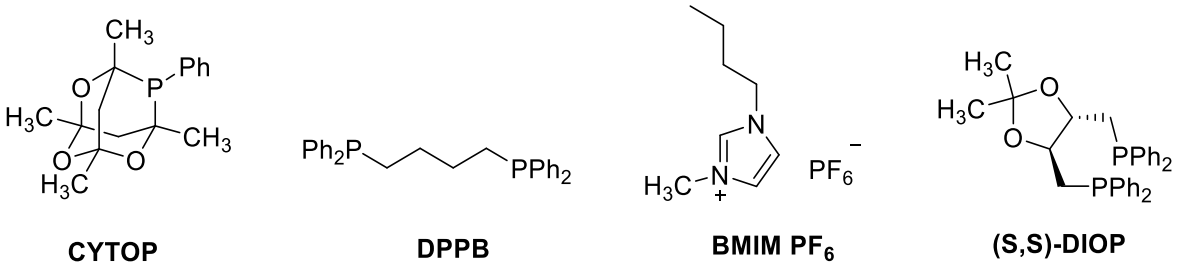

Figure 2.33 Cyclocarbonylation ligands and ionic liquid.

At full conversion, the catalyst formed from **DPPDMP** also yields more 5-membered lactone product than the catalyst formed from **DPPP** (15% vs 3% yield), although the 7-membered lactone remains the major product obtained for both ligands (runs 6 and 7, **Figure 2.33**).

2.7 Conclusions and Outlook

A series of C_3-bridged diphosphine ligands with *gem*-dialkyl groups of varying steric bulk at the central carbon of the ligand backbone has been synthesised. X-ray crystallographic analysis of the solid-state structures of the [Pd(diphosphine)Cl_2] complexes showed simultaneous external R-C-R bond angle expansion and internal C-C-C bond angle compression as a result of the *gem*-dialkyl effect. These changes are accompanied by a distortion in the conformation of the 6-membered chelate formed between the ligand and the Pd metal centre.

DFT calculations have predicted that the external angle widens with increasing R group size, but the internal angle goes to a minimum of about 107° before reverting to the ideal tetrahedral angle. Further inspection reveals that after the initial decrease in internal angle, additional tension generated by further external angle perturbation appears to be released via distortion of the 6-membered chair conformation toward a half-chair and eventually a twist-boat conformation. The compounding effects of external angle expansion, internal angle compression and chelate distortion complicate the relationship between the *gem*-dialkyl effect and ligand bite angle. However, ligand buried volume calculations indicate that increasing R group size results in a more crowded coordination sphere around the metal centre.

The PPh_2 ligand series has been evaluated in palladium catalysed hydroformylation of olefins. For 1-octene as the substrate, a decrease in hydroformylation activity was observed as a result of the *gem*-dialkyl effect. The bulkier **DPPIPIPP** (R = iPr/iPent) and **DPPDIPP** (R = iPr) ligands showed a change in chemoselectivity with increased reductive hydroformylation to the alcohol product. **DPPP** (R = H) and

DPPDMP (R = Me) have also been evaluated for the hydroformylation of internal alkenes (*trans*-4-octene and *trans*-2-octene) and an alkenoate ester (methyl 4-pentenoate). Runs using the *gem*-dimethylated ligand **DPPDMP** showed poorer isomerising hydroformylation activity for internal octenes but similar performance to the undecorated **DPPP** for methyl 4-pentenoate.

DTBPP (R = H) and **DTBPDMP** (R = Me) have also been evaluated in palladium catalysed methoxycarbonylation of olefins. For terminal alkenes (1-hexene and 1-octene) at 105 °C, the *gem*-dialkyl effect reduced olefin isomerisation and increased methoxycarbonylation activity. However, it should also be noted that significant catalyst degradation has been observed after 1 h. Decreased olefin isomerisation activity also makes catalysts formed from **DTBPDMP** poor candidates for methoxycarbonylation of internal *trans*-4-octene, while facile isomerisation exhibited by catalysts formed from **DTBPP** results in similar performance for both internal and terminal olefin substrates. For methyl 4-pentenoate as a substrate, catalysts formed from **DTBPP** again maintains a similar activity as that for octene substrates while catalysts formed from **DTBPDMP** exhibited poor methoxycarbonylation activity.

The *gem*-dialkyl effect in diphosphine ligands can be considered a relevant parameter, in addition to ligand backbone structure and the nature of P-substituents, in affecting catalytic performance. It would be interesting to further probe the mechanism for palladium catalysed carbonylation using a combination of experimental and computational methods to ascertain how the *gem*-dialkyl effect impacts the catalytic cycle. Expanding the scope to explore the viability of other nucleophiles such as amines for aminocarbonylation may be another interesting avenue to pursue. Further experiments outside of the scope of carbonylation, such as palladium catalysed hydrogenation of aldehydes to alcohols, may also aid in finding out how the *gem*-dialkyl effect influences chemoselectivity to favour reductive hydroformylation. A better understanding of the impact of *gem*-dialkyl effect on diphosphine ligands may see it mature as an effective tool in modulating catalyst activity and selectivity in future.

2.8 Chapter 2 References

1. Jung, M. E.; Piizzi, G., *Chem. Rev.* **2005,** *105*, 1735-1766.
2. Beesley, R. M.; Ingold, C. K.; Thorpe, J. F., *J. Chem. Soc., Trans.* **1915,** *107*, 1080-1106.
3. Ingold, C. K., *J. Chem. Soc.* **1921,** *119*, 951-970.
4. Galli, C.; Giovannelli, G.; Illuminati, G.; Mandolini, L., *J. Org. Chem.* **1979,** *44*, 1258-1261.
5. Bruice, T. C.; Pandit, U. K., *J. Am. Chem. Soc.* **1960,** *82*, 5858-5865.
6. Allinger, N. L.; Zalkow, V., *J. Org. Chem.* **1960,** *25*, 701-704.

7. Parker, K. A.; Adamchuk, M. R., *Tetrahedron Lett.* **1978,** *19*, 1689-1692.

8. Baldwin, S. W.; Wilson, J. D.; Aube, J., *J. Org. Chem.* **1985,** *50*, 4432-4439.

9. Ghosh, S. K.; Sarkar, T. K., *Tetrahedron Lett.* **1986,** *27*, 525-528.

10. Harfenist, M.; Thom, E., *J. Org. Chem.* **1972,** *37*, 841-848.

11. Crandall, J. K.; Tindell, G. L., *J. Chem. Soc. D* **1970**, 1411-1412.

12. Freixa, Z.; van Leeuwen, P. W. N. M., *Dalton Trans.* **2003**, 1890-1901.

13. Dierkes, P.; W. N. M. van Leeuwen, P., *J. Chem. Soc., Dalton Trans.* **1999**, 1519-1530.

14. van Rijn, J. A.; Siegler, M. A.; Spek, A. L.; Bouwman, E.; Drent, E., *Organometallics* **2009,** *28*, 7006-7014.

15. Arthur, K. L.; Wang, Q. L.; Bregel, D. M.; Smythe, N. A.; O'Neil, B. A.; Goldberg, K. I.; Moloy, K. G., *Organometallics* **2005,** *24*, 4624-4628.

16. Marcone, J. E.; Moloy, K. G., *J. Am. Chem. Soc.* **1998,** *120*, 8527-8528.

17. van Rijn, J. A.; Gouré, E.; Siegler, M. A.; Spek, A. L.; Drent, E.; Bouwman, E., *J. Organomet. Chem.* **2011,** *696*, 1899-1903.

18. van Rijn, J. A.; Lutz, M.; von Chrzanowski, L. S.; Spek, A. L.; Bouwman, E.; Drent, E., *Adv. Synth. Catal.* **2009,** *351*, 1637-1647.

19. van Rijn, J. A.; Dunnen, A. d.; Bouwman, E.; Drent, E., *J. Mol. Catal. A: Chem.* **2010,** *329*, 96-102.

20. Mul, W. P.; van der Made, A. W.; Smaardijk, A. A.; Drent, E., Catalytic Synthesis of Copolymers and Terpolymers. In *Catalytic Synthesis of Alkene-Carbon Monoxide Copolymers and Cooligomers*, Sen, A., Ed. Springer US: 2003; pp 87-140.

21. O'Neill, M. J.; Riesebeck, T.; Cornella, J., *Angew. Chem. Int. Ed.* **2018,** *57*, 9103-9107.

22. Henderson, W. A.; Buckler, S. A., *J. Am. Chem. Soc.* **1960,** *82*, 5794-5800.

23. Eberhard, M. R. New Strategies In 9-Phosphabicyclononane Chemistry. Ph.D. Thesis, University of Bristol, United Kingdom, 2001.

24. Ozturk, T.; Saygili, N.; Ozkara, S.; Pilkington, M.; Rice, C. R.; Tranter, D. A.; Turksoy, F.; Wallis, J. D., *J. Chem. Soc., Perkin Trans. 1* **2001**, 407-414.

25. Calvo-Flores, F. G.; García-Mendoza, P.; Hernández-Mateo, F.; Isac-García, J.; Santoyo-González, F., *J. Org. Chem.* **1997,** *62*, 3944-3961.

26. Kabalka, G. W.; Varma, M.; Varma, R. S.; Srivastava, P. C.; Knapp, F. F., *J. Org. Chem.* **1986,** *51*, 2386-2388.

27. Gao, Y.; Sharpless, K. B., *J. Am. Chem. Soc.* **1988,** *110*, 7538-7539.

28. Appel, R., *Angew. Chem. Int. Ed. Engl.* **1975,** *14*, 801-811.

29. Misra, G. S.; Srivastava, S. B., *J. Prakt. Chem.* **1958,** *6*, 170-173.

30. Kuchen, W.; Buchwald, H., *Chem. Ber.* **1958,** *91*, 2871-2877.

31. Dodds, D. L.; Haddow, M. F.; Orpen, A. G.; Pringle, P. G.; Woodward, G., *Organometallics* **2006,** *25*, 5937-5945.

32. Harris, T. V.; Pretzer, W. R., *Inorg. Chem.* **1985,** *24*, 4437-4439.

33. Van Overschelde, M.; Vervecken, E.; Modha, S. G.; Cogen, S.; Van der Eycken, E.; Van der Eycken, J., *Tetrahedron* **2009,** *65*, 6410-6415.

34. Seebach, D., *Angew. Chem. Int. Ed. Engl.* **1979,** *18*, 239-258.

35. Seetz, J. W. F. L.; Hartog, F. A.; Böhm, H. P.; Blomberg, C.; Akkerman, O. S.; Bickelhaupt, F., *Tetrahedron Lett.* **1982,** *23*, 1497-1500.

36. Steffen, W. L.; Palenik, G. J., *Inorg. Chem.* **1976,** *15*, 2432-2439.

37. Frew, J. J. R.; Damian, K.; Van Rensburg, H.; Slawin, A. M. Z.; Tooze, R. P.; Clarke, M. L., *Chem. Eur. J.* **2009,** *15*, 10504-10513.

38. Van Leeuwen, P. W. N. M.; Freixa, Z., Bite Angle Effects of Diphosphines in Carbonylation Reactions. In *Modern Carbonylation Methods*, Kollár, L., Ed. Wiley-VCH Verlag GmbH & Co. KGaA: Germany, 2008; pp 1-20.

39. Tolman, C. A., *Chem. Rev.* **1977,** *77*, 313-348.

40. Falivene, L.; Credendino, R.; Poater, A.; Petta, A.; Serra, L.; Oliva, R.; Scarano, V.; Cavallo, L., *Organometallics* **2016,** *35*, 2286-2293.

41. Falivene, L.; Cao, Z.; Petta, A.; Serra, L.; Poater, A.; Oliva, R.; Scarano, V.; Cavallo, L., *Nat. Chem.* **2019,** *11*, 872-879.

42. Frisch, M. J.; Trucks, G. W.; Schlegel, H. B.; Scuseria, G. E.; Robb, M. A.; Cheeseman, J. R.; Scalmani, G.; Barone, V.; Petersson, G. A.; Nakatsuji, H.; Li, X.; Caricato, M.; Marenich, A. V.; Bloino, J.; Janesko, B. G.; Gomperts, R.; Mennucci, B.; Hratchian, H. P.; Ortiz, J. V.; Izmaylov, A. F.; Sonnenberg, J. L.; Williams; Ding, F.; Lipparini, F.; Egidi, F.; Goings, J.; Peng, B.; Petrone, A.; Henderson, T.; Ranasinghe, D.; Zakrzewski, V. G.; Gao, J.; Rega, N.; Zheng, G.; Liang, W.; Hada, M.; Ehara, M.; Toyota, K.; Fukuda, R.; Hasegawa, J.; Ishida, M.; Nakajima, T.; Honda, Y.; Kitao, O.; Nakai, H.; Vreven, T.; Throssell, K.; Montgomery Jr., J. A.; Peralta, J. E.; Ogliaro, F.; Bearpark, M. J.; Heyd, J. J.; Brothers, E. N.; Kudin, K. N.; Staroverov, V. N.; Keith, T. A.; Kobayashi, R.; Normand, J.; Raghavachari, K.; Rendell, A. P.; Burant, J. C.; Iyengar, S. S.; Tomasi, J.; Cossi, M.; Millam, J. M.; Klene, M.; Adamo, C.; Cammi, R.; Ochterski, J. W.; Martin, R. L.; Morokuma, K.; Farkas, O.; Foresman, J. B.; Fox, D. J. *Gaussian 16 Rev. B.01*, Wallingford, CT, 2016.

43. Lee, C.; Yang, W.; Parr, R. G., *Phys. Rev. B* **1988,** *37*, 785-789.

44. Becke, A. D., *J. Chem. Phys.* **1993,** *98*, 5648-5652.

45. Weigend, F.; Ahlrichs, R., *PCCP* **2005,** *7*, 3297-3305.

46. Weigend, F., *PCCP* **2006,** *8*, 1057-1065.

47. Grimme, S., *Wiley Interdiscip. Rev.: Comput. Mol. Sci.* **2011,** *1*, 211-228.

48. Johnson, E. R.; Becke, A. D., *J. Chem. Phys.* **2005,** *123*, 024101.

49. Johnson, E. R.; Becke, A. D., *J. Chem. Phys.* **2006,** *124*, 174104.

50. Kireev, N. V.; Filippov, O. A.; Gulyaeva, E. S.; Shubina, E. S.; Vendier, L.; Canac, Y.; Sortais, J.-B.; Lugan, N.; Valyaev, D. A., *Chem. Commun.* **2020,** *56*, 2139-2142.

51. Drent, E.; Budzelaar, P. H. M., *J. Organomet. Chem.* **2000,** *593–594*, 211-225.

52. Drent, E., *Pure Appl. Chem.* **1990,** *62*, 661-669.

53. Červený, L., *Chem. Eng. Commun.* **1989,** *83*, 31-63.

54. Inoue, H.; Ueda, K.; Yoshida, Y.; Ogata, S.; Iwakura, C., *Denki Kagaku oyobi Kogyo Butsuri Kagaku* **1997,** *65*, 1061-1065.

55. Boudjouk, P.; Han, B.-H., *J. Catal.* **1983,** *79*, 489-492.

56. Brunel, J. M., *Tetrahedron* **2007,** *63*, 3899-3906.

57. Linstead, R. P.; Braude, F. A.; Mitchell, P. W. D.; Wooldridge, K. R. H.; Jackman, L. M., *Nature* **1952,** *169*, 100-103.

58. Braude, E. A.; Linstead, R. P.; Mitchell, P. W. D., *J. Chem. Soc.* **1954**, 3578-3585.

59. Casey, C. P.; Cyr, C. R., *J. Am. Chem. Soc.* **1973,** *95*, 2248-2253.

60. Tolman, C. A., *J. Am. Chem. Soc.* **1972,** *94*, 2994-2999.

61. Hendrix, W. T.; Von Rosenberg, J. L., *J. Am. Chem. Soc.* **1976,** *98*, 4850-4852.

62. Konya, D.; Almeida Leñero, K. Q.; Drent, E., *Organometallics* **2006,** *25*, 3166-3174.

63. Jennerjahn, R.; Piras, I.; Jackstell, R.; Franke, R.; Wiese, K.-D.; Beller, M., *Chem. Eur. J.* **2009,** *15*, 6383-6388.

64. Morrill, T. C.; D'Souza, C. A., *Organometallics* **2003,** *22*, 1626-1629.

65. Chen, Q.-A.; Ye, Z.-S.; Duan, Y.; Zhou, Y.-G., *Chem. Soc. Rev.* **2013,** *42*, 497-511.

66. Franke, R.; Selent, D.; Börner, A., *Chem. Rev.* **2012,** *112*, 5675-5732.

67. Vilches-Herrera, M.; Domke, L.; Börner, A., *ACS Catal.* **2014,** *4*, 1706-1724.

68. Kathe, P.; Fleischer, I., *ChemCatChem* **2019,** *11*, 3343-3354.

69. Slaugh, L. H.; Mullineaux, R. D. Shell Oil Co, Hydroformylation of Olefins. US3239569A, 1966.

70. Winkle, J. L. V.; Morris, R. C.; Mason, R. F. Shell Oil Company, Single Stage Hydroformylation of Olefins to Alcohols. US3420898A, 1969.

71. Meessen, P.; Vogt, D.; Keim, W., *J. Organomet. Chem.* **1998,** *551*, 165-170.

72. Drent, E.; Van Ginkel, R.; Jager, W. W. Shell Internationale Research Maatschappij B.V., Process for the Hydroformylation of an Ethylenically Unsaturated Compound. WO2004028689A2, 2004.

73. Goldbach, V.; Roesle, P.; Mecking, S., *ACS Catal.* **2015,** *5*, 5951-5972.

74. Behr, A.; Obst, D.; Westfechtel, A., *Eur. J. Lipid Sci. Technol.* **2005,** *107*, 213-219.

75. Pospech, J.; Fleischer, I.; Franke, R.; Buchholz, S.; Beller, M., *Angew. Chem. Int. Ed.* **2013,** *52*, 2852-2872.

76. Baya, M.; Houghton, J.; Konya, D.; Champouret, Y.; Daran, J.-C.; Almeida Leñero, K. Q.; Schoon, L.; Mul, W. P.; Oort, A. B. v.; Meijboom, N.; Drent, E.; Orpen, A. G.; Poli, R., *J. Am. Chem. Soc.* **2008,** *130*, 10612-10624.

77. Zuidema, E.; Bo, C.; van Leeuwen, P. W. N. M., *J. Am. Chem. Soc.* **2007,** *129*, 3989-4000.

78. Tay, D. W. P.; Nobbs, J. D.; Romain, C.; White, A. J. P.; Aitipamula, S.; van Meurs, M.; Britovsek, G. J. P., *ACS Catal.* **2020,** *10*, 663-671.

79. van Leeuwen, P. W. N. M.; Zuideveld, M. A.; Swennenhuis, B. H. G.; Freixa, Z.; Kamer, P. C. J.; Goubitz, K.; Fraanje, J.; Lutz, M.; Spek, A. L., *J. Am. Chem. Soc.* **2003,** *125*, 5523-5539.

80. Doherty, S.; Robins, E. G.; Knight, J. G.; Newman, C. R.; Rhodes, B.; Champkin, P. A.; Clegg, W., *J. Organomet. Chem.* **2001,** *640*, 182-196.

81. Roesle, P.; Dürr, C. J.; Möller, H. M.; Cavallo, L.; Caporaso, L.; Mecking, S., *J. Am. Chem. Soc.* **2012,** *134*, 17696-17703.

82. Zhao, L.; Pudasaini, B.; Genest, A.; Nobbs, J. D.; Low, C. H.; Stubbs, L. P.; van Meurs, M.; Rösch, N., *ACS Catal.* **2017**, 7070-7080.

83. Pearson, J. M.; Hadden, R. A. Lucite International UK Limited, Process for the Palladium and Phosphine Ligand Catalyzed Carbonylation of Ethylene. US6489506B2, 2001.

84. Nobbs, J. D.; Low, C. H.; Stubbs, L. P.; Wang, C.; Drent, E.; van Meurs, M., *Organometallics* **2017,** *36*, 391-398.

85. Dahl, D. B.; Davies, C.; Hyden, R.; Kirova, M. L.; Lloyd, W. G., *J. Mol. Catal. A: Chem.* **1997,** *123*, 91-101.

86. Chuc, L. T. N.; Chen, C.-S.; Lo, W.-S.; Shen, P.-C.; Hsuan, Y.-C.; Tsai, H.-H. G.; Shieh, F.-K.; Hou, D.-R., *ACS Omega* **2017,** *2*, 698-711.

87. Parrill, A. L.; Dolata, D. P., *J. Mol. Struct.: THEOCHEM* **1996,** *370*, 187-202.

88. Delolo, F. G.; dos Santos, E. N.; Gusevskaya, E. V., *Green Chem.* **2019**.

89. Gerlach, M.; Kirschtowski, S.; Seidel-Morgenstern, A.; Hamel, C., *Chem. Ing. Tech.* **2018,** *90*, 673-678.

90. van Leeuwen, P. W. N. M., *Appl. Catal., A* **2001,** *212*, 61-81.

91. Crabtree, R. H., *Chem. Rev.* **2015,** *115*, 127-150.

92. Bianchini, C.; Meli, A.; Oberhauser, W., *Dalton Trans.* **2003**, 2627-2635.

93. Johnson, L. K.; Mecking, S.; Brookhart, M., *J. Am. Chem. Soc.* **1996,** *118*, 267-268.

94. Zeni, G.; Larock, R. C., *Chem. Rev.* **2004,** *104*, 2285-2310.

95. Muzart, J., *Tetrahedron* **2005,** *61*, 9423-9463.

96. Paddon-Jones, G. C.; McErlean, C. S. P.; Hayes, P.; Moore, C. J.; Konig, W. A.; Kitching, W., *J. Org. Chem.* **2001,** *66*, 7487-7495.

97. Roelens, F.; Huvaere, K.; Dhooge, W.; Van Cleemput, M.; Comhaire, F.; De Keukeleire, D., *Eur. J. Med. Chem.* **2005,** *40*, 1042-1051.

98. Zhang, X.-f.; Wang, H.-m.; Song, Y.-l.; Nie, L.-h.; Wang, L.-f.; Liu, B.; Shen, P.-p.; Liu, Y., *Bioorg. Med. Chem. Lett.* **2006,** *16*, 949-953.

99. Amézquita-Valencia, M.; Alper, H., *Org. Lett.* **2014,** *16*, 5827-5829.

100. Ye, F.; Alper, H., *Adv. Synth. Catal.* **2006,** *348*, 1855-1861.

101. Abu Seni, A.; Kollár, L.; Pongrácz, P., *Mol. Catal.* **2019**, 110673.

Chapter 3 – Impact of Diphobane Ligand Variation on Olefin Carbonylation

3.1 Introduction to Phobane Chemistry

The bicyclic secondary phosphine known as 9-phosphabicyclononane or phobane, was first reported by Shell in 1966[1-2] for their cobalt catalysed alkene hydroformylation process.[3] Since then, the catalytic applications of phobane ligands have been expanding to include allylic substitution,[4-9] nickel catalysed ethylene oligomerisation,[10] asymmetric hydrogenation,[11] heterocyclic C-H arylation,[12] ruthenium catalysed olefin metathesis,[13-16] asymmetric hydroboration[9] and palladium catalysed olefin carbonylation.[17-19]

Phobane is a phosphacycle possessing a strained C-P-C bridgehead resulting in a bond angle smaller than the 107° typical for trigonal pyramidal structures (**Figure 3.1**).[20] For example, the C-P-C bond angle of phobane in the solid state structure of its platinum(II) chloride complex is 97°.[18]

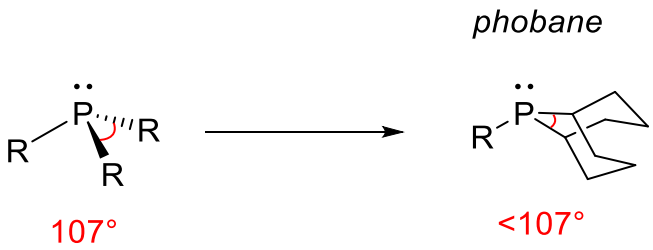

Figure 3.1 Restricted C-P-C bond angle in phobane structure. R = alkyl.

This strained geometry of the C-P-C bridgehead (**Figure 3.1**) decreases energy of the HOMO, which corresponds to the phobane lone pair. The constriction of the C-P-C angle also results in a destabilisation of the P-C σ-bonding orbitals due to poorer overlap.[21] The electronic effects of conformational distortions in tertiary phosphines and their impact on coordination chemistry have been documented by Orpen and co-workers.[22-24]

The unique characteristics of phobane have been leveraged for several catalytic carbonylation processes, for example in the direct production of alcohols from olefins.[25] The Shell reductive hydroformylation cobalt catalyst modified with eicosyl phobane produces detergent alcohols via in situ reduction of an intermediate aldehyde (**Figure 3.2**). The long eicosyl chain serves to increase the boiling point of the ligand to prevent it being distilled off with the desired alcohol product.[26-27] Palladium catalysts based on bidentate diphobanes that perform isomerising reductive hydroformylation of internal olefins to linear alcohols have also been devised by Shell for analogous reactions (**Figure 3.2**).[19] However, despite showing improvements in alcohol yield and a reduction in undesired olefin hydrogenation versus the cobalt catalysts, they were never commercialised.

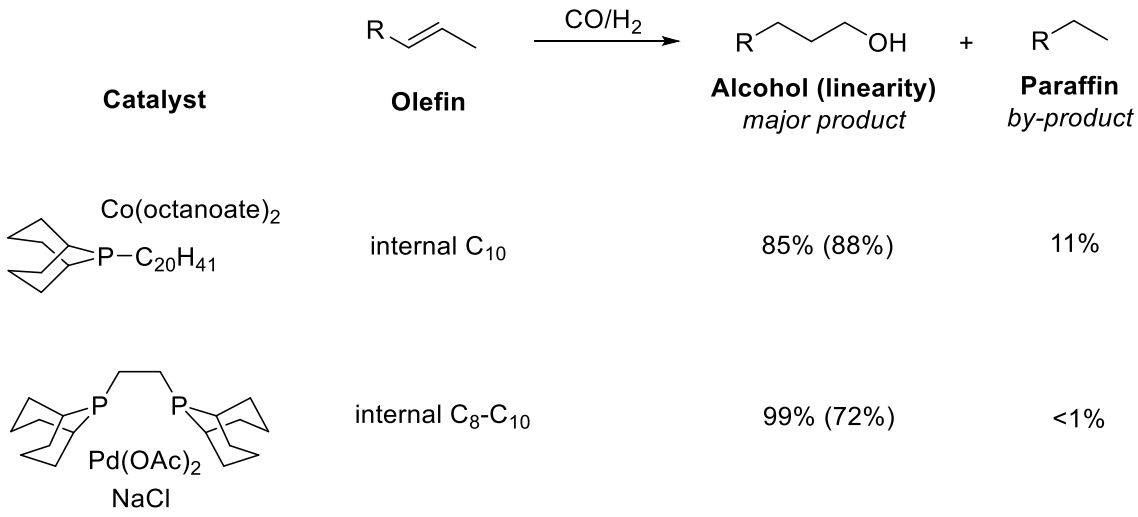

Figure 3.2 Reductive hydroformylation of internal olefins by eicosyl phobane[28] and diphobane[19] catalysts. OAc = acetate ($CH_3CO_2^-$).

Palladium-based hydroformylation catalysts are uncommon[29] compared to their rhodium- or cobalt-based counterparts that have been employed industrially.[30] However, despite its high activity and excellent selectivity,[19] there are surprisingly few reports of the Pd-diphobane system.[31-32] This may be due in part to the non-trivial synthesis of secondary phobanes involving the use of pyrophoric PH_3 gas under pressure at elevated temperatures[33] to produce a mixture of phobane isomers (**Figure 3.3**).

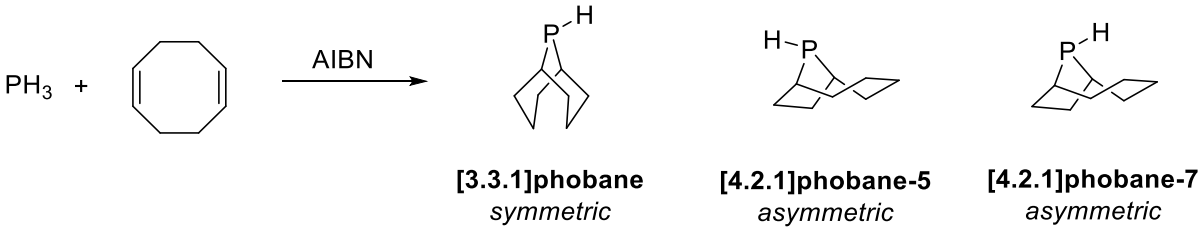

Figure 3.3 Synthesis of phobane isomers from PH_3 and 1,5-cyclooctadiene. AIBN = azobisisobutyronitrile.

PH_3 undergoes radical addition to 1,5-cyclooctadiene in the presence of a suitable initiator such as AIBN to give three possible phobane isomers, [3.3.1]phobane, [4.2.1]phobane-5 and [4.2.1]phobane-7 (**Figure 3.3**). Differences in reactivity,[34-36] spectroscopic properties,[34] coordination behaviour[37-38] and catalytic activity[18] have been reported between symmetric [3.3.1]phobane and asymmetric [4.2.1]phobane. Tertiary asymmetric [4.2.1]phobane-5 and [4.2.1]phobane-7 have also been noted to exhibit differences in donor properties.[20] The two isomers of asymmetric [4.2.1]phobane differ in the position of the H atom, where the number refers to its orientation either toward the 5- or 7-membered ring of the bicyclic structure. [4.2.1]phobane-7 however, has been reported to isomerise to the more thermodynamically stable [4.2.1]phobane-5 isomer at high temperatures (250 °C) or in the presence of water, resulting in similar catalytic performance observed for both [4.2.1]phobane isomers under

certain reaction conditions.[20] Comprehensive studies on the unique characteristics of phobanes and on their applications have been conducted by Pringle and co-workers.[20]

This chapter explores ligand backbone modification in C_2-bridged diphobane ligands (**Figure 3.4**), its influence on coordination behaviour and its impact on catalytic performance in palladium catalysed olefin carbonylation.

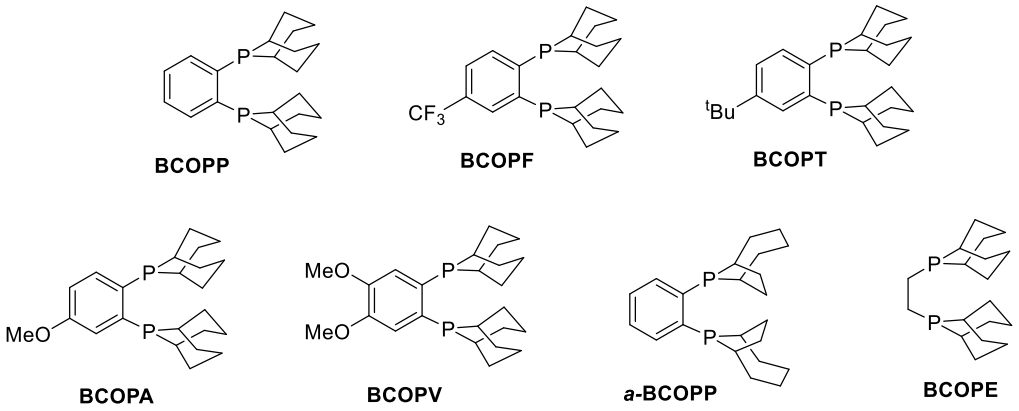

Figure 3.4 Series of C_2-bridged diphobane ligands.

1,2-Substituted-aryl-bridged diphobane ligands (**Figure 3.4**) have been synthesised and compared with the benchmark **BCOPE**. Single crystals of a selection of [Pd(diphobane)Cl_2] complexes were grown and studied via X-ray diffraction to investigate the geometries of their solid state structures. The catalytic performance of the diphobane ligands have been evaluated in palladium catalysed hydroformylation, alkoxycarbonylation and hydroxycarbonylation of olefins. In the concluding remarks, an outlook on the application of diphobane ligands in palladium catalysed olefin carbonylation will also be discussed.

3.2 Synthesis and Characterisation

3.2.1 Ligand Synthesis

Mixtures of secondary phobane isomers were separated via selective protonation of [3.3.1]phobane with aqueous HCl as reported by Pringle and co-workers.[18] Ethylene-bridged diphobane (**BCOPE**) and 1,2-phenylene-bridged diphobane (**BCOPP**) were synthesised following reported procedures.[39-40] The syntheses of 1,2-phenylene-bridged asymmetric diphobane (***a*-BCOPP**) and functionalised aryl-bridged diphobanes were achieved via palladium catalysed coupling of secondary phobane with their corresponding aryl bromide precursors, a route adapted from literature.[40] The compounds were obtained in moderate yields of 32 – 58% (**Table 3.1**). Yamaguchi and co-workers have also described an alternative preparation for sterically hindered diphosphines using bi(phosphine)boronium salts as key building blocks.[41]

Table 3.1 Synthesis of C_2-bridged diphobane ligands.[a]

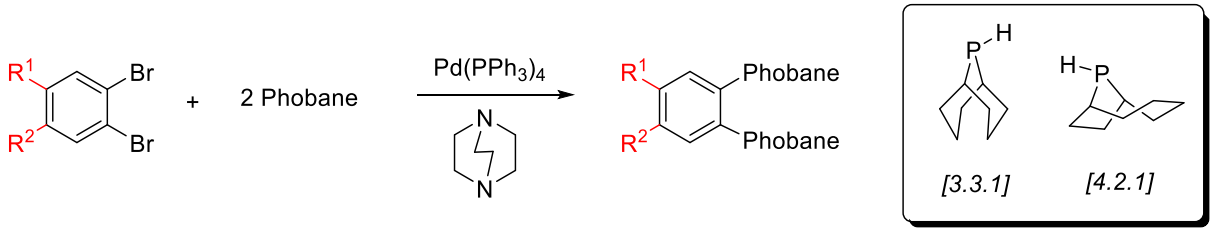

Ligand	R^1	R^2	Phobane	Isolated Yield / %	$^{31}P\{^1H\}$ / δ
BCOPF	H	CF_3	[3.3.1]	47	-15.7, -16.2
BCOPP	H	H	[3.3.1]	58	-17.3
BCOPA	H	OMe	[3.3.1]	54	-16.7, -18.7
BCOPV	OMe	OMe	[3.3.1]	33	-17.7
BCOPT	H	^{t}Bu	[3.3.1]	32	-16.7, -18.3
***α*-BCOPP**	H	H	[4.2.1]	37	3.8

[a]Conditions: dibromobenzene precursor (1 eq), phobane (2.1 eq), $Pd(PPh_3)_4$ (0.1 eq), 1,4-diazabicyclo[2.2.2]octane (5 eq), xylenes, 140 °C, 72 h.

The dry conditions and reaction temperature of 140 °C do not fulfil the conditions reported to facilitate inversion at the P atom to interconvert asymmetric [4.2.1]phobane isomers.[42] The [4.2.1]phobane isomer obtained thus maintains its integrity to exclusively give a single ***α*-BCOPP** diastereomer ($^{31}P\{^1H\}$ NMR = 3.8 ppm) that is assumed to be the conformation with minimum steric hindrance. For reference, **BCOPE** possesses a ^{31}P chemical shift of -31.2 ppm, far upfield to the aryl-bridged diphobanes, likely due to its ethylene bridge having no π-electron system for the P lone pair to delocalise into and the electron-donating effect of its alkyl chain further shielding the P atom.

3.2.2 Ligand Electronic Properties

The symmetric [3.3.1]phobane ligands exhibited chemical shifts between -16 and -18 ppm, a surprisingly small range despite the variety of electron-withdrawing (CF_3) and electron-donating (OMe, ^{t}Bu) substituents present on their aryl backbones. However, a similarly restricted chemical shift range has been observed for their analogues bearing phenyl groups on the P atom. 1,2-Bis(diphenylphosphino)benzene has a reported ^{31}P chemical shift of -12.7 ppm,[43] while its dimethoxy-substituted analogue, 1,2-bis(diphenylphosphino)-4,5-dimethoxybenzene, has a similar ^{31}P chemical shift of -12.9 ppm despite possessing two additional OMe groups on its phenylene backbone.[44] However, the difference between phenylene-bridged di-[3.3.1]phobane or di-[4.2.1]phobane is a significant downfield shift of about 20 ppm, which is indicative of the difference in their electronic properties.

The small differences in chemical shift observed despite the variety of aryl substituents suggest that ^{31}P NMR may not be the best measure of electronic properties for the respective diphobane ligands. For example, Hammett parameters indicate that a tert-butyl group should be electron-donating in both the meta and para position,[45] however, ^{31}P NMR instead shows a divergence of chemical shifts for **BCOPT**, one upfield and one downfield of the unsubstituted analogue, **BCOPP**.

A classic measure of ligand electronic properties, the Tolman electronic parameter, is determined by measuring the frequency of the A_1 CO vibrational mode in [Ni(ligand)$(CO)_3$] complexes.[46] An analogous system measuring the CO-stretching frequencies of [Rh(phosphine)(CO)Cl] complexes in solution[47] may also be adopted to avoid the toxicity associated with nickel carbonyl complexes.[48] However, mixing 1 equivalent of diphobane with 0.5 equivalents of [Rh(μ-Cl)$(CO)_2]_2$ in CH_2Cl_2 did not give a clean mononuclear [Rh(diphobane)(CO)Cl] complex as desired. Instead, ^{31}P{^{1}H} NMR of the product indicated the formation of a more symmetrical structure (**Figure 3.5**). Symmetrical Rh(I) macrocyclic and cage-like structures formed from phenylene-bridged diphosphines exhibiting similar NMR features have been reported.[49]

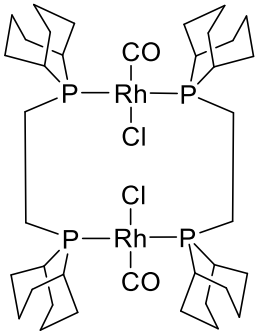

Figure 3.5 Proposed symmetric rhodium complex obtained.

3.2.3 Inductive and Mesomeric Effects of Aryl Substituents

The introduction of a single methoxy substituent on the phenylene bridge of **BCOPP** to give **BCOPA** renders the P atoms inequivalent, diverging their electronic environments based on their relative position to the methoxy group. When the methoxy group is meta to phobane, the electron-withdrawing inductive effect of the methoxy group deshields the P atom (**Figure 3.6**). Alternatively, when the methoxy group is para to phobane, a positive mesomeric effect dominates the electron-withdrawing inductive effect (that is relatively weaker over the 4-bond distance) to exert an overall shielding effect. The combination of these two effects results in **BCOPA** showing chemical shifts that are split one upfield (-1.4 ppm) and one downfield (+0.7 ppm) of unsubstituted **BCOPP** (-17.3 ppm).

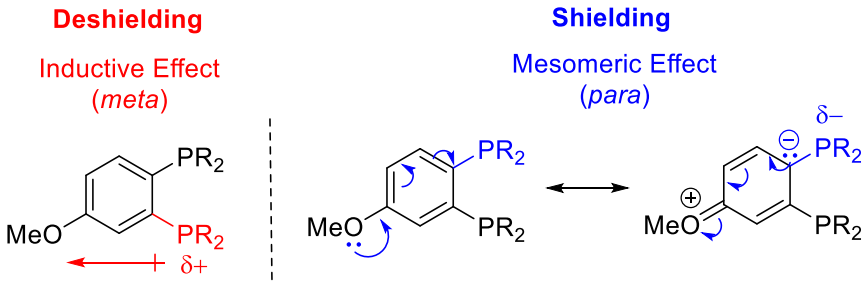

Figure 3.6 Inductive and mesomeric effects in **BCOPA**.

The introduction of a second methoxy group to give symmetrically substituted **BCOPV** results in a single ^{31}P chemical shift slightly upfield (-0.4 ppm) of **BCOPP** (-17.3 ppm), suggesting that the positive mesomeric effect outweighs the electron-withdrawing inductive effect to result in an overall shielding effect on the P atoms.

The trifluoromethyl group in **BCOPF** does not possess π electrons that can interact with the π-electron system on the aromatic phenylene ring and hence is unable to influence the phosphorus atoms via mesomeric effects. The electron-withdrawing inductive effect of the trifluoromethyl group should thus deshield each P nucleus proportionate to its relative distance to give two slightly different ^{31}P chemical shifts both downfield (+1.6 and +1.1 ppm) of **BCOPP** (-17.3 ppm).

It should be noted however, that phosphorus NMR shifts can also be significantly influenced by the circulation of electrons between its ground and excited states induced by the external magnetic field, resulting in unexpected NMR shifts unaccounted for by inductive and mesomeric effects.

3.2.4 Palladium(II) Chloride Complexes

Palladium(II) chloride complexes of ethylene-bridged di-[3.3.1]phobane (**BCOPE**), phenylene-bridged di-[3.3.1]phobane (**BCOPP**) and phenylene-bridged di-[4.2.1]phobane (***α*-BCOPP**) were prepared by mixing equimolar amounts of diphobane ligand with [Pd(1,5-cyclooctadiene)Cl_2] in CH_2Cl_2 (**Figure 3.7**). ^{31}P{^{1}H} NMR of the complexes revealed that [Pd(***α*-BCOPP**)Cl_2] (65.1 ppm) was the furthest downfield of the three as expected from [4.2.1]phobane. However, [Pd(**BCOPP**)Cl_2] (38.2 ppm) was found significantly upfield from [Pd(**BCOPE**)Cl_2] (51.3 ppm), despite having sp^2 carbon centres adjacent to its P atoms that should be more electron-withdrawing than the sp^3 ethylene carbon centres adjacent to the P atoms in **BCOPE**. Crystals suitable for X-ray diffraction were grown via slow vapour diffusion of cyclohexane into CH_2Cl_2 solutions of the complexes. Their molecular structures, along with selected bond angles and lengths, are shown in **Figure 3.8** and **Table 3.2**.

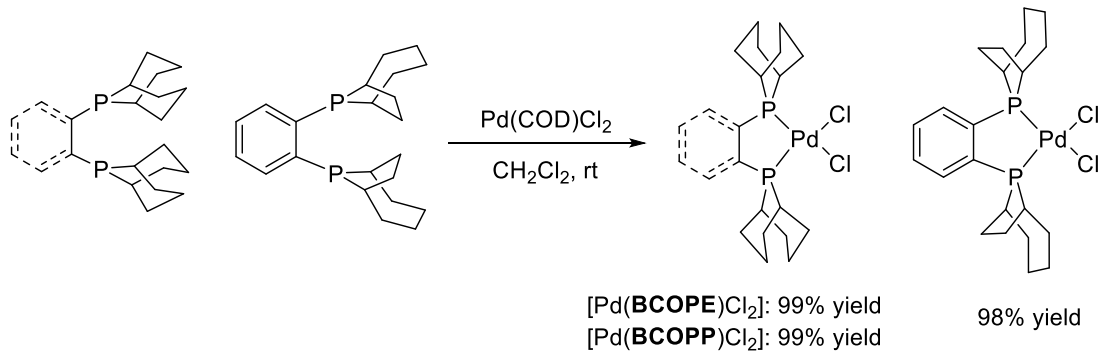

Figure 3.7 Synthesis of [Pd(diphobane)Cl_2] complexes. COD = 1,5-cyclooctadiene.

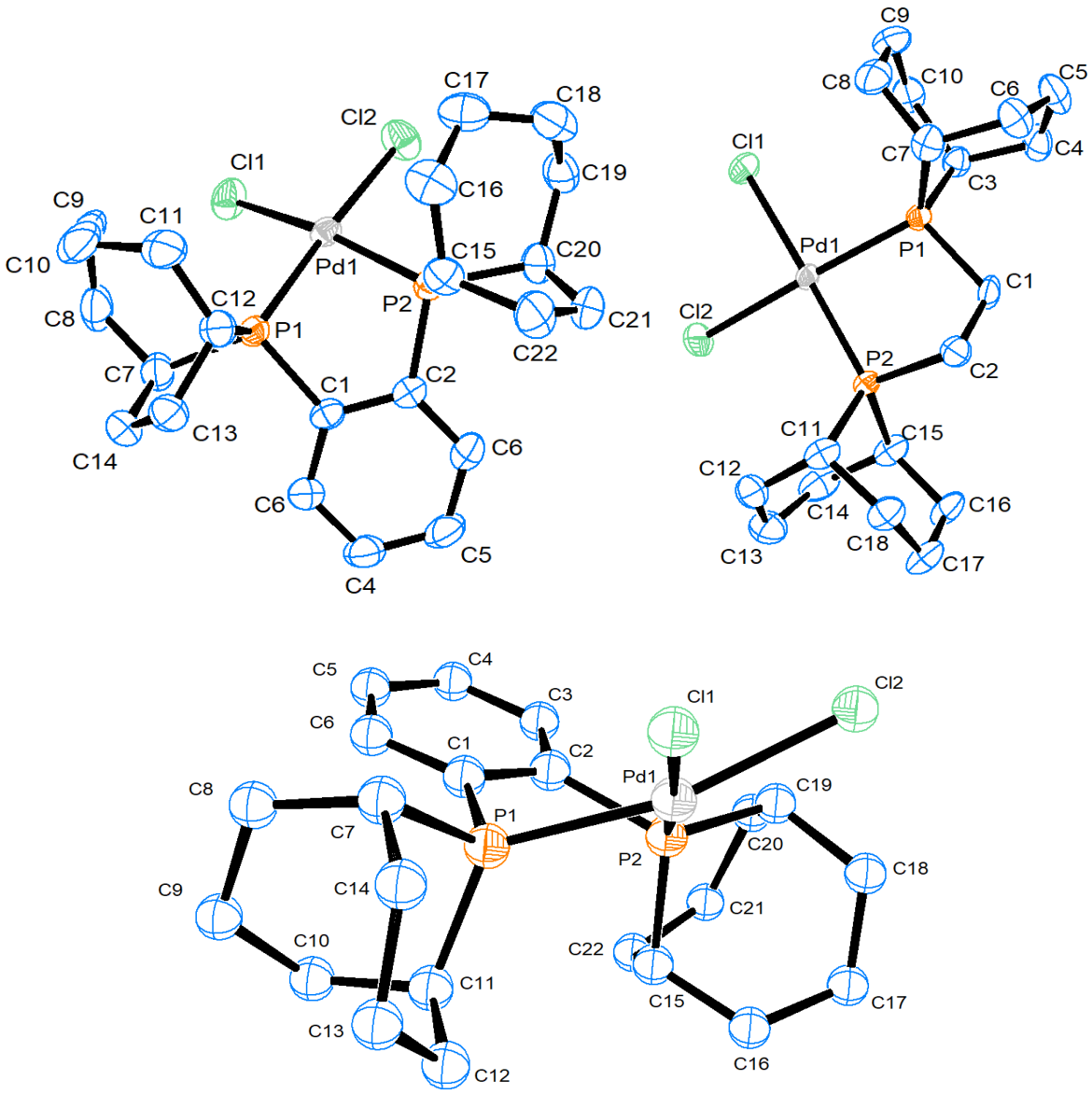

Figure 3.8 Molecular structures of [Pd(***a*-BCOPE**)Cl_2] (*top left*), [Pd(**BCOPE**)Cl_2] (*top right*) and [Pd(**BCOPP**)Cl_2] (*bottom*). Structures refined by Dr. Andrew White.

Table 3.2 Selected bond angles (°) and bond lengths (Å) of [Pd(diphobane)Cl_2] complexes.

	[Pd(**BCOPE**)Cl_2]	[Pd(**BCOPP**)Cl_2]	[Pd(***α*-BCOPP**)Cl_2]
P^1-Pd^1-P^2	85.45(5)	82.31(3)	82.18(2)
P^2-C^2-C^1	108.7(5)	115.2(2)	115.19(18)
C^2-C^1-P^1	107.4(5)	115.2(2)	115.91(19)
C^2-P^2-Pd^1	106.1(2)	99.93(11)	99.95(8)
C^1-P^1-Pd^1	106.0(2)	99.59(11)	100.81(8)
C-P^1-C (bridgehead)	96.4(3)	95.52(15)	92.74(13)
C-P^2-C (bridgehead)	96.6(3)	95.95(15)	92.64(13)
P^1-Pd^1	2.2840(15)	2.2817(8)	2.2752(6)
P^2-Pd^1	2.2752(15)	2.2484(4)	2.2661(6)
C^1-P^1	1.824(7)	1.855(3)	1.833(2)
C^2-P^2	1.834(6)	1.823(4)	1.831(3)
C^1-C^2	1.500(9)	1.405(5)	1.402(4)

Comparison of the symmetric diphobane complexes [Pd(**BCOPE**)Cl_2] and [Pd(**BCOPP**)Cl_2] show that both are 4-coordinate in the solid state and adopt square planar arrangements characteristic of d^8 complexes. Their square planar geometries, however, are slightly distorted in different ways. [Pd(**BCOPP**)Cl_2] distorts toward a square pyramidal geometry with Cl^1-P^1-P^2-Cl^2 lying within 0.09 Å of the same plane and Pd^1 displaced 0.20 Å away from that plane. [Pd(**BCOPE**)Cl_2] on the other hand, asymmetrically distorts towards a tetrahedral geometry by twisting its Cl atoms, resulting in Cl^1 shifting 0.22 Å away and Cl^2 shifting 0.19 Å away from the Pd^1-P^1-P^2 plane on opposite sides.

Due to the rigid aromatic phenylene backbone of **BCOPP**, P^1-C^1-C^2-P^2 are nearly co-planar while P^1-C^1-C^2 and P^2-C^2-C^1 bond angles are strained toward the ideal 120° for sp^2 carbon centres. This results in an 8-9° increase for its P^1-C^1-C^2 and P^2-C^2-C^1 bond angles compared to those found in the twisted sp^3 ethylene bridge in [Pd(**BCOPE**)Cl_2]. Consequently, the P atoms in [Pd(**BCOPP**)Cl_2] are about 0.1 Å closer together than in [Pd(**BCOPE**)Cl_2], resulting in [Pd(**BCOPP**)Cl_2] possessing a P^1-Pd^1-P^2 ligand bite angle of 82.31(3)° that is about 3° smaller than the 85.48(2)° found in [Pd(**BCOPE**)Cl_2]. The impact of ligand bite angle effects on catalyst performance in various reactions including hydroformylation, hydrocyanation and CO/ethylene copolymerisation have been reviewed by van Leeuwen and co-workers.[50-52]

The 5-membered chelate formed between the C_2 ligand backbone, the two P atoms and the Pd metal centre in both complexes pucker, staggering its spatial arrangement to minimise torsional strain. The phenylene backbone in [Pd(**BCOPP**)Cl_2] adopts a well-defined "envelope" conformation with C_s symmetry while the more flexible ethylene backbone in [Pd(**BCOPE**)Cl_2] allows it to twist into a C_2 symmetric "half-chair" conformation. Both complexes exhibit similar [3.3.1]phobane geometries, with the quaternary bridgehead P held in a strained position to give a C-P-C angle of about 96° and both propylene bridges folded away from the P atom in a similar conformation to that observed for the solid state structure of secondary [3.3.1]phobane in its platinum(II) chloride complex.[18]

The asymmetric diphobane complex [Pd(***a*-BCOPP**)Cl_2] is 4-coordinate in the solid state and adopts a distorted square planar geometry similar to that found in [Pd(**BCOPP**)Cl_2]. The square planar geometry distorts towards a square pyramidal arrangement with Cl^1-P^1-P^2-Cl^2 within 0.06 Å of the same plane and Pd^1 displaced 0.13 Å away from that plane. Many of the other geometric features of [Pd(***a*-BCOPP**)Cl_2] mirror those of [Pd(**BCOPP**)Cl_2], such as the reduced P^1-Pd^1-P^2 ligand bite angle compared to [Pd(**BCOPE**)Cl_2] and a 5-member chelate adopting a well-defined "envelope" conformation. The difference in asymmetric [4.2.1]phobane however, is in its asymmetric bicyclic phobane that appears to favour the conformation where the 5-membered ring is oriented toward the phenylene bridge the 7-membered ring is oriented toward the Pd atom (**Figure 3.8**). The C-P-C bridgehead of [Pd(***a*-BCOPP**)Cl_2] also shows an even more strained angle of around 93° compared with the roughly 96° found in the symmetric [3.3.1]phobanes of [Pd(**BCOPE**)Cl_2] and [Pd(**BCOPP**)Cl_2].

3.3 Phobane Coordination Chemistry

3.3.1 Implications for Catalyst Formation

Earlier work by Marson, Oort and Mul noted that in situ preparation of palladium diphosphine catalysts may be complicated by the formation of inactive bis-chelates such as [Pd(diphosphine)$_2$](OAc)$_2$.[53] They found that the formation of bis-chelates are kinetically favoured but convert to their catalytically active mono-chelate species over time. Addition of a strong acid however, locks the inactive bis-chelate species and prevents any further conversion (**Figure 3.9**).[53] They believed that the reason for this was because the conversion of the kinetically favoured bis-chelate species to the thermodynamically favoured mono-chelate species was assisted by acetate.

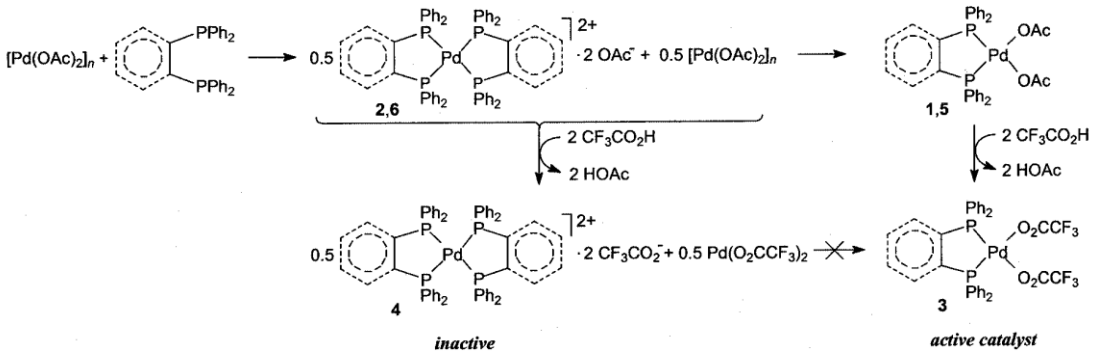

Figure 3.9[c] Reactions observed during preparation of some palladium diphosphine catalysts in situ.[53]

3.3.2 Mono- and Bischelate Formation

The mixing of 1 equivalent of Pd(OAc)$_2$ with 1.4 equivalents of **BCOPE** followed by the immediate addition of excess methanesulfonic acid was monitored by $^{31}P\{^1H\}$ NMR. The formation of two singlets at 70.2 ppm and 54.5 ppm were observed in a 1:2 ratio (**Figure 3.10**). The singlets were assigned as the mono- and bis-chelate complexes respectively based on the ^{31}P chemical shifts of similar species in literature.[54] A second experiment where the Pd(OAc)$_2$/**BCOPE** mixture was first stirred overnight before addition of excess methanesulfonic acid gave an identical composition with no difference in the ratio of the two complexes, indicating that the timing of methanesulfonic acid addition had no impact on the ratio of mono- to bis-chelate complex obtained.

[c] Reproduced with permission of the rights holder, John Wiley and Sons.

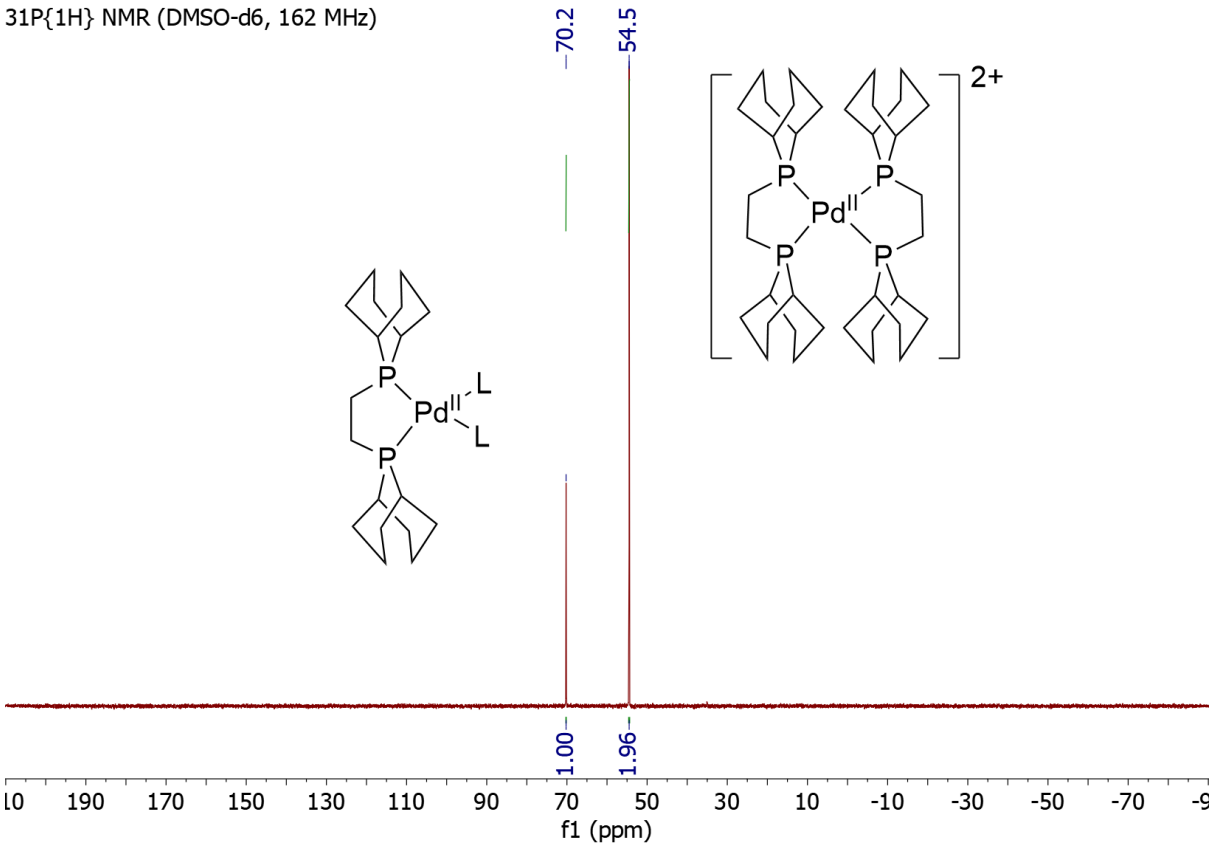

Figure 3.10 $^{31}P\{^{1}H\}$ NMR (162 MHz, DMSO-d_6, 25 °C) spectrum of mixture of 1 $Pd(OAc)_2$:1.4 **BCOPE** in DMSO-d_6 with excess CH_3SO_3H. L = $CH_3SO_3^-$ or DMSO-d_6.

In subsequent experiments, the ratio of $Pd(OAc)_2$/**BCOPE** was varied to investigate its influence on the formation of the proposed complexes. The reduction of $Pd(OAc)_2$/**BCOPE** ratio from 1/1.4 to 1/1 with immediate addition of excess methanesulfonic acid resulted in the expected increase of mono-chelate to roughly 1:1 relative to the bis-chelate species. After standing for 24 h, the ratio changed to 3:1 in favour of the thermodynamically favoured mono-chelate complex, concurring with earlier reports that the bis-chelate species is the kinetic product[53] and indicating that even in the presence of strong acid, interconversion between the bis-chelate and mono-chelate species is facile for Pd-**BCOPE** complexes. The ratio of mono-chelate to bis-chelate could also be controlled through the addition of more $Pd(OAc)_2$ or **BCOPE** respectively to favour the formation of mono-chelate or bis-chelate, again supporting that the two species readily interconvert in the presence of methanesulfonic acid.

3.3.3 Catalyst Interaction with Aqueous NaCl

The addition of a sub-stoichiometric amount of NaCl with respect to palladium has been reported to improve reductive hydroformylation activity by an order of magnitude and increase linear selectivity from 68% to 79%.[19] To investigate this phenomenon, a 1/1.5 mixture of $Pd(OAc)_2$/**BCOPE** was mixed with excess methanesulfonic acid, then 0.25 equivalents of aqueous NaCl (with respect to $Pd(OAc)_2$) added while being monitored by $^{31}P\{^{1}H\}$ NMR. The addition of aqueous NaCl resulted in the

disappearance of the singlet at 70.2 ppm corresponding to the mono-chelate species to give two new broad signals at 66.3 ppm and 59.7 ppm respectively (**Figure 3.11**).

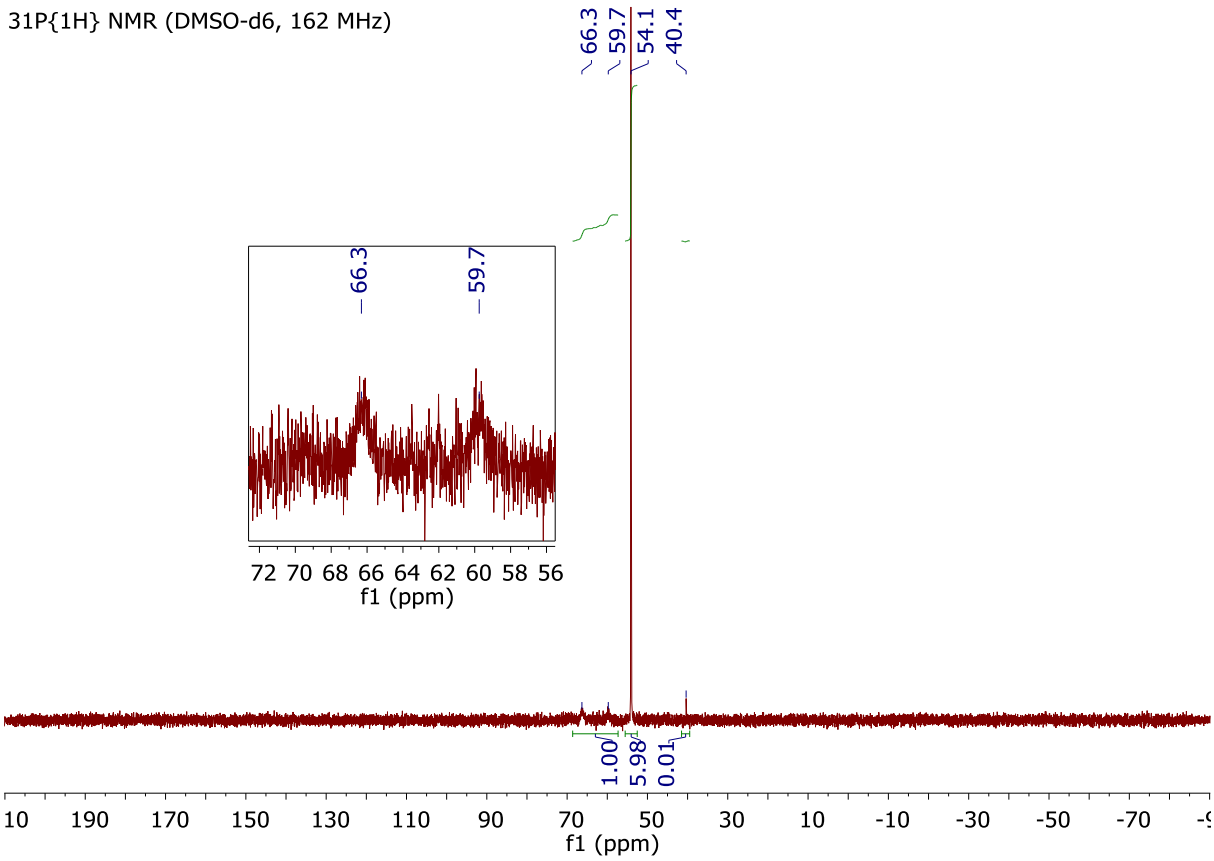

Figure 3.11 $^{31}P\{^{1}H\}$ NMR (162 MHz, DMSO-d_6, 25 °C) spectrum of mixture of 1 $Pd(OAc)_2$:1.5 **BCOPE**:0.25 aqueous NaCl in DMSO-d_6 with excess CH_3SO_3H.

The singlet at 54.1 ppm corresponding to the bis-chelate species remained untouched, indicating that the aqueous NaCl added only interacted with the mono-chelate species. The introduction of Cl^- to the solution likely displaced a solvent or $CH_3SO_3^-$ ligand to give an asymmetric [Pd(**BCOPE**)(L)Cl] complex (**Figure 3.12**), hence splitting the mono-chelate singlet to two broad signals.

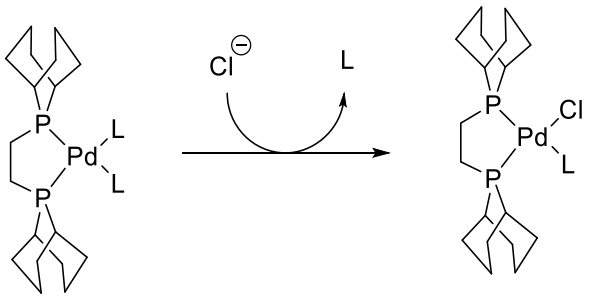

Figure 3.12 Substitution of chloride (Cl^-) to give asymmetric [Pd(**BCOPE**)(L)Cl] complex. L = $CH_3SO_3^-$ or DMSO-d_6.

The asymmetric [Pd(**BCOPE**)(L)Cl] structure differentiates the chemical environments of the P atoms depending on if they are trans to Cl^- or to the solvent/$CH_3SO_3^-$ ligand. The significant broadening of ^{31}P signals observed (from 0.5 ppm to 2 ppm width), may be due to hydrogen bonding interactions between H_2O and Cl^- or due to unresolved ^2J couplings.

Adding an equivalent of $Ag(CH_3SO_3)$ to [Pd(**BCOPE**)Cl_2] in a less coordinating solvent such as $CDCl_3$ resulted in the formation of a singlet at 71.4 ppm. In the absence of a more coordinating ligand, Cl^- preferentially bridges a second mono-chloride complex to give a dimeric structure with bridging chlorides [Pd(**BCOPE**)Cl]$_2$(CH_3SO_3)$_2$ (**Figure 3.13**).

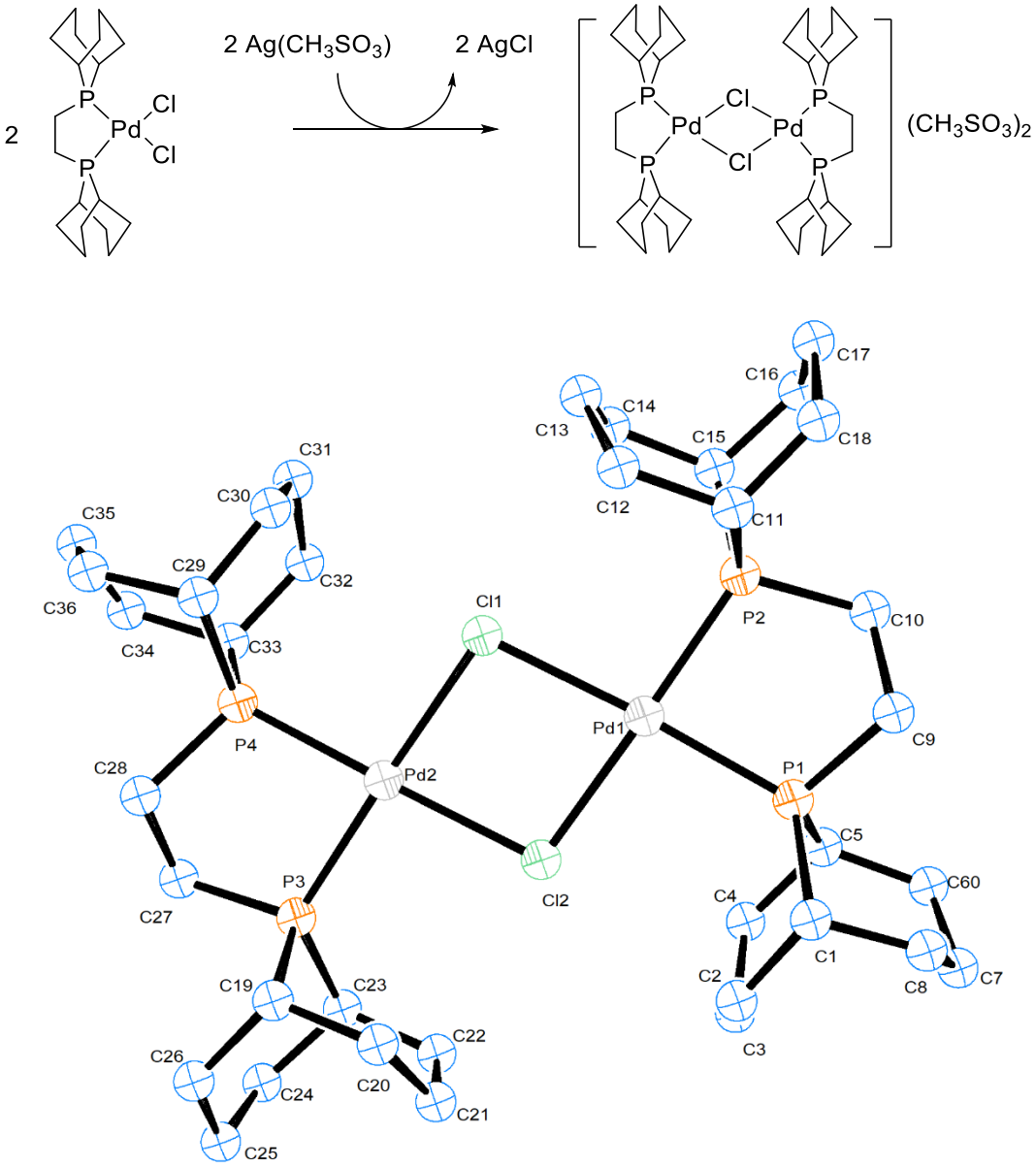

Figure 3.13 Formation and molecular structure of the cation in [Pd(**BCOPE**)Cl]$_2$(CH_3SO_3)$_2$. Structure refined by Dr. Martin Schreyer.

Addition of a second equivalent of $Ag(CH_3SO_3)$ to $[Pd(\textbf{BCOPE})Cl]_2(CH_3SO_3)_2$ broke up the dimer to give $[Pd(\textbf{BCOPE})(CH_3SO_3)_2]$ and shifted the ^{31}P singlet downfield to 73.6 ppm.

3.4 Olefin Hydroformylation

The series of C_2-bridged diphobane ligands have been evaluated in palladium catalysed hydroformylation of 1-hexene and internal hexenes and the results are summarised in **Table 3.3**. The catalyst was prepared in situ via the sequential combination of $Pd(OAc)_2$, diphobane, CH_3SO_3H and aqueous NaCl in diglyme (see section **5.5.3** for details).[19]

Table 3.3 Palladium catalysed hydroformylation of 1-hexene and internal hexenes.[a]

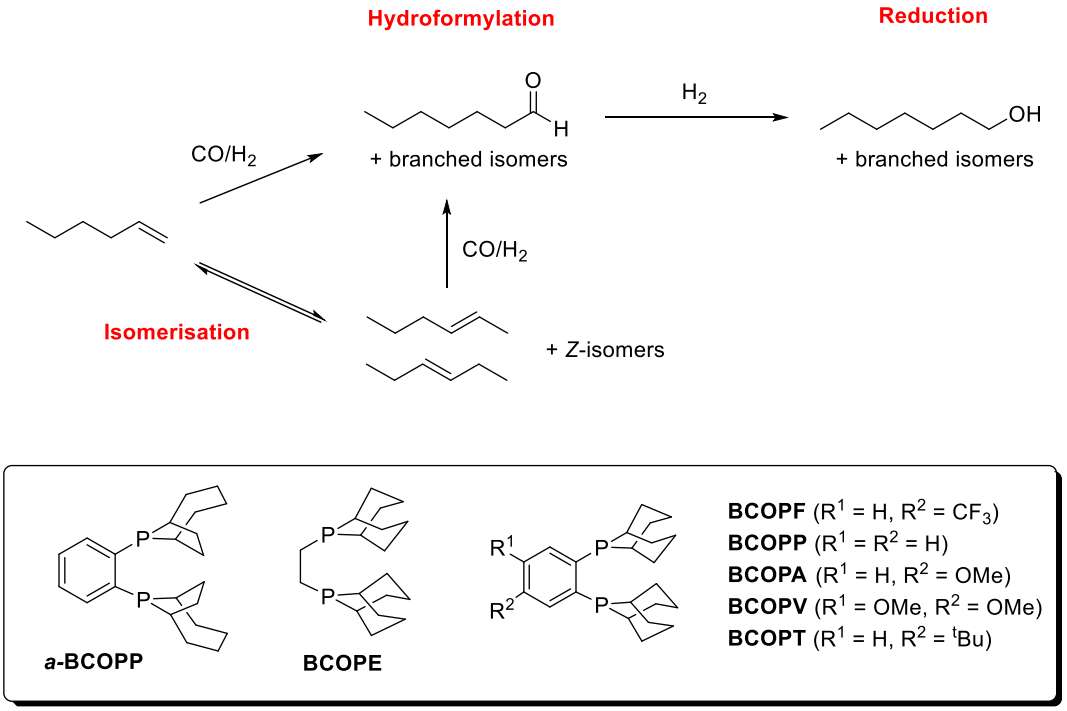

Substrate	Ligand	Conv / %	Internal Hexenes / %	Heptanal (lin)[b] / %	Heptanol (lin)[b] / %	Alcohol/ Aldehyde	TON[c]
1-Hexene[d]	**BCOPF**	97	42	38 (77)	5 (82)	0.1	850
1-Hexene	**BCOPP**	100	40	42 (75)	16 (78)	0.4	1150
1-Hexene	**BCOPA**	100	32	45 (75)	19 (79)	0.4	1200
1-Hexene	**BCOPV**	100	25	19 (69)	41 (76)	2.2	1300
1-Hexene	**BCOPT**	100	30	40 (72)	20 (77)	0.5	1200
1-Hexene	**BCOPE**	100	5	4 (81)	89 (78)	22.3	1850
1-Hexene	***a*-BCOPP**	100	56	34 (69)	1 (71)	<0.1	700
Hexene Mix[e]	**BCOPP**	100	73	17 (42)	10 (49)	0.6	550

Hexene Mix[e]	**BCOPA**	100	66	16 (40)	18 (48)	1.1	700
Hexene Mix[e]	**BCOPE**	100	9	6 (81)	84 (78)	14.0	1800

[a]Conditions: 1-hexene (161.12 mmol), $Pd(OAc)_2$ (0.05 mol%), Ligand (L/Pd = 1.4), CH_3SO_3H (Acid/Pd = 40), 1 mL aqueous NaCl (NaCl/Pd = 0.4), 60 bar CO/H_2 (1:2), diglyme (60 mL), 100 °C, 2 h. Yields were determined via gas chromatography using anisole as an internal standard. [b]Linearity = moles of 1-isomer/moles of all regioisomers. [c]TON = sum of moles of heptanal and heptanol/moles of catalyst. [d]1-hexene (53.9 mmol), diglyme (20 mL). [e]Hexene mix = 3% 1-hexene, 75% 2-hexene and 22% 3-hexene. Note: minor amounts (0.1-3%) of C_{13} ketones and heptanoic acids were detected in all runs. All single runs.

Near quantitative conversions were achieved for all runs to give a mixture of internal hexenes and the linear and branched isomers of heptanal and heptanol. Linear selectivities were similar (ca. 75%) across the series of diphobane ligands despite the variety of electron-donating (methoxy, tert-butyl) and electron-withdrawing (trifluoromethyl) groups present, suggesting that regioselectivity is primarily determined by steric not electronic factors. This is in line with a study by Drent and Budzelaar that observed a direct correlation between product linearity and ligand steric bulk for palladium catalysed olefin hydrocarbonylation.[55]

3.4.1 Influence of Electronic Effects on Hydroformylation Activity

Hydroformylation activity for 1-hexene appears to correlate with electron density at the P donor atom in the order **BCOPE** > **BCOPP** ≈ **BCOPA** ≈ **BCOPV** ≈ **BCOPT** > **BCOPF** ≈ ***α*-BCOPP**. The poorest hydroformylation activities were observed for the runs using **BCOPF**, which possesses an electron-withdrawing trifluoromethyl group on its phenylene backbone, and ***α*-BCOPP**, which has the less basic [4.2.1]phobane moiety. Moderate hydroformylation activities were observed for runs using phenylene-bridged diphobane (**BCOPP**) and aryl-bridged diphobanes (**BCOPA**/**BCOPV**/**BCOPT**) that could decrease electron density on the P donor atoms via delocalisation of the P lone pair into the aromatic ring. The highest hydroformylation activity was obtained in the run using ethylene-bridged **BCOPE**, that possesses an alkyl bridge with no π electron system to resonate with the P lone pair and also has an electron-donating inductive effect on the P donor atoms.

3.4.2 Impact of Backbone Modification on Reductive Hydroformylation Activity

Taking the alcohol/aldehyde ratio as an indication of aldehyde reduction ability, the diphobane series reveals a trend like that for hydroformylation with the more electron-rich phosphines giving a greater ratio of alcohol products. Ethylene-bridged **BCOPE** afforded the highest (89%) yield of heptanol from 1-hexene, while runs using **BCOPF** (5%) and ***α*-BCOPP** (1%) gave the lowest heptanol yields (**Table 3.3**). However, this time, the run using dimethoxy-substituted **BCOPV** stood out as an exception from amongst the aryl-bridged diphobanes, reducing 68% of the aldehydes produced in situ to alcohols, roughly double that in the runs using **BCOPP** (28%), **BCOPA** (30%) or **BCOPT** (33%). Zhou and co-

workers have proposed a mechanism for the homogeneous palladium catalysed reduction of aldehydes to alcohols (**Figure 3.14**).[56]

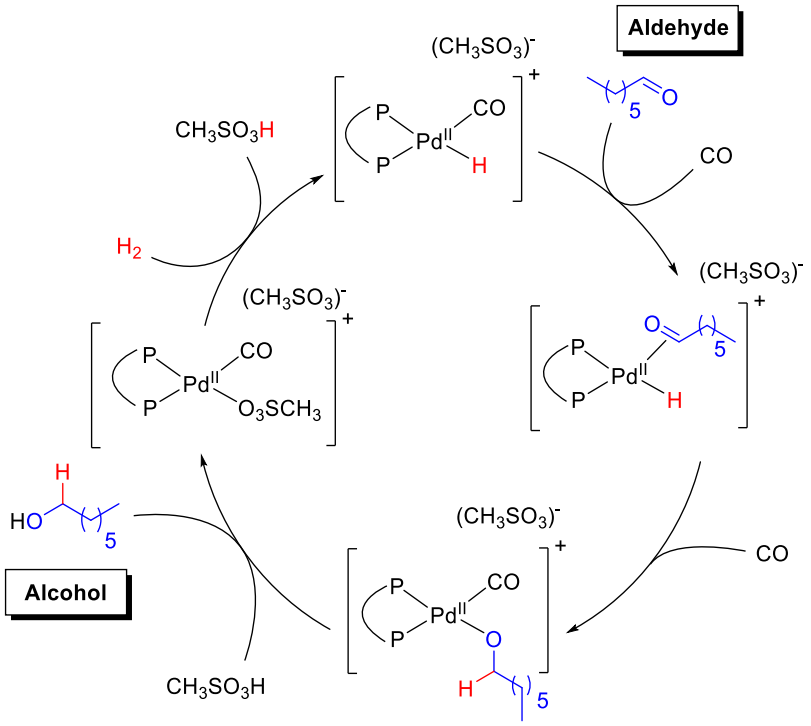

Figure 3.14 Proposed mechanism for palladium catalysed reduction of heptanal to heptanol, adapted from literature.[56]

In the mechanism proposed above (**Figure 3.14**), Pd-hydride attacks the carbonyl group in heptanal to give a Pd-alkoxy species that is protonated by CH_3SO_3H to yield the heptanol product. An increase in electron density at the P donor atoms and hence, at the Pd centre may facilitate this process by increasing the nucleophilicity of the hydride ligand in the Pd-hydride complex. If the nucleophilic attack of Pd-hydride on heptanal is rate-determining, reductive hydroformylation activity would then directly correlate with electron density and more electron-rich ligands such as **BCOPV** and **BCOPE** would yield the most alcohol product.

3.4.3 Hydroformylation of a Mixture of 1-, 2- and 3-Hexenes

A mixture of 1-, 2- and 3-hexenes was also investigated as the substrate using **BCOPP**, **BCOPA** and **BCOPE** (**Table 3.3**). Both the runs using **BCOPP** or **BCOPA** showed reduced hydroformylation activities compared to when 1-hexene was the substrate, while the run using **BCOPE** showed nearly identical activity as that with 1-hexene as substrate. For the run using **BCOPE**, isomerisation must be fast relative to hydroformylation, thus allowing isomerising hydroformylation of internal olefins to occur in an equally facile fashion as the hydroformylation of terminal olefins. The reduced hydroformylation activities observed for the runs using aryl-bridged **BCOPP** and **BCOPA** however, suggest olefin

isomerisation as the rate-determining step that limits overall hydroformylation activity to give reduced yields of heptanal and heptanol.

3.4.4 Solvent Effects

Investigations into the use of various solvents for palladium catalysed hydroformylation of 1-hexene using **BCOPE** and **BCOPP** also revealed dramatic changes in product selectivity (**Figure 3.15**).

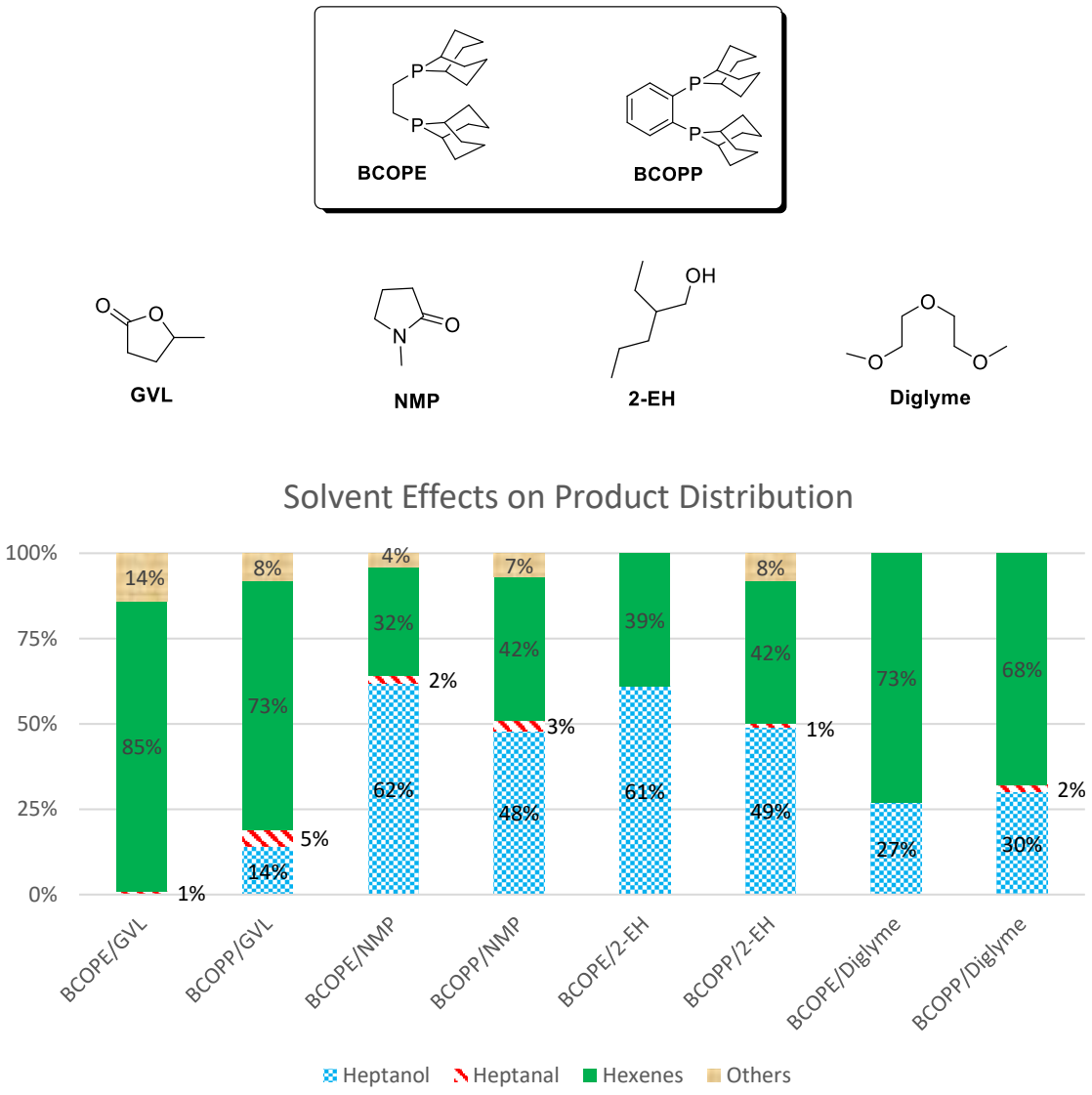

Figure 3.15 Bar chart of product distributions from palladium catalysed hydroformylation of 1-hexene in different solvents. Conditions: 1-hexene (16.1 mmol), $Pd(OAc)_2$ (0.1 mol%), ligand (L/Pd = 1.4), CH_3SO_3H (acid/Pd = 40), 0.1 mL aqueous NaCl (NaCl/Pd = 0.4), 60 bar CO/H_2 (1:2), solvent (6 mL), 100 °C, 2 h.

In the run using γ-valerolactone (GVL), **BCOPE** is nearly inactive for hydroformylation while **BCOPP** yields 14% heptanol as the major product. However, in the runs for both n-methyl-2-pyrrolidone (NMP) and 2-ethylhexanol (2-EH) solvents, **BCOPE** outperforms **BCOPP** to convert more 1-hexene to

heptanol (**Figure 3.15**). Finally, in diglyme, both **BCOPE** and **BCOPP** exhibit similar activities to give about 30% heptanol as the major product. Their similar performance in diglyme opposes earlier observations in **Table 3.3** where **BCOPE** was about 1.5 times more active than **BCOPP** in diglyme and **BCOPP** favoured heptanal as the major product in about a 3:1 ratio to heptanol. However, unlike the experiments in **Table 3.3**, the solvent screening experiments were conducted at 1/10th the scale and in reactors mixed with magnetic stirrer bars instead of overhead mechanical stirrers. The mechanical setup influences the rate of mass transfer that in turn, may alter product distributions. Alternatively, the smaller absolute amount of catalyst present in the solvent screening experiments may be decomposing at a similar absolute rate to give a larger ratio of Pd black that may be unable to carbonylate hexene but can still hydrogenate heptanal to afford a higher ratio of heptanol in its hydroformylation products.

3.4.5 Hydroformylation of Methyl 4-Pentenoate (M4P)

The performance of the diphobane ligands, **BCOPE** and **BCOPP**, has also been evaluated in palladium catalysed hydroformylation of methyl pentenoate and the results are summarised in **Table 3.4**.

Table 3.4 Palladium catalysed hydroformylation of methyl pentenoate.[a]

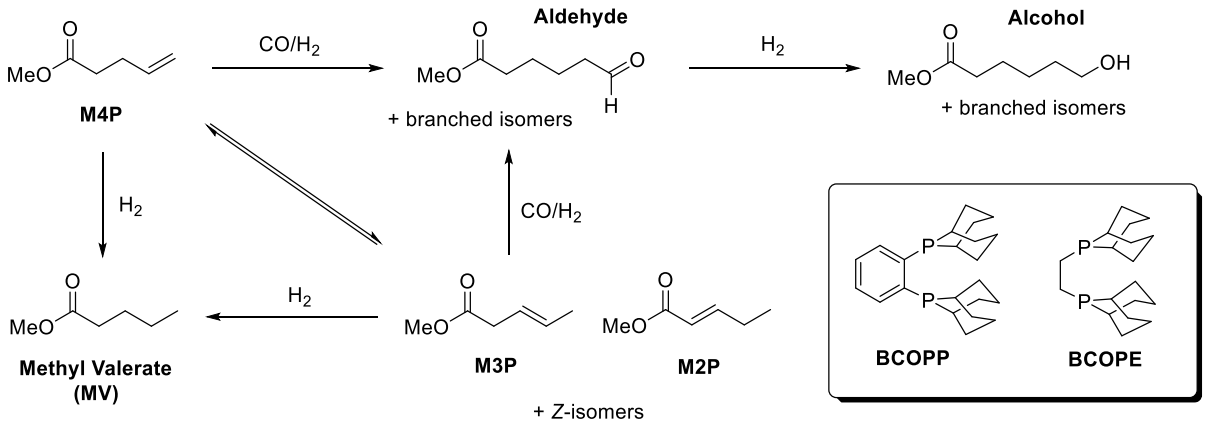

#	Olefin	Ligand	Acid (Acid /Pd)	Conv / %	M2P / %	M3P / %	M4P / %	MV / %	Aldehyde (lin)[b] / %	Alcohol[c] (lin)[b] / %	TON[d]
1	M4P	**BCOPE**	MSA (40)	100	0	0	0	54	0 (n.a.)	32 (71)	650
2	M4P	**BCOPP**	MSA (40)	100[e]	4	3	<1	5	3 (79)	78 (74)	1450
3	M4P	**BCOPE**	MSA (4)	99	6	2	1	11	8 (76)	68 (63)	1550

4	M4P	**BCOPP**	MSA (4)	93	1	14	7	<1	70 (79)	4 (80)	1500
5	M4P	**BCOPE**	TFA (40)	99	16	28	1	1	47 (79)	3 (72)	1000
6	M4P	**BCOPP**	TFA (40)	61	1	9	39	<1	47 (82)	1 (76)	950
7	M2P	**BCOPE**	TFA (40)	52	48	10	1	9	23 (73)	2 (43)	500
8	M2P	**BCOPP**	TFA (40)	7	93	2	<1	2	<1 (n.d.)	0 (n.a.)	0

[a]Conditions: methyl pentenoate (40.3 mmol), $Pd(OAc)_2$ (0.05 mol%), Ligand (L/Pd = 1.4), 60 bar CO/H_2 (1:2), diglyme, 100 °C, 4 h. MSA = methanesulfonic acid, CH_3SO_3H. TFA = trifluoroacetic acid, CF_3CO_2H. n.a. = not applicable. n.d. = not determined. Yields were determined via gas chromatography using anisole as an internal standard. [b]Linearity = moles of 1-isomer/moles of all regioisomers. [c]Inclusive of ε-caprolactone. [d]TON = sum of moles of aldehyde and alcohol/moles of catalyst. [e]dimethyl adipate (7%) detected. Note: all single runs.

Initial hydroformylation experiments with methyl 4-pentenoate (M4P) were carried out with methanesulfonic acid (MSA) in 40:1 excess relative to palladium (runs 1 and 2, **Table 3.4**). Full conversion was achieved in both runs to give methyl 6-hydroxyhexanoate as the major carbonylation product. **BCOPP** was about 2-fold more active than **BCOPE** for the reductive hydroformylation of M4P. The run using **BCOPE** instead exhibited greater olefin hydrogenation to yield 54% methyl valerate versus the 5% afforded in the run using **BCOPP**. Competing olefin hydrogenation to these lower-value methyl esters is an undesired side reaction[57] that is often exacerbated for functionalised olefin substrates like M4P.[58] The significant reduction in olefin hydrogenation (54% to 5%) and concomitant increase in methyl 6-hydroxyhexanoate yield represents a dramatic improvement, suggesting ligand backbone modification of diphosphines as a viable avenue to address such issues.

3.4.6 Effect of Acid Concentration on Product Selectivity

Decreasing the equivalents of MSA added from 40 to 4 with respect to palladium (runs 3 and 4, **Table 3.4**) has a significant impact on both olefin hydrogenation as well as aldehyde reduction. This can be seen in the 5-fold drop in olefin hydrogenation for both runs (**BCOPE**, 54% to 11% and **BCOPP**, 5% to <1%) and in the decrease in aldehyde reduction for the run using **BCOPP** resulting in the major product changing from methyl 6-hydroxyhexanoate (78%) to methyl 6-oxohexanoate (70%). The decrease in olefin hydrogenation activity for the run using **BCOPE** is accompanied by a 2-fold increase in methyl 6-hydroxyhexanoate yield (32% to 68%) so that the carbonylation activities of **BCOPE** and **BCOPP** become similar. However, a remarkable difference in chemoselectivity between **BCOPE** (68% methyl

6-hydroxyhexanoate yield) and **BCOPP** (70% methyl 6-oxohexanoate yield) is observed. Similar results were observed for their performance in palladium catalysed hydroformylation of 1-hexene (**Table 3.3**) where **BCOPE** favoured 1-heptanol and **BCOPP** favoured 1-heptanal as their respective major products, although the MSA/Pd ratio was 40 in that case.

3.4.7 Effect of Acid Strength on Product Selectivity

Given the dramatic reduction in olefin hydrogenation observed by lowering acid concentration, investigations into the effect of acid strength were also conducted. The replacement of MSA (pK_a = -1.9)[59] with trifluoroacetic acid, TFA (pK_a = 0.23),[60] at 40:1 excess relative to palladium (runs 5 and 6, **Table 3.4**) also led to a dramatic reduction in hydrogenation of both olefins and aldehydes. Near quantitative conversion was observed for **BCOPE** (99%) but a significantly reduced conversion for **BCOPP** (61%) was observed due to a reduction in olefin isomerisation. Hydroformylation activity for both **BCOPE** and **BCOPP** were similar and lower than their respective runs using MSA. Using TFA also afforded 47% methyl oxohexanoate as the major product while olefin hydrogenation was suppressed to negligible levels. The change in major product from methyl 6-hydroxyhexanoate to methyl 6-oxohexanoate and the suppression of olefin hydrogenation effected by changing acid co-catalyst suggests an active role played by the acid in the catalytic cycle. Drent and Budzelaar proposed that the acid anion may affect the catalytic cycle in 3 different ways:[55]

(1) altering electrophilicity of the Pd centre
    a. weaker acids have conjugate base anions that generally exhibit stronger coordination to the Pd centre and decrease the electrophilicity of the Pd centre
(2) blocking coordination sites
    a. anions that are strongly coordinated to the Pd centre may not be easily displaced and hence would hinder catalytic activity
(3) assisting in the heterolytic dissociation of H_2
    a. by temporarily binding H^+ to facilitate hydrogenolysis

At TFA/Pd = 40, the catalytic performance of **BCOPE** and **BCOPP** also diverge when it comes to olefin isomerisation, resulting in the difference observed in conversion. **BCOPE** exhibits facile isomerisation of M4P to give a 16:28:1 composition of 2-, 3- and 4-pentenoates (run 5, **Table 3.4**) while **BCOPP** showed weaker isomerisation ability to leave most of the starting M4P untouched in a 1:9:39 composition of 2-, 3- and 4-pentenoates (run 6, **Table 3.4**). This was mirrored in their performance for the palladium catalysed hydroformylation of 1-hexene and internal hexenes (**Table 3.3**). The superior isomerising ability of **BCOPE** allowed it to hydroformylate both 1-hexene and internal hexene

substrates equally well while **BCOPP** showed reduced hydroformylation activity for internal hexene substrates.

3.4.8 Hydroformylation of Methyl 2-Pentenoate (M2P)

The lower isomerisation ability of **BCOPP** makes it less efficient in converting internal olefins like M2P compared to **BCOPE** (runs 7 and 8, **Table 3.4**) as terminal hydroformylation is preferred (ca. 80% linear selectivity) for both **BCOPE** and **BCOPP** regardless of the starting isomer. In the isomerising hydroformylation of M2P, the run using **BCOPE** gave 23% conversion to methyl 6-oxohexanoate (approximately half the activity for M4P as substrate), while the run using **BCOPP** gave negligible conversion. Drent and co-workers noted that ligand steric bulk inversely correlates with hydroformylation activity for internal olefin substrates.[19] Bulkier ligands result in more congested coordination spheres that are expected to hinder the formation of sterically demanding branched Pd-alkyl intermediates obtained from the insertion of internal olefins into the proposed catalytically active Pd-hydride species. A comparison of ligand buried volumes (%V_Bur, see section **2.2.8**) show that **BCOPE** (33.2%) is less bulky than **BCOPP** (35.1%), concurring with the higher hydroformylation activity exhibited by **BCOPE** over **BCOPP** for internal olefin substrates like internal hexenes (**Table 3.3**) and M2P (**Table 3.4**).

Moving from terminal M4P to internal M2P as substrate also gave an increase in olefin hydrogenation from negligible levels to 9% and 2% for **BCOPE** and **BCOPP** respectively. Conjugated alkenoate esters such as M2P have been noted in the literature to be more prone to hydrogenation than their non-conjugated analogues.[61-62]

3.4.9 Composition of Isomers

The distribution of methyl pentenoate isomers found in the product mixture from runs 4 and 5 (**Table 3.4**) both favour M3P instead of M2P. M2P is expected to more abundant due to the stability afforded by the conjugation of its double bond with the carbonyl group of the ester functionality. M3P however, may also be derived via β-hydride elimination from 5-membered palladacycles (**Figure 3.16**).

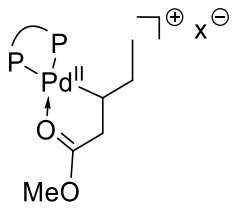

Figure 3.16 5-membered palladacycle. P⌢P = **BCOPE** or **BCOPP**. X^- = $CF_3CO_2^-$ or $CH_3SO_3^-$.

5-membered chelates with carbonyl coordinating to the palladium centre have been described in the literature as intermediates during polymerisation reactions.[63-64] Such chelates have also been

implicated as the driving force for functionalisation favouring the 3-position in palladium catalysed hydroxycarbonylation of pentenoic acids.[65] The unexpected abundance of M3P in the isomer distribution is thus attributed to chelate-driven selectivity originating from the formation of such stable 5-membered palladacycles.

3.4.10 By-Product Formation – Hydroacylation

Run 1 (**Table 3.4**) using **BCOPE** and MSA in 40:1 excess relative to palladium has 14% of its mole balance uncharacterised. In the GC spectrum of the product mixture (**Figure 6.32**, supplementary information) from run 1 (**Table 3.4**), there were several unknown peaks observed eluting later, especially around the retention time expected for the ketone product. Ketones may be formed via hydroacylation of the Pd-acyl intermediate according to the mechanism proposed in **Figure 3.17**.

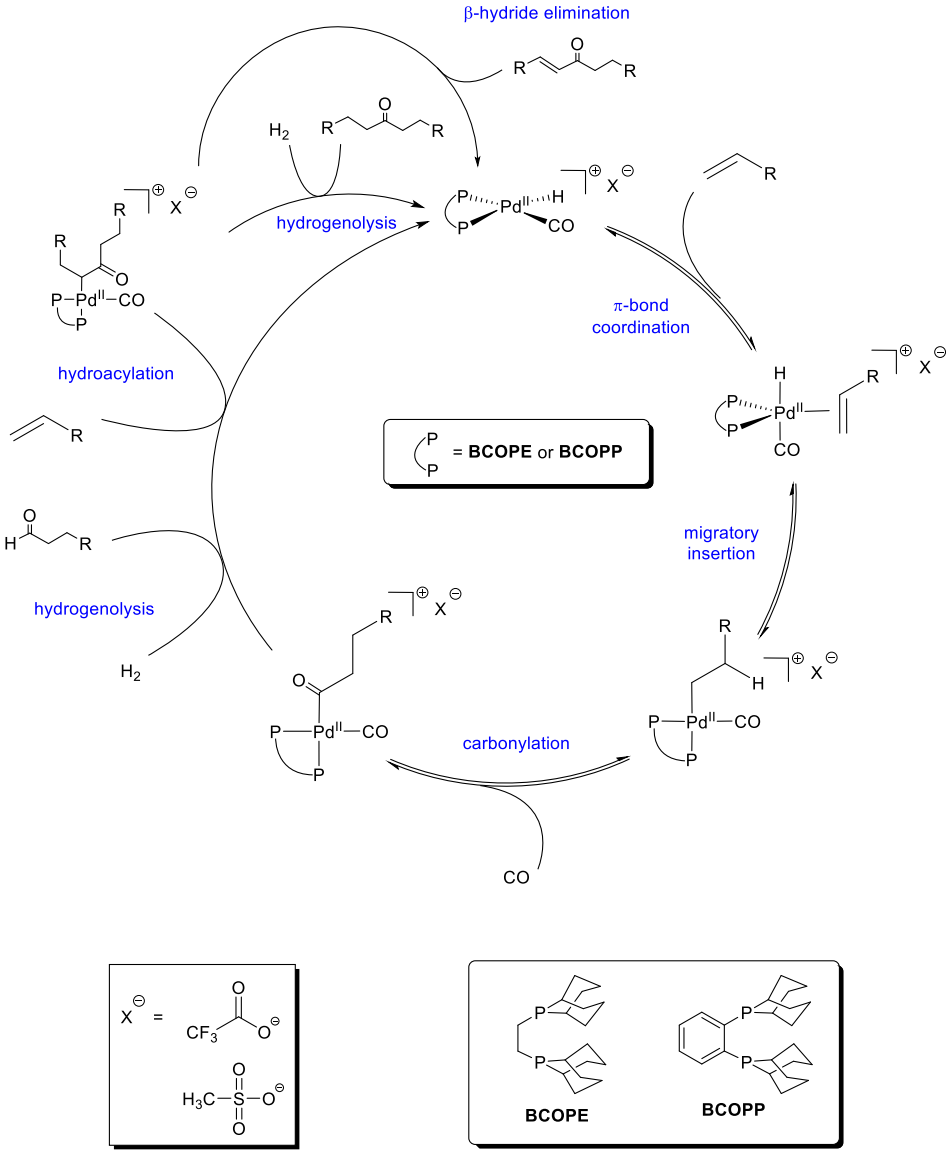

Figure 3.17 Mechanism of palladium catalysed hydroformylation of M4P, adapted from literature.[55]

In the catalytic cycle adapted from Drent and Budzelaar,[55] M4P first coordinates to a cationic Pd-hydride complex in an associative fashion to give a 5-coordinate intermediate before inserting to give a Pd-alkyl complex (**Figure 3.17**). Subsequent coordination and insertion of CO yields the key Pd-acyl intermediate from which several products may be derived. Hydrogenolysis of the Pd-acyl intermediate yields methyl oxohexanoate and returns the starting Pd-hydride complex that can then repeat the cycle. Alternatively, a second M4P molecule can coordinate and insert into the Pd-acyl species to give a Pd-alkyl complex. The Pd-alkyl species can undergo hydrogenolysis to yield a saturated ketone or perform β-hydride elimination to give an unsaturated ketone.[55] As M4P can insert in a 1,2-linear or 2,1-branched fashion and may isomerise to M2P/M3P before insertion, multiple structurally isomeric ketone products may be obtained (**Figure 3.18**).

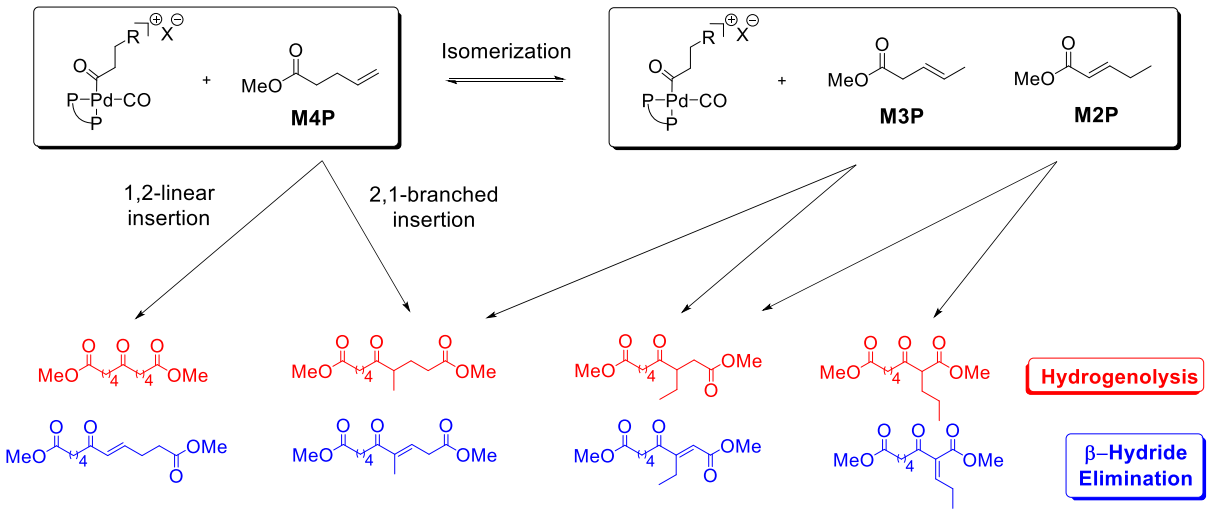

Figure 3.18 Possible ketone products derived from the linear Pd-acyl intermediate. P⌒P = diphobane. X^- = $CF_3CO_2^-$ or $CH_3SO_3^-$.

The linear Pd-acyl intermediate obtained from the carbonylation of the linear Pd-alkyl complex may give 8 different ketones as shown above in **Figure 3.18**. If the various possible branched Pd-acyl intermediates were to also be taken into consideration, 32 different ketone products are possible in total. The retention times of these structurally similar ketones of similar mass are expected to fall within a narrow range on the GC spectrum, complicating the identification and quantification of individual ketone isomers.

3.4.11 By-Product Formation – Alcohol Derivatives

Side reactions involving methyl 6-hydroxyhexanoate obtained from the reductive hydroformylation of M4P (**Figure 3.19**) may also contribute to the uncharacterised mole balance from run 1 (**Table 3.4**).

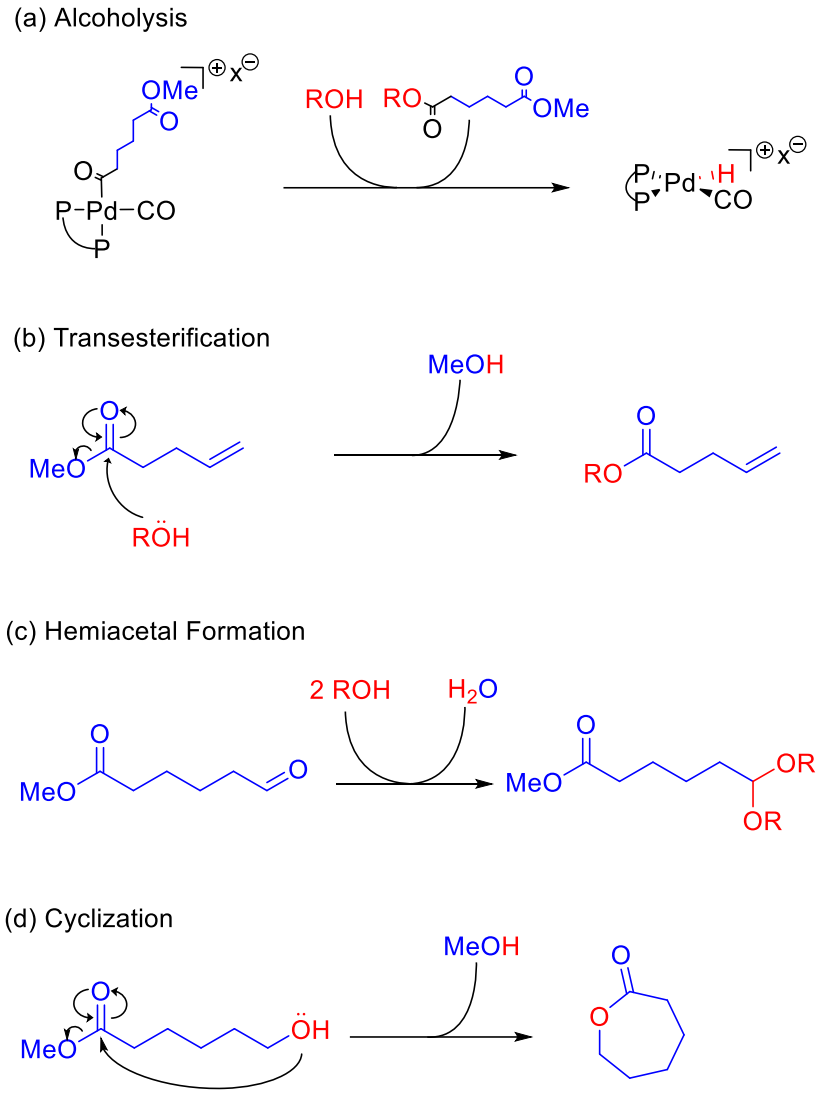

Figure 3.19 Side reactions involving the alcohol product from palladium catalysed hydroformylation of M4P: (a) alcoholysis, (b) transesterification, (c) hemiacetal formation and (d) cyclisation.

If methyl 6-hydroxyhexanoate were to be involved in the alcoholysis of Pd-acyl as shown in **Figure 3.19a**, a dimeric ester product may be obtained. Alternatively, methyl 6-hydroxyhexanoate can attack its own (**Figure 3.19d**) or other ester functionalities present (such as in M4P) in a transesterification reaction (**Figure 3.19b**) to produce caprolactone or an oligomeric ester respectively and release MeOH as a by-product. GC analysis of the product mixture from run 1 (**Figure 6.32**, supplementary information) does indeed show the presence of MeOH (17%), likely generated from such side reactions.

Methyl 6-hydroxyhexanoate may also react with methyl 6-oxohexanoate to form hemiacetal or acetal by-products and release H_2O (**Figure 3.19c**). Finally, if the H_2O or MeOH released were to take part in the catalytic cycle via hydrolysis or methanolysis of the Pd-acyl intermediate, carboxylic acids or diesters may also be obtained.

3.4.12 Hydroformylation of 1-Octene in 2-Ethylhexanol – Competition with Alkoxycarbonylation

The diphobane ligand series has been evaluated in palladium catalysed hydroformylation of 1-octene in 2-ethylhexanol and the results are summarised in **Table 3.5**. 2-Ethylhexanol was selected as the reaction solvent in order to benchmark previous reports.[19] 2-Ethylhexanol is a common industrial solvent owing to its low volatility,[66] and around 2.5 million tonnes are produced annually via aldol condensation of n-butyraldehyde followed by hydrogenation of the resulting hydroxyaldehyde.[67] In the presence of an alcohol solvent however, competing alkoxycarbonylation to 2-ethylhexyl nonanoate was observed.

Table 3.5 Palladium catalysed hydroformylation of 1-octene.[a]

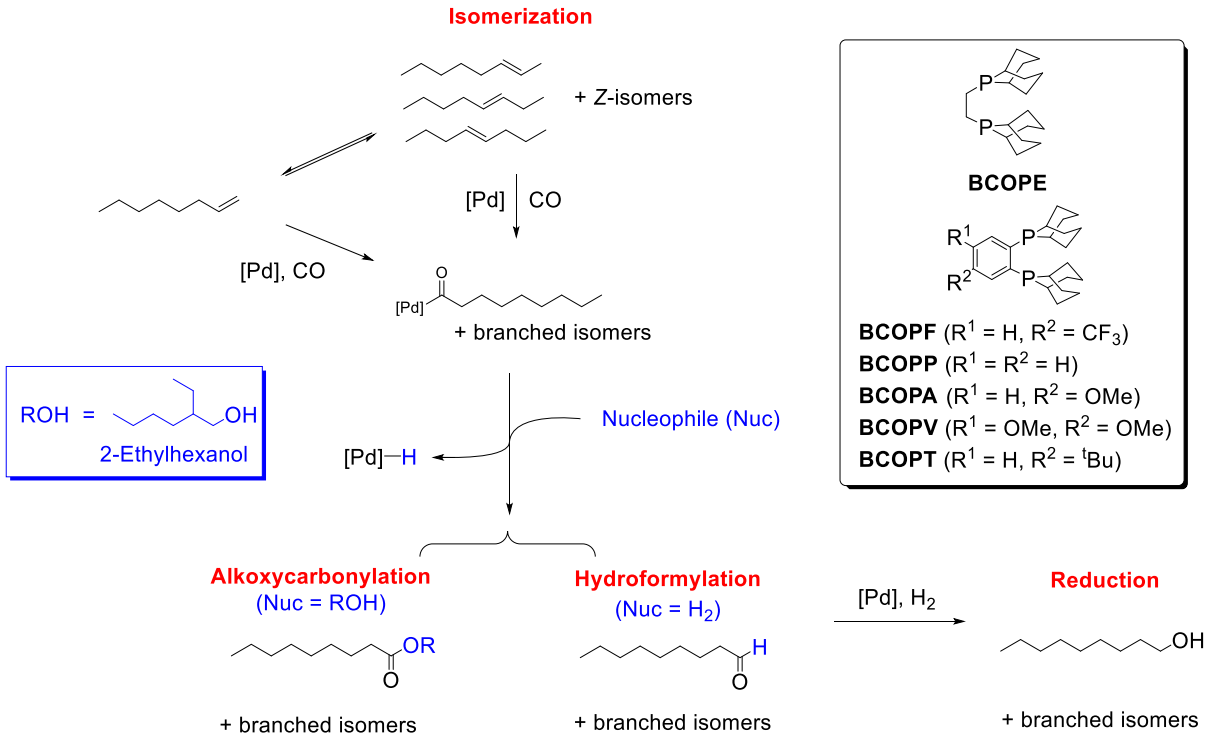

Ligand	Conv / %	Isomerisation: Internal Octenes / %	Hydroformylation: Nonanal (lin)[b] / %	Hydroformylation: Nonanol (lin)[b] / %	Alkoxycarbonylation: 2-Ethylhexyl Nonanoate (lin)[b] / %	Alkoxy/ Hydrof.	TON[c]
BCOPF	98	51	9 (68)	4 (79)	35 (82)	2.7	950
BCOPP	98	46	12 (65)	17 (73)	16 (76)	0.6	900
BCOPA	98	50	14 (66)	17 (76)	13 (77)	0.4	900
BCOPV	98	52	5 (69)	20 (72)	17 (78)	0.7	850

BCOPT	98	52	8 (63)	14 (72)	18 (80)	0.8	850
BCOPE	99	35	1 (73)	61 (74)	2 (72)	<0.1	1300

[a]Conditions: 1-octene (80.6 mmol), $Pd(OAc)_2$ (0.05 mol%), ligand (L/Pd = 1.4), CH_3SO_3H (acid/Pd = 40), 1 mL aqueous NaCl (NaCl/Pd = 0.4), 60 bar CO/H_2 (1:2), 2-ethylhexanol (20 mL), 100 °C, 2 h. Yields were determined via gas chromatography using anisole as an internal standard. [b]Linearity = 1-isomer/sum of all regioisomers. [c]TON = sum of moles of nonanal, nonanol and 2-ethylhexyl nonanoate/moles of catalyst. Note: Minor amounts (0.2 – 3%) of nonyl nonanoate and nonanoic acid were detected in the product mixtures of all runs. All single runs.

Near quantitative conversions (≥98%) were achieved for all runs to give a mixture of internal octenes, nonanal, nonanol and 2-ethylhexyl nonanoate. The hydroformylation activities of the diphobane ligand series for 1-octene mirrored that for 1-hexene with **BCOPV** and **BCOPE** favouring reductive hydroformylation to nonan-1-ol.

In the presence of 2-ethylhexanol solvent however, the aryl-bridged diphobane ligands also yielded significant amounts of 2-ethylhexyl nonanoate, as opposed to **BCOPE** which selectively produced nonan-1-ol as the major carbonylation product. Alkoxycarbonylation and hydroformylation are closely related processes, albeit with different nucleophiles (ROH or H_2) attacking the Pd-acyl intermediate.[54, 68] Palladium-based systems however, are more well-known for alkoxycarbonylation than for hydroformylation.[69-71]

The run employing electron-poor **BCOPF** gave the highest alkoxycarbonylation activity to yield about 3-fold more alkoxycarbonylation than hydroformylation products (35% vs 13%). van Leeuwen and co-workers described an alcoholysis mechanism involving the deprotonation of a coordinated alcohol species to form a Pd-alkoxy intermediate that subsequently undergoes reductive elimination to yield the ester product (**Figure 3.20**).[68]

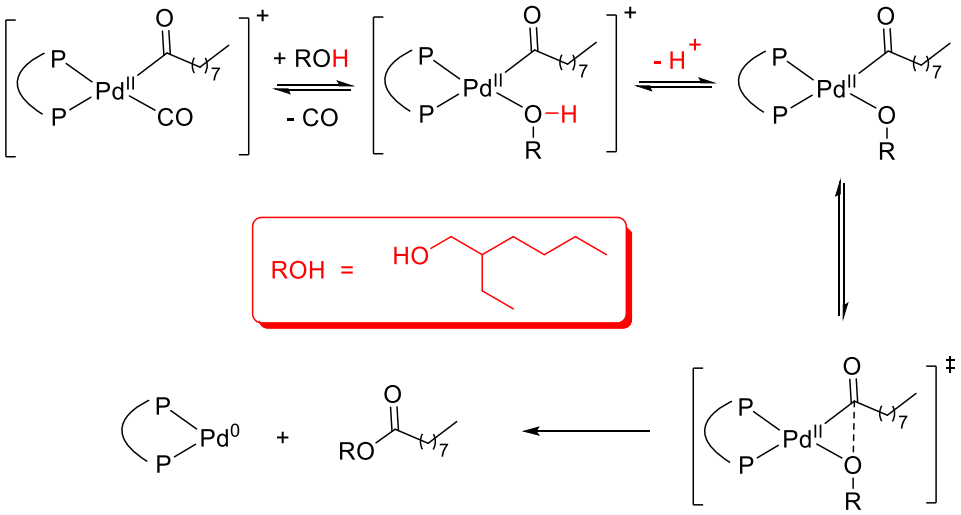

Figure 3.20 Alcoholysis mechanism adapted from van Leeuwen and co-workers.[68]

BCOPF bears an electron-withdrawing trifluoromethyl group that draws electron density away from the P donor atoms and consequently results in a more electrophilic Pd centre. More electrophilic Pd centres should be better able to polarise the O-H bond of a coordinated 2-ethylhexanol ligand, facilitate its deprotonation, and accelerate the alcoholysis of the Pd-acyl species to favour the formation of 2-ethylhexyl esters.

3.5 Alkoxycarbonylation of 1-Octene

In order to study the alkoxycarbonylation activity of the Pd-diphobane catalysts independently from hydroformylation, a series of alkoxycarbonylation experiments using pure CO and alcohol solvent was conducted. The series of diphobane ligands were thus evaluated in palladium catalysed alkoxycarbonylation of 1-octene and the results are summarised in **Table 3.6**. The effect of using primary, secondary and tertiary alcohol solvents and the effect of NaCl and H_2O as additives were also investigated.

Table 3.6 Palladium catalysed alkoxycarbonylation of 1-octene.[a]

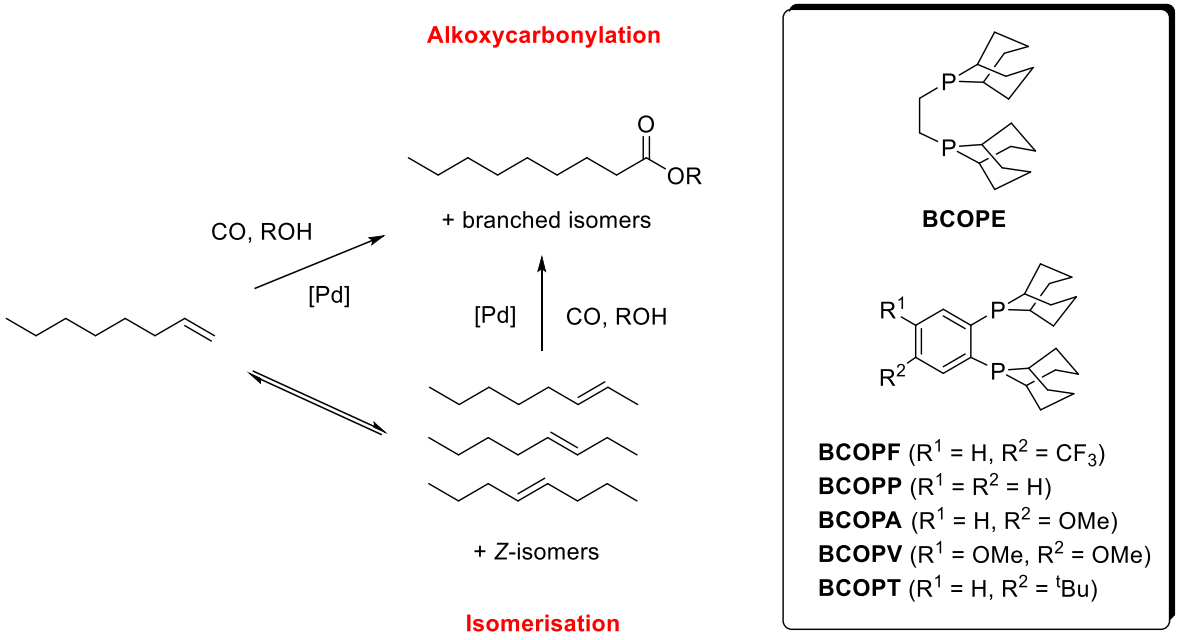

#	Ligand	ROH	Additive[b]	Conv / %	Internal Octenes (isom.)[c] / %	Ester (linear)[d] / %	TON[e]
1	**BCOPF**	2-Ethylhexanol	NaCl (aq)	92	39 (82)	51 (82)	1000
2	**BCOPP**	2-Ethylhexanol	NaCl (aq)	64	39 (52)	22 (80)	450
3	**BCOPA**	2-Ethylhexanol	NaCl (aq)	31	19 (22)	11 (76)	200
4	**BCOPV**	2-Ethylhexanol	NaCl (aq)	78	48 (69)	30 (78)	600

5	**BCOPT**	2-Ethylhexanol	NaCl (aq)	56	36 (46)	20 (81)	400
6	**BCOPE**	2-Ethylhexanol	NaCl (aq)	98	92 (98)	2 (71)	50
7	**BCOPE**	MeOH	-	100	94 (97)	3 (77)	50
8	**BCOPF**	MeOH	-	99	37 (98)	56 (73)	1150
9	**BCOPA**	MeOH	-	98	79 (98)	12 (76)	250
10	**BCOPV**	MeOH	-	98	77 (98)	15 (77)	300
11	**BCOPT**	MeOH	-	98	77 (98)	15 (76)	300
12	**BCOPP**	MeOH	-	98	76 (98)	16 (74)	300
13	**BCOPP**	MeOH	NaCl (aq)	99	62 (98)	35 (74)	700
14	**BCOPP**	MeOH	NaCl	97	78 (97)	12 (76)	250
15	**BCOPP**	MeOH	H_2O	99	35 (98)	55 (73)	1100
16	**BCOPF**	^{t}BuOH	H_2O	99	30 (98)	7 (68)	150

[a]Conditions: 1-octene (80.6 mmol), $Pd(OAc)_2$ (0.05 mol%), ligand (L/Pd = 1.4), CH_3SO_3H (acid/Pd = 40), 50 bar CO, ROH solvent (20 mL), 100 °C, 2 h. Yields were determined via gas chromatography using anisole as an internal standard. [b]NaCl (aq) (1 mL solution, NaCl/Pd = 0.4), NaCl (NaCl/Pd = 0.4), H_2O (1 mL). [c]Isomerised = moles of internal octenes/moles of all octenes. [d]Linearity = 1-isomer/all regioisomers. [e]TON = moles of esters/moles of catalyst. Note: minor amounts of oligomeric esters were detected for runs using MeOH and minor amounts of nonanal, nonanol and nonanoic acid were detected for runs using H_2O or NaCl (aq). Note: all single runs.

The trend in alkoxycarbonylation activity for the diphobane series was the same for primary (MeOH) and secondary (2-ethylhexanol) alcohols in the order **BCOPF** > **BCOPP ≈ BCOPT ≈ BCOPV ≈ BCOPA > BCOPE**, the inverse of that observed for their hydroformylation activities (**Table 3.3**). The run using **BCOPE** showed negligible alkoxycarbonylation activity (2% ester yield) even in the absence of H_2, likely due to a less electrophilic Pd centre hindering the rate-determining alcoholysis step.

3.5.1 Effect of NaCl and H_2O on Alkoxycarbonylation Activity

The effect of aqueous NaCl was investigated over multiple alkoxycarbonylation experiments (runs 12 – 15, **Table 3.6**). Comparison with a control experiment (run 12, **Table 3.6**) revealed that adding aqueous NaCl promoted alkoxycarbonylation activity (16% to 35% ester yield) with no change in regioselectivity (74%) or olefin isomerisation (98% of remaining octene as internal octenes). Adding NaCl as a solid (run 14, **Table 3.6**) however, had a mild inhibiting effect (16% to 12% ester yield) instead. Chloride may act as a ligand to strongly coordinate with the palladium catalyst, blocking coordination sites and hindering alkoxycarbonylation activity. Comparison of the runs using H_2O (run 15, **Table 3.6**) and aqueous NaCl (run 13, **Table 3.6**) as additives show that the presence of NaCl does indeed appear to have an inhibitory effect on alkoxycarbonylation activity (55% to 35% ester yield), in contrast to the promoting effect of NaCl observed in the palladium catalysed hydroformylation of 1-octene.[19] The addition of H_2O without NaCl on the other hand (run 15, **Table 3.6**), had a significant

promoting effect, nearly quadrupling ester yield from 16% to 55%. It is possible that the addition of H_2O interacts with MeOH (via hydrogen bonding) to facilitate dissociation of H^+ to accelerate the rate-determining alcoholysis step (**Figure 3.20**) as H_2O (pKa = 14.0) is slightly more acidic than MeOH (pKa = 15.5).[72] Alternatively, H_2O may be hydrolysing the Pd-acyl intermediate to give an intermediate carboxylic acid that may undergo further acid-catalysed esterification with MeOH to yield the ester product at a faster rate than direct olefin alkoxycarbonylation.

3.5.2 Olefin Isomerisation

Despite the similar alkoxycarbonylation activity trend for the diphobane ligand series for primary (MeOH) and secondary (2-ethylhexanol) alcohols, there is a difference in conversion due mainly to their varying olefin isomerisation abilities. In MeOH solvent (runs 7 – 15, **Table 3.6**), the catalysts exhibit facile isomerisation to give octene isomer distributions near that of the thermodynamic composition[73] (1:99 ratio of 1-octene to internal octenes). In 2-ethylhexanol however, only **BCOPE** shows good isomerisation ability to give a 1:49 ratio of 1-octene to internal octenes (run 6, **Table 3.6**) while the aryl-bridged diphobanes exhibit varying degrees of olefin isomerisation (runs 1 – 5, **Table 3.6**). Methanol[74] and 2-ethylhexanol[66] differ in several properties such as dielectric constant, polarity, lipophilicity, nucleophilicity and acidity. These different properties give rise to different CO and H_2[75-76] gas solubilities and varying solvent behaviour when interacting with aqueous NaCl. For example, the long alkyl chain in 2-ethylhexanol increases its lipophilicity to the point where it forms an immiscible biphasic system with aqueous NaCl even at 100 °C, as opposed to the miscible single layer system observed for MeOH. Differences in reaction solvent have been noted in the literature to cause changes in olefin isomerisation mechanism for the same metal-ion catalyst,[77] and in this case, may be giving rise to the differences in olefin isomerisation observed.

3.5.3 Tert-Butoxycarbonylation of 1-Octene

The rate of alcoholysis in alkoxycarbonylation has been reported to decrease with increasing steric bulk of the alcohol nucleophile.[78-79] The synthesis of linear tert-butyl esters via olefin alkoxycarbonylation with ^{t}BuOH has been particularly challenging and modest yields in the 30% range are common.[80-81] Encouraged by the alkoxycarbonylation activity of **BCOPF** and the promoting effect of H_2O as an additive, ^{t}BuOH was investigated as the solvent for the production of linear tert-butyl esters from 1-octene (run 16, **Table 3.6**) using H_2O as a promoter (H_2O/1-octene = 0.7). Regretfully, only 7% of the desired tert-butyl ester product was obtained. The major product was instead nonanoic acid (60% yield), derived from the hydroxycarbonylation of 1-octene (**Figure 3.21**). The smaller H_2O nucleophile appears to be favoured over the bulkier tertiary alcohol nucleophile under these conditions despite the abundance of tert-butanol present as the solvent.

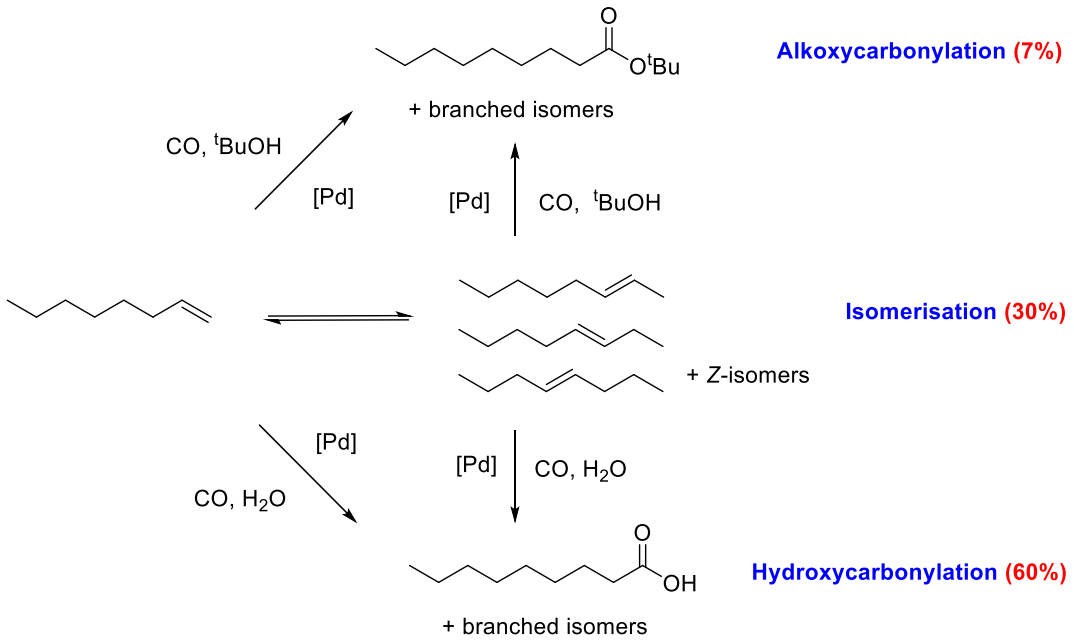

Figure 3.21 Palladium catalysed tert-butoxycarbonylation of 1-octene (run 16, **Table 3.6**), yields given in brackets.

The presence of excess strong acid CH_3SO_3H (acid/Pd = 40) also facilitated the acid catalysed dehydration of ^tBuOH to give H_2O and isobutene. The former increased H_2O concentration in situ to encourage hydroxycarbonylation, while the latter acted as an alternative substrate for palladium catalysed alkoxycarbonylation and hydroxylation to give isopentanoic acid and tert-butyl 3-methylbutanoate respectively (**Figure 3.22**).

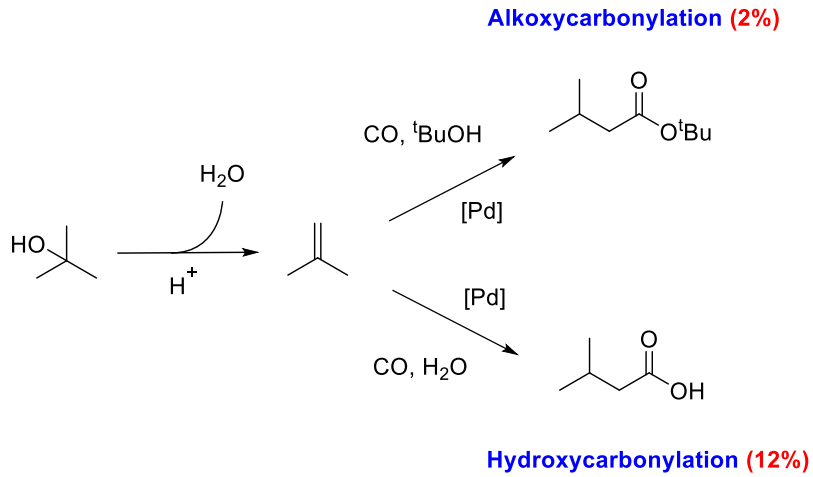

Figure 3.22 Acid catalysed dehydration of tBuOH and subsequent alkoxycarbonylation and hyroxycarbonylation (run 16, **Table 3.6**), yields given in brackets are relative to 1-octene.

In order to encourage alkoxycarbonylation activity with tertiary alcohols, hydroxycarbonylation to carboxylic acid products should be suppressed. Future attempts may explore this by excluding H_2O

and using Lewis acids such as $SnCl_2$ or $Ti(O^iPr)_4$ in place of Brønsted acids[82] or removing the acid co-catalyst altogether[71] to address the issue of acid catalysed dehydration of tertiary alcohols.

3.6 Hydroxycarbonylation of Olefins

3.6.1 Hydroxycarbonylation of 1-Hexene

Encouraged by the hydroxycarbonylation activity observed in the alkoxycarbonylation experiments in **Table 3.6**, the diphobane ligand series was also evaluated in palladium catalysed hydroxycarbonylation of 1-hexene and the results are summarised in **Table 3.7**.

Table 3.7 Palladium catalysed hydroxycarbonylation of 1-hexene.[a]

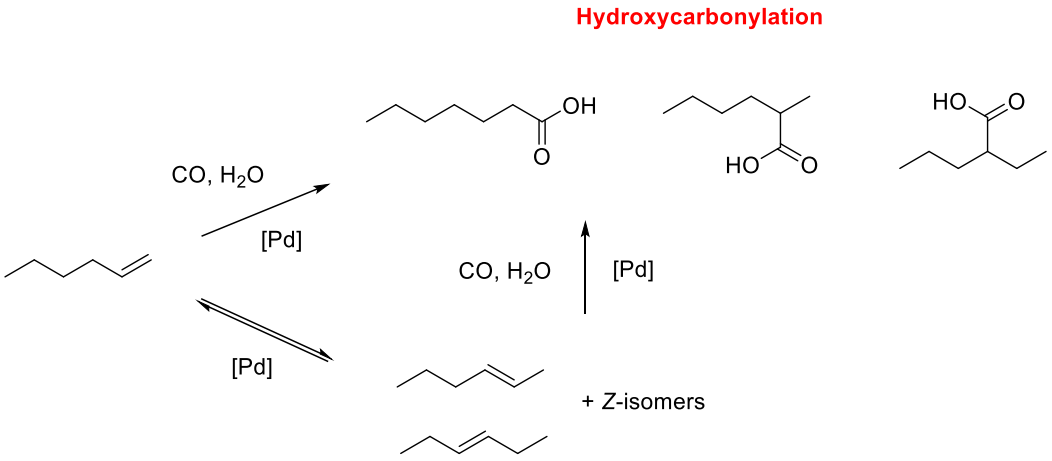

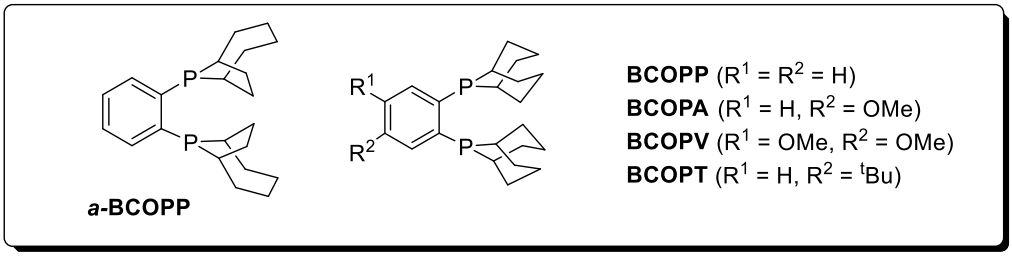

Ligand	Conv. / %	Internal Hexenes / %	Heptanoic Acids (linear)[b] / %	TON[c]
BCOPP	100	44	42 (68)	420
BCOPA	100	43	35 (68)	350
BCOPV	100	34	49 (69)	490
BCOPT	100	41	37 (69)	370
***α*-BCOPP**	100	47	35 (68)	350

[a]Conditions: 1-hexene (20.0 mmol), $Pd(OAc)_2$ (0.1 mol%), ligand (L/Pd = 1.4), CH_3SO_3H (acid/Pd = 10), H_2O (0.5 mL), 40 bar CO, diglyme (7 mL), 100 °C, 21 h. Yields were determined by gas chromatography

using anisole as an internal standard. [b]Linear = moles of terminal acid/moles of all acids. [c]TON = moles of acids/moles of catalyst. Note: Minor amounts (0.3 – 1%) of C_{13} ketones and heptanal detected in all runs and a small amount (3 – 4%) of heptanol was detected in all runs except the one using ***α*-BCOPP**. All single runs.

Quantitative conversions were achieved across the series to give a product mixture containing mainly internal hexenes and heptanoic acids. Linear selectivities were similar (68 – 69%) despite the difference in basicity between [4.2.1]phobane in ***α*-BCOPP** and [3.3.1]phobane in other diphobanes, suggesting that regioselectivity is not significantly affected by the electrophilicity of the Pd centre. Hydroxycarbonylation activities were similar across the series with electron-rich dimethoxy-substituted **BCOPV** yielding slightly more heptanoic acid.

3.6.2 Hydroxycarbonylation of 4-Pentenoic Acid (4PA)

The route from biomass-derived γ-valerolactone (GVL) to adipic acid (ADA), a monomer for the industrial production of nylon-6,6,[83] has been achieved using a combination of heterogeneous and homogenous catalysis.[84] One of the key steps in that process is the hydroxycarbonylation of pentenoic acids obtained from the reactive distillation of GVL,[65] a step that can be catalysed by Pd-diphobane catalysts. The diphobane ligand series has been evaluated in palladium catalysed hydroxycarbonylation of 4-pentenoic acid (4PA) to ascertain their applicability in such processes and the results are summarised in **Table 3.8**.

Table 3.8 Palladium catalysed hydroxycarbonylation of 4-pentenoic acid (4PA).[a]

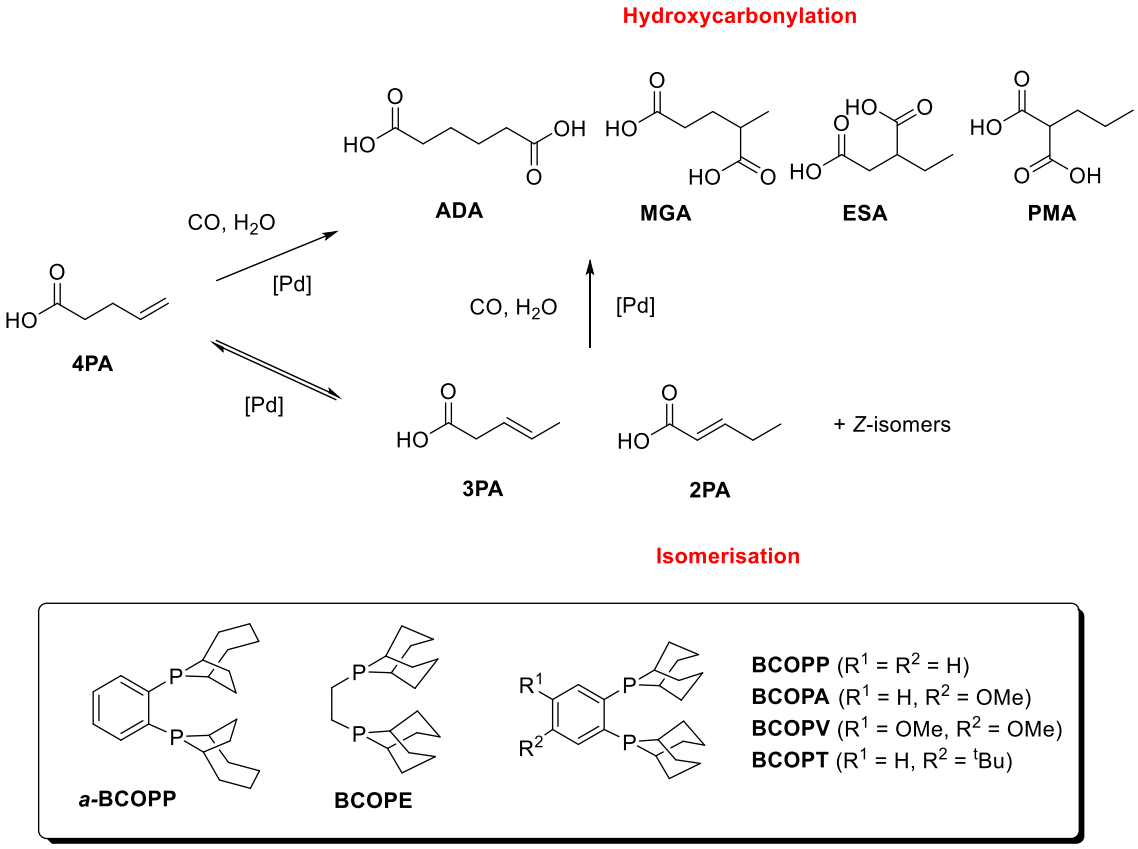

			Isomerisation		Hydroxycarbonylation				
	Conv	4PA	3PA	2PA	ADA	MGA	ESA	PMA	
Ligand	/ %	/ %	/ %	/ %	/ %	/ %	/ %	/ %	TON[b]
***a*-BCOPP**	97	3	38	17	2	1	39	0	420
BCOPE	98	2	29	67	0	0	2	0	20
BCOPP	96	4	57	22	1	1	15	<1	170
BCOPA	96	4	59	17	1	1	18	0	200
BCOPV	97	3	46	27	2	1	21	0	240
BCOPT	95	5	63	12	1	1	18	0	200

[a]Conditions: 4-pentenoic acid (20.0 mmol), $Pd(OAc)_2$ (0.1 mol%), ligand (L/Pd = 1.4), CH_3SO_3H (acid/Pd = 10), H_2O (0.5 mL), 40 bar CO, diglyme (7.5 mL), 100 °C, 21 h. Yields were determined by gas chromatography using anisole as an internal standard. [b]TON = sum of moles of ADA, MGA, ESA and PMA/moles of catalyst. ADA = adipic acid. MGA = 2-methylglutaric acid. ESA = ethylsuccinic acid. PMA = propylmalonic acid. Note: all single runs.

There are near quantitative conversions (≥95%) across the series to give a mixture of internal pentenoic acid and diacid products. The hydroxycarbonylation activity trend for the diphobane ligands appears to match that for alkoxycarbonylation, in the order ***a*-BCOPP > BCOPP ≈ BCOPA ≈ BCOPV ≈ BCOPT > BCOPE**. The major product in all cases is ethylsuccinic acid (ESA), where functionalisation

occurs at the 3-position. Palladium catalysed hydroxycarbonylation of pentenoic acids favouring functionalisation at the 3-position has been described in the literature.[65] Chelation of the carboxylic acid functionality to the Pd centre can form stable 5-membered palladacycles that are subsequently carbonylated and hydrolysed to give ESA.

The major internal pentenoic acid isomer observed in most of the product mixtures (**Table 3.8**) is 3-pentenoic acid (3PA), which can be derived from β-hydride elimination of such stable 5-membered palladacycles. **BCOPE** is the exception, producing 2-pentenoic acid (2PA) as the major isomer in its product mixture in the ratio 67:29:2 for 2-, 3- and 4-pentenoic acids (**Table 3.8**). 2PA is expected to be the major pentenoic acid isomer due to the stability conferred by conjugation with the carboxylic acid group. The observed chelate-driven regioselectivity for the aryl-bridged diphobane ligands compared to **BCOPE** suggests a stronger chelate effect that favours the formation of 5-membered palladacycles. This effect could be related to the different flexibility of the ligand backbones.

3.7 Conclusions and Outlook for Pd-Diphobane Catalysed Olefin Carbonylation

Pd-diphobanes are active hydroformylation catalysts giving excellent yields and selectivities in isomerising reductive hydroformylation of olefins.[19] A series of C_2-bridged diphobane ligands with modified backbones have been synthesised to investigate the impact of systematic ligand variation on co-ordination behaviour and catalytic performance. X-ray crystallographic analysis of the solid-state structures of a selection of [Pd(diphobane)Cl_2] complexes show several differences in geometry, including:

(1) smaller P-Pd-P ligand bite angles for 1,2-phenylene-bridged diphobanes (**BCOPP** and ***α*-BCOPP**) versus ethylene-bridged diphobane (**BCOPE**)
(2) more strained C-P-C bond angle for [4.2.1]phobane than for [3.3.1]phobane
(3) 5-membered chelate formation to give either a clearly defined “envelope” conformation (**BCOPP** and ***α*-BCOPP**) or a “half-chair” conformation (**BCOPE**)

For palladium catalysed hydroformylation of 1-hexene, higher hydroformylation and reductive hydroformylation activities appeared to be favoured by electron-rich ligands. However, the benchmark **BCOPE** remains the best candidate to produce heptanol from either terminal or internal hexenes. For functionalised olefins such as methyl pentenoates, the picture is more complex owing to the influence of the acid co-catalyst on product selectivity. Lower acid concentrations or weaker acids decrease hydrogenation of both olefins and aldehydes, resulting in significant changes in chemoselectivity. In general, however, ethylene-bridged diphobane (**BCOPE**) is more reducing than

phenylene-bridged diphobane (**BCOPP**) with methanesulfonic acid and exhibits superior olefin isomerisation abilities with weaker acids such as trifluoroacetic acid.

Evaluation of the diphobane ligand series in palladium catalysed hydroformylation of 1-octene in 2-ethylhexanol resulted in competing alkoxycarbonylation that was favoured by electron-poor ligands. Alkoxycarbonylation activity was also found to be promoted by H_2O or hindered by NaCl. For palladium catalysed hydroxycarbonylation of 1-hexene, functionalisation at the 3-position was found to be favoured to give ethylsuccinic acid (ESA) as the major product. The high selectivity for branched products was attributed to the formation of stable 5-membered palladacycles resulting in chelate-driven regioselectivity favouring ESA.

A study of the co-ordination chemistry and electronic properties of these diphobane ligands may give hints toward the design of more active palladium-based hydroformylation catalysts that have thus far proved elusive. It would be intriguing to see if the linear selectivity of **BCOPE** can be further enhanced while retaining its high activity. For example, by increasing steric bulk (**Figure 3.23**) to disfavour the formation of sterically demanding branched Pd-alkyl intermediates leading to branched aldehyde products.

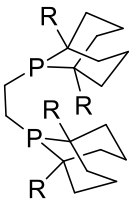

Figure 3.23 Proposed bulkier **BCOPE** analogue. R = alkyl.

Further mechanistic studies on palladium catalysed hydroformylation may also lead to improvements in catalytic performance as current understanding is still lacking when compared with the knowledge gathered on the analogous rhodium catalysed processes.

3.8 Chapter 3 References

1. Shell Internationale Research Maatschappij N.V., Ditertiary Phosphines and Application thereof as Catalyst Components for Alcohol Production. GB1127965A, 1966.

2. Mason, R. F.; Winkle, J. L. V. Shell Oil Company, Hydrocarbylene-Bis (monophosphobicyclononanes) and the Preparation Thereof. US3401204A, 1968.

3. Winkle, J. L. V.; Morris, R. C.; Mason, R. F. Shell Oil Company, Single Stage Hydroformylation of Olefins to Alcohols. US3420898A, 1969.

4. Abbenhuis, H. C. L.; Burckhardt, U.; Gramlich, V.; Koellner, C.; Pregosin, P. S.; Salzmann, R.; Togni, A., *Organometallics* **1995,** *14*, 759-766.

5. Hamada, Y.; Seto, N.; Ohmori, H.; Hatano, K., *Tetrahedron Lett.* **1996,** *37*, 7565-7568.

6. Hamada, Y.; Seto, N.; Takayanagi, Y.; Nakano, T.; Hara, O., *Tetrahedron Lett.* **1999,** *40*, 7791-7794.

7. Hamada, Y.; Sakaguchi, K.-e.; Hatano, K.; Hara, O., *Tetrahedron Lett.* **2001,** *42*, 1297-1299.

8. Butti, P.; Rochat, R.; Sadow, A. D.; Togni, A., *Angew. Chem. Int. Ed.* **2008,** *47*, 4878-4881.

9. Abbenhuis, H. C. L.; Burckhardt, U.; Gramlich, V.; Martelletti, A.; Spencer, J.; Steiner, I.; Togni, A., *Organometallics* **1996,** *15*, 1614-1621.

10. Luo, H.-K.; Li, D.-G., *Appl. Organomet. Chem.* **2000,** *14*, 389-393.

11. Braun, W.; Salzer, A.; Spindler, F.; Alberico, E., *Appl. Catal., A* **2004,** *274*, 191-203.

12. Lewis, J. C.; Berman, A. M.; Bergman, R. G.; Ellman, J. A., *J. Am. Chem. Soc.* **2008,** *130*, 2493-2500.

13. Meyer, W. H.; McConnell, A. E.; Forman, G. S.; Dwyer, C. L.; Kirk, M. M.; Ngidi, E. L.; Blignaut, A.; Saku, D.; Slawin, A. M. Z., *Inorg. Chim. Acta* **2006,** *359*, 2910-2917.

14. Williams, D. B. G.; Ajam, M.; Ranwell, A., *Organometallics* **2006,** *25*, 3088-3090.

15. Dwyer, C. L.; Kirk, M. M.; Meyer, W. H.; Janse van Rensburg, W.; Forman, G. S., *Organometallics* **2006,** *25*, 3806-3812.

16. Forman, G. S.; McConnell, A. E.; Tooze, R. P.; Janse van Rensburg, W.; Meyer, W. H.; Kirk, M. M.; Dwyer, C. L.; Serfontein, D. W., *Organometallics* **2005,** *24*, 4528-4542.

17. Drent, E.; De Castro, M. M.; Giilespie, H. M.; Savage, P. D.; Van Helden, A. K.; McKenna, E. G. Shell Internationale Research Maatschappij B.V., Process for the Carbonylation of Ethylenically Unsaturated Compounds. WO9738964, 1997.

18. Eberhard, M. R.; Carrington-Smith, E.; Drent, E. E.; Marsh, P. S.; Orpen, A. G.; Phetmung, H.; Pringle, P. G., *Adv. Synth. Catal.* **2005,** *347*, 1345-1348.

19. Konya, D.; Almeida Leñero, K. Q.; Drent, E., *Organometallics* **2006,** *25*, 3166-3174.

20. Carreira, M.; Charernsuk, M.; Eberhard, M.; Fey, N.; Ginkel, R. v.; Hamilton, A.; Mul, W. P.; Orpen, A. G.; Phetmung, H.; Pringle, P. G., *J. Am. Chem. Soc.* **2009,** *131*, 3078-3092.

21. Eberhard, M. R. New Strategies In 9-Phosphabicyclononane Chemistry. Ph.D. Thesis, University of Bristol, United Kingdom, 2001.

22. Orpen, A. G.; Connelly, N. G., *J. Chem. Soc., Chem. Commun.* **1985**, 1310-1311.

23. Orpen, A. G.; Connelly, N. G., *Organometallics* **1990,** *9*, 1206-1210.

24. Dunne, B. J.; Morris, R. B.; Orpen, A. G., *J. Chem. Soc., Dalton Trans.* **1991**, 653-661.

25. Torres, G. M.; Frauenlob, R.; Franke, R.; Borner, A., *Catal. Sci. Technol.* **2015,** *5*, 34-54.

26. Drent, E.; Van Ginkel, R.; Jager, W. W. Shell Internationale Research Maatschappij B.V., Process for Producing Olefins. WO2008034894 A1, 2008.

27. Mul, W. P. Shell Internationale Research Maatschappij B.V., Hydroformylation Process for Production of Alcohols and Aldehydes. WO2007003589A1, 2007.

28. Bungu, P. N.; Otto, S., *Dalton Trans.* **2007**, 2876-2884.

29. Pospech, J.; Fleischer, I.; Franke, R.; Buchholz, S.; Beller, M., *Angew. Chem. Int. Ed.* **2013,** *52*, 2852-2872.

30. Franke, R.; Selent, D.; Börner, A., *Chem. Rev.* **2012,** *112*, 5675-5732.

31. Drent, E.; Jager, W. W. Shell Oil Company, Hydroformylation Reactions. US5780684, 1997.

32. Drent, E.; Van Ginkel, R.; Jager, W. W. Shell Oil Company, Process for the Hydroformylation of an Ethylenically Unsaturated Compound. US7414155B2, 2008.

33. Elsner, G.; Heymer, G.; Stephan, H.-W. Hoechst AG, Continuous Production of Organic Phosphines. US4163760A, 1979.

34. Bungu, P. N.; Otto, S., *J. Organomet. Chem.* **2007,** *692*, 3370-3379.

35. Fawcett, J.; Hoye, P. A. T.; Kemmitt, R. D. W.; Law, D. J.; Russell, D. R., *J. Chem. Soc., Dalton Trans.* **1993**, 2563-2568.

36. Downing, J. H.; Gee, V.; G. Pringle, P., *Chem. Commun.* **1997**, 1527-1528.

37. J. Coles, S.; G. Edwards, P.; B. Hursthouse, M.; M. Abdul Malik, K.; L. Thick, J.; P. Tooze, R., *J. Chem. Soc., Dalton Trans.* **1997**, 1821-1830.

38. Wolf, J.; Thommes, K.; Briel, O.; Scopelliti, R.; Severin, K., *Organometallics* **2008,** *27*, 4464-4474.

39. Dunne, J. P.; Aiken, S.; Duckett, S. B.; Konya, D.; Almeida Leñero, K. Q.; Drent, E., *J. Am. Chem. Soc.* **2004,** *126*, 16708-16709.

40. Drent, E.; Van Ginkel, R.; Jager, W. W. Shell Internationale Research Maatschappij B.V., Process for the Hydroformylation of an Ethylenically Unsaturated Compound. WO2004028689A2, 2004.

41. Yamamoto, Y.; Koizumi, T.; Katagiri, K.; Furuya, Y.; Danjo, H.; Imamoto, T.; Yamaguchi, K., *Org. Lett.* **2006,** *8*, 6103-6106.

42. Lewis, J. C.; Wu, J. Y.; Bergman, R. G.; Ellman, J. A., *Angew. Chem. Int. Ed.* **2006,** *45*, 1589-1591.

43. Farrer, N. J.; McDonald, R.; Piga, T.; McIndoe, J. S., *Polyhedron* **2010,** *29*, 254-261.

44. Chuong, R.; Luck, K. A.; Luck, R. L.; Nguyen, L. P.; Phan, D.; Pignotti, L. R.; Urnezius, E.; Valente, E. J., *J. Organomet. Chem.* **2013,** *724*, 45-50.

45. Hansch, C.; Leo, A.; Taft, R. W., *Chem. Rev.* **1991,** *91*, 165-195.

46. Tolman, C. A., *J. Am. Chem. Soc.* **1970,** *92*, 2953-2956.

47. Moloy, K. G.; Petersen, J. L., *J. Am. Chem. Soc.* **1995,** *117*, 7696-7710.

48. Roodt, A.; Otto, S.; Steyl, G., *Coord. Chem. Rev.* **2003,** *245*, 121-137.

49. Arcau, J.; Ferrer, M.; Aguiló, E.; Rodríguez, L., *Transition Met. Chem.* **2017,** *42*, 57-67.

50. Freixa, Z.; van Leeuwen, P. W. N. M., *Dalton Trans.* **2003**, 1890-1901.

51. Van Leeuwen, P. W. N. M.; Freixa, Z., Bite Angle Effects of Diphosphines in Carbonylation Reactions. In *Modern Carbonylation Methods*, Kollár, L., Ed. Wiley-VCH Verlag GmbH & Co. KGaA: Germany, 2008; pp 1-20.

52. Dierkes, P.; W. N. M. van Leeuwen, P., *J. Chem. Soc., Dalton Trans.* **1999**, 1519-1530.

53. Marson, A.; van Oort, A. B.; Mul, Wilhelmus P., *Eur. J. Inorg. Chem.* **2002,** *2002*, 3028-3031.

54. Baya, M.; Houghton, J.; Konya, D.; Champouret, Y.; Daran, J.-C.; Almeida Leñero, K. Q.; Schoon, L.; Mul, W. P.; Oort, A. B. v.; Meijboom, N.; Drent, E.; Orpen, A. G.; Poli, R., *J. Am. Chem. Soc.* **2008,** *130*, 10612-10624.

55. Drent, E.; Budzelaar, P. H. M., *J. Organomet. Chem.* **2000,** *593–594*, 211-225.

56. Chen, Q.-A.; Ye, Z.-S.; Duan, Y.; Zhou, Y.-G., *Chem. Soc. Rev.* **2013,** *42*, 497-511.

57. Slaugh, L. H.; Mullineaux, R. D. Shell Oil Co, Hydroformylation of Olefins. US3239569A, 1966.

58. Meessen, P.; Vogt, D.; Keim, W., *J. Organomet. Chem.* **1998,** *551*, 165-170.

59. Guthrie, J. P., *Can. J. Chem.* **1978,** *56*, 2342-2354.

60. Milne, J. B.; Parker, T. J., *J. Solution Chem.* **1981,** *10*, 479-487.

61. Goldbach, V.; Roesle, P.; Mecking, S., *ACS Catal.* **2015,** *5*, 5951-5972.

62. Behr, A.; Obst, D.; Westfechtel, A., *Eur. J. Lipid Sci. Technol.* **2005,** *107*, 213-219.

63. Bianchini, C.; Meli, A.; Oberhauser, W., *Dalton Trans.* **2003**, 2627-2635.

64. Johnson, L. K.; Mecking, S.; Brookhart, M., *J. Am. Chem. Soc.* **1996,** *118*, 267-268.

65. Low, C. H.; Nobbs, J. D.; van Meurs, M.; Stubbs, L. P.; Drent, E.; Aitipamula, S.; Pung, M. H. L., *Organometallics* **2015,** *34*, 4281-4292.

66. Bahrmann, H.; Hahn, H.-D.; Mayer, D.; Frey, G. D., 2-Ethylhexanol. In *Ullmann's Encyclopedia of Industrial Chemistry*, Wiley-VCH Verlag GmbH & Co. KGaA, 2013.

67. Kohlpaintner, C.; Schulte, M.; Falbe, J.; Lappe, P.; Weber, J., Aldehydes, Aliphatic. In *Ullmann's Encyclopedia of Industrial Chemistry*, Elvers, B., Ed. Wiley-VCH Verlag GmbH & Co. KGaA.: 2008; Vol. 2, pp 304-305.

68. Zuidema, E.; Bo, C.; van Leeuwen, P. W. N. M., *J. Am. Chem. Soc.* **2007,** *129*, 3989-4000.

69. Nobbs, J. D.; Low, C. H.; Stubbs, L. P.; Wang, C.; Drent, E.; van Meurs, M., *Organometallics* **2017,** *36*, 391-398.

70. Roesle, P.; Caporaso, L.; Schnitte, M.; Goldbach, V.; Cavallo, L.; Mecking, S., *J. Am. Chem. Soc.* **2014,** *136*, 16871-16881.

71. Fang, X.; Li, H.; Jackstell, R.; Beller, M., *Angew. Chem. Int. Ed.* **2014,** *53*, 9030-9034.

72. Ballinger, P.; Long, F. A., *J. Am. Chem. Soc.* **1960,** *82*, 795-798.

73. Morrill, T. C.; D'Souza, C. A., *Organometallics* **2003,** *22*, 1626-1629.

74. English, A.; E&C, J. B.; Rovner, J.; Davies, S., Methanol. In *Kirk-Othmer Encyclopedia of Chemical Technology*, John Wiley & Sons: 2015; pp 1-19.

75. Battino, R.; Bo, S.; Clever, H. L.; Gjaldbaek, J. C.; Wiesenburg, D. A.; Wilheim, E.; Yampol'skii, Y. P.; Young, C. L., Carbon Monoxide. In *Solubility Data Series*, Lorimer, J. W.; Clever, H. L.; Young, C. L.; Barton, A. F. M.; Cohen-Adad, R.; Crovetto, R.; Fermeglia, M.; Fogg, P. G. T.; Gerrad, W.; Getzen, F. W.; Gevantman, L. H.; Hayduk, W.; Hefter, G. T.; Mather, A. E.; Salomon, M.; Scharlin, P.; Tomkins, R. P. T.; Gujral, P. D., Eds. Pergamon: Oxford, New York, 1990; Vol. 43, pp 152-207.

76. Young, C. L., Hydrogen and Deuterium. In *Solubility Data Series*, Kertes, A. S.; Akaiwa, H.; Barton, A. F. M.; Battino, R.; Bylicki, A.; Clever, H. L.; Cohen-Adad, R.; Gerrad, W.; Getzen, F. W.; Gevantman, L. H.; Haulait-Pirson, M. C.; Hayduk, W.; Horvath, A. L.; Huyskens, P.; Kalidas, C.; Lorimer, J. W.; Maczynski, A.; Navratil, J. D.; Salomon, M.; Schindler, P. W.; Shaw, D. G.; Vanderzee, C. E.; Vesala, A.; Wilhelm, E.; Woolley, E. M.; Yalkowsky, S. H.; Young, C. L., Eds. Pergamon: Elmsford, New York, 1981; Vol. 5/6, pp 435-480.

77. Harrod, J. F.; Chalk, A. J., *J. Am. Chem. Soc.* **1966,** *88*, 3491-3497.

78. Cavinato, G.; Toniolo, L., *J. Mol. Catal. A: Chem.* **1996,** *104*, 221-227.

79. Vavasori, A.; Toniolo, L.; Cavinato, G., *J. Mol. Catal. A: Chem.* **2003,** *191*, 9-21.

80. Estorach, C. T.; Masdeu-Bultó, A. M., *Catal. Lett.* **2008,** *122*, 76-79.

81. Li, H.; Dong, K.; Jiao, H.; Neumann, H.; Jackstell, R.; Beller, M., *Nat. Chem.* **2016,** *8*, 1159.

82. Amézquita-Valencia, M.; Achonduh, G.; Alper, H., *J. Org. Chem.* **2015,** *80*, 6419-6424.

83. Palmer, R. J., Polyamides, Plastics. In *Encyclopedia of Polymer Science and Technology*, John Wiley & Sons: 2001.

84. Wong, P.; Li, C.; Stubbs, L.; Van Meurs, M.; Kumbang, D.; Lim, S.; Drent, E. A*STAR, Synthesis of Diacids. WO2012134397, 2012.

Chapter 4 – Ru-Catalysed Olefin Carbonylation Utilising CO_2 as a CO Surrogate

4.1 Introduction to Ru-catalysed Reverse Water-Gas Shift (rWGS) Reactions

The reduction of CO_2 to CO catalysed by Ru carbonyl clusters has been reported as early as 1985.[1] This work was further developed by Tominaga and Sasaki in 1994, who employed anionic Ru clusters generated from $Ru_3(CO)_{12}$ to catalyse conversion of CO_2 to CO via the reverse Water-Gas Shift (rWGS) reaction (**Equation 4.1**).[2]

Equation 4.1 The reverse Water-Gas Shift (rWGS) reaction.

$$CO_2 + H_2 \rightleftharpoons CO + H_2O \qquad \Delta H^0_{298K} = +42.1 \text{ kJ mol}^{-1}$$

Their homogeneous Ru-based system operated under milder temperatures than their heterogeneous counterparts, allowing it to be coupled to Ru-catalysed olefin hydroformylation to utilise the CO generated in situ to produce alcohols from a variety of olefins.[3-9] Due to the presence of H_2 however, undesired olefin hydrogenation to alkanes competes as an side reaction.

The Ru-based system pioneered by Tominaga and Sasaki[10-12] has since garnered considerable interest, notably from Beller and co-workers, who first employed the use of bulky monodentate phosphite ligands to decrease undesired olefin hydrogenation side reactions and improve alcohol yields (**Figure 4.1**).[13]

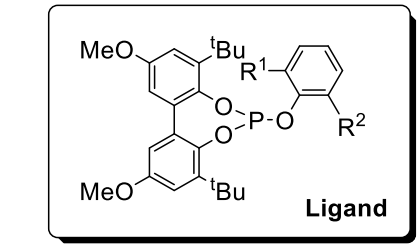

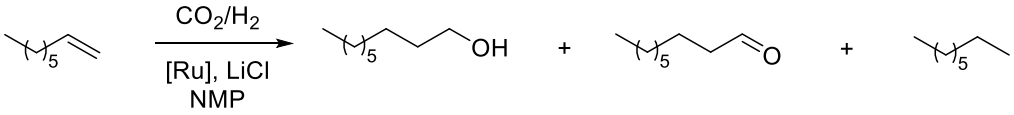

No Ligand	33%	6%	22%
$R^1 = R^2 = H$	76%	1.5%	12%
$R^1 = H, R^2 = Me$	76%	1%	15%
$R^1 = R^2 = Me$	63%	2%	13%
$R^1 = H, R^2 = {}^tBu$	72%	6%	12%

Figure 4.1 Ru-catalysed hydroformylation of 1-octene with CO_2.[13] NMP = N-Methyl-2-pyrrolidone.

They also found that variation at the *ortho*-position of the phenol ring of the phosphite ligand (**Figure 4.1**) had a significant impact on the reaction outcome. Introduction of a single *ortho*-methyl on the phenol ring gave similar performance to the unsubstituted analogue but o,o-dimethylation led to diminished activities and formation of uncharacterised side products (**Figure 4.1**).[13] For analogues bearing a single ortho *tert*-butyl on the phenol ring, slower hydrogenation of the intermediate nonanal to the desired nonanol product was observed instead.

Ligands possess considerable potential to influence catalytic performance and tune reaction outcomes. Some examples of their application to systems utilising CO_2 to produce oxo products from olefins include Rh-catalysed hydroformylation,[14] Rh-catalysed hydroxycarbonylation[15] and Cu-catalysed reductive hydroxymethylation.[16] For the Ru-based system proceeding via the rWGS reaction however, reports of employing ligands to tune the reaction are rare,[13] possibly owing to the ambiguous role played by Ru clusters and the potential for ligands to disperse them. However, Tominaga and co-workers have recently shown that mononuclear Ru complexes are also able to catalyse the rWGS reaction.[9] The rWGS reaction shows great promise in combating rising anthropogenic CO_2 emissions that have serious environmental consequences.[17] For example, when producing fuels from CO_2 captured from flue gas or from the atmosphere, the rWGS reaction has been estimated to possess the highest potential efficiency compared to a selection of light-driven and electrocatalytic processes.[18] The application of the rWGS reaction to convert CO_2 to gasoline alone has the potential to reduce atmospheric CO_2 influx by more than a third, assuming a readily available green source of H_2.[17]

This chapter explores the effect of several monodentate and bidentate ligands on the Ru-based system pioneered by Tominaga and Sasaki.[19] Two variants on the monodentate phosphite framework have been synthesised and characterised. The synthesised phosphite ligands, together with several commercially available ligands have been evaluated in the tandem Ru-catalysed rWGS-hydroformylation-reduction of olefins to alcohols. The ligand free Ru-based system was then studied to better understand how catalyst loading, salt additives and choice of solvent affected reaction outcomes and to provide an indication of how reaction optimisation could proceed. The chapter then concludes with an outlook on this area of research.

4.2 Monodentate Phosphite Ligand Synthesis

Transesterification of triphenylphosphite, $P(OPh)_3$, with an equivalent of diol gave the desired monodentate phosphite ligands in moderate yield (**Figure 4.2**).

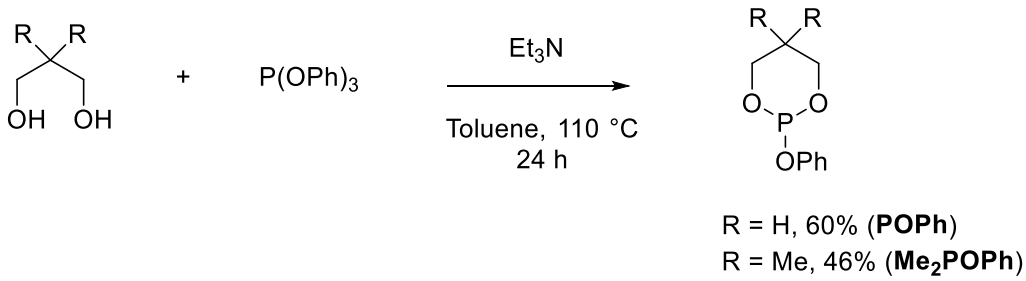

Figure 4.2 Synthesis of monodentate phosphite ligands.

Initial transesterification attempts were performed under neat conditions without base and yielded no desired product. The addition of an equivalent of Et_3N was essential to deprotonate the relatively acidic phenol released from alcohol exchange, precipitating it as a salt and driving the equilibrium in favour of the desired product. An alternative synthetic route to analogous cyclic phosphites has been reported to proceed via substitution of dichloroalkylphosphine with diol, albeit with poorer yields.[20]

The boiling points of the cyclic phosphite products are reported to be 88 °C (**POPh**)[21] and 90 – 95 °C (**Me$_2$POPh**)[22] respectively, well below that of the starting triphenylphosphite (365 °C)[23] or diol (R = H, 217 °C, R = Me, 238 – 240 °C)[24-25] reactants. The differentiated boiling points between reactants and products allow for a convenient purification via distillation under reduced pressure. The desired products were thus obtained as either translucent crystals (**POPh**) or a clear oil (**Me$_2$POPh**) at room temperature and pressure, suggesting that the presence of two additional methyl groups on the 6-membereded ring may be disrupting packing of the dimethylated analogue to give a lower melting point despite its relatively higher molecular weight.

4.2.1 Phosphite Stability

Phosphites have been known to degrade through hydrolysis,[26] alcoholysis, transesterification and Arbusov rearrangement mechanisms.[27] The Ru-catalysed rWGS-hydroformylation-reduction of olefins produces H_2O through the rWGS reaction (**Equation 4.1**) that may cause hydrolysis, while subsequent Ru-catalysed hydroformylation-reduction of olefins produces alcohol products that may result in alcoholysis or transesterification. This is especially so in the case of **POPh** and **Me$_2$POPh** (**Figure 4.3**) as they lack multiple bulky aryl substituents that are typically included to combat such degradation.[27-28] Aliphatic phosphites are also known to be more susceptible to Arbusov rearrangements than their aryl analogues.[27]

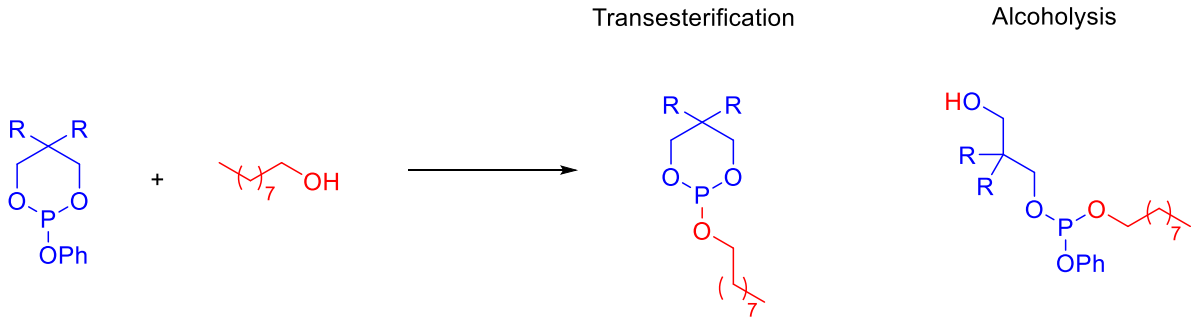

Figure 4.3 Decomposition of **POPh** and **Me$_2$POPh** by reacting with 1-nonanol. R = H or Me.

To test the stability of **POPh** and **Me$_2$POPh**, a 0.33:1:1 mixture of $Ru_3(CO)_{12}$/ligand/1-nonanol was prepared in NMP and monitored by $^{31}P\{^1H\}$ NMR. The mixture showed no change in phosphorus species between the initial and final mixes after standing at 130 °C for 3 h, indicating its robustness under those conditions. However, the stability of **POPh** and **Me$_2$POPh** against hydrolysis was not tested and caution should be exercised when drawing conclusions from catalysis runs with these ligands as a significant amount of water is expected to be generated through the reverse Water-Gas Shift reaction. The following investigation into Ru-catalysed rWGS-hydroformylation-reduction of 1-octene was also conducted at the same temperature (130 °C). Union Carbide have also performed similar investigations into phosphite stability as part of their patents on transition metal-diorganophosphite complex catalysed hydroformylation reactions, though not specifically on **POPh** and **Me$_2$POPh**.[29-30]

4.3 Ligands Effects in Ru-Catalysed rWGS-Hydroformylation-Reduction of 1-Octene

The monodentate phosphite ligands **POPh** and **Me$_2$POPh** together with a selection of commercially available ligands were evaluated in tandem Ru-catalysed rWGS-hydroformylation-reduction of 1-octene and the results have been summarised in **Table 4.1**. The catalyst was formed in situ by mixing $Ru_3(CO)_{12}$ with ligand in N-methyl-2-pyrrolidone (NMP) followed by the addition of LiCl (Cl/[Ru] = 16.7). Halide anions have been noted to be essential for Ru-catalysed rWGS reactions.[2, 11] The order of catalytic activity has also been observed to decrease down the group in the order $Cl^- > Br^- > I^-$. The exact role the halide anions play is still under debate, however one of the hypotheses put forward by Tominaga and Sasaki theorizes that the halide acts to abstract or facilitate the abstraction of a proton from a Ru complex, thus enhancing electron density at the Ru centre to enable CO_2 coordination. The phosphite-Ru system reported by Beller and co-workers was used as a benchmark despite imperfect mole balances (56 – 101%) reported as good alcohol yields were obtained using a ligand-promoted Ru-based system.[13] However, it should also be noted that ruthenium cluster carbonyls have been

observed to interact with phosphine ligands such as 1,8-bis(diphenylphosphino)napthlene in C-H and C-P bond cleavage reactions,[31] and an analogous reaction between $Ru_3(CO)_{12}$ and PPh_3 in this system may likewise occur.

Table 4.1 Ru-catalysed tandem rWGS-hydroformylation-reduction of 1-octene.[a]

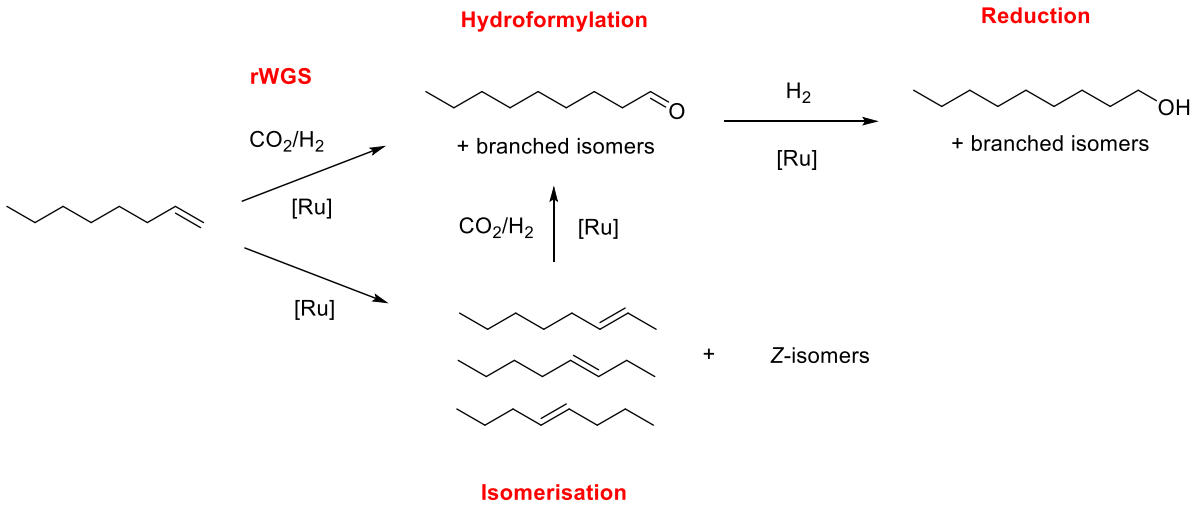

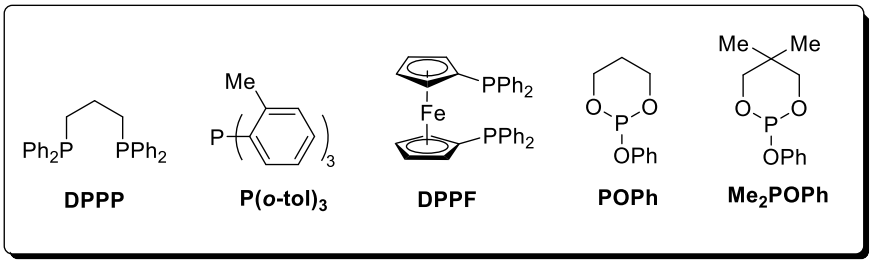

Ligand	L/ [Ru]	Conv / %	Internal Octenes / %	Octane / %	Nonanal (lin)[b] / %	Nonanol (lin)[b] / %	TON[c]	Mole Balance[d] / %
none	n.a.	100	1	40	1 (49)	42 (50)	90	84
$P(OPh)_3$	1.1	99	10	46	4 (57)	28 (52)	60	89
Me_2POPh	1.1	100	2	54	1 (53)	30 (48)	60	87
POPh	1.1	100	5	43	1 (55)	35 (49)	70	84
PPh_3	1.1	100	3	35	1 (55)	49 (52)	100	88
$P(o\text{-tol})_3$	1.1	100	1	39	1 (58)	40 (52)	80	81
DPPF	1.1	100	0	66	<1 (n.d.)	<1 (n.d.)	<1	66
DPPP	1.1	100	1	78	1 (48)	11 (54)	20	91
DPPP	0.37	100	2	67	1 (46)	21 (52)	40	91

[a]Conditions: 1-octene (12.7 mmol), $Ru_3(CO)_{12}$ (0.5 mol%), ligand, LiCl (25 mol%), 30 bar CO_2/H_2 (1:1), NMP (15 mL), 130 °C, 24 h. Yields were determined via gas chromatography using anisole as an internal standard. [b]Linear = 1-isomer/all regioisomers. [c]TON = sum of moles of nonanal and nonanol/moles of

catalyst. [d]Mole balance = moles of all identified products/moles of starting 1-octene. n.a. = not applicable. n.d. = not determined. Note: all single runs.

Quantitative conversions were achieved for nearly all runs to give product mixtures consisting of internal octenes, octane, nonanal and nonanol. The similar ratios of branched to linear products observed across all runs indicated that there was no significant difference in regioselectivity between different ligands.

4.3.1 Monodentate Ligands

In terms of increasing alcohol yields and suppressing olefin hydrogenation, the monodentate phosphite ligands performed in the order **P(OPh)$_3$** < **Me$_2$POPh** < **POPh**. All three phosphites however, gave lower alcohol yields than the ligand free system. Triphenylphosphine, **PPh$_3$**, was the only ligand tested that reduced olefin hydrogenation and increased alcohol yield to 49% (up from 42% in the ligand free system). The phosphite analogue of **PPh$_3$**, triphenylphosphite, **P(OPh)$_3$** however, had the opposite effect of reducing alcohol yield from 42% to 28% and slightly increasing octane yield from 40% to 46%. **PPh$_3$** and **P(OPh)$_3$** differ in both steric and electronic properties. The bridging oxygens connecting the phenyl groups to the phosphorus atom in **P(OPh)$_3$** result in a less sterically demanding arrangement around the phosphorus centre than in **PPh$_3$**, as indicated by its smaller Tolman cone angle of 121° versus 145° for **PPh$_3$**.[32] The greater steric demand of **PPh$_3$** over **P(OPh)$_3$** has also been noted to lengthen the metal-phosphorus bond in their respective rhodium adducts.[33] The CO stretching frequencies of the Ni(CO)$_3$(ligand) complexes for **PPh$_3$** (2068.9 cm^{-1}) and **P(OPh)$_3$** (2085.3 cm^{-1})[34] indicate that **P(OPh)$_3$** is a poorer σ-donor, better π-acceptor and should thus result in a more electrophilic metal centre.[35]

The monodentate phosphite employed by Beller and co-workers (**Figure 4.1**) bears electron-donating methoxy and *tert*-butyl groups on the biphenyl moiety to modulate the electronic properties of the ligand.[13] The combination of these electron-donating substituents and its steric bulk appears to modify the **P(OR)$_3$** framework toward resembling **PPh$_3$**, which may explain its superior performance despite the general trend of monodentate phosphites showing poor catalytic performance in the reaction. In order to favour these characteristics, an *ortho*-methyl substituent can be introduced to each of the phenyl groups in **PPh$_3$** to give **P(*o*-tol)$_3$**, simultaneously increasing both ligand steric bulk (Tolman cone angle, 194°)[32] and electron density on the phosphorus donor atom (Ni(CO)$_3$(ligand) CO stretching frequency, 2066.6 cm^{-1}).[34] The results, however, show that **P(*o*-tol)$_3$** gave 40% alcohol yield, about the same as the ligand free system (42%) and worse than **PPh$_3$** (49%).

Our two variants on the **P(OR)$_3$** framework, **POPh** and **Me$_2$POPh**, are likely less sterically hindered than **PPh$_3$** due to the replacement of two bulky phenyl groups with alkyl groups and the constraints

imposed by the 6-membered ring. The $Ni(CO)_3$(ligand) complexes of **POPh** and **Me_2POPh** have not been synthesised but generally, replacement of phenoxy with alkoxy groups is expected to decrease CO stretching frequency, indicating better σ-donor/poorer π-acceptor properties and a less electrophilic metal centre.[34] The overall result however, is that the modified monodentate phosphites, **POPh** and **Me_2POPh**, gave alcohol yields between those obtained from **PPh_3** and **$P(OPh)_3$**.

4.3.2 Bidentate Ligands

The bidentate phosphine ligands, **DPPF** and **DPPP**, were selected for their structural similarity to the best performing monodentate ligand, **PPh_3**. However, both runs employing **DPPF** or **DPPP** gave mostly octane (66% and 78% respectively, **Table 4.1**). Beller and co-workers tested a bulky bidentate ligand (**Figure 4.4**) in their study of Ru-catalysed rWGS-hydroformylation-reduction of 1-octene.[13] In that case, only olefin hydrogenation to octane and isomerisation to internal octenes was observed. Their bulky bidentate ligand was based on the Xantphos scaffold known for its rigid aromatic backbone that enforces wide bite angles (>100°).[36]

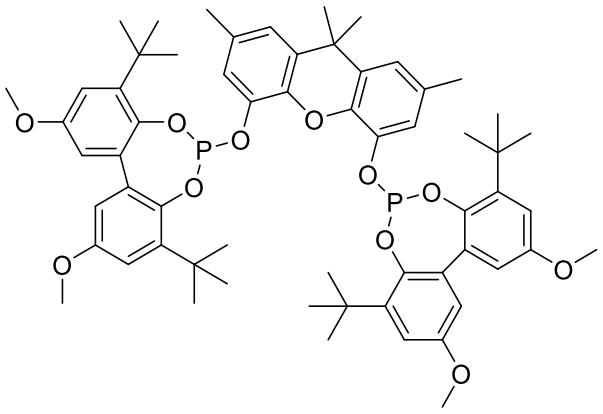

Figure 4.4 Bulky bidentate ligand based on Xantphos backbone.

It is noteworthy however, that decreasing **DPPP**/[Ru] ratio from 1.1 to 0.37 nearly doubled alcohol yield (11% to 21%) with a concomitant reduction in octane yield (78% to 67%, **Table 4.1**). Beller and co-workers noted that increasing **PPh_3**/[Ru] ratio from 1 to 3 limited both hydroformylation of 1-octene and reduction of 1-nonanal but did not significantly affect hydrogenation of 1-octene under reaction conditions.[13] A single equivalent of bidentate **DPPP** can act as two equivalents of **PPh_3** in terms of coordination, and may result in a similar inhibiting effect observed for excess **PPh_3**. The reduction of **DPPP**/[Ru] from 1.1 to 0.37 may then possibly be either limiting the amount of Ru being chelated by **DPPP** and deactivated toward hydroformylation or allowing the limited amount of **DPPP** to coordinate in a monodentate fashion to multiple Ru centres in a way that does not deactivate the catalyst toward hydroformylation, thus leading to the improvement in alcohol yield and reduction in octane yield observed.

Overall however, poor mole balances like those obtained by Beller and co-workers were observed. Poor mole balances such as the 66% for the run employing **DPPF**, suggest possible side reactions and uncharacterised products. This prompted an investigation into the simpler ligand-free Ru-catalysed rWGS-hydroformylation-reduction of 1-octene to establish a better understanding of the system that may perhaps provide an indication of how reaction optimisation could proceed.

4.4 Ru-Catalysed rWGS-Hydroformylation-Reduction

The Ru-based rWGS-hydroformylation-reduction system was investigated by varying substrate, solvent, salt additive and catalyst loading (**Table 4.2**). These variables were selected as previous investigations by Arai and co-workers have already shown the beneficial effects of increasing LiCl/[Ru] ratio and higher CO_2/H_2 pressures on alcohol yield.[10] Studies by Tominaga and Sasaki on reaction temperature have also shown that alcohol yield reaches a maximum at 130 °C, above which competing olefin hydrogenation to alkanes begins to accelerate and take over as the major product.[6]

Table 4.2 Ru-catalysed rWGS-hydroformylation-reduction of olefins.[a]

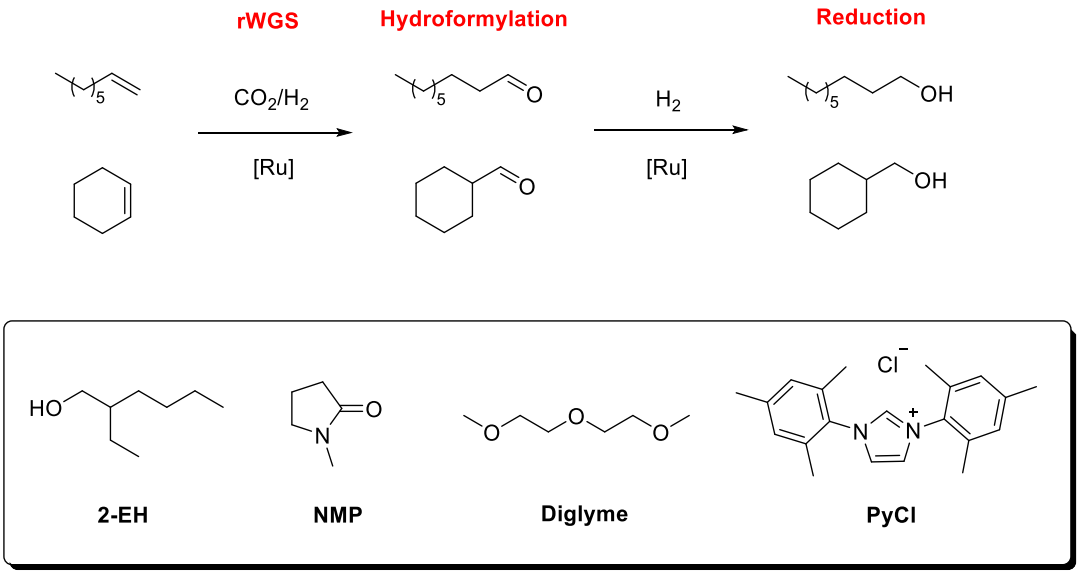

#	Olefin	Solvent	Salt	Conv / %	Aldehyde / %	Alcohol / %	Alkane / %	Mole Balance[b] / %
Lit[6]	Cyclohexene	NMP	LiCl	100	2	88	6	96
1[c]	Cyclohexene	NMP	LiCl	99	3	90	3	99
2	1-Octene	NMP	LiCl	99	5	60	26	92
3[d]	1-Octene	NMP	LiCl	98	2	18	52	85
4[e]	1-Octene	Diglyme	LiCl	100	0	0	96	96

5	1-Octene	Diglyme	PPh_4Cl	100	0	3	87	90
6	1-Octene	Toluene	PyCl	100	0	2	95	97
7	1-Octene	2-EH	PPh_4Cl	100	4	13	80	97
8[f]	1-Octene	1,4-Dioxane	LiCl	99	0	10	84	94
9[g]	1-Octene	NMP/1,4-Dioxane (1:1)	LiCl	99	4	17	52	92
10	1-Octene	NMP/1,4-Dioxane (2:3)	LiCl	99	2	65	31	99

[a]Conditions: olefin (12.5 mmol), $Ru_3(CO)_{12}$ (2 mol%), salt (8 mol%), solvent (20 mL), 80 bar CO_2/H_2 (1:1), 140 °C, 30 h. Yields were determined via gas chromatography using anisole as an internal standard. [b]Mole Balance = moles of all identified products/moles of starting olefin. [c]Reaction time 30 h, 2% cyclohexylethanol detected in product mixture. [d]$Ru_3(CO)_{12}$ (0.2 mol%), LiCl (0.8 mol%). 12% internal octenes detected. [e]$Ru_3(CO)_{12}$ (0.5 mol%), LiCl (25 mol%), 30 bar CO_2/H_2 (1:1). [f]1,4-Dioxane (14 mL). [g]19% internal octenes detected. Note: all single runs.

An initial Ru-catalysed rWGS-hydroformylation-reduction experiment (run 1, **Table 4.2**) duplicating the work of Tominaga and Sasaki was run for benchmarking purposes.[6] The results were similar, indicating that despite the different scale and apparatus used, the conditions described in previous reports of the Ru-based rWGS-hydroformylation-reduction system have been replicated.

4.4.1 Mole Balance

Previous reports describing the Ru-catalysed rWGS-hydroformylation-reduction of 1-octene substrates gave poor mole balances (ca. 70%),[13] as was the case observed for our experiments on 1-octene in **Table 4.1** (66 – 91%). For run 2 (**Table 4.2**), initial mole balance for the reaction was 78%. Ring-opening hydrolysis of NMP that has an activated amide functionality is known.[37] It is possible that the Li^+ present in the mixture may act as a Lewis acid to activate the amide functionality in NMP, allowing a similar ring-opening alcoholysis between 1-nonanol and NMP (**Figure 4.5**) to give by-products, decrease 1-nonanol yield and lower mole balance.

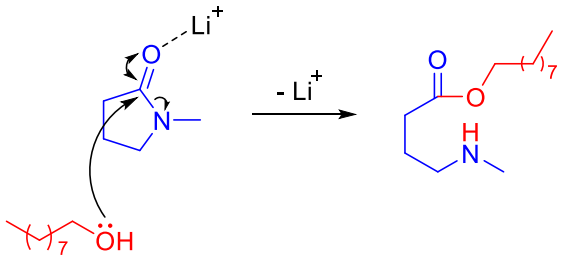

Figure 4.5 Ring-opening alcoholysis of NMP with 1-nonanol.

A control experiment mixing 1-heptanol, $Ru_3(CO)_{12}$ (2 mol%) and LiCl (8 mol%) in NMP at 140 °C overnight however, showed that there was no significant reaction between the 1-heptanol and NMP

under those conditions. All major peaks (>0.5% area) on the GC spectra of the product mixture had been characterised. No residue remained in the reactor after catalysis, indicating that no insoluble products had been formed. Extension of the GC method to allow for the elution of heavier products in solution also showed no significant vaporisable products with longer retention times present in the product mixture.

Finally, independent solubility experiments between NMP and each component revealed that hydrocarbons such as 1-octene and octane were only sparingly miscible in NMP. The separation of immiscible hydrocarbons from the rest of the product mixture after catalysis had been difficult to detect as they formed a thin colourless film on top of clear orange NMP solutions, giving the appearance of a homogeneous solution. Sampling the bulk solution via needle for GC analysis would then exclude the immiscible top layer and explain the combination of clean, well characterised GC spectra yet lacking mole balances obtained. It is possible that similar circumstances resulted in the imperfect mole balances obtained from Beller's system.[13]

Addition of a 1:1 mixture of Acetone/MeCN homogenised the product mixture and increased mole balance from 78% to 92% (run 2, **Table 4.2**), with the majority of the missing mole balance coming from octane.

4.4.2 Effect of Catalyst Loading

Lowering catalyst loading from 2 mol% to 0.2 mol% reduced alcohol yield from 60% to 18% and increased the amount of octane produced from 26% to 52% (comparing runs 2 and 3, **Table 4.2**). Slower reaction rates at lower catalyst loadings is expected, however this is typically not accompanied by a change in product distribution. In the case of Ru-catalysed rWGS-hydroformylation-reduction however, the Ru catalyst performs a dual role in catalysing the production of both reactants (the rWGS reaction to CO) and products (hydroformylation and reduction). The concentration of CO is catalyst-dependent and a reduction in catalyst loading will result in lower concentrations of CO that likely gives slower rates of olefin hydroformylation. On the other hand, since H_2 is provided in abundance as part of the 80 bar CO_2/H_2 (1:1) mixture charged to the reactor, olefin hydrogenation may proceed unhindered.

4.4.3 Effect of Salt Additives

The effect of numerous salt additives have been described in the literature.[6, 11] Tominaga and Sasaki have demonstrated that halide anions were essential for the reaction and that activity decreased down in the group in the order $Cl^- > Br^- > I^-$.[6] Salt additives without halide anions such as Li_2CO_3 may also be employed, however, the halide must then be incorporated elsewhere such as within the

$Ru_2(CO)_6Cl_2$ precatalyst.[11] Jääskeläinen and Haukka found that metal cation size in the metal halide additive was inversely correlated with alcohol yield but the metal cations themselves were not essential for activity as HCl was also found to be a suitable additive.[11] Given the poor solubility of LiCl in non-polar aprotic solvents such as toluene or highly lipophilic solvents like 2-ethylhexanol, other chloride salts such as the pyrazole derivative, PyCl (**Table 4.2**), and PPh_4Cl have been employed to allow other solvents to be tested in the Ru-catalysed rWGS-hydroformylation-reduction of 1-octene.

4.4.4 Solvent Effects

Tominaga and Sasaki have reported 70 – 91% cyclohexylmethanol as the major product from Ru-catalysed rWGS-hydroformylation-reduction of cyclohexene in a variety of solvents including toluene, benzene, tetrahydrofuran (THF) and dimethoxyethane (DME). However, when the same reaction conditions were applied with 1-octene as the substrate, hydrogenation to octane was observed as the major product for all examples excluding NMP (runs 4 – 8, **Table 4.2**).

Diglyme is a high boiling industrial solvent favoured for its chemical and thermal stability.[38] As a polar aprotic solvent similar to NMP, diglyme was anticipated to be a suitable solvent for the Ru-catalysed rWGS-hydroformylation-reduction of olefins to alcohols. However, both attempts using diglyme (runs 4 and 5, **Table 4.2**) demonstrated that olefin hydrogenation dominated to give 87 – 96% octane. The first attempt (run 4, **Table 4.2**) gave no alcohol product at all while the second attempt (run 5, **Table 4.2**) gave only 3% nonanol despite increasing catalyst loading from 0.5 to 2 mol%. As discussed above (sub-section **4.4.2**), higher catalyst loadings likely produce more CO and increase the rate of hydroformylation, resulting in higher alcohol yields.

As the rate of hydroformylation can be limited by the availability of CO, the solubility of CO in each solvent is another relevant parameter. CO is noted to be nearly twice as soluble in toluene than in 1,4-dioxane and should promote hydroformylation activity.[39] Running the reaction in toluene however, resulted in predominantly olefin hydrogenation to octane (95%) occurring (run 6, **Table 4.2**) despite 10% nonanol being produced when run in 1,4-dioxane (run 8, **Table 4.2**). This suggests that at the low concentrations of CO produced in situ via rWGS, CO solubility in solvent is not the limiting factor hindering hydroformylation activity.

4.4.5 CO_2 Expanded Solvents

Unexpectedly, during the testing of various solvents, varying initial pressures were observed at 140 °C despite identical starting solvent volumes and CO_2/H_2 pressures at room temperature for runs 2 – 7 (**Table 4.2**). A review of the literature revealed that at high CO_2 pressures, organic solvents can dissolve a significant amount of CO_2, expand in volume and undergo changes in their physical properties (**Table**

4.3).[40] In lieu of the lack of data on 2-ethylhexanol, data on petan-1-ol and undecan-2-ol have been provided instead.

Table 4.3 Properties of solvents under high pressures (40 – 45 bar) of CO_2.

Solvent	CO_2 Pressure / bar	Temperature / K	CO_2 Mole Fraction	Volume Expansion / %
Pentan-1-ol[41]	43	308	0.31	n.d.
NMP[42-43]	40	308	0.33	49
Undecan-2-ol[44]	43	313	0.36	n.d.
Toluene[45]	43	308	0.46	n.d.
Diglyme[46-47]	45	313	0.59	n.d.
1,4-Dioxane[48]	44	313	0.61	159

n.d. = not determined.

By varying CO_2 pressure and hence the composition of the liquid media, solvent properties can be tuned on a continuum between neat organic solvent and supercritical CO_2.[40] Despite the lack of volume expansion data, the trend of expansion is expected to mirror that for its CO_2 solubility as volume expansion is dependent on mole fraction of CO_2 in the liquid phase. Solvent polarity also changes as CO_2 is incorporated as part of the liquid phase, affecting the solubility of the solid, liquid and gas components present in the system.

4.4.6 Solubility in CO_2 Expanded Solvents

The different phase behaviour of CO_2 expanded solvents has been leveraged to precipitate solids from its solution. Examples of foodstuffs,[49] explosives[50] and pharmaceuticals[51] have been prepared from their solutions via incorporation of CO_2 as an anti-solvent. In homogeneous catalysis, organic solvents are typically chosen for their dielectric properties to dissolve substrates and catalysts to promote reaction rate. In the case of CO_2 expanded solvents however, the incorporation of non-polar CO_2 to polar solvent mixtures containing dissolved catalysts may instead cause catalyst precipitation and reduce catalytic activity. Precipitation of the Ru catalyst may have gone unnoticed as observations of the reaction mixture pre- and post-catalysis were done at room temperature and pressure instead of the CO_2 expanded solvent state under high CO_2 pressure when catalyst precipitation may occur.

The use of CO_2 expanded toluene in homogeneous Rh-catalysed hydroformylation of 1-hexene has been reported to give more rapid reaction rates than in supercritical CO_2 but slower than in neat toluene.[52] The slower rate of reaction in CO_2 expanded toluene compared to neat toluene was attributed to phase transfer of a portion of the hexene substrate out of the liquid phase and into the

CO_2 phase, thus lowering the concentration of hexene available to the catalyst. Toluene, CO_2 and hexene are all non-polar compounds, resulting in the partitioning of hexene substrate between the liquid and CO_2 phases. For polar solvents such as NMP however, hydrocarbons like octene are only sparingly soluble. Despite a similar partitioning of the octene substrate between the CO_2 and liquid phases expected, the incorporation of non-polar CO_2 in the liquid phase may increase solubility of the octene substrate in the liquid phase to a greater extent, raise available octene concentration in solution and improve reaction rates instead.

A study on the use of CO_2 expanded acetone in Rh-catalysed hydroformylation of 1-octene showed that incorporation of CO_2 enhanced reaction rate and linear selectivity.[53] The incorporation of CO_2 into acetone was hypothesized to increase syngas availability in solution through enhanced solubility and mass transfer rates, resulting in a faster rate of reaction. The increased syngas availability was also hypothesised to promote hydroformylation over isomerisation, resulting in higher yields of the linear product. The incorporation of CO_2 was observed to encourage hydroformylation up to a point, after which additional CO_2 begins to lower reaction rates instead as substrate dilution becomes more prominent. In our case of Ru-catalysed rWGS-hydroformylation-reduction of 1-octene however, CO_2 also acts a reactant in the rWGS reaction to produce CO in the initial step of the catalytic process. The high concentration of CO_2 in the CO_2 expanded solvent may promote rate of formation of CO via the rWGS reaction, increase CO concentration and encourage hydroformylation.

The high pressure phase equilibria for several (CO_2, CO or H_2) + organic solvent binary systems along with other more complex multicomponent systems have been reviewed by Dohrn and Brunner.[54] Despite the emerging interest in the application of CO_2 expanded solvents for catalytic reactions involving gaseous reagents (such as in hydrogenation or carbonylation), publications on CO_2 + organic solvent + (CO or H_2 or both) ternary and quaternary systems are rare.[40] Furthermore, in the case of Ru-catalysed rWGS-hydroformylation-reduction of 1-octene, there is the added complexity of the rWGS reaction producing both H_2O and CO, octene hydroformylation producing nonanal, octene hydrogenation producing octane and nonanal reduction producing nonanol, resulting in an even more complicated multicomponent system.

4.4.7 Solvent Mixtures

The use of neat NMP as solvent gave the highest nonanol yield (60%, run 2, **Table 4.2**) but also resulted in phase separation of octenes and octane in the product mixture due to the poor miscibility of hydrocarbons in NMP. On the other hand, using neat 1,4-dioxane gave octane as the major product (84%) but fully dissolved all components present in a single homogeneous phase (run 8, **Table 4.2**). 1,4-Dioxane also incorporates a greater mole fraction of CO_2 compared to NMP at similar pressures,

which may be beneficial for the formation of CO via the rWGS reaction. In an attempt to leverage on the high activity in NMP and the good CO_2 incorporation properties of 1,4-dioxane, mixtures of NMP and 1,4-dioxane in different ratios were tested in the Ru-catalysed rWGS-hydroformylation-reduction of 1-octene (runs 9 and 10, **Table 4.2**).

Employing a 1:1 mixture of NMP/1,4-dioxane (run 9, **Table 4.2**) gave a homogeneous product mixture showing reduced nonanol yield and increased octane and internal octenes compared to running the reaction in neat NMP (run 2, **Table 4.2**). The incorporation of 1,4-dioxane decreases hydroformylation activity, despite the expected increase in CO_2 incorporation that should favour the rWGS reaction, higher CO concentrations and hydroformylation rates. The use of a 2:3 mixture of NMP/1,4-dioxane (run 10, **Table 4.2**) showed similar results to the run in neat NMP (run 2, **Table 4.2**) while remaining as a single homogeneous phase, suggesting that exclusion of octane by poor hydrocarbon solubility in NMP does not drive the reaction. Intuitively, the solvent system closer to neat NMP (1:1 mix) should resemble it closer than the one that has been altered more (2:3 mix). However, these unexpected results suggest a complicated balance between the one pot tandem rWGS-hydroformylation-reduction reaction, CO_2 solvent expansion affecting solvent properties, gas solubility, substrate concentration and catalyst stability that is yet to be fully understood.

4.5 Conclusions and Outlook

Two monodentate phosphite ligand variants have been synthesised and characterised. The synthesised ligands together with a selection of commercially available monodentate and bidentate ligands have been evaluated in the Ru-catalysed rWGS-hydroformylation-reduction of 1-octene to nonanol. In terms of encouraging nonanol production and suppressing octene hydrogenation, the ligands performed in the order **DPPF** < **DPPP** < **$P(OPh)_3$** < **Me_2POPh** < **POPh** < **no ligand** ≈ **P(*o*-tol)$_3$** < **PPh_3**. In general, monodentate ligands exhibited superior performance to the bidentate ligands tested. Reducing the ligand/[Ru] ratio of bidentate ligands was also found to improve performance.

Investigations into the ligand free Ru-catalysed rWGS-hydroformylation-reduction of olefins revealed that hydrocarbons such as octene and octane were only sparingly soluble in NMP. Lowering catalyst loadings resulted in more octene hydrogenation and decreased nonanol yields. Lower concentrations of Ru catalyst likely resulted in a slower rate of CO production via the rWGS reaction, and the lower CO concentrations in turn reduced hydroformylation rates. Choice of reaction solvent was found to have a significant impact on catalytic activity and chemoselectivity. Solvent properties can also be influenced by the incorporation of CO_2 at high pressure. CO_2 expanded solvents have altered properties that may affect solubility of reactants or cause catalyst precipitation.

CO_2 capture and utilisation remains an important area of research to address environmental concerns over rising anthropogenic CO_2 emissions. Catalytic conversion of CO_2 to valuable chemicals is an important part in that area, and the use of ligands to tune the stereo-electronic properties of catalysts holds much potential for reaction optimisation. For example, increasing desired alcohol yields and suppressing undesired olefin hydrogenation in Ru-catalysed rWGS-hydroformylation-reduction of olefins using **PPh_3**. Given the complexity of the Ru-based system however, further research first into the significant impact reaction solvents have on the ligand-free system to optimise activity would be beneficial. Alternatively, experiments using CO/H_2 instead of CO_2/H_2 to test the tandem hydroformylation-reduction activity of the system may be fruitful.

4.6 Chapter 4 References

1. Chang, B.-H., *J. Organomet. Chem.* **1985,** *291*, c31-c33.
2. Tominaga, K.-i.; Yoshiyuki, S.; Kohnosuke, H.; Taiki, W.; Masahiro, S., *Chem. Lett.* **1994,** *23*, 1391-1394.
3. Tominaga, K.-i.; Sasaki, Y.; Watanabe, T.; Saito, M., *J. Chem. Soc., Chem. Commun.* **1995**, 1489-1490.
4. Tominaga, K.-I.; Sasaki, Y.; Watanabe, T.; Saito, M., *Energy* **1997,** *22*, 169-176.
5. Tominaga, K.-i.; Sasaki, Y., *Catal. Commun.* **2000,** *1*, 1-3.
6. Tominaga, K.-i.; Sasaki, Y., *J. Mol. Catal. A: Chem.* **2004,** *220*, 159-165.
7. Tominaga, K.-i.; Yoshiyuki, S., *Chem. Lett.* **2004,** *33*, 14-15.
8. Tominaga, K.-i., *Catal. Today* **2006,** *115*, 70-72.
9. Tsuchiya, K.; Huang, J.-D.; Tominaga, K.-i., *ACS Catal.* **2013,** *3*, 2865-2868.
10. Fujita, S.-i.; Okamura, S.; Akiyama, Y.; Arai, M., *Int. J. Mol. Sci.* **2007,** *8*, 749-759.
11. Jääskeläinen, S.; Haukka, M., *Appl. Catal., A* **2003,** *247*, 95-100.
12. Kontkanen, M.-L.; Oresmaa, L.; Moreno, M. A.; Jänis, J.; Laurila, E.; Haukka, M., *Appl. Catal., A* **2009,** *365*, 130-134.
13. Liu, Q.; Wu, L.; Fleischer, I.; Selent, D.; Franke, R.; Jackstell, R.; Beller, M., *Chem. Eur. J.* **2014,** *20*, 6888-6894.
14. Ren, X.; Zheng, Z.; Zhang, L.; Wang, Z.; Xia, C.; Ding, K., *Angew. Chem. Int. Ed.* **2017,** *56*, 310-313.
15. Ostapowicz, T. G.; Schmitz, M.; Krystof, M.; Klankermayer, J.; Leitner, W., *Angew. Chem. Int. Ed.* **2013,** *52*, 12119-12123.
16. Gui, Y.-Y.; Hu, N.; Chen, X.-W.; Liao, L. L.; Ju, T.; Ye, J.-H.; Zhang, Z.; Li, J.; Yu, D.-G., *J. Am. Chem. Soc.* **2017,** *139*, 17011-17014.

17. Daza, Y. A.; Kuhn, J. N., *RSC Adv.* **2016,** *6*, 49675-49691.

18. Mallapragada, D. S.; Singh, N. R.; Curteanu, V.; Agrawal, R., *Ind. Eng. Chem. Res.* **2013,** *52*, 5136-5144.

19. Ken-ichi, T.; Yoshiyuki, S.; Kohnosuke, H.; Taiki, W.; Masahiro, S., *Chem. Lett.* **1994,** *23*, 1391-1394.

20. Edmundson, R. S., *Tetrahedron* **1964,** *20*, 2781-2795.

21. Ayres, D. C.; Rydon, H. N., *J. Chem. Soc.* **1957**, 1109-1114.

22. Hooker Chemical Corp, Improvements in or Relating to Dioxaphosphorinanes and Their Preparation. GB853798A, 1960.

23. Sagadeev, E. V.; Safina, Y. G.; Sopin, V. F.; Cherkasov, R. A., *Russ. J. Gen. Chem.* **2003,** *73*, 1702-1708.

24. Goia, C.; Matijević, E.; Goia, D. V., *J. Mater. Res.* **2005,** *20*, 1507-1514.

25. Bestian, H.; Günther, D., *Angew. Chem. Int. Ed. Engl.* **1963,** *2*, 608-613.

26. Zhang, B.; Jiao, H.; Michalik, D.; Kloß, S.; Deter, L. M.; Selent, D.; Spannenberg, A.; Franke, R.; Börner, A., *ACS Catal.* **2016,** *6*, 7554-7565.

27. van Leeuwen, P. W. N. M., *Appl. Catal., A* **2001,** *212*, 61-81.

28. Kloß, S.; Selent, D.; Spannenberg, A.; Franke, R.; Börner, A.; Sharif, M., *Catalysts* **2019,** *9*, 1036.

29. Billig, E.; Abatjoglou, A. G.; Bryant, D. R.; Murray, R. E.; Maher, J. M. Union Carbide Corp, Transition Metal Complex Catalyzed Reactions. US4717775A, 1986.

30. Billig, E.; Abatjoglou, A. G.; Bryant, D. R.; Murray, R. E.; Maher, J. M. Union Carbide Corp, Transition Metal Complex Catalyzed Reactions. US4737588A, 1986.

31. Bruce, M. I.; Humphrey, P. A.; Okucu, S.; Schmutzler, R.; Skelton, B. W.; White, A. H., *Inorg. Chim. Acta* **2004,** *357*, 1805-1812.

32. Tolman, C. A., *J. Am. Chem. Soc.* **1970,** *92*, 2956-2965.

33. Bursten, B. E.; Cotton, F. A., *Inorg. Chem.* **1981,** *20*, 3042-3048.

34. Tolman, C. A., *J. Am. Chem. Soc.* **1970,** *92*, 2953-2956.

35. Oswald, A. A.; Hendriksen, D. E.; Kastrup, R. V.; Mozeleski, E. J., Electronic Effects on the Synthesis, Structure, Reactivity, and Selectivity of Rhodium Hydroformylation Catalysts. In *Homogeneous Transition Metal Catalyzed Reactions*, American Chemical Society: 1992; Vol. 230, pp 395-418.

36. Kamer, P. C. J.; van Leeuwen, P. W. N. M.; Reek, J. N. H., *Acc. Chem. Res.* **2001,** *34*, 895-904.

37. Lammens, T. M.; Franssen, M. C. R.; Scott, E. L.; Sanders, J. P. M., *Green Chem.* **2010,** *12*, 1430-1436.

38. Tang, S.; Zhao, H.; Song, Z.; Olubajo, O., *Bioresour. Technol.* **2013,** *139*, 107-112.

39. Battino, R.; Bo, S.; Clever, H. L.; Gjaldbaek, J. C.; Wiesenburg, D. A.; Wilheim, E.; Yampol'skii, Y. P.; Young, C. L., Carbon Monoxide. In *Solubility Data Series*, Lorimer, J. W.; Clever, H. L.; Young, C. L.; Barton, A. F. M.; Cohen-Adad, R.; Crovetto, R.; Fermeglia, M.; Fogg, P. G. T.; Gerrad, W.; Getzen, F. W.; Gevantman, L. H.; Hayduk, W.; Hefter, G. T.; Mather, A. E.; Salomon, M.; Scharlin, P.; Tomkins, R. P. T.; Gujral, P. D., Eds. Pergamon: Oxford, New York, 1990; Vol. 43, pp 123, 236.

40. Jessop, P. G.; Subramaniam, B., *Chem. Rev.* **2007,** *107*, 2666-2694.

41. Gui, X.; Tang, Z.; Fei, W., *J. Chem. Eng. Data* **2011,** *56*, 2420-2429.

42. Rajasingam, R.; Lioe, L.; Pham, Q. T.; Lucien, F. P., *J. Supercrit. Fluids* **2004,** *31*, 227-234.

43. Bohloul, M. R.; Vatani, A.; Peyghambarzadeh, S. M., *Fluid Phase Equilib.* **2014,** *365*, 106-111.

44. Petrova, E.; Crampon, C.; Ali, E.; Neau, E.; Badens, E.; Charbit, G.; Jaubert, J. N., *Fluid Phase Equilib.* **2003,** *213*, 153-162.

45. Lay, E. N.; Taghikhani, V.; Ghotbi, C., *J. Chem. Eng. Data* **2006,** *51*, 2197-2200.

46. Kodama, D.; Kanakubo, M.; Kokubo, M.; Hashimoto, S.; Nanjo, H.; Kato, M., *Fluid Phase Equilib.* **2011,** *302*, 103-108.

47. Henni, A.; Tontiwachwuthikul, P.; Chakma, A., *Can. J. Chem. Eng.* **2005,** *83*, 358-361.

48. Kordikowski, A.; Schenk, A. P.; Van Nielen, R. M.; Peters, C. J., *J. Supercrit. Fluids* **1995,** *8*, 205-216.

49. Kokot, K.; Knez, Z.; Bauman, D., *Acta Aliment.* **1999,** *28*, 197-208.

50. Pourmortazavi, S. M.; Hajimirsadeghi, S. S., *Ind. Eng. Chem. Res.* **2005,** *44*, 6523-6533.

51. Palakodaty, S.; York, P., *Pharm. Res.* **1999,** *16*, 976-985.

52. Hemminger, O.; Marteel, A.; Mason, M. R.; Davies, J. A.; Tadd, A. R.; Abraham, M. A., *Green Chem.* **2002,** *4*, 507-512.

53. Jin, H.; Subramaniam, B.; Ghosh, A.; Tunge, J., *AlChE J.* **2006,** *52*, 2575-2581.

54. Dohrn, R.; Brunner, G., *Fluid Phase Equilib.* **1995,** *106*, 213-282.

Chapter 5 – Experimental

5.1 General Considerations

Unless stated otherwise, all manipulations were performed under N_2 using standard Schlenk line techniques on a dual manifold vacuum/inert gas line or in an MBraun Labmaster DP glovebox. Glassware was dried at 150 °C overnight prior to use. Solvents and solutions were transferred using a positive pressure of nitrogen through stainless steel cannulas, or via plastic syringes for volumes less than or equal to 20 mL. Filtrations were performed using modified stainless-steel cannulas fitted with glass microfibre filters.

5.2 Instrumentation and Analyses

NMR spectroscopy: NMR spectra (^{1}H at 400 MHz, ^{13}C at 101 MHz, ^{31}P at 162 MHz and ^{19}F at 376 MHz) was recorded using Bruker AV400 spectrometers at 25 °C unless otherwise specified. ^{1}H and ^{13}C chemical shifts, δ in parts per million (ppm), are given relative to Me_4Si and are referenced to the residual solvent peak. ^{13}C chemical shifts were proton decoupled. $^{31}P\{^{1}H\}$ chemical shifts were referenced externally in $CDCl_3$ to 85% aqueous H_3PO_4. ^{19}F chemical shifts were referenced externally from $CFCl_3$. Air or moisture sensitive samples were prepared inside the glovebox using oven-dried NMR tubes fitted with J. Young valves. NMR spectra are reported as follows: chemical shift (δ ppm), integration, multiplicity, coupling constant (Hz) and assignment. Multiplicities are given as follows (or combinations thereof): s – singlet, d – doublet, t – triplet, q – quartet, m – multiplet, br – broad. Detailed NMR assignments were elucidated via cross-referencing 2D NMR experiments (^{1}H,^{1}H COSY and ^{1}H,^{13}C HSQC) with 1D NMR experiments (^{1}H, $^{13}C\{^{1}H\}$, $^{31}P\{^{1}H\}$ and DEPT-135). Acquired data was processed and analysed by MestReNova version 11.0.0-17609.

Gas Chromatography: Agilent 6890N Gas Chromatograph instrument fitted with a Agilent 7683 Automatic Liquid Sampler and FID on a HP-5 (5%-Phenyl)-methylpolysiloxane column, length 30 m, internal diameter 0.32 mm, film 0.25 µm, using Helium as a carrier gas starting with a flow rate of 2 mL min^{-1} for 1 min after injection then ramped at 1 mL min^{-2} to 5 mL min^{-1} and held for 5 min before ramping at 10 mL min^{-2} to 25 mL min^{-1} for the remainder of the run. The oven was kept isothermal at 40 °C for 5 min after injection then heated at 20 K min^{-1} to 240 °C and kept isothermal for a further 5 min. GC yields were determined with anisole as an internal standard.

Mass Spectrometry: High resolution mass spectrometry samples (HRMS; EI & ESI) were recorded by Dr. L. Haigh using either a Micromass Autospec Premier or a Micromass LCT Premier spectrometer or by Ms. Angeline Seo using Agilent 6545B Q-TOF LC/MS.

Tandem Gas Chromatography/Mass Spectrometry (GCMS): Agilent 7890B Gas Chromatograph instrument coupled with 5977B MSD.

Elemental Analysis: C, H and N elemental analysis was conducted by Mr S. Boyer of the London Metropolitan University or by Ms. Angeline Seo using Thermo Scientific Flash 2000.

X-Ray Analysis: X-Ray diffraction analyses were carried out by Dr Andrew White at Imperial College London using Agilent Xcalibur 3 E diffractometer or by Dr Srinivasulu Aitipamula using Rigaku Oxford Diffraction SuperNova diffractometer.

High Pressure Reactors: Carbonylation experiments were carried out in stainless steel pressure Parr reactors (452HC9) equipped with overhead stirrers, pressure sensors, sampling dip tubes and electrical heating jackets as part of the Parr®5500 series compact reactor system or in SPR16 AMTECH automated slurry phase reactor system on 16 parallel batch reactors (stainless steel 316L) stirred with cross-shaped polytetrafluoroethylene (PTFE) coated magnetic stirrer bars, heated with electrical heating jackets and pressure automatically controlled via pressure sensor and a selection valve system.

Thin Layer Chromatography (TLC): Performed on Merck TLC plates, Silica gel 60. Visualisation was accomplished using $KMnO_4$ stain or ceric ammonium molybdate (CAM) stain followed by heating with a heat gun set to 300 °C until colour developed.

Column Chromatography: Supelco Silica gel, high-purity grade, 40, 35 – 70 mesh purchased from Sigma-Aldrich.

5.3 Solvents and Reagents

Solvents: Toluene, pentane, hexane, methanol, dichloromethane were dried using Innovative Technology Pure Solv SPS-400, while tetrahydrofuran (THF) and diethyl ether were distilled over Na/fluorenone. Diglyme, 1,4-dioxane, 2-ethylhexanol, n-methyl-2-pyrrolidone (NMP) were purchased from Sigma-Aldrich and degassed by sparging with N_2. All solvents were stored in gas-tight graduated ampules over 3 Å molecular sieves apart from diethyl ether which was stored over a potassium mirror. $CDCl_3$ and CD_2Cl_2 purchased from Cambridge Isotope Laboratories was freeze-pump-thaw degassed, dried, and stored over 3 Å molecular sieves in the glovebox. DMSO-d_6 was purchased from Cambridge Isotope Laboratories and used as received.

Gases: Ar, N_2, CO, CO_2, H_2 and premixed CO/H_2 or CO_2/H_2 gases were purchased from the BOC group or from Air Liquide and used as received.

Chapter 2: Neopentyl glycol, 2-isopropyl-5-methyl-2-hexenal, potassium iodide, 4-methylbenzenesulfonyl chloride, triphenyl phosphine, 1,3-bis(diphenylphosphino)propane, isopropyl bromide, 1,3-dibromopropane, diethyl malonate, sodium hydride, lithium aluminium hydride,

triethylamine, pyridine, sodium periodate, ruthenium(III) chloride hydrate, 1-octene, trans-2-octene, trans-4-octene, trifluoroacetic acid, methanesulfonic acid, palladium(II) chloride, bromine and thionyl chloride were purchased from Sigma-Aldrich and used as received. 1,3-dichloropropane was purchased from Tokyo Chemical Industry and used as received. Palladium(II) acetate was purchased from Strem and used as received. Pd(1,5-cyclooctadiene)Cl_2 was synthesized via literature procedures.[1]

Chapter 3: Mixtures of secondary [3.3.1]phobane and [4.2.1]phobane as a 60 wt% solution in toluene were obtained from Rhodia (now Solvay). 1,2-dibromobenzene, 1,2-dibromoethane, tetrakis(triphenylphosphine)palladium(0), 1,4-diazabicyclo[2.2.2]octane, methanesulfonic acid, 1-hexene, sodium chloride, diglyme, anisole, 1-octene, 2-ethylhexanol, tert-butyl alcohol and 4-pentenoic acid were purchased from Sigma-Aldrich and used as received. 1,2-dibromo-4-(1,1-dimethylethyl)benzene, 1,2-dibromoveratrole, 1,2-dibromoanisole, 1,2-dibromo-4-(trifluoromethyl)benzene were purchased from Fluorochem and used as received. Methyl 4-pentenoate was synthesised from 4-pentenoic acid via acid-catalysed esterification in methanol.

Chapter 4: Propan-1,3-diol, triphenylphosphite, triethylamine, neopentyl glycol, $Ru_3(CO)_{12}$, lithium chloride, n-methyl-2-pyrrolidone (NMP), 1-octene and anisole were purchased from Sigma-Aldrich and used as received.

5.4 Experimental Procedures for Chapter 2

5.4.1 Precursor Synthesis

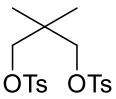

2,2-Dimethylpropane-1,3-diyl bis(4-methylbenzenesulfonate) 2,2-Dimethylpropane-1,3-diol (3.12 g, 30 mmol, 1 eq) was taken up in CH_2Cl_2 (30 mL) then pyridine (9.7 mL, 120 mmol, 4 eq) was added and the reaction mixture cooled to 0 °C. To the stirred cold mixture was added 4-methylbenzenesulfonyl chloride (14.3 g, 75 mmol, 2.5 eq) in 2 portions. The resulting solution was stirred at 0 °C for 3 h then warmed to room temperature and left to stir overnight under air. The bulk of the solvent was removed under vacuum then CH_2Cl_2 (30 mL) and H_2O (40 mL) were added. The layers were separated, and the aqueous layer extracted with CH_2Cl_2 (30 mL). The combined organic phases were washed with 2 M HCl, saturated aqueous $NaHCO_3$, H_2O then saturated aqueous NaCl. A white emulsion formed. More H_2O (20 mL) was added and gentle swirling employed to separate the emulsion. The resulting organic layer was dried over anhydrous Na_2SO_4 then concentrated under reduced pressure to give 2,2-dimethylpropane-1,3-diyl bis(4-methylbenzenesulfonate) as a white solid (12.3 g, 99%). ^{1}H NMR (400

MHz, $CDCl_3$): δ 7.72 (4H, d, $^3J_{HH}$ = 8.0 Hz, ArH), 7.36 (4H, d, $^3J_{HH}$ = 8.0 Hz, ArH), 3.71 (4H, s, CH_2), 2.45 (6H, s, $ArCH_3$) and 0.88 ppm (6H, s, CCH_3). $^{13}C\{^1H\}$ NMR (101 MHz, $CDCl_3$): δ 145.0 (Ar), 132.5 (Ar), 130.0 (Ar), 127.9 (Ar), 73.7 (CH_2), 35.4 (tert. C), 21.7 (CH_3) and 21.0 ppm (CH_3).

1,3-Diiodo-2,2-dimethylpropane Potassium iodide (2.04 g, 12.3 mmol, 2 eq) was taken up in dimethylformate (50 mL). To the stirred mixture was added 2,2-dimethylpropane-1,3-diyl bis(4-methylbenzenesulfonate) (2.53 g, 6.13 mmol, 1 eq). The reaction mixture was refluxed overnight to give a dark red solution. After cooling to room temperature, it was diluted with H_2O (60 mL). The aqueous layer was extracted with ethyl acetate (3 x 15 mL). The combined organic extracts were washed with H_2O, saturated aqueous NaCl, dried over Na_2SO_4 then concentrated under reduced pressure to give the crude product as a black oil. The crude product was purified via column chromatography (9:1 hexane/ethyl acetate, R_f = 0.63) to give 1,3-diiodo-2,2-dimethylpropane as an amber oil (0.8 g, 43%). ^1H NMR (400 MHz, $CDCl_3$): δ 3.27 (4H, s, CH_2) and 1.24 ppm (6H, s, CH_3). $^{13}C\{^1H\}$ NMR (101 MHz, $CDCl_3$): δ 33.7, 26.1 and 21.5 ppm. MS (+ve EI): m/z (calcd), $[M]^+$ 323; found 323.

General procedure for conversion of diol to cyclic sulfate

Diol (1 eq) was taken up in CH_2Cl_2 (20 mL) then triethylamine (4 eq) was added. To the stirred 0 °C solution was added $SOCl_2$ (1.5 eq) dropwise and the resulting mixture stirred at 0 °C for 4 h before being quenched with 0 °C H_2O (10 mL). The layers were separated, and the organic layer washed with 0 °C H_2O (2 x 30 mL). The organic layer was washed with saturated aqueous NaCl, dried over anhydrous Na_2SO_4 then concentrated under reduced pressure to give the intermediate cyclic sulfite. The crude intermediate product was used in the next step without any further purification. The crude cyclic sulfite was taken up in MeCN/H_2O (6:5, 55 mL), cooled to 0 °C then $NaIO_4$ (2 eq) followed by $RuCl_3.H_2O$ (10 mol%) was added. The reaction mixture was gradually warmed to room temperature then stirred overnight under air. The mixture was extracted with Et_2O (3 x 20 mL). The combined organic extracts were washed with saturated aqueous NaCl, dried over anhydrous Na_2SO_4 then concentrated under reduced pressure to give the crude product that was then purified by column chromatography.

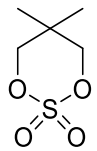

5,5-Dimethyl-1,3,2-dioxathiane 2,2-dioxide Synthesized via the general procedure for conversion of diol to cyclic sulfate. Starting diol = neopentyl glycol. Purified via column chromatography (1:1

hexane/Et_2O, R_f = 0.38) and isolated as a white solid. Yield = 70%. ^1H NMR (400 MHz, $CDCl_3$): δ 4.34 (4H, s, CH_2) and 1.14 ppm (6H, s, CH_3). $^{13}C\{^1H\}$ NMR (101 MHz, $CDCl_3$): δ 81.9, 30.9 and 21.0 ppm. MS (-ve ESI): m/z (calcd), $[M+HCOO]^-$ 211; found $[M+HCOO]^-$ 211. Note: $HCOO^-$ was used as part of the buffer solution for the MS.

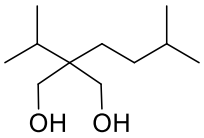

2-Isopentyl-2-isopropylpropane-1,3-diol 2-Isopropyl-5-methyl-2-hexenal (5.9 mL, 32.4 mmol, 1 eq), 10 wt% palladium on carbon (138 mg, 0.13 mmol, 0.004 eq) and NaOEt 21 wt% in EtOH (0.48 mL, 1.3 mmol, 0.04 eq) were sequentially added to a Parr reactor containing EtOH (30 mL). The reactor was flushed with H_2 for 2 min before being sealed and pressurized to 5 bar. The pressure was maintained at 5 bar and the reactor heated to 75 °C and stirred for 5 h before it was cooled to 10 °C then vented. GC analysis of the reaction mixture showed that starting material was completely consumed. The mixture was filtered and immediately used in the next step without further purification. A H_2O (10 mL) solution of K_2CO_3 (2.69 g, 19.4 mmol, 0.6 eq) and formaldehyde 37 wt% in H_2O (8.4 mL, 113.4 mmol, 3.5 eq) was added and the mixture refluxed overnight to give a dark amber solution. The solution was cooled to room temperature, diluted with H_2O (20 mL) and adjusted to pH 6.5 with 1 M aqueous HCl. It was then cooled to 0 °C and adjusted to pH 9 with 35 wt% aqueous ammonia before being further diluted with H_2O (10 mL). The resulting solution was extracted with ethyl acetate (2 x 20 mL). The combined organic extracts were washed with H_2O which formed a stable emulsion. The emulsion was separated by washing with 90 °C H_2O (3 x 40 mL). The organic phase was washed with saturated aqueous NaCl, dried over anhydrous Na_2SO_4 then concentrated under reduced pressure to give 2-isopentyl-2-isopropylpropane-1,3-diol as an amber oil (5.55 g, 91%). ^1H NMR (400 MHz, $CDCl_3$): δ 3.75 (2H, d, $^2J_{HH}$ = 10.8 Hz, OCH_2), 3.61 (2H, d, $^2J_{HH}$ = 10.8 Hz, OCH_2), 2.86 (2H, s, OH), 1.89 (1H, m, iPr-CH), 1.44 (1H, m, iPent-CH), 1.36 – 1.29 (2H, m, CH_2), 1.13 – 1.05 (2H, m, $CHCH_2$) and 0.90 – 0.85 ppm (12H, m, CH_3). $^{13}C\{^1H\}$ NMR (101 MHz, $CDCl_3$): δ 68.0, 42.1, 32.1, 29.1, 28.2, 27.1, 22.6 and 17.1 ppm. MS (+ve EI): m/z (calcd), $[M-H_2O-CHO]^+$ 141; found $[M-H_2O-CHO]^+$ 141. Note: proposed EI fragmentation pattern (**Figure 6.13**, supplementary information).

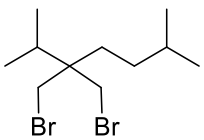

3,3-Bis(bromomethyl)-2,6-dimethylheptane Triphenylphosphine (4.4 g, 16.8 mmol, 2 eq) was taken up in MeCN (35 mL) then cooled to 0 °C to give a cloudy white solution. To the 0 °C stirred mixture

was added bromine (0.86 mL, 16.8 mmol, 2 eq) to give a cloudy yellow solution. 2-isopentyl-2-isopropylpropane-1,3-diol (1.58 g, 8.39 mmol, 1 eq) was then added as a solution in MeCN (15 mL). The resulting mixture was stirred for 2 h at 0 °C then warmed to room temperature to give a clear amber solution that was then further warmed to 80 °C and stirred for a further 72 h. The resulting black reaction mixture was concentrated under reduced pressure to give a black solid, which was then washed with hexane (3 x 10 mL) and filtered to give a yellow filtrate that was concentrated under reduced pressure to give 3,3-bis(bromomethyl)-2,6-dimethylheptane as an amber oil (1.78 g, 68%). 1H NMR (400 MHz, $CDCl_3$): δ 3.53 (4H, s, $BrCH_2$), 1.96 (1H, septet, $^3J_{HH}$ = 7.1 Hz, iPr-CH), 1.46 (3H, m, iPent-CH, iPent-$CHCH_2$), 1.23 (2H, m, CH_2CH_2), 1.01 (6H, d, $^3J_{HH}$ = 6.9 Hz, CH_3(iPr)) and 0.91 ppm (6H, d, $^3J_{HH}$ = 6.4 Hz, CH_3(iPent)). $^{13}C\{^1H\}$ NMR (101 MHz, $CDCl_3$): δ 41.6 (tert. C), 40.7 (BrC), 33.3 (CH_2CH_2), 32.4 (iPr-CH), 31.2 (CH_2CH_2), 29.1 (iPent-CH), 22.7 (CH_3(iPent)) and 18.2 ppm (CH_3(iPr)). HR-MS (+ve EI): m/z (calcd), $[M]^+$ 314.0068; found 314.0085.

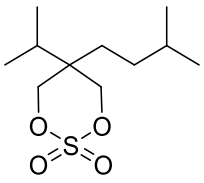

5-Isopentyl-5-isopropyl-1,3,2-dioxathiane 2,2-dioxide Synthesized via the general procedure for conversion of diol to cyclic sulfate. Starting diol = 2-isopentyl-2-isopropylpropane-1,3-diol. Purified via column chromatography (4:1 hexane/Et_2O, R_f = 0.34) and isolated as a clear oil. Yield = 61%. ^1H NMR (400 MHz, $CDCl_3$): δ 4.61 (2H, d, $^2J_{HH}$ = 11.6 Hz, CH_2), 4.41 (2H, d, $^2J_{HH}$ = 11.6 Hz, CH_2), 1.95 (1H, m, iPr-CH), 1.59 – 1.45 (3H, m, iPent-CH, CH_2), 1.20 – 1.12 (2H, m, CH_2), 0.97 (6H, d, $^3J_{HH}$ = 4.0 Hz, CH_3 (iPr)) and 0.92 (6H, d, $^3J_{HH}$ = 4.0 Hz, CH_3 (iPent)). $^{13}C\{^1H\}$ NMR (101 MHz, $CDCl_3$): δ 78.4, 37.7, 32.2, 28.8, 28.3, 27.0, 22.6 and 17.2 ppm. MS (+ve ESI): m/z (calcd), $[M+H]^+$ 251.1; found 251.0.

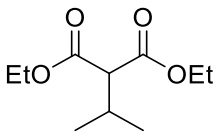

Diethyl 2-isopropylmalonate Diethyl malonate (5.0 mL, 0.03 mol, 1 eq) was taken up in EtOH (35 mL) then sodium ethoxide (2.69 g, 0.04 mol, 1.2 eq) was added. The orange solution was refluxed for 2 h to give a milky yellow mixture. After cooling to room temperature, isopropyl bromide (3.1 mL, 0.03 mol, 1 eq) was added and the mixture refluxed overnight. After cooling to room temperature, the milky yellow mixture was diluted with H_2O (50 mL) to give a clear amber solution. The aqueous phase was extracted with Et_2O (3 x 20 mL). The combined organic extracts were washed with saturated aqueous NaCl, dried over anhydrous $MgSO_4$ then concentrated to give a yellow oil which was then

purified via column chromatography (1:1 Et_2O/hexanes, R_f = 0.58) to give diethyl 2-isopropyl malonate as a colourless oil (2.84 g, 47%). ^{1}H NMR (400 MHz, $CDCl_3$): δ 4.20 (4H, q, $^3J_{HH}$ = 7.2 Hz, OCH_2), 3.11 (1H, d, $^3J_{HH}$ = 8.8 Hz, COCH), 2.43 – 2.33 (1H, m, CH), 1.26 (6H, t, $^3J_{HH}$ = 7.2 Hz, CH_2CH_3) and 1.00 ppm (6H, d, $^3J_{HH}$ = 6.8 Hz, $CHCH_3$). $^{13}C\{^1H\}$ NMR (101 MHz, $CDCl_3$) δ 169.0, 61.3, 59.2, 28.9, 20.5 and 14.3 ppm.

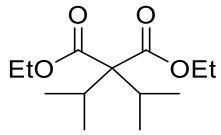

Diethyl 2,2-diisopropylmalonate Sodium hydride (0.62 g, 26.0 mmol, 1.5 eq) was taken up in toluene (20 mL). To the stirred white mixture was added diethyl 2-isopropylmalonate (3.5 g, 17.3 mmol, 1 eq) as a solution in toluene (10 mL) before warming to 70 °C and stirring for 1 h. Isopropyl bromide (1.9 mL, 20.8 mmol, 1.2 eq) was added and the reaction mixture refluxed overnight. The reaction was monitored by TLC and additional equivalents of isopropyl bromide added until no starting material remained. The milky off-white mixture was cooled to room temperature, diluted with H_2O (30 mL) and the layers separated. The aqueous layer was extracted with ethyl acetate (3 x 20 mL). The combined organic layers were washed with saturated aqueous NaCl, dried over anhydrous $MgSO_4$ then concentrated in vacuo to give diethyl 2,2-diisopropylmalonate as a yellow oil (4.2 g, 99%). ^{1}H NMR (400 MHz, $CDCl_3$): δ 4.22 (4H, q, $^3J_{HH}$ = 7.1 Hz, $COCH_2$), 2.53 (2H, septet, $^3J_{HH}$ = 6.9 Hz, CH), 1.28 (6H, t, $^3J_{HH}$ = 7.1 Hz, CH_2CH_3) and 0.94 ppm (12H, d, $^3J_{HH}$ = 6.9 Hz, CH_3). $^{13}C\{^1H\}$ NMR (101 MHz, $CDCl_3$): δ 170.4, 60.5, 30.5, 18.7 and 14.4 ppm.

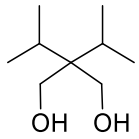

2,2-Diisopropylpropane-1,3-diol Lithium aluminium hydride (0.5 g, 13.1 mmol, 4 eq) was taken up in Et_2O (15 mL) then cooled to 0 °C. To the 0 °C stirred grey mixture was carefully added dropwise diethyl 2,2-diisopropylmalonate (0.8 g, 3.27 mmol, 1 eq) as a solution in Et_2O (5 mL), effervescence was observed. The resulting mixture was warmed to room temperature and stirred overnight. The grey mixture was cooled to 0 °C then carefully quenched with H_2O (50 mL) to give a white milky mixture (note: quenching excess lithium aluminium hydride is highly exothermic and releases H_2), which was then extracted with Et_2O (3 x 20 mL). The emulsion formed during extraction was separated by applying heat with gentle swirling. The combined organic extracts were washed with saturated aqueous NaCl, dried over anhydrous $MgSO_4$ and concentrated in vacuo to give 2,2-diisopropylpropane-1,3-diol as a yellow oil (0.37 g, 71%). ^{1}H NMR (400 MHz, $CDCl_3$): δ 3.76 (4H, br.s,

CH_2), 2.34 (2H, m, OH), 1.97 (2H, septet, $^3J_{HH}$ = 7.0 Hz, CH) and 0.98 ppm (12H, d, $^3J_{HH}$ = 7.0 Hz, CH_3). $^{13}C\{^1H\}$ NMR (101 MHz, $CDCl_3$): δ 66.6, 44.2, 29.5 and 18.7 ppm.

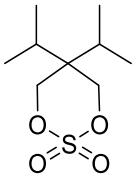

5,5-Diisopropyl-1,3,2-dioxathiane 2,2-dioxide Synthesized via the general procedure for conversion of diol to cyclic sulfate. Starting diol = 2,2-diisopropylpropane-1,3-diol. Purified via column chromatography (4:1 hexane/ethyl acetate, R_f = 0.44) and isolated as a white solid. Yield = 43%. ^1H NMR (400 MHz, $CDCl_3$): δ 4.57 (4H, s, CH_2), 2.05 (2H, $^3J_{HH}$ = 7.0 Hz, CH) and 1.04 ppm (12H, d, $^3J_{HH}$ = 7.0 Hz, CH_3). $^{13}C\{^1H\}$ NMR (101 MHz, $CDCl_3$): δ 76.8, 39.9, 29.6 and 18.3 ppm. HR-MS (+ve ESI): m/z (calcd), $[M+H]^+$ 223.0999; found 223.0999. Elem. Anal. Calcd. For $C_9H_{18}O_4S$: C, 48.63; H, 8.16; Found: C, 49.53; H, 8.24. Note: the experimental elemental analysis values obtained were outside the 0.4% tolerance. Therefore, NMR spectra has been included to demonstrate the absence of detectable contaminants except for H_2O (**Figure 6.1** and **Figure 6.2**, supplementary information).

5.4.2 Ligand Synthesis

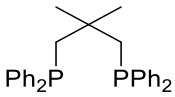

(2,2-Dimethylpropane-1,3-diyl)bis(diphenylphosphane) (DPPDMP) Diphenylphosphine (1.4 mL, 8.23 mmol, 2.1 eq) was taken up in tetrahydrofuran (15 mL) then cooled to 0 °C. To the stirred 0 °C solution was added dropwise ^{n}BuLi (2.5 M in hexane, 3.3 mL, 8.23 mmol, 2.1 eq) to give a bright orange-red solution that was left to stir for a further 30 min at 0 °C. 1,3-Dichloro-2,2-dimethylpropane (0.51 mL, 3.94 mmol, 1 eq) was added and the reaction mixture gradually warmed to 65 °C. The reaction was monitored by $^{31}P\{^1H\}$ NMR by taking aliquots of the reaction mixture, and the reaction run until diphenylphosphine was completely consumed. The reaction mixture was cooled to room temperature and volatiles removed under vacuum to give a black oil. The crude product was diluted with H_2O (30 mL) and the aqueous layer extracted with Et_2O (3 x 10 mL). The combined organic extracts were dried over anhydrous Na_2SO_4 then concentrated to give a grey oil which solidified overnight to give a grey solid (2.07 g). The grey solid was triturated with MeOH (3 x 10 mL) to give (2,2-dimethylpropane-1,3-diyl)bis(diphenylphosphane) as a white solid (1.67 g, 96%). ^1H NMR (400 MHz, $CDCl_3$): δ 7.46 – 7.38 (8H, m, ArH), 7.35 – 7.22 (12H, m, ArH), 2.33 (4H, d, $^2J_{HP}$ = 3.2 Hz, CH_2) and 1.03 ppm (6H, s, CH_3). $^{13}C\{^1H\}$ NMR (101 MHz, $CDCl_3$): δ 140.1 (d, $^1J_{CP}$ = 13.1 Hz), 133.1 (d, $^2J_{CP}$ = 22.2 Hz), 128.3 (d, J_{CP} = 7.1 Hz), 44.2 (dd, J_{CP} = 8.4 Hz), 35.2 (d, $^2J_{CP}$ = 14.1 Hz) and 30.4 ppm (t, $^3J_{CP}$ = 9.1 Hz). $^{31}P\{^1H\}$ NMR (162

MHz, $CDCl_3$): δ -24.6 ppm. MS (+ve ESI): m/z (calcd), $[M+H]^+$ 441.2; found 441.2. Elem. Anal. Calcd for $C_{29}H_{30}P_2$: C, 79.07; H, 6.86. Found: C, 79.02, H 6.78.

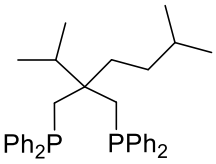

(2-Isopentyl-2-isopropylpropane-1,3-diyl)bis(diphenylphosphane) (DPPIPIPP) Diphenylphosphine (1.1 mL, 6.00 mmol, 2.1 eq) was taken up in tetrahydrofuran (15 mL) then cooled to 0 °C. To the stirred 0 °C solution was added dropwise ^{n}BuLi (2.5 M in hexane, 2.4 mL, 6.00 mmol, 2.1 eq) to give a bright orange-red solution which was left to stir for a further 30 min at 0 °C. 5-isopentyl-5-isopropyl-1,3,2-dioxathiane 2,2-dioxide (715 mg, 2.86 mmol, 1 eq) was added dropwise and the resulting mixture gradually warmed to 65 °C. The reaction mixture was monitored by $^{31}P\{^1H\}$ NMR by taking aliquots and the reaction run until diphenylphosphine was completely consumed. The reaction mixture was cooled to room temperature, volatiles removed under vacuum then diluted with H_2O (20 mL). The aqueous phase was extracted with Et_2O (3 x 10 mL) and the combined organic extracts dried over anhydrous Na_2SO_4 then concentrated to give a viscous brown liquid (1.82 g). To the crude product was added an excess of BH_3.THF (38 mL, 38.1 mmol, 11 eq) and stirred at room temperature and monitored by $^{31}P\{^1H\}$ NMR till all phosphorus signals corresponding to the crude product were absent. The crude borane-protected product was then purified by column chromatography (1:1 hexane/CH_2Cl_2, R_f = 0.34) to give a white gel (160 mg). The purified borane-protected product was refluxed in EtOH (3 mL) to give (2-isopentyl-2-isopropylpropane-1,3-diyl)bis(diphenylphosphane) as a light beige gel (152 mg, 10%). ^1H NMR (400 MHz, $CDCl_3$): δ 7.53 – 7.48 (4H, m, ortho-ArH), 7.48 – 7.42 (4H, m, ortho-ArH), 7.36 – 7.27 (12H, m, meta/para-ArH), 2.48 (2H, dd, $^2J_{HH}$ = 14.9 Hz, $^2J_{HP}$ = 4.1 Hz, PCH_2), 2.32 (2H, dd, $^2J_{HH}$ = 14.6 Hz, $^2J_{HP}$ = 2.5 Hz, PCH_2), 2.06 (1H, septet, $^3J_{HH}$ = 6.9 Hz, iPr-CH), 1.50 – 1.42 (2H, m, CH_2), 1.03 – 0.93 (3H, m, CH_2, iPent-CH), 0.90 (6H, d, $^3J_{HH}$ = 6.9 Hz, CH_3(iPr)) and 0.62 ppm (6H, d, $^3J_{HH}$ = 6.2 Hz, CH_3(iPent)). $^{13}C\{^1H\}$ NMR (101 MHz, $CDCl_3$): δ 140.7 (m, ipso-Ar), 133.3 (m, ortho-Ar), 128.4 (m, meta/para-Ar), 42.7 (t, J = 11 Hz, tert. C), 38.0 (d, J = 14 Hz, PCH_2), 37.9 (d, J = 14 Hz, PCH_2), 37.2 (t, J = 8 Hz, CH_2), 35.3 (t, J = 7 Hz, CH(iPr)), 33.3 (CH_2), 28.9 (CH(iPent)), 22.5 (CH_3(iPent)) and 18.1 ppm (CH_3(iPr)). $^{31}P\{^1H\}$ NMR (162 MHz, $CDCl_3$): δ -25.2 ppm. HR-MS (+ve ESI): $[M+H]^+$ 525.2835; found 525.2834. Elem. Anal. Calcd for $C_{35}H_{42}P_2$: C, 80.12; H, 8.07. Found: C, 76.48; H, 7.79. Note: the experimental elemental analysis values obtained were outside the 0.4% tolerance. Therefore, NMR spectra has been included to demonstrate the absence of detectable organic contaminants except for silicon grease (**Figure 6.3**, **Figure 6.4** and **Figure 6.5**, supplementary information).

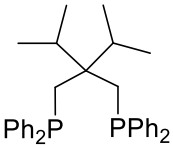

(2,2-Diisopropylpropane-1,3-diyl)bis(diphenylphosphane) (DPPDIPP) Diphenylphosphine (0.6 mL, 3.59 mmol, 2.1 eq) was taken up in tetrahydrofuran (15 mL) then cooled to 0 °C. To the stirred 0 °C solution was added dropwise ^{n}BuLi (2.0 M in cyclohexane, 1.8 mL, 3.59 mmol, 2.1 eq) to give an amber solution which was left to stir for a further 30 min at 0 °C. 5,5-diisopropyl-1,3,2-dioxathiane 2,2-dioxide (380 mg, 1.71 mmol, 1 eq) was added dropwise as a solution in tetrahydrofuran (10 mL) and the resulting mixture gradually warmed to 65 °C. The reaction mixture was monitored by $^{31}P\{^{1}H\}$ NMR by taking aliquots of the reaction mixture and the reaction run until diphenylphosphine was completely consumed. The reaction mixture was cooled to room temperature, volatiles removed under vacuum to give a red gel that was then diluted with H_2O (20 mL) to give a cloudy yellow mixture. The aqueous phase was extracted with Et_2O (3 x 10 mL) and the combined organic extracts dried over anhydroyus $MgSO_4$ then concentrated to give a reddish-brown gel (0.93 g). To the crude gel product was added an excess of BH_3.THF (1M in THF, 10 mL, 10 mmol) and then stirred overnight at room temperature. The clear solution was concentrated in vacuo to give a pale-yellow cloudy gel (1.19 g) that was then purified by column chromatography (4:1 hexane/ethyl acetate, R_f = 0.43) to give a white solid (100 mg). The purified borane-protected product was refluxed in EtOH (5 mL) to give (2,2-diisopropylpropane-1,3-diyl)bis(diphenylphosphane) as a white solid (94 mg, 11%). ^{1}H NMR (400 MHz, $CDCl_3$): δ 7.45 – 7.38 (8H, m, ArH), 7.30 – 7.24 (12H, m, ArH), 2.33 (4H, d, $^{2}J_{PH}$ = 3.7 Hz, PCH_2), 2.22 (2H, septet, $^{3}J_{HH}$ = 6.9 Hz, CH) and 0.90 ppm (12H, $^{3}J_{HH}$ = 6.9 Hz, CH_3). $^{13}C\{^{1}H\}$ NMR (101 MHz, $CDCl_3$): δ 140.8 (d, J = 22 Hz), 133.2 (d, J = 21 Hz), 128.4 (m), 45.4 (t, J = 10 Hz), 36.4 (dd, J = 20 Hz and 12 Hz), 34.9 (t, J = 5 Hz) and 19.4 ppm (t, J = 3 Hz). $^{31}P\{^{1}H\}$ NMR (162 MHz, $CDCl_3$): δ -23.8 ppm. HR-MS (+ve ESI): $[M+H]^+$ 497.2522; Found: 497.2521. Elem. Anal. Calcd for $C_{33}H_{38}P_2$: C, 79.81; H, 7.71. Found: C, 77.41; H, 7.47 Note: the experimental elemental analysis values obtained were outside the 0.4% tolerance. Therefore, NMR spectra has been included to demonstrate the absence of detectable organic contaminants except for silicon grease (**Figure 6.6**, **Figure 6.7** and **Figure 6.8**, supplementary information).

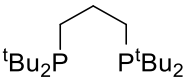

1,3-Bis(di-tert-butylphosphaneyl)propane (DTBPP) Di-tert-butylphosphine (10 wt% in hexane, 22.1 mL, 10.3 mmol, 2.1 eq) was mixed with THF (30 mL) then cooled to 0 °C. To the stirred 0 °C solution was added dropwise ^{n}BuLi (1.6 M in hexane, 6.5 mL, 10.3 mmol, 2.1 eq) to give a bright yellow solution

which was left to stir for a further 30 min at 0 °C. 1,3-Dibromopropane (0.5 mL, 4.93 mmol, 1 eq) was added and the reaction mixture gradually warmed to 65 °C and left to stir overnight. The slightly cloudy reaction mixture was cooled to room temperature and volatiles removed under vacuum before diluting with degassed H_2O (20 mL) to give a cloudy white mixture. The aqueous layer was extracted with pentane (3 x 10 mL). The combined organic extracts were dried over anhydrous $MgSO_4$ then concentrated to give a clear oil (1.74 g) which was then distilled under reduced pressure (0.6 mbar, 135 – 140 °C) to give 1,3-bis(di-tert-butylphosphaneyl)propane as a clear oil (1.04 g, 63%). ^{1}H NMR (400 MHz, $CDCl_3$): δ 1.79 – 1.66 (2H, m, CH_2CH_2), 1.50 – 1.42 (4H, m, PCH_2) and 1.10 ppm (36H, d, $^3J_{HP}$ = 10.9 Hz, CH_3). $^{31}P\{^1H\}$ NMR (162 MHz, $CDCl_3$): δ 27.5 ppm.

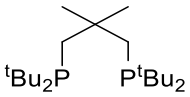

(2,2-Dimethylpropane-1,3-diyl)bis(di-tert-butylphosphane) (DTBPDMP) Di-tert-butylphosphine (1.2 g, 8.21 mmol, 2.1 eq) was taken up in tetrahydrofuran (15 mL) then cooled to 0 °C. To the stirred 0 °C solution was added dropwise ^{n}BuLi (2.5 M in hexane, 3.3 mL, 8.21 mmol, 2.1 eq) and left to stir for a further 15 min at 0 °C before being cooled to -78 °C. 5,5-Dimethyl-1,3,2-dioxathiane 2,2-dioxide (650 mg, 3.91 mmol, 1 eq) was added as a solution in tetrahydrofuran (5 mL) and the reaction mixture warmed to 60 °C and then left to stir overnight. The reaction mixture was monitored by $^{31}P\{^1H\}$ NMR by taking aliquots of the reaction mixture until all starting di-tert-butylphosphine was consumed. The reaction mixture then was cooled to room temperature and volatiles removed under vacuum before diluting with H_2O (25 mL). The aqueous layer was extracted with Et_2O (3 x 12 mL). The combined organic extracts were dried over anhydrous Na_2SO_4 then concentrated to give a grey solid (0.8 g) which was triturated with MeOH (3 x 10 mL) to give (2,2-dimethylpropane-1,3-diyl)bis(di-tert-butylphosphane) as an off-white powder (275 mg, 20%). ^{1}H NMR (400 MHz, $CDCl_3$): δ 1.51 (4H, d, $^2J_{HP}$ = 5.8 Hz, PCH_2), 1.16 (36H, d, $^3J_{HP}$ = 10.8 Hz, CH_3) and 1.07 ppm (6H, s, CH_3). $^{13}C\{^1H\}$ NMR (101 MHz, $CDCl_3$): δ 36.8 (dd, J = 25 Hz and 6 Hz), 33.3 (t, J = 17 Hz), 31.7 (d, J = 21 Hz), 30.7 ppm (d, J = 13 Hz) and 30.4 ppm. $^{31}P\{^1H\}$ NMR (162 MHz, $CDCl_3$): δ 17.2 ppm. MS (+ve EI): m/z (calcd), $[M\text{-}C_4H_8]^+$ 304; found $[M\text{-}C_4H_8]^+$ 304. Elem. Anal. Calcd for $C_{21}H_{46}P_2$: C, 69.96; H, 12.86. Found: C, 69.98; H, 13.02. Note: proposed EI fragmentation pattern (**Figure 6.14**, supplementary information).

5.4.3 [Pd(Ligand)Cl_2] Synthesis

General procedure for synthesis of Pd(ligand)Cl_2 complexes

Diphosphine (0.1 mmol, 1 eq) and Pd(1,5-cyclooctadiene)Cl_2 (28.6 mg, 0.1 mmol, 1 eq) were dissolved in CH_2Cl_2 (2 mL) then stirred overnight. Volatiles were removed under vacuum to obtain the desired complex. Crystals suitable for single crystal x-ray diffraction were grown from saturated CH_2Cl_2

solutions of the complex layered with pentane or via slow diffusion of cyclohexane into saturated CH_2Cl_2 solutions of the complex.

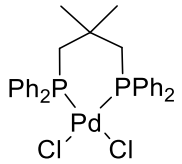

(2,2-Dimethylpropane-1,3-diyl)bis(diphenylphosphane)dichloropalladium(II) complex, Pd(DPPDMP)Cl₂ Synthesized via the general procedure for synthesis of Pd(ligand)Cl_2 complexes. Ligand = (2,2-dimethylpropane-1,3-diyl)bis(diphenylphosphane). ^{1}H NMR (400 MHz, CD_2Cl_2): δ 7.95 – 7.89 (8H, m, ortho-ArH), 7.58 – 7.49 (12H, m, meta/para-ArH), 2.34 (4H, d, 2JHP = 9.0 Hz, CH_2) and 0.65 ppm (6H, br.s, CH_3). $^{13}C\{^1H\}$ NMR (101 MHz, CD_2Cl_2): δ 134.8 (t, J = 5.1 Hz), 131.9, 129.1 (t, J = 5.9 Hz), 39.6 (PCH_2), 35.7 (tert. C) and 32.6 ppm (CH_3). $^{31}P\{^1H\}$ NMR (162 MHz, CD_2Cl_2): δ 17.5 ppm. MS (+ve ESI): m/z (calcd), $[M\text{-}2Cl+HCOO]^+$ 591.0829; found 591.0897 (^{106}Pd). Elem. Anal. Calcd for $C_{29}H_{30}Cl_2P_2Pd$: C, 56.38; H, 4.89. Found: C, 56.16; H, 5.06.

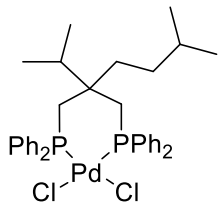

(2-Isopentyl-2-isopropylpropane-1,3-diyl)bis(diphenylphosphane)dichloropalladium(II) complex, Pd(DPPIPIPP)Cl₂ Synthesized via the general procedure for synthesis of Pd(ligand)Cl_2 complexes. Ligand = (2-isopentyl-2-isopropylpropane-1,3-diyl)bis(diphenylphosphane). ^{1}H NMR (400 MHz, $CDCl_3$): δ 8.33 – 8.25 (4H, m, ortho-ArH), 7.68 – 7.62 (4H, m, ortho-ArH), 7.56 – 7.51 (6H, m, meta/para-ArH), 7.47 – 7.41 (6H, m, meta/para-ArH), 2.43 (2H, dd, $^2J_{PH}$ = 15.0 Hz, $^2J_{HH}$ = 11.3 Hz, PCH_2), 2.21 (2H, dd, $^2J_{PH}$ = 15.2 Hz, $^2J_{HH}$ = 7.1 Hz, PCH_2), 1.63 – 1.54 (1H, m, $CH(CH_3)_2$), 0.81 (6H, d, $^3J_{HH}$ = 10.7 Hz, CH_3(iPr)), 0.75 – 0.69 (2H, br.m, CH_2) and 0.13 ppm (9H, br.s, CH_3(iPent) & CH(iPent) & CH2). $^{13}C\{^1H\}$ NMR (101 MHz, $CDCl_3$): δ 136.4 (t, $^2J_{PC}$ = 5.7 Hz, ortho), 132.8 (t, $^2J_{PC}$ = 4.9 Hz, ortho) 132.0, 130.7, 128.9 (t, J = 5.6 Hz), 128.7 (t, J = 5.7 Hz), 43.1 (tert. C), 36.0 (t, J = 9.4 Hz), 35.0 (t, J = 5.3 Hz), 33.2, 33.0, 32.8, 31.2, 27.9, 21.8 and 16.2 ppm. $^{31}P\{^1H\}$ NMR (162 MHz, $CDCl_3$): δ 16.6 ppm. MS (+ve ESI): m/z (calcd), $[M\text{-}2Cl+HCOO]^+$ 675.1768; found 675.1786 (^{106}Pd). Elem. Anal. Calcd for $C_{35}H_{42}Cl_2P_2Pd$: C, 59.88; H, 6.03. Found: C, 57.30; H, 5.55. Note: the experimental elemental analysis values obtained were outside the 0.4% tolerance. This is likely due to the presence of Et_2O and H_2O as observed in the ^{1}H NMR spectra (**Figure 6.9**, supplementary information).

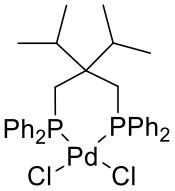

(2,2-Diisopropylpropane-1,3-diyl)bis(diphenylphosphane)dichloropalladium(II) complex, Pd(DPPDIPP)Cl₂ Synthesized via the general procedure for synthesis of Pd(ligand)Cl_2 complexes. Ligand = (2,2-diisopropylpropane-1,3-diyl)bis(diphenylphosphane). ^{1}H NMR (400 MHz, CD_2Cl_2): δ 7.97 – 7.89 (8H, m, ArH), 7.57 – 7.46 (12H, m, ArH), 2.40 (4H, d, $^{2}J_{PH}$ = 9.8 Hz, PCH_2), 1.91 (2H, septet, $^{3}J_{HH}$ = 6.7 Hz, CH) and 0.49 ppm (12H, $^{3}J_{HH}$ = 6.7 Hz, CH_3). $^{13}C\{^{1}H\}$ NMR (101 MHz, CD_2Cl_2): δ 135.1 (t, J = 5 Hz), 131.8, 129.1 (t, J = 5 Hz), 48.2, 35.3 (t, J = 7 Hz), 32.6, 32.4, 32.2 and 19.1 ppm. $^{31}P\{^{1}H\}$ NMR (162 MHz, CD_2Cl_2): δ 17.6 ppm. MS (+ve ESI): m/z (calcd), $[M+Na]^+$ 695.0753; found 695.0773 (^{106}Pd/^{35}Cl/^{35}Cl or ^{104}Pd/^{37}Cl/^{35}Cl). Elem. Anal. Calcd for $C_{33}H_{38}Cl_2P_2Pd.CH_2Cl_2$: C, 58.81; H, 5.68; Found: C, 54.33; H, 5.33.

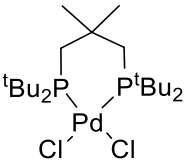

(2,2-Dimethylpropane-1,3-diyl)bis(di-tert-butylphosphane)dichloropalladium(II) complex, Pd(DTBPDMP)Cl₂ Synthesized via the general procedure for synthesis of Pd(ligand)Cl_2 complexes. Ligand = (2,2-dimethylpropane-1,3-diyl)bis(di-tert-butylphosphane). ^{1}H NMR (400 MHz, CD_2Cl_2): δ 1.69 (4H, dd, $^{2}J_{HP}$ = 10.5 Hz, $^{2}J_{HH}$ = 1.6 Hz, CH_2), 1.58 (36H, d, $^{3}J_{HP}$ = 14.2 Hz) and 1.30 ppm (6H, br.s, CH_3). $^{13}C\{^{1}H\}$ NMR (101 MHz, CD_2Cl_2): δ 40.8 (d, J = 20 Hz), 35.4, 35.1 (t, J = 5 Hz), 32.4 and 31.6 (dd, J = 13 Hz and 6 Hz). $^{31}P\{^{1}H\}$ NMR (162 MHz, CD_2Cl_2): δ 47.9 ppm. MS (+ve ESI): m/z (calcd), $[M-Cl]^+$ 501.1793; found 501.1789 (^{106}Pd/^{35}Cl or ^{104}Pd/^{37}Cl). Elem. Anal. Calcd for $C_{21}H_{46}Cl_2P_2Pd$: C, 46.89; H, 8.62. Found: C, 44.29; H, 8.05. Note: the experimental elemental analysis values obtained were outside the 0.4% tolerance. Therefore, NMR spectra has been included to demonstrate the absence of detectable organic contaminants (**Figure 6.10**, **Figure 6.11** and **Figure 6.12**, supplementary information).

5.4.4 Chelation Competition

General procedure for chelation competition experiments

A Schlenk tube was taken into the glovebox and sequentially charged with **DPPP** (2.9 mg, 7.0 µmol, 1 eq), **DPPDMP** (3.1 mg, 7.0 µmol, 1 eq), Pd(1,5-cyclooctadiene)Cl_2 (2 mg, 7.0 µmol, 1 eq) then CH_2Cl_2 (0.7 mL). The resulting mixture was stirred for 2 min to give a clear yellow solution that was then transferred to a NMR tube equipped with a $C_2D_2Cl_4$ capillary that had PPh_3 dissolved within as an internal standard before being submitted for $^{31}P\{^{1}H\}$ NMR analysis.

5.4.5 Computational Details

Geometry optimisations: Density functional theory (DFT) calculations were performed with the Gaussian 16 package[2] using the B3LYP3 functional[3] and the DEF2TZVPP[4-5] basis set on C, H, O and P atoms and the Stuttgart-Dresden (SDD)[6] effective core potential (ECP) with the corresponding basis set for Pd. All calculations were performed at 298.15 K and at 423.15 K with Grimme dispersion correction[7] and Becke-Johnson damping.[8-9] All geometries were localised in the gas phase at the B3LYP level. All structures were confirmed to be at a minimum through frequency calculations.

Mechanistic studies: DFT calculations were performed using Gaussian 09. Unless stated otherwise, calculations used B3LYP density functional with 6-31G(d,p)[10-11] for C, H, O, P atoms and the Stuttgart-Dresden (SDD) effective core potential (ECP) with the corresponding basis set for Pd. All calculations were performed with an ultrafine grid (integral=grid=ultrafine) and at 298.15 K (default). All transition states were characterised by normal coordinate analysis revealing precisely one imaginary mode corresponding to the intended reaction. The vibrational mode corresponding to the imaginary frequency was used to deduce the corresponding minima. In addition, for **II-TS** (**Figure 2.28**) IRC calculations were performed to confirm the identity of the transition state. Full coordinates for all the stationary points are available at: 10.14469/hpc/6231. For ligand with gem-di-*tert*-butyl substituents (as per Table 6.2), calculations also were performed using Gaussian 16 (revision A03) including Grimme dispersion correction with Becke-Johnson damping (empiricaldispersion=gd3bj) and self-consistent reaction cavity continuum solvation model with THF as solvent (scrf=cpcm=THF) at 423.15 K.

Ligand buried volume (%V_Bur): Pd(ligand)Cl_2 structures obtained from XRD and DFT calculations were subjected to ligand buried volume (%V_Bur) calculations using SambVca 2.[12-13] The Pd atom was set as the coordination centre, P donor atoms were selected for z-axis definition (z-negative) and the central carbon of the C_3-bridge selected as the atom for xz-plane definition. The Pd and Cl atoms were deleted and thus not considered in the buried volume calculation. Atomic radii were set at Bondi radii and sphere radius set to 5 Å. Mesh spacing for numerical integration was set to 0.10 Å and hydrogen atoms were omitted from the calculation.

5.4.6 Carbonylation Procedures

General procedure for DPPP modified palladium catalysed hydroformylation of 1-octene (Table 2.3)

Parr reactor was assembled then cycled 3 times with N_2. A Schlenk flask was charged sequentially with diglyme, $Pd(OAc)_2$ then DPPP (if any). The catalyst mixture was injected into the Parr reactor under a stream of N_2. A stock solution of CF_3CO_2H in diglyme (or pure diglyme) was used to wash out the Schlenk flask that previously held the catalyst mixture and the washes injected into the Parr reactor

under a stream of N_2. Anisole (internal standard) followed by 1-octene was then injected into the Parr reactor a stream of N_2 then the mixture stirred at 1000 rpm with a magnetic stirrer bar and the reactor pressurised to 60 bar with a 1:1 CO/H_2 syngas premix at room temperature. The reactor was then sealed and heated to reaction temperature and stirred at 1000 rpm for 5 h. The reactor was then slowly cooled to 0 °C then carefully vented before being sampled for GC analysis.

General procedure for palladium catalysed hydroformylation of olefins (Table 2.4)

Parr reactor was assembled and cycled 3 times with Ar. A Schlenk flask was charged sequentially with $Pd(OAc)_2$, ligand and diglyme. The mixture was stirred for 5 min before CF_3CO_2H was injected and stirred for a further 5 min. The catalyst mixture was injected into the Parr reactor under a stream of Ar and diglyme used to wash the Schlenk flask that held the catalyst mixture and the washes injected into the Parr reactor under a stream of Ar. Anisole (internal standard) then olefin was injected into the Parr reactor under a stream of Ar and the reactor was sealed. The reaction mixture was stirred at 1000 rpm and pressurised to 60 bar CO/H_2 (1:1) by sequential introduction of first 30 bar pure CO then making up the pressure to 60 bar with pure H_2. The Parr reactor was sealed and warmed to 125 °C and stirred at 1000 rpm for 5 h. The Parr reactor was slowly cooled to 0 °C then vented and sampled for GC analysis.

General procedure for palladium catalysed methoxycarbonylation of olefins (Table 2.6)

Parr reactor was assembled and cycled 3 times with Ar. A Schlenk flask was charged sequentially with $Pd(OAc)_2$, ligand then a stock solution of CH_3SO_3H in MeOH. The catalyst mixture was injected into the Parr reactor under a stream of Ar. The Schlenk flask containing the catalyst mixture was washed with MeOH and the washes injected into the Parr reactor under a stream of Ar. Anisole (internal standard) and olefin was injected into the Parr reactor under a stream of Ar then the reactor sealed and stirred at 1000 rpm. The reactor was pressurised to 50 bar CO then sealed, warmed to reaction temperature and stirred at 1000 rpm for 4 h. The reaction mixture was sampled throughout the reaction period via dip tube and analysed via GC. The Parr reactor was slowly cooled to 0 °C then vented and sampled for GC analysis.

General procedure for palladium catalysed cyclocarbonylation of 2-allylphenol (Table 2.7)

Parr reactor was assembled and cycled 3 times with N_2. A Schlenk flask was charged sequentially with toluene, $Pd(OAc)_2$ then ligand and stirred for 5 min. The catalyst mixture was injected into the Parr reactor under a stream of N_2 then the Schlenk flask containing the catalyst mixture washed with toluene and the washes injected into the Parr reactor under a stream of N_2. 2-Allylphenol was injected into the Parr reactor under a stream of N_2 and the reactor flushed briefly with 20 bar 1:1 CO/H_2 syngas

premix before being pressurised to 40 bar with 1:1 CO/H_2 syngas premix. The reactor was sealed, stirred at 1000 rpm with a magnetic stirrer bar and warmed to 90 °C for the reaction time period specified. The reactor was allowed to cool to room temperature then vented and the product mixture concentrated under reduced pressure to remove toluene. 1,4-Dioxane was added as an internal standard and the product mixture stirred and sampled for NMR analysis.

5.5 Experimental Procedures for Chapter 3

5.5.1 Ligand Synthesis

Mixtures of secondary [3.3.1]phobane and [4.2.1]phobane isomers were separated by selective protonation following literature.[14] 1,2-di(9-phosphabicyclo[3.3.1]nonan-9-yl)benzene (**BCOPP**) and 1,2-di(9-phosphabicyclo[3.3.1]nonan-9-yl)ethane (**BCOPE**) were synthesized via reported procedures.[15-16]

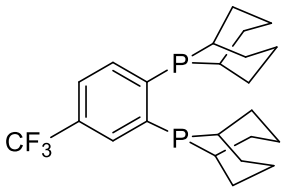

9,9'-(4-(trifluoromethyl)-1,2-phenylene)bis(9-phosphabicyclo[3.3.1]nonane) (BCOPF) 9-phosphabicyclo[3.3.1]nonane (0.60 g, 4.20 mmol, 2.1 equiv), tetrakis(triphenylphosphine)palladium(0) (0.23 g, 0.20 mmol, 0.1 equiv), 1,4-diazabicyclo[2.2.2]octane (1.12 g, 10.0 mmol, 5.0 equiv) and 1,2-dibromo-4-(trifluoromethyl)benzene (0.61 g, 2.00 mmol, 1.0 equiv) were taken up in xylenes (15 mL) then stirred at 140 °C for 72 h. The resulting mixture was filtered and the filtrate concentrated under vacuum to give a red solid. The red solid was flashed through a short pad of silica with toluene (20 mL) and concentrated to give a crude solid. The crude product was washed with pentane (2 x 10 mL), MeOH (2 x 10 mL) and dried under vacuum to yield 9,9'-(4-(1,1,1-trifluoromethyl)-1,2-phenylene)bis(9-phosphabicyclo[3.3.1]nonane) as an off-white powder (0.40 g, 47%). ^{1}H (400 MHz, $CDCl_3$): δ 7.53 – 7.48 (1H, m, ArH), 7.43 – 7.37 (2H, m, ArH), 2.71 (4H, br.s, CH), 2.29 – 2.07 (10H, m, CH_2), 2.00 – 1.84 (6H, m, CH_2), 1.80 – 1.69 (6H, m, CH_2) and 1.37 – 1.28 ppm (2H, m, CH_2). $^{13}C\{^{1}H\}$ NMR (101 MHz, $CDCl_3$): δ 131.3 (dd, J = 9 Hz, 3 Hz), 127.7 (m), 122.3 (br.s), 32.1 (dd, J = 15 Hz, 4 Hz), 25.6 (dd, J = 15 Hz, 4 Hz), 24.8 (quintet, J = 7 Hz), 22.9 (br.s) and 21.9 (s) ppm. $^{31}P\{^{1}H\}$ NMR (162 MHz, $CDCl_3$): δ -15.7 and -16.2 ppm. ^{19}F NMR (376 MHz, $CDCl_3$): δ -62.8 ppm. HR-MS (+ve ESI): m/z (calcd), $[M+H]^+$ 427.1926; found 427.1942. Elem. Anal. Calcd for $C_{23}H_{31}F_3P_2$: C, 64.78; H, 7.33. Found: C, 64.14; H, 6.97. NMR spectra have been included to

demonstrate the absence of detectable organic contaminants except for silicon grease (**Figure 6.21**, **Figure 6.22** and **Figure 6.23**, supplementary information).

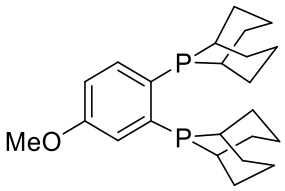

9,9'-(4-methoxy-1,2-phenylene)bis(9-phosphabicyclo[3.3.1]nonane) (BCOPA) 9-phosphabicyclo[3.3.1]nonane (0.65 g, 4.52 mmol, 2.2 equiv), tetrakis(triphenylphosphine)palladium(0) (0.29 g, 0.21 mmol, 0.1 equiv), 1,4-diazabicyclo[2.2.2]octane (0.69 g, 6.15 mmol, 3.0 equiv) and 1,2-dibromoanisole (0.3 mL, 2.00 mmol, 1.0 equiv) were taken up in xylenes (15 mL) then stirred at 140 °C for 16 h. The resulting mixture was filtered and the filtrate concentrated under reduced pressure at 65 °C to give a reddish-brown solid. The residue was washed with pentane (2 x 10 mL) then flashed through a short pad of silica with toluene (20 mL) and concentrated to give a crude solid product. The crude product was subsequently triturated with MeOH (2 x 20 mL) to yield 9,9'-(4-methoxy-1,2-phenylene)bis(9-phosphabicyclo[3.3.1]nonane) as a white solid (0.44 g, 54%). ^{1}H (400 MHz, $CDCl_3$): δ 7.23 – 7.18 (1H, m, ArH), 6.89 – 6.85 (1H, m, ArH), 6.76 (1H, dd, $^{3}J_{HH}$ = 8.6 Hz, $^{4}J_{HH}$ = 2.8 Hz, ArH), 3.80 (3H, s, CH_3), 2.67 (2H, br.s, PCH), 2.61 (2H, br.s, PCH), 2.26 – 1.92 (16H, m, CH_2), 1.77 – 1.66 (6H, m, CH_2) and 1.38 – 1.29 ppm (2H, m, CH_2). ^{13}C{^{1}H} NMR (101 MHz, $CDCl_3$): δ 157.8 (d, J = 2 Hz), 144.0 (dd, J = 31 Hz, 15 Hz), 132.8 (dd, J = 28 Hz, 14 Hz), 132.5 (dd, J = 9 Hz, 4 Hz), 117.4 (dd, J = 9 Hz, 4 Hz), 111.4 (s), 55.1 (s), 32.1 (dd, J = 15 Hz, 7 Hz), 25.6 (dd, J = 18 Hz, 4 Hz), 24.9 (m), 23.0 (dd, J = 10 Hz, 5 Hz) and 22.0 ppm (d, J = 11 Hz). ^{31}P{^{1}H} NMR (162 MHz, $CDCl_3$): δ -16.7 and -18.7 ppm. HR-MS (+ve ESI): m/z (calcd), $[M+H]^+$ 389.2158; found 389.2165. Elem. Anal. Calcd for $C_{23}H_{34}OP_2$: C, 71.11; H, 8.82. Found: C, 68.91; H, 8.15. NMR spectra have been included to demonstrate the absence of detectable organic contaminants except for silicon grease (**Figure 6.24**, **Figure 6.25** and **Figure 6.26**, supplementary information).

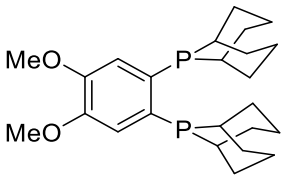

9,9'-(4,5-dimethoxy-1,2-phenylene)bis(9-phosphabicyclo[3.3.1]nonane) (BCOPV) 9-phosphabicyclo[3.3.1]nonane (0.63 g, 4.40 mmol, 2.2 equiv), tetrakis(triphenylphosphine)palladium(0) (0.23 g, 0.20 mmol, 0.1 equiv), 1,4-diazabicyclo[2.2.2]octane (1.12 g, 10.0 mmol, 5.0 equiv) and 1,2-dibromoveratrole (0.59 g, 2.00 mmol,

1.0 equiv) were taken up in xylenes (15 mL) then stirred at 140 °C for 72 h. The resulting mixture was filtered and the filtrate concentrated under vacuum at 50 °C to give a dark red solid. The solid was triturated with pentane (2 x 10 mL) then MeOH (2 x 10 mL) and dried under vacuum to yield 9,9'-(4,5-dimethoxy-1,2-phenylene)bis(9-phosphabicyclo[3.3.1]nonane) as a pale orange powder (0.28 g, 33%). ^{1}H (400 MHz, $CDCl_3$): δ 6.84 – 6.82 (2H, dd, J = 5.2 Hz, 2.3 Hz), 3.86 (6H, s, OCH_3), 2.62 (4H, br.s, PCH), 2.25 – 1.95 (16H, m, CH_2), 1.78 – 1.67 (6H, m, CH_2) and 1.37 – 1.28 ppm (2H, m, CH_2). ^{13}C{^{1}H} NMR (101 MHz, $CDCl_3$): δ 147.3 (s), 133.7 (dd, J = 29 Hz, 15 Hz), 129.0, 128.8, 128.6, 128.6, 114.4 (dd, J = 9 Hz, 5 Hz), 55.8 (s), 47.5 (s), 32.0 (d, J = 15 Hz), 25.6 (d, J = 4 Hz), 25.2 (dd, J = 13 Hz, 7 Hz), 23.0 (d, J = 5 Hz) and 22.0 (s) ppm. ^{31}P{^{1}H} NMR (162 MHz, $CDCl_3$): δ -17.7 ppm. HR-MS (+ve ESI): m/z (calcd), $[M+H]^+$ 419.2263; found 419.2276. Elem. Anal. Calcd for $C_{24}H_{36}O_2P_2$: C, 68.88; H, 8.67. Found: C, 68.72; H, 8.54.

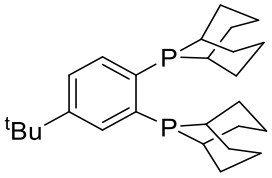

9,9'-(4-(tert-butyl)-1,2-phenylene)bis(9-phosphabicyclo[3.3.1]nonane) (BCOPT) 9-phosphabicyclo[3.3.1]nonane (0.64 g, 4.48 mmol, 2.8 equiv), tetrakis(triphenylphosphine)palladium(0) (0.19 g, 0.16 mmol, 0.1 equiv), 1,4-diazabicyclo[2.2.2]octane (0.90 g, 8.00 mmol, 5.0 equiv) and 1,2-dibromo-4-(1,1-dimethylethyl)benzene (0.3 mL, 1.60 mmol, 1.0 equiv) were taken up in xylenes (15 mL) then stirred at 140 °C for 72 h. The resulting mixture was filtered and the filtrate concentrated under vacuum to give an orange solid. The solid was triturated with MeOH (3 x 10 mL) then pentane (3 x 5 mL) to yield 9,9'-(4-(1,1-dimethylethyl)-1,2-phenylene)bis(9-phosphabicyclo[3.3.1]nonane) as an off-white powder (0.21 g, 32%). ^{1}H (400 MHz, $CDCl_3$): δ 7.33 – 7.29 (1H, m, ArH), 7.24 – 7.17 (2H, m, ArH), 2.68 (2H, br.s, PCH), 2.64 (2H, br.s, PCH), 2.31 – 1.89 (16H, m, CH_2), 1.77 – 1.67 (6H, m, CH_2) and 1.31 ppm (11H, m, tBu & CH_2). ^{13}C{^{1}H} NMR (101 MHz, $CDCl_3$): δ 148.2 (s), 141.3 (dd, J = 29 Hz, 14 Hz), 138.3 (dd, J = 29 Hz, 14 Hz), 130.9 (dd, J = 8 Hz, 4 Hz), 128.5 (dd, J = 8 Hz, 4 Hz), 123.0 (s), 34.6 (s), 32.1 (dd, J = 14 Hz, 5 Hz), 31.1 (s), 25.7 (t, J = 4 Hz), 24.9 (m), 23.1 (t, J = 5 Hz) and 22.1 ppm (d, J = 8 Hz). ^{31}P{^{1}H} NMR (162 MHz, $CDCl_3$): δ -16.7 and -18.3 ppm. HR-MS (+ve ESI): m/z (calcd), $[M+H]^+$ 415.2639; found 415.2692. Elem. Anal. Calcd for $C_{26}H_{40}P_2$: C, 75.33; H, 9.73. Found: C, 75.23; H, 9.45.

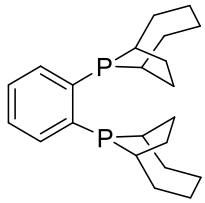

1,2-Di(9-phosphabicyclo[4.2.1]nonan-9-yl)benzene (*a*-BCOPP) 9-phosphabicyclo[4.2.1]nonane (0.70 g, 4.92 mmol, 2.2 equiv), tetrakis(triphenylphosphine)palladium(0) (0.13 g, 0.11 mmol, 0.05 equiv), 1,4-diazabicyclo[2.2.2]octane (1.26 g, 11.2 mmol, 5.0 equiv) and 1,2-dibromobenzene (0.27 mL, 2.24 mmol, 1.0 equiv) were taken up in xylenes (15 mL) then stirred at 140 °C for 72 h. The resulting mixture was filtered and the filtrate concentrated under vacuum. The residue obtained was filtered through a short pad of silica with toluene (20 mL) then concentrated under reduced pressure to give a crude solid product. The crude product was triturated with MeOH (3 x 10 mL) and dried under vacuum to yield 9,9'-(1,2-phenylene)bis(9-phosphabicyclo[4.2.1]nonane) as a white solid (0.29 g, 37%). ^{1}H NMR (400 MHz, $CDCl_3$): δ 7.28 – 7.22 (2H, m, ArH), 7.17 – 7.11 (2H, m, ArH), 3.00 – 2.91 (4H, m, CH), 2.26 – 2.16 (4H, m, CH_2), 2.04 – 1.93 (4H, m, CH_2) and 1.86 – 1.50 ppm (16H, m, CH_2). ^{13}C NMR (101 MHz, $CDCl_3$): δ 130.0, 127.0, 40.0, 40.0, 40.0, 35.0, 34.9, 34.8, 25.7, 25.7 and 25.6 ppm. $^{31}P\{^{1}H\}$ NMR (162 MHz, $CDCl_3$): δ 3.8 ppm. HR-MS (+ve ESI): m/z (calcd), $[M+H]^+$ 359.2052; found 359.2066. Elem. Anal. Calcd for $C_{22}H_{32}P_2$: C, 73.72; H, 9.00. Found: C, 70.70; H, 8.33. Note: the experimental elemental analysis values obtained were outside the 0.4% tolerance. This is likely due to the presence of acetone and grease as observed in the ^{1}H NMR spectra (**Figure 6.27**, supplementary information).

5.5.2 [Pd(Ligand)Cl_2] Synthesis

General procedure for synthesis of Pd(ligand)Cl_2 complexes

Ligand (0.1 mmol, 1 eq) and Pd(1,5-cyclooctadiene)Cl_2 (28.6 mg, 0.1 mmol, 1 eq) were dissolved in CH_2Cl_2 (2 mL) then stirred overnight. Volatiles were removed under vacuum to obtain the desired complex. Crystals suitable for single crystal x-ray diffraction were grown via slow vapor diffusion of cyclohexane into CH_2Cl_2 solutions of the complex.

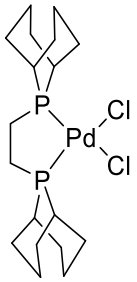

(1,2-di(9-phosphabicyclo[3.3.1]nonan-9-yl)ethane)dichloropalladium(II) complex, [Pd(BCOPE)Cl_2] Synthesized via the general procedure for synthesis of Pd(ligand)Cl_2 complexes. Ligand = 1,2-di(9-phosphabicyclo[3.3.1]nonan-9-yl)ethane (**BCOPE**). ^{1}H NMR (400 MHz, CD_2Cl_2): δ 3.38 (4H, br.s, PCH), 2.35 – 2.26 (4H, m, CH_2), 2.25 – 2.13 (6H, m, CH_2) and 2.10 – 1.80 ppm (14H, m, CH_2). $^{13}C\{^{1}H\}$ NMR (101 MHz, CD_2Cl_2): δ 29.3, 29.2, 28.4, 28.2, 27.9, 27.7, 21.0 and 20.8 ppm. $^{31}P\{^{1}H\}$ NMR (162 MHz, CD_2Cl_2): δ 51.3 ppm. HR-MS (+ve ESI): m/z (calcd), $[M+H]^+$ 487.0464; found 487.0528 ($^{105}Pd/^{35}Cl/^{35}Cl$).

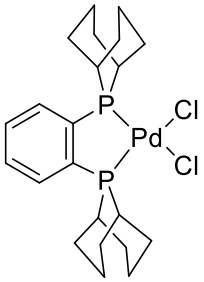

(1,2-di(9-phosphabicyclo[3.3.1]nonan-9-yl)benzene)dichloropalladium(II) complex, [Pd(BCOPP)Cl_2] Synthesized via the general procedure for synthesis of Pd(ligand)Cl_2 complexes. Ligand = 1,2-di(9-phosphabicyclo[3.3.1]nonan-9-yl)benzene (**BCOPP**)**.** ^{1}H NMR (400 MHz, CD_2Cl_2): δ 8.11 – 8.04 (2H, m, ArH), 7.58 – 7.51 (2H, m, ArH), 3.12 (4H, br.s, PCH), 2.90 – 2.80 (4H, m, CH_2), 2.50 – 2.37 (4H, m, CH_2), 2.36 – 2.18 (2H, m, CH_2), 2.14 – 1.92 (12H, m, CH_2) and 1.85 – 1.75 ppm (2H, m, CH_2). $^{13}C\{^{1}H\}$ NMR (101 MHz, CD_2Cl_2): δ 133.3 (d, J = 17 Hz), 131.7, 31.8, 31.5, 31.4, 29.1 (t, J = 3 Hz), 21.2, 21.2, 21.1 and 19.5 ppm (t, J = 3 Hz). $^{31}P\{^{1}H\}$ NMR (162 MHz, CD_2Cl_2): δ 38.6 ppm. HR-MS (+ve ESI): m/z (calcd), $[M+H]^+$ 537.0464; found 537.0306 ($^{106}Pd/^{35}Cl/^{37}Cl$ or $^{108}Pd/^{35}Cl/^{35}Cl$). Elem. Anal. Calcd for $C_{22}H_{32}Cl_2P_2Pd.CH_2Cl_2$: C, 44.51; H, 5.52. Found: C, 44.22; H, 5.45.

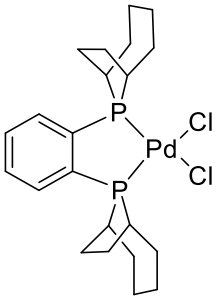

(1,2-Di(9-phosphabicyclo[4.2.1]nonan-9-yl)benzene)dichloropalladium(II) complex, [Pd(*α*-BCOPP)Cl$_2$] Synthesized via the general procedure for synthesis of Pd(ligand)Cl_2 complexes. Ligand = 1,2-di(9-phosphabicyclo[4.2.1]nonan-9-yl)benzene (***α*-BCOPP**). ^{1}H NMR (400 MHz, $CDCl_3$): δ 7.54 – 7.34 (4H, m, ArH), 3.54 – 2.84 (4H, m), 2.79 – 2.07 (8H, m), 1.97 – 1.82 (4H, m) and 1.74 – 1.34 ppm (12H, m). $^{13}C\{^1H\}$ NMR (101 MHz, $CDCl_3$): δ 131.8 (q, J = 4 Hz), 129.6 (d, J = 16 Hz), 33.0, 32.0, 28.1 and 27.0 ppm. $^{31}P\{^1H\}$ NMR (162 MHz, $CDCl_3$): δ 65.1 ppm. HR-MS (+ve ESI): m/z (calcd), $[M+Na]^+$ 557.0284; found 557.0292 ($^{104}Pd/^{35}Cl/^{37}Cl$ or $^{106}Pd/^{35}Cl/^{35}Cl$).

5.5.3 Carbonylation Procedures

General procedure for palladium catalysed hydroformylation of hexene (Table 3.3)

Parr reactor was assembled and cycled 3 times with Ar. A Schlenk flask was charged sequentially with $Pd(OAc)_2$, ligand, CH_3SO_3H as a solution in diglyme then aqueous NaCl. The mixture was stirred for 5 min before it was injected into the Parr reactor under a stream of Ar. Diglyme was used to wash the Schlenk flask that held the catalyst mixture and the washes injected into the Parr reactor under a stream of Ar. Anisole (internal standard) then hexene was injected into the Parr reactor under a stream of Ar and the reactor sealed. The reaction mixture was stirred at 1000 rpm and pressurised to 60 bar CO/H_2 (1:2) by sequential introduction of first 20 bar pure CO then making up the pressure to 60 bar with pure H_2. The Parr reactor was sealed and warmed to 100 °C and stirred at 1000 rpm for 2 h. The Parr reactor was slowly cooled to 0 °C vented and sampled for GC analysis.

General procedure for solvent screening experiments (Figure 3.15)

Solvent screening was carried out in parallel reactors on the SPR16 AMTECH system. Catalyst solutions were made up from stock solutions of $Pd(OAc)_2$, ligand, CH_3SO_3H and aqueous NaCl in solvent. The catalyst mixtures were stirred for 5 min then left to stand for 72 h. The SPR16 AMTECH system flushed the reactors with Ar for 3 cycles then the catalyst mixtures, anisole (internal standard) and 1-hexene were injected into the reactors and the system programmed to maintain pressure at 60 bar of (1:2) CO/H_2 premix, stirring speed of 1000 rpm and temperature of 100 °C for 2 h. The reactors were then cooled to room temperature and the reactors vented and sampled for GC analysis.

General procedure for palladium catalysed hydroformylation of methyl pentenoate (Table 3.4)

Parr reactor was assembled and cycled 3 times with Ar. A Schlenk flask was charged sequentially with $Pd(OAc)_2$, ligand then CH_3SO_3H as a solution in diglyme. The mixture was stirred for 5 min before it was injected into the Parr reactor under a stream of Ar. Diglyme was used to wash the Schlenk flask that held the catalyst mixture and the washes injected into the Parr reactor under a stream of Ar. Anisole (internal standard) then methyl pentenoate was injected into the Parr reactor under a stream of Ar then the reactor sealed. The reaction mixture was stirred at 1000 rpm and then pressurised to 60 bar CO/H_2 (1:2) by sequential introduction of first 20 bar pure CO then making up the pressure to 60 bar with pure H_2. The Parr reactor was sealed and warmed to 100 °C and stirred at 1000 rpm for 2 h. The Parr reactor was then slowly cooled to 0 °C and vented. Runs 1 – 4 were diluted with excess MeOH and refluxed overnight before being concentrated under reduced pressure and sampled for GC analysis. Runs 5 – 8 were directly sampled for GC analysis.

General procedure for palladium catalysed hydroformylation of 1-octene (Table 3.5)

Parr reactor was assembled and cycled 3 times with Ar. A Schlenk flask was charged sequentially with $Pd(OAc)_2$, ligand, CH_3SO_3H as a solution in 2-ethylhexanol then aqueous NaCl (note: aqueous phase was immiscible with 2-ethylhexanol phase). The mixture was stirred for 5 min before it was injected into the Parr reactor under a stream of Ar. 2-Ethylhexanol was used to wash the Schlenk flask that held the catalyst mixture and the washes injected into the Parr reactor under a stream of Ar. Anisole (internal standard) then 1-octene was injected into the Parr reactor under a stream of Ar then the reactor sealed. The reaction mixture was stirred at 1000 rpm and pressurised to 60 bar CO/H_2 (1:2) by sequential introduction of first 20 bar pure CO then making up the pressure to 60 bar with pure H_2. The Parr reactor was sealed and warmed to 100 °C and stirred at 1000 rpm for 2 h. The Parr reactor was then slowly cooled to 0 °C, vented and sampled for GC analysis.

General procedure for palladium catalysed alkoxycarbonylation of 1-octene (Table 3.6)

Parr reactor was assembled and cycled 3 times with Ar. A Schlenk flask was charged sequentially with $Pd(OAc)_2$, ligand, CH_3SO_3H as a solution in alcohol (ROH) then additive (note: aqueous NaCl and H_2O was immiscible with 2-ethylhexanol phase). The mixture was stirred for 5 min before it was injected into the Parr reactor under a stream of Ar. Alcohol (ROH) was used to wash the Schlenk flask that held the catalyst mixture and the washes injected into the Parr reactor under a stream of Ar. Anisole (internal standard) then 1-octene was injected into the Parr reactor under a stream of Ar and the reactor sealed. The reaction mixture was stirred at 1000 rpm and pressurised to 50 bar CO. The Parr reactor was sealed and warmed to 100 °C and stirred at 1000 rpm for 2 h. The Parr reactor was then

slowly cooled to 0 °C, vented and sampled for GC analysis. Note: Run 13 employing aqueous NaCl additive in MeOH solvent resulted in the separation of the product mixture into 2 different phases. CH_2Cl_2 was added post-catalysis in order to homogenise the mixture.

General procedure for palladium catalysed hydroxycarbonylation of olefins (Table 3.7 and Table 3.8)

Hydroxycarbonylation experiments were carried out in parallel reactors on the SPR16 AMTECH system. Catalyst solutions were made up from stock solutions of $Pd(OAc)_2$, ligand and CH_3SO_3H in diglyme. H_2O was added and the catalyst mixtures stirred for 5 min. The SPR16 AMTECH system flushed the reactors with Ar for 3 cycles then the catalyst mixtures, anisole (internal standard) and olefin were injected into the reactors and the system programmed to maintain pressure at 40 bar of CO, stirring speed of 1000 rpm and temperature of 100 °C for 21 h. The reactors were then cooled to room temperature and the reactors vented and sampled for GC analysis.

5.6 Experimental Procedures for Chapter 4

5.6.1 Ligand Synthesis

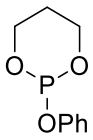

2-phenoxy-1,3,2-dioxaphosphinane A Schlenk flask was charged sequentially with propan-1,3-diol (0.55 mL, 7.63 mmol, 1 eq), toluene (15 mL), triphenylphosphite (2 mL, 7.63 mmol, 1 eq) then triethylamine (0.1 mL, 0.76 mmol, 0.1 eq) and warmed to 110 °C and stirred for 24 h. The reaction mixture was cooled to room temperature and volatiles removed under reduced pressure to give a clear viscous liquid. The crude product was distilled under reduced pressure (0.1 mbar, 115 °C) to give 2-phenoxy-1,3,2-dioxaphosphinane as translucent crystals (0.9 g, 60%). ^{1}H NMR (400 MHz, $CDCl_3$): δ 7.36 – 7.29 (2H, m, ArH), 7.13 – 7.06 (3H, m, ArH), 4.72 – 4.62 (2H, m, CH_2), 3.97 – 3.88 (2H, m, CH_2), 2.63 – 2.48 (1H, m, CH_2) and 1.71 – 1.61 ppm (1H, m, CH_2). $^{13}C\{^1H\}$ NMR (101 MHz, $CDCl_3$): δ 153.0 (d, $^2J_{CP}$ = 7 Hz, ipso), 129.8 (ortho), 123.4, 120.0 (d, J = 7 Hz), 60.0 (OCH_2) and 28.5 ppm (d, J = 5 Hz, CH_2). $^{31}P\{^1H\}$ NMR (162 MHz, $CDCl_3$): δ 123.2 ppm. MS (+ve ESI): m/z (calcd), $[M+H]^+$ 199.0519; found 199.0510. Elem. Anal. Calcd for $C_9H_{11}O_3P$: C, 54.55; H, 5.60. Found: C, 54.70, H 5.66.

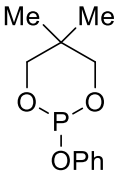

5,5-dimethyl-2-phenoxy-1,3,2-dioxaphosphinane A Schlenk flask was charged sequentially with neopentyl glycol (0.80 g, 7.63 mmol, 1 eq), toluene (15 mL), triphenylphosphite (2 mL, 7.63 mmol, 1 eq) then triethylamine (0.1 mL, 0.76 mmol, 0.1 eq) and warmed to 110 °C and stirred for 24 h. The reaction mixture was cooled to room temperature and volatiles removed under reduced pressure to give a clear viscous liquid. The crude product was distilled under reduced pressure (0.1 mbar, 115 °C) to give 2-phenoxy-1,3,2-dioxaphosphinane as translucent crystals (0.8 g, 46%). ^{1}H NMR (400 MHz, $CDCl_3$): δ 7.36 – 7.28 (2H, m, ArH), 7.12 – 7.05 (3H, m, ArH), 4.33 (br.d, 2H, J = 10.7 Hz, OCH_2), 3.46 (tt, 2H, J = 10.7 Hz, J = 1.4 Hz, OCH_2), 1.32 (s, 3H, CH_3) and 0.80 ppm (s, 3H, CH_3). $^{13}C\{^{1}H\}$ NMR (101 MHz, $CDCl_3$): δ 152.9 (d, J = 7 Hz), 129.8, 123.4, 120.0, 120.0, 69.5, 33.0, 22.9 and 22.7 ppm. $^{31}P\{^{1}H\}$ NMR (162 MHz, $CDCl_3$): δ 115.3 ppm. MS (+ve ESI): m/z (calcd), $[M+H]^+$ 227.0837; found 227.0838.

5.6.2 Carbonylation Procedures

General procedure for ligand modified Ru-catalysed tandem rWGS-hydroformylation-reduction of 1-octene (Table 4.1)

A hot Parr reactor (150 °C) was charged sequentially with $Ru_3(CO)_{12}$ and LiCl then assembled and allowed to cool to room temperature under vacuum before being cycled twice with N_2. A Schlenk flask was charged sequentially with ligand and n-methyl-2-pyrrolidone (NMP), stirred for 5 min then injected into the Parr reactor under a stream of N_2. The Schlenk flask that held the ligand solution was washed twice with NMP and the washes also injected into the Parr reactor under a stream of N_2. 1-Octene was then injected into the Parr reactor under a stream of N_2 and the reactor purged with 4 bar CO_2 for 5 min before being sealed. The Parr reactor was stirred at 1000 rpm with a magnetic stirrer bar and pressurised to 10 bar CO_2 before being topped up to 30 bar with a 1:3 CO_2/H_2 premix then heated to 130 °C and stirred at 1000 rpm for 24 h. The Parr reactor was cooled to room temperature then vented. Anisole (internal standard) was added and the mixture stirred for 5 min before being sampled for GC analysis.

General procedure for Ru-catalysed tandem rWGS-hydroformylation-reduction of olefins (Table 4.2)

A hot Parr reactor (150 °C) was charged sequentially with $Ru_3(CO)_{12}$ and chloride salt then assembled and allowed to cool to room temperature under vacuum before being cycled twice with Ar. Solvent, olefin then anisole (internal standard) was injected into the Parr reactor under a stream of Ar. The Parr reactor was sealed, stirred at 1000 rpm and pressurised to 80 bar 1:1 CO_2/H_2 by first the

introduction of 40 bar pure CO_2 then topped up to 80 bar with pure H_2. The Parr reactor was heated to 140 °C and stirred at 1000 rpm for 24 h. The Parr reactor was then cooled to 0 °C, vented and sampled for GC analysis. Note: Initial pressures at reaction temperature can vary due to the CO_2 expansion properties of each solvent.

5.7 Chapter 5 References

1. Erami, R.; Díaz-García, D.; Prashar, S.; Rodríguez-Diéguez, A.; Fajardo, M.; Amirnasr, M.; Gómez-Ruiz, S., *Catalysts* **2017,** *7*, 76.

2. Frisch, M. J.; Trucks, G. W.; Schlegel, H. B.; Scuseria, G. E.; Robb, M. A.; Cheeseman, J. R.; Scalmani, G.; Barone, V.; Petersson, G. A.; Nakatsuji, H.; Li, X.; Caricato, M.; Marenich, A. V.; Bloino, J.; Janesko, B. G.; Gomperts, R.; Mennucci, B.; Hratchian, H. P.; Ortiz, J. V.; Izmaylov, A. F.; Sonnenberg, J. L.; Williams; Ding, F.; Lipparini, F.; Egidi, F.; Goings, J.; Peng, B.; Petrone, A.; Henderson, T.; Ranasinghe, D.; Zakrzewski, V. G.; Gao, J.; Rega, N.; Zheng, G.; Liang, W.; Hada, M.; Ehara, M.; Toyota, K.; Fukuda, R.; Hasegawa, J.; Ishida, M.; Nakajima, T.; Honda, Y.; Kitao, O.; Nakai, H.; Vreven, T.; Throssell, K.; Montgomery Jr., J. A.; Peralta, J. E.; Ogliaro, F.; Bearpark, M. J.; Heyd, J. J.; Brothers, E. N.; Kudin, K. N.; Staroverov, V. N.; Keith, T. A.; Kobayashi, R.; Normand, J.; Raghavachari, K.; Rendell, A. P.; Burant, J. C.; Iyengar, S. S.; Tomasi, J.; Cossi, M.; Millam, J. M.; Klene, M.; Adamo, C.; Cammi, R.; Ochterski, J. W.; Martin, R. L.; Morokuma, K.; Farkas, O.; Foresman, J. B.; Fox, D. J. *Gaussian 16 Rev. B.01*, Wallingford, CT, 2016.

3. Becke, A. D., *J. Chem. Phys.* **1993,** *98*, 5648-5652.

4. Weigend, F., *PCCP* **2006,** *8*, 1057-1065.

5. Weigend, F.; Ahlrichs, R., *PCCP* **2005,** *7*, 3297-3305.

6. Dunning, T. H.; Hay, P. J., Methods of Electronic Structure Theory. In *Modern Theoretical Chemistry*, Schaefer, H. F., Ed. Plenum: New York, 1977; Vol. 3, pp 1-28.

7. Grimme, S., *Wiley Interdiscip. Rev.: Comput. Mol. Sci.* **2011,** *1*, 211-228.

8. Johnson, E. R.; Becke, A. D., *J. Chem. Phys.* **2006,** *124*, 174104.

9. Johnson, E. R.; Becke, A. D., *J. Chem. Phys.* **2005,** *123*, 024101.

10. Petersson, G. A.; Bennett, A.; Tensfeldt, T. G.; Al-Laham, M. A.; Shirley, W. A.; Mantzaris, J., *J. Chem. Phys.* **1988,** *89*, 2193-2218.

11. Petersson, G. A.; Al-Laham, M. A., *J. Chem. Phys.* **1991,** *94*, 6081-6090.

12. Falivene, L.; Credendino, R.; Poater, A.; Petta, A.; Serra, L.; Oliva, R.; Scarano, V.; Cavallo, L., *Organometallics* **2016,** *35*, 2286-2293.

13. Falivene, L.; Cao, Z.; Petta, A.; Serra, L.; Poater, A.; Oliva, R.; Scarano, V.; Cavallo, L., *Nat. Chem.* **2019,** *11*, 872-879.

14. Eberhard, M. R.; Carrington-Smith, E.; Drent, E. E.; Marsh, P. S.; Orpen, A. G.; Phetmung, H.; Pringle, P. G., *Adv. Synth. Catal.* **2005,** *347*, 1345-1348.

15. Drent, E.; Van Ginkel, R.; Jager, W. W. Shell Internationale Research Maatschappij B.V., Process for the Hydroformylation of an Ethylenically Unsaturated Compound. WO2004028689A2, 2004.

16. Eberhard, M. R. New Strategies In 9-Phosphabicyclononane Chemistry. Ph.D. Thesis, University of Bristol, United Kingdom, 2001.

Chapter 6 – Supplementary Information

6.1 Copyright Permission

Table 6.1 Table of reproduced works and permissions from copyright holders.

Page No.	Type of work:	Name of work	Source of work	Copyright holder and contact	permission requested on	I have permission yes /no	Permission note
23	Image	Photos for everyone	Photographs	© Unsplash	30 Dec 2019	yes	Written permission (Appendix A)
37	Graph	Fig. 1. Schematic representation of chemoselectivity as a function of ligand and acid properties.	Drent, E.; Budzelaar, P. H. M., The oxo-synthesis catalyzed by cationic palladium complexes, selectivity control by neutral ligand and anion. *J. Organomet. Chem.* **2000,** *593–594*, 211-225.	© Elsevier	29 Dec 2019	yes	Written permission (Appendix B)
69 – 97	Journal Article	gem-Dialkyl Effect in Diphosphine Ligands: Synthesis, Coordination Behavior, and Application in Pd-Catalyzed Hydroformylation	Tay, D. W. P.; Nobbs, J. D.; Romain, C.; White, A. J. P.; Aitipamula, S.; van Meurs, M.; Britovsek, G. J. P., *ACS Catal.* **2020,** *10* (1), 663-671.	© American Chemical Society	16 Mar 2020	yes	Written permission (Appendix C)
124	Figure	Scheme 1. Reactions observed during preparation of some palladium diphosphane catalysts in situ; P-P _ dppe (1-4) or dppbz (5,6)	Marson, A.; van Oort, A. B.; Mul, Wilhelmus P., In Situ Preparation of Palladium Diphosphane Catalysts. *Eur. J. Inorg. Chem.* **2002,** *2002* (11), 3028-3031.	© John Wiley and Sons	2 Jan 2020	yes	Written permission (Appendix D)

6.2 Supplementary Information for Chapter 2

6.2.1 NMR Spectra

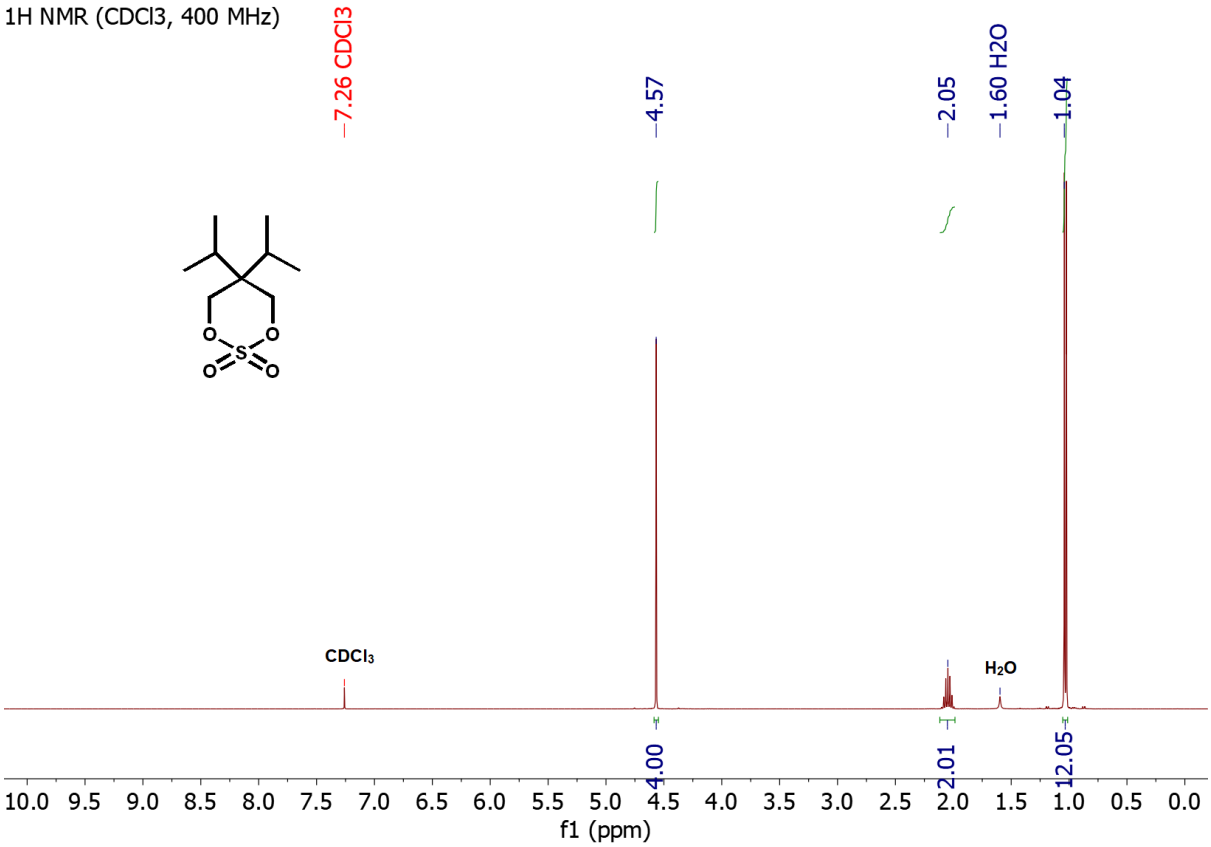

Figure 6.1 ^{1}H NMR (400 MHz, $CDCl_3$, 25 °C) spectrum of 5,5-diisopropyl-1,3,2-dioxathiane 2,2-dioxide.

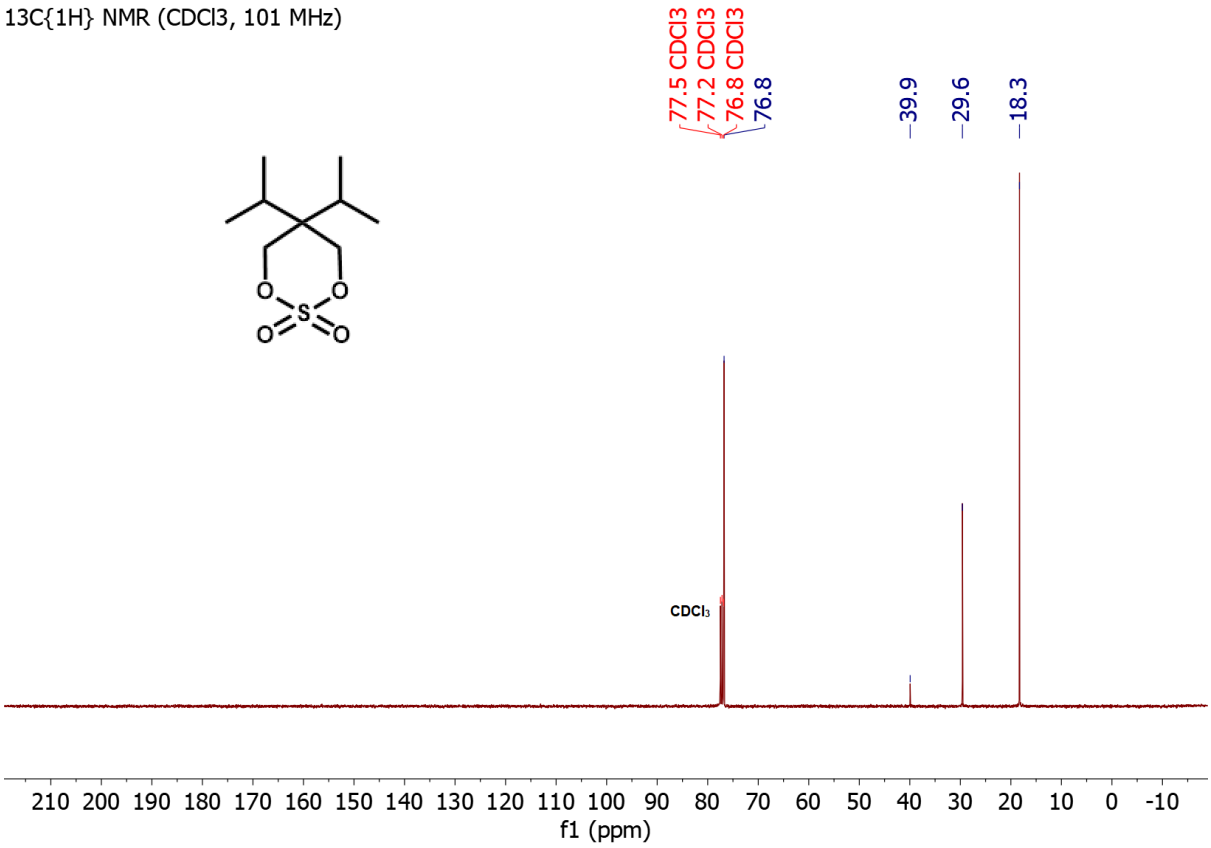

Figure 6.2 $^{13}C\{^{1}H\}$ NMR (101 MHz, $CDCl_3$, 25 °C) spectrum of 5,5-diisopropyl-1,3,2-dioxathiane 2,2-dioxide.

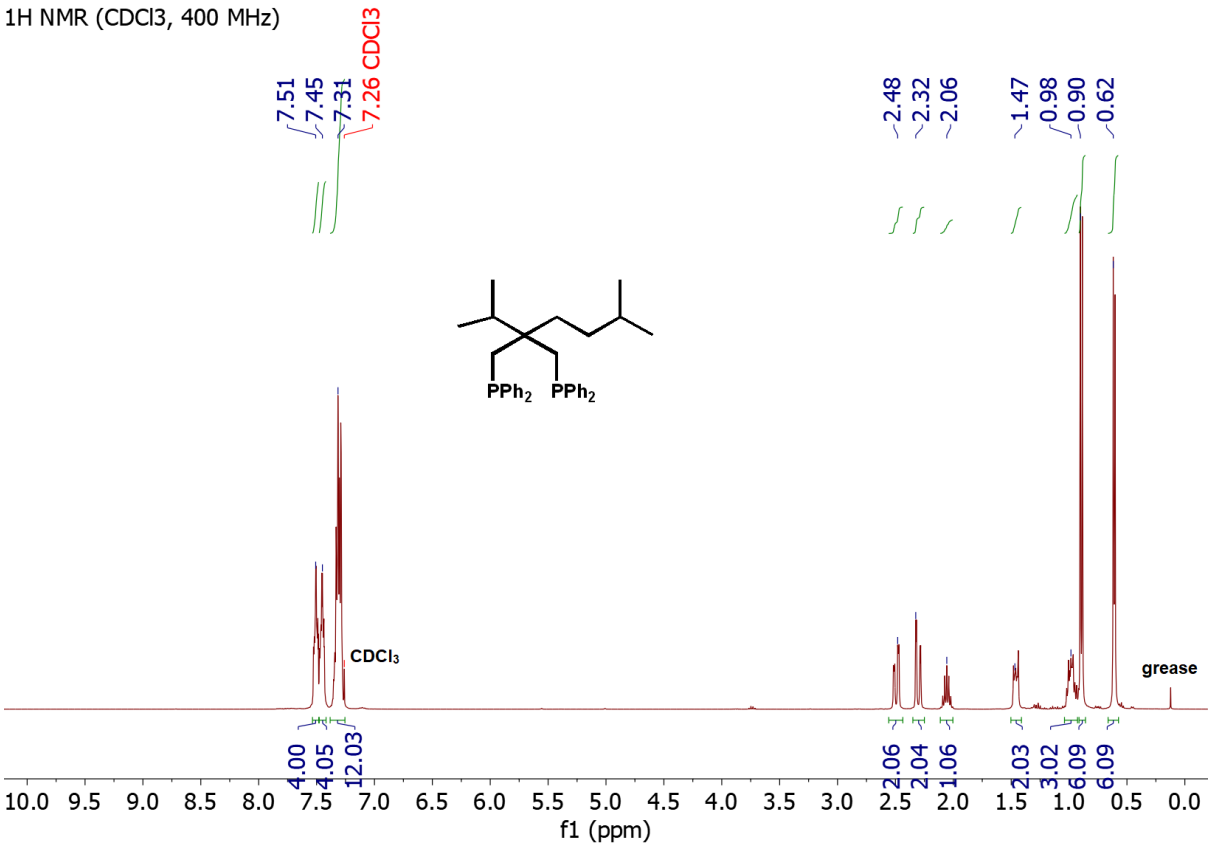

Figure 6.3 ^{1}H NMR (400 MHz, $CDCl_3$, 25 °C) spectrum of (2-isopentyl-2-isopropylpropane-1,3-diyl)bis(diphenylphosphane), **DPPIPIPP**.

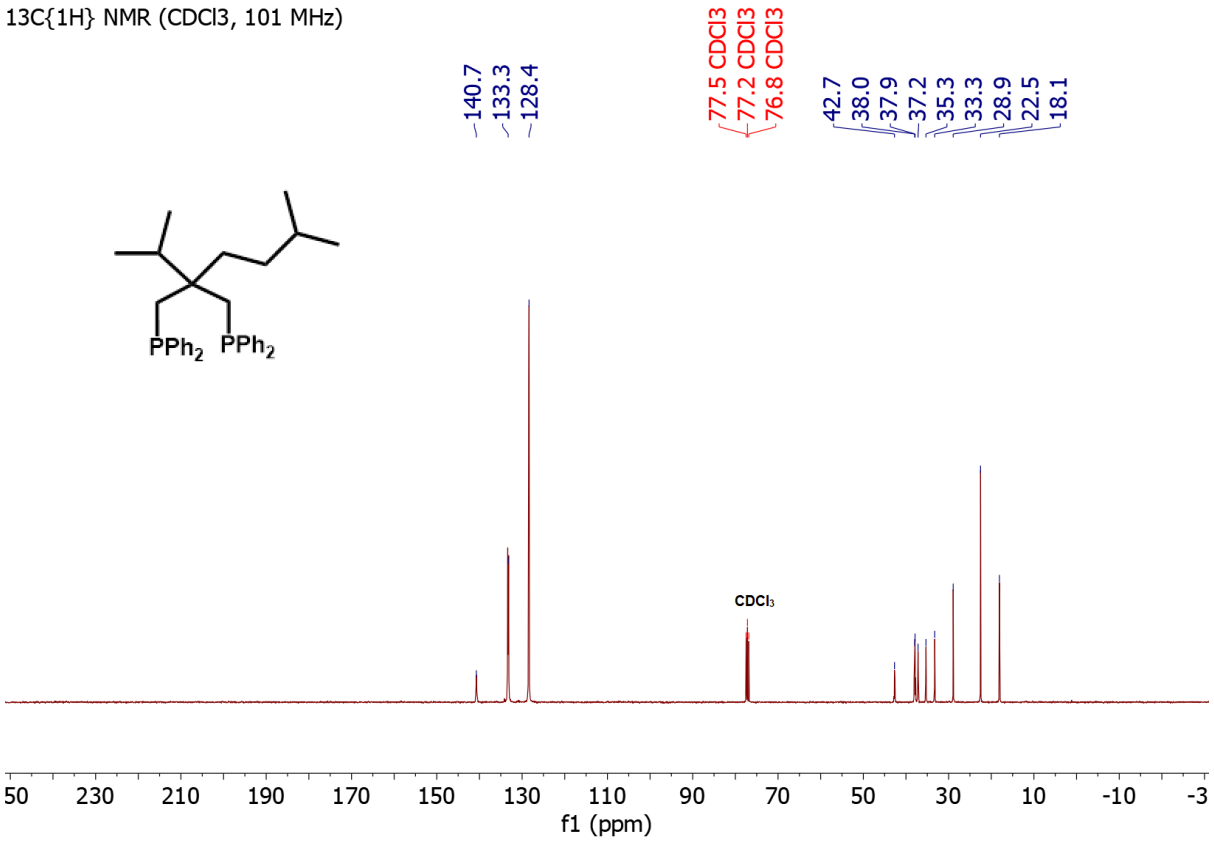

Figure 6.4 $^{13}C\{^{1}H\}$ NMR (101 MHz, $CDCl_3$, 25 °C) spectrum of (2-isopentyl-2-isopropylpropane-1,3-diyl)bis(diphenylphosphane), **DPPIPIPP**.

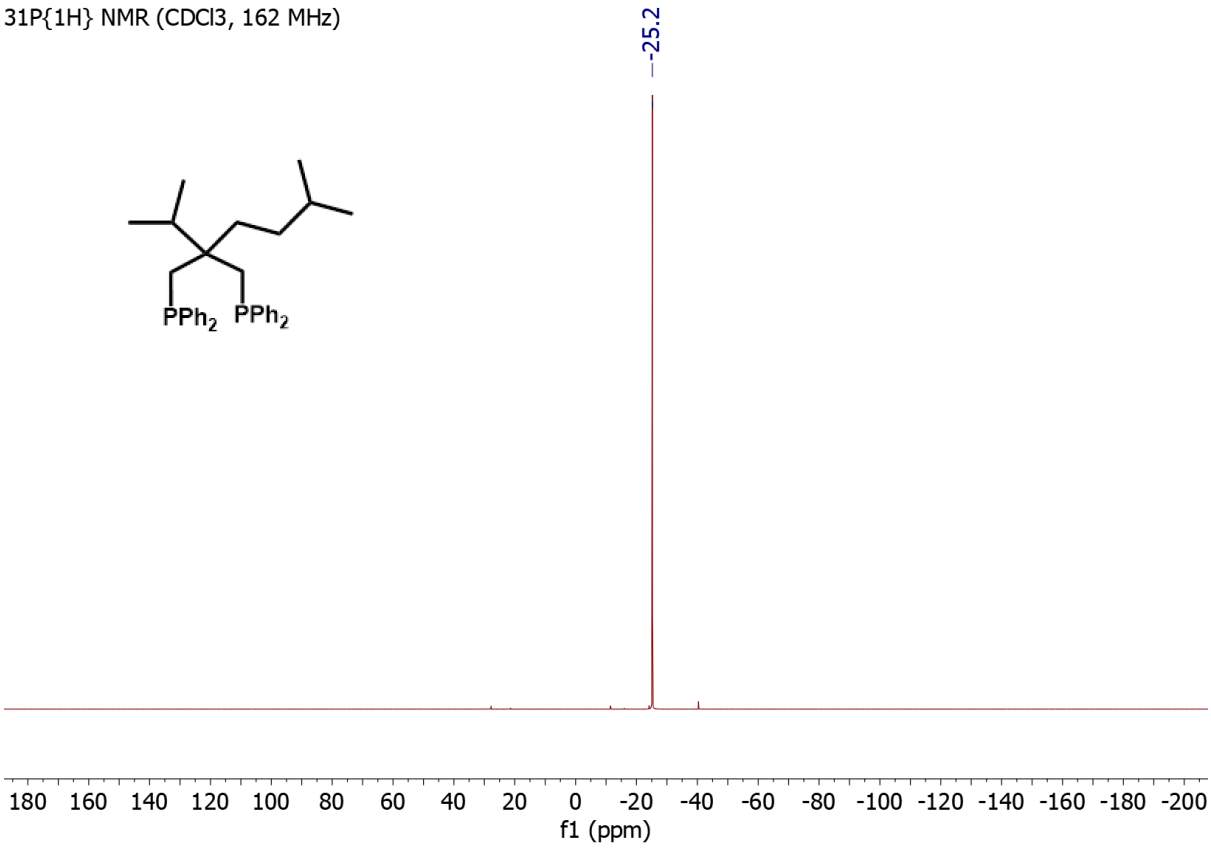

Figure 6.5 $^{31}P\{^{1}H\}$ NMR (162 MHz, $CDCl_3$, 25 °C) spectrum of (2-isopentyl-2-isopropylpropane-1,3-diyl)bis(diphenylphosphane), **DPPIPIPP**.

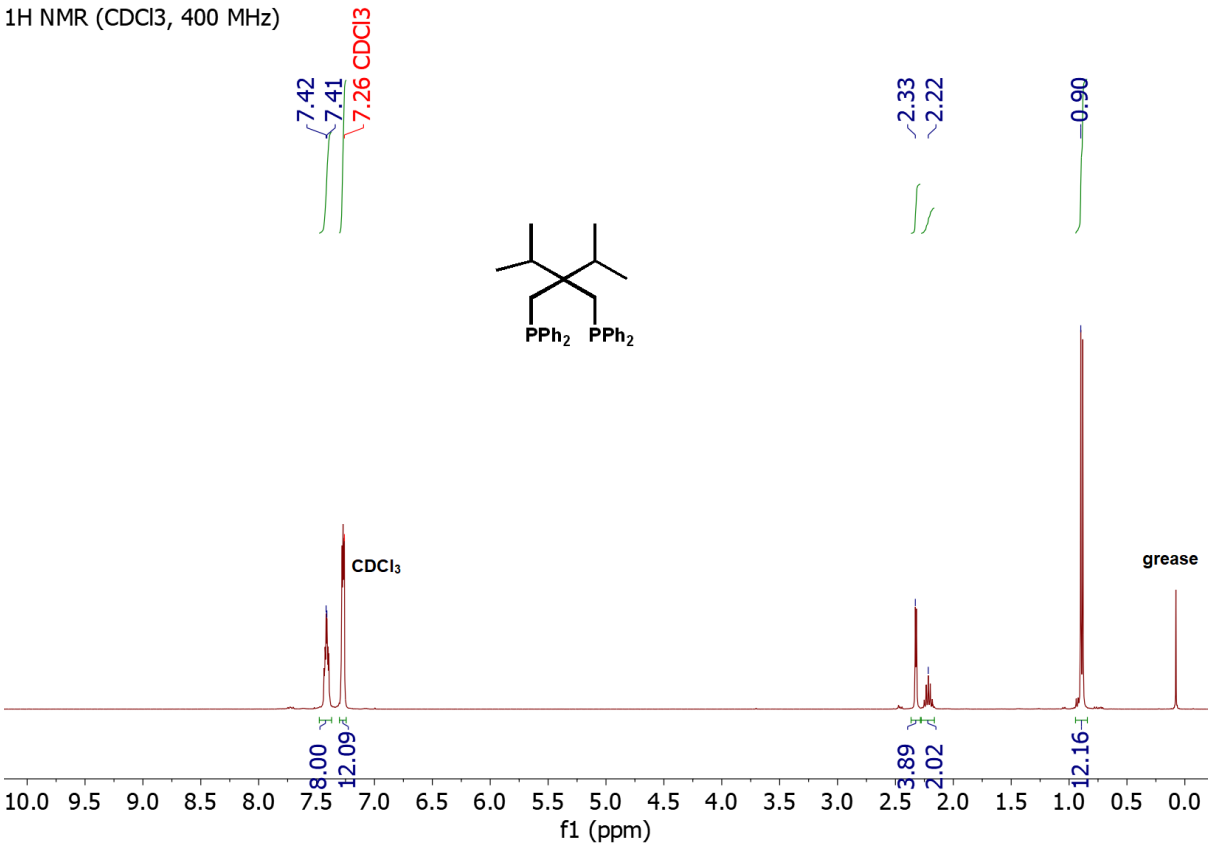

Figure 6.6 ^{1}H NMR (400 MHz, $CDCl_3$, 25 °C) spectrum of (2,2-diisopropylpropane-1,3-diyl)bis(diphenylphosphane), **DPPDIPP**.

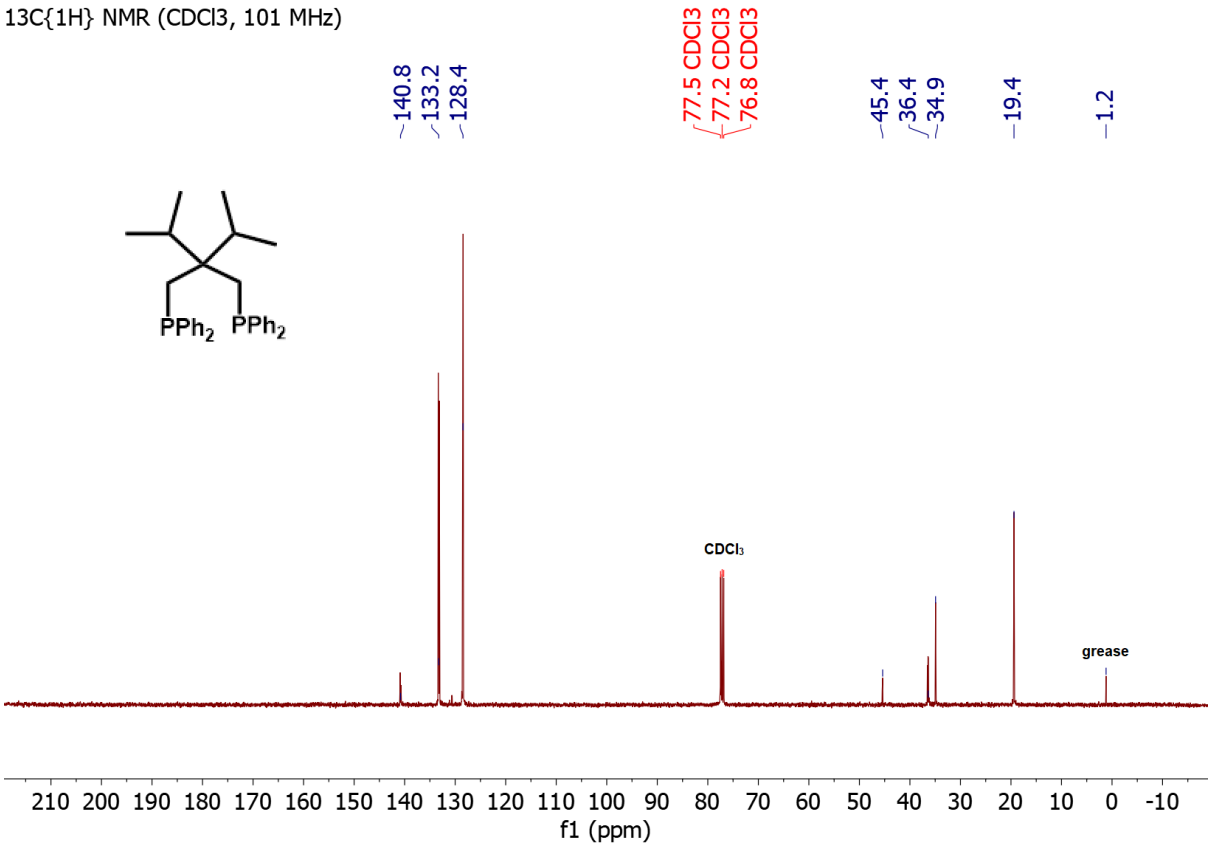

Figure 6.7 $^{13}C\{^{1}H\}$ NMR (101 MHz, $CDCl_3$, 25 °C) spectrum of (2,2-diisopropylpropane-1,3-diyl)bis(diphenylphosphane), **DPPDIPP**.

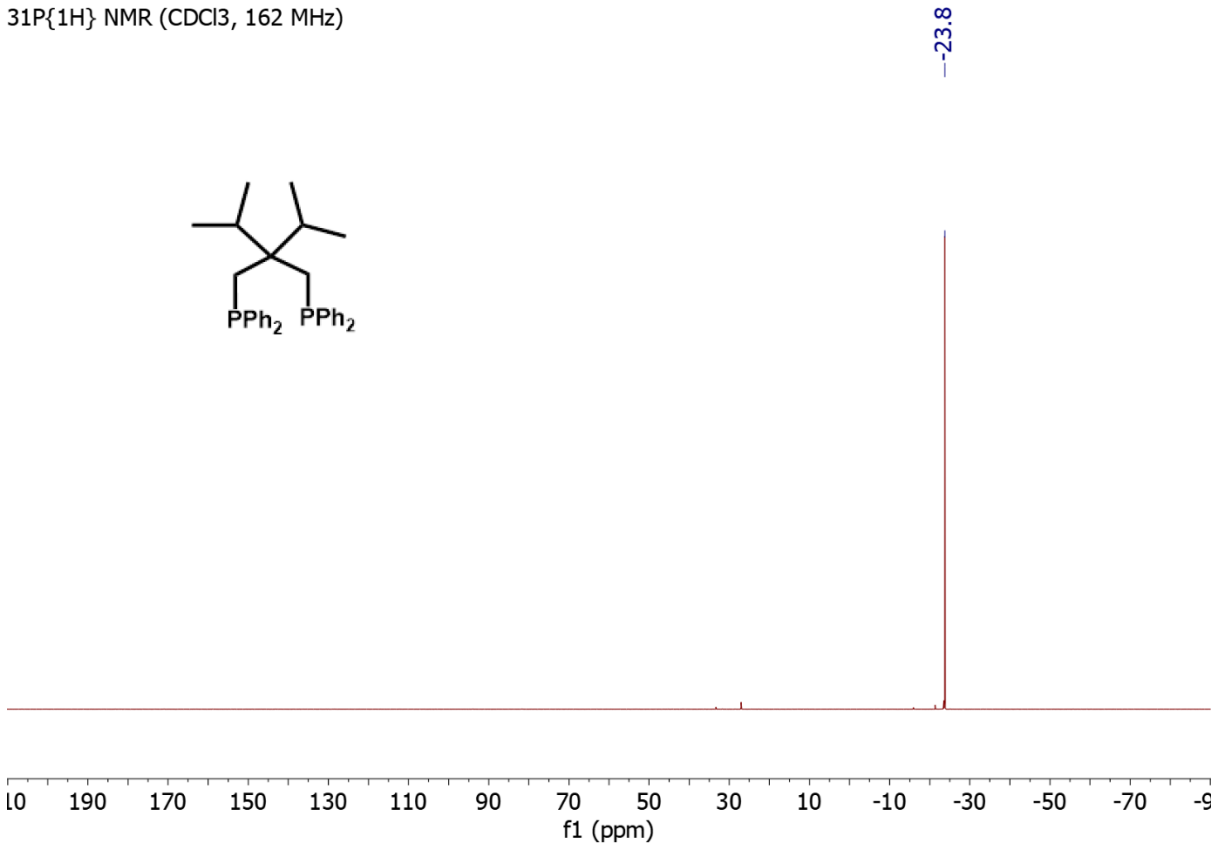

Figure 6.8 $^{31}P\{^{1}H\}$ NMR (162 MHz, $CDCl_3$, 25 °C) spectrum of (2,2-diisopropylpropane-1,3-diyl)bis(diphenylphosphane), **DPPDIPP**.

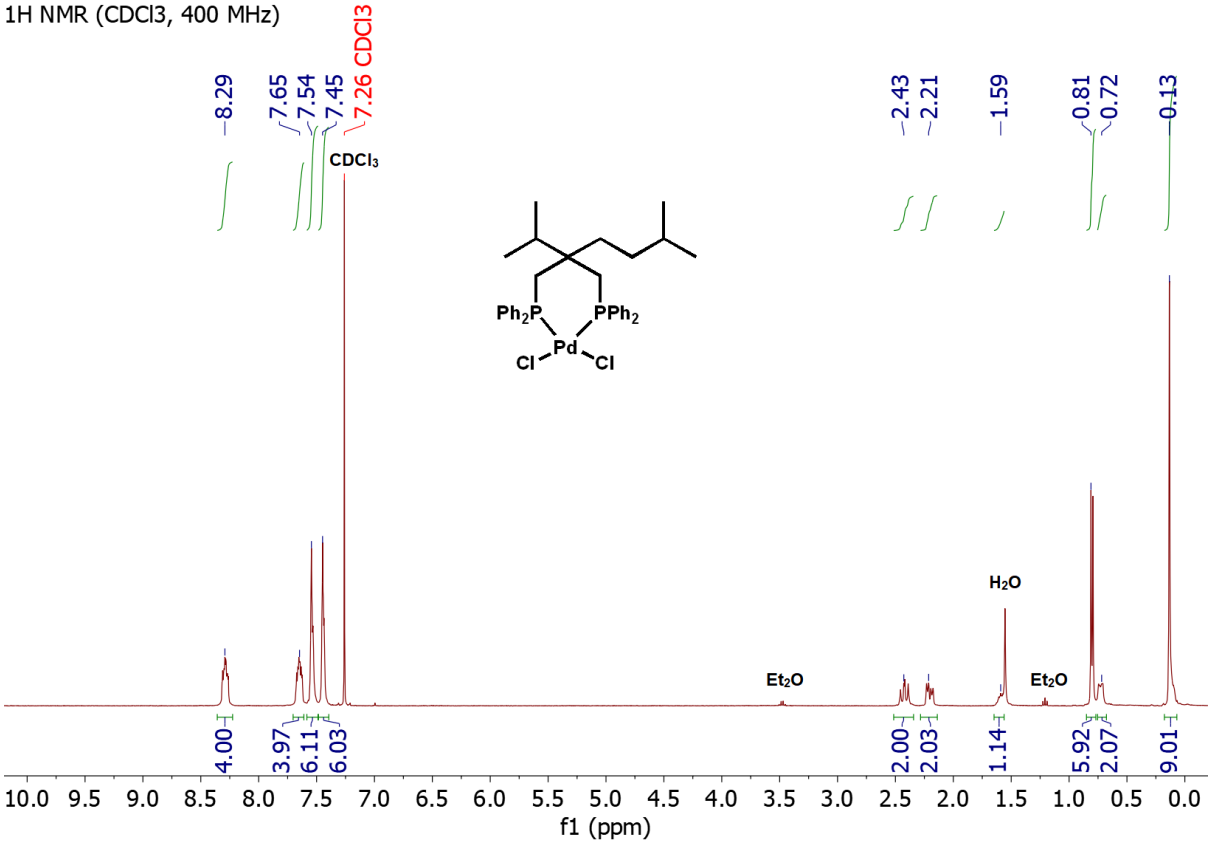

Figure 6.9 ^{1}H NMR (400 MHz, $CDCl_3$, 25 °C) spectrum of (2-isopentyl-2-isopropylpropane-1,3-diyl)bis(diphenylphosphane)dichloropalladium(II) complex, Pd(**DPPIPIPP**)Cl_2.

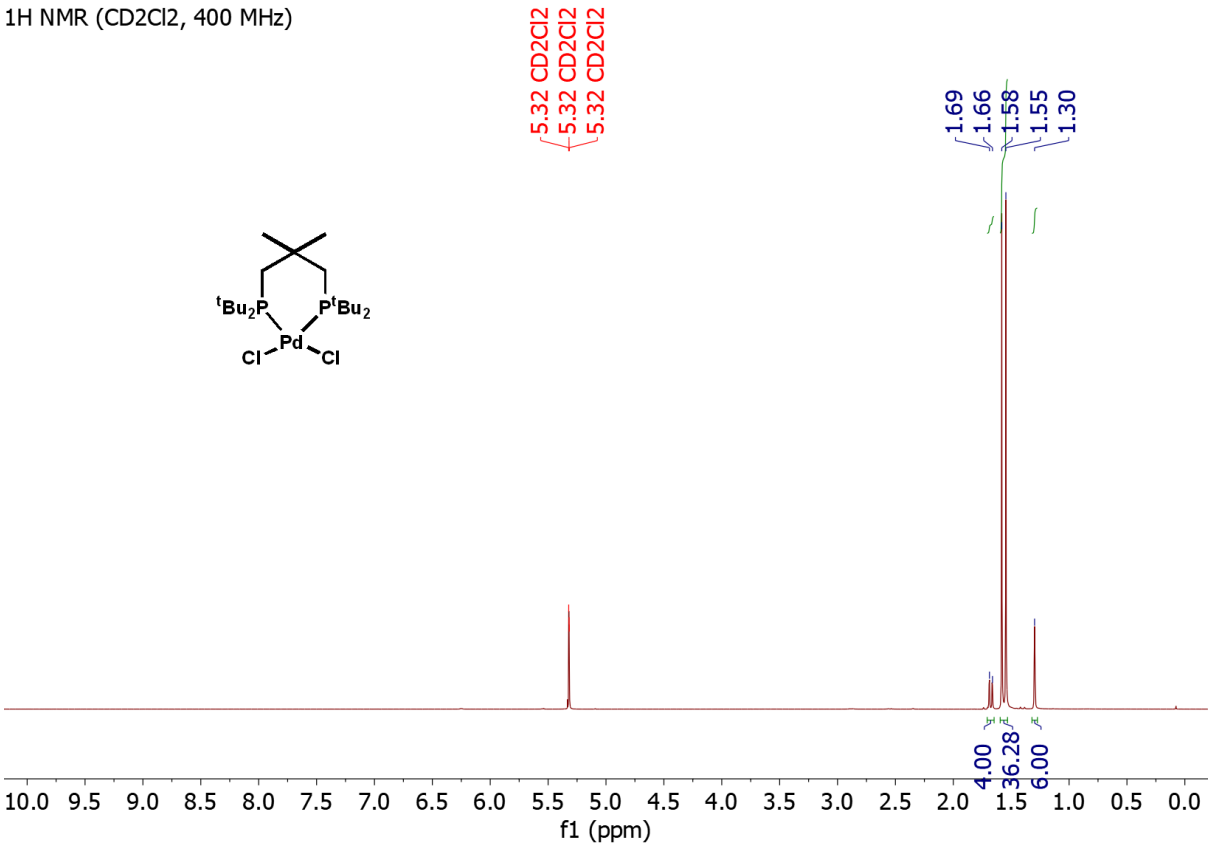

Figure 6.10 ^{1}H NMR (400 MHz, CD_2Cl_2, 25 °C) spectrum of (2,2-Dimethylpropane-1,3-diyl)bis(di-tert-butylphosphane)dichloropalladium(II) complex, Pd(**DTBPDMP**)Cl_2.

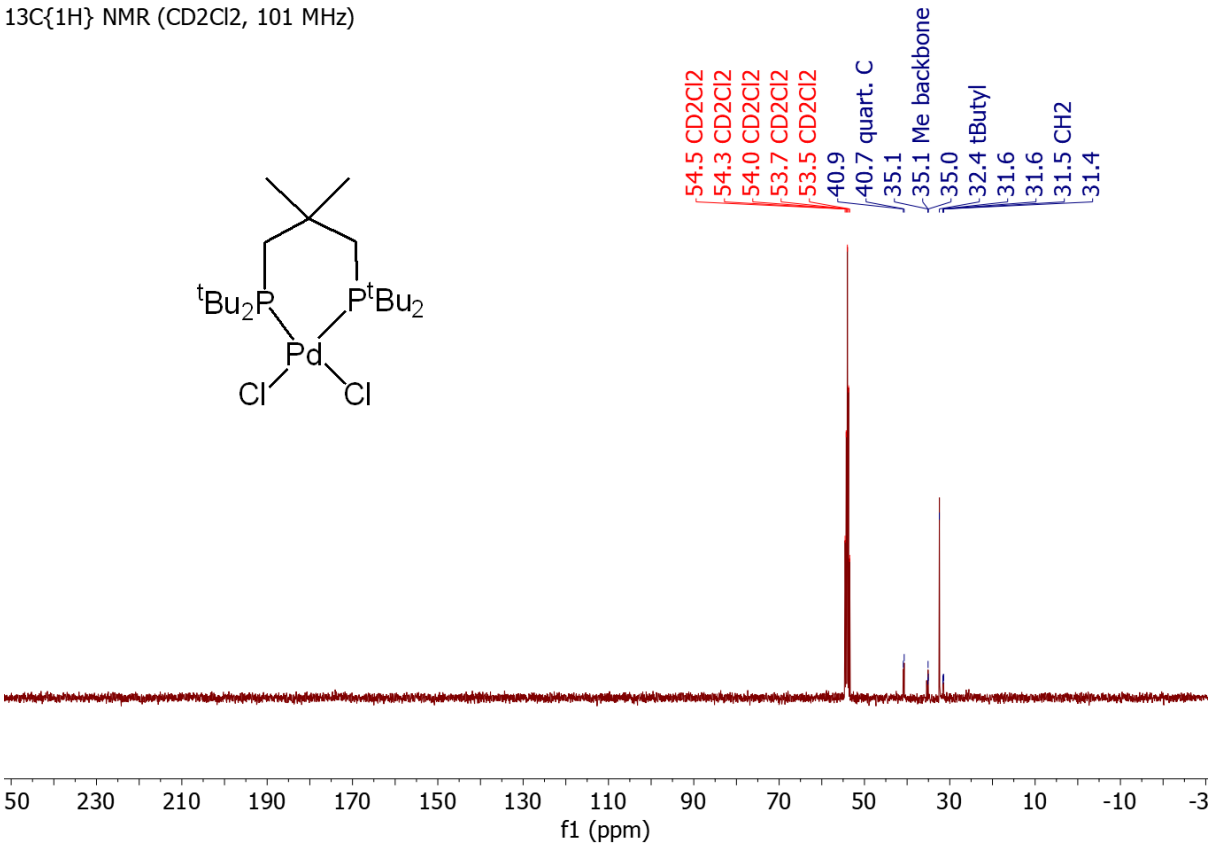

Figure 6.11 $^{13}C\{^{1}H\}$ NMR (101 MHz, CD_2Cl_2, 25 °C) spectrum of (2,2-Dimethylpropane-1,3-diyl)bis(di-tert-butylphosphane)dichloropalladium(II) complex, Pd(**DTBPDMP**)Cl_2.

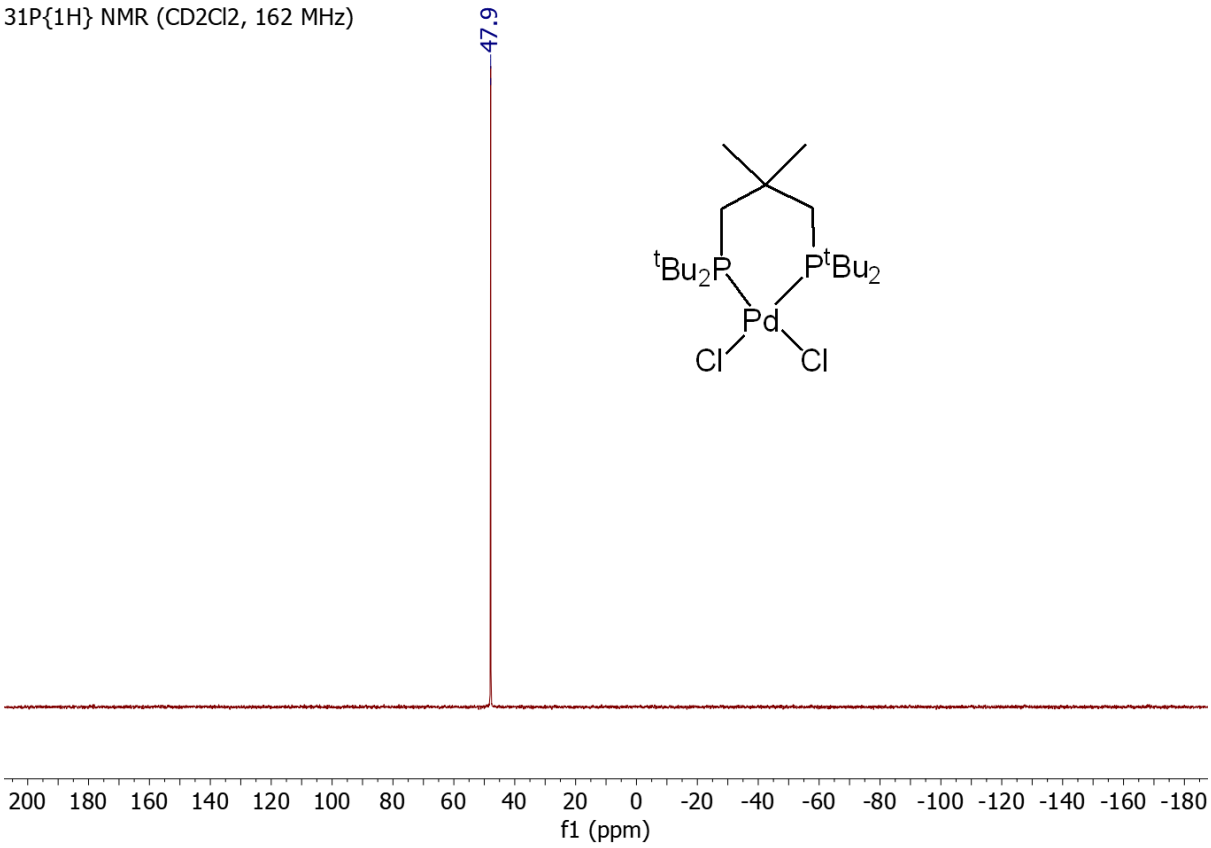

Figure 6.12 $^{31}P\{^{1}H\}$ NMR (162 MHz, CD_2Cl_2, 25 °C) spectrum of (2,2-Dimethylpropane-1,3-diyl)bis(di-tert-butylphosphane)dichloropalladium(II) complex, Pd(**DTBPDMP**)Cl_2.

6.2.2 Mass Spectrometry

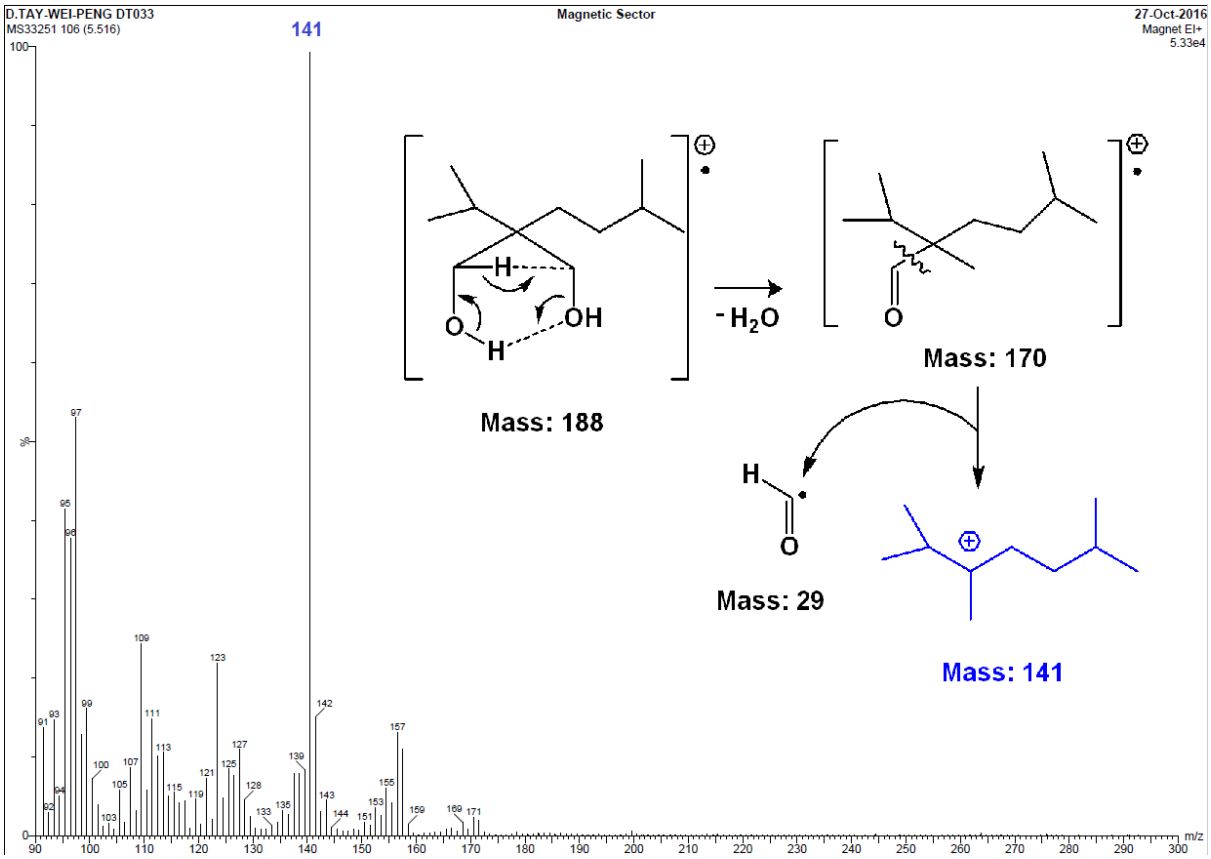

Figure 6.13 MS (+ve EI) spectrum of 2-isopentyl-2-isopropylpropane-1,3-diol and a proposed fragmentation pattern.

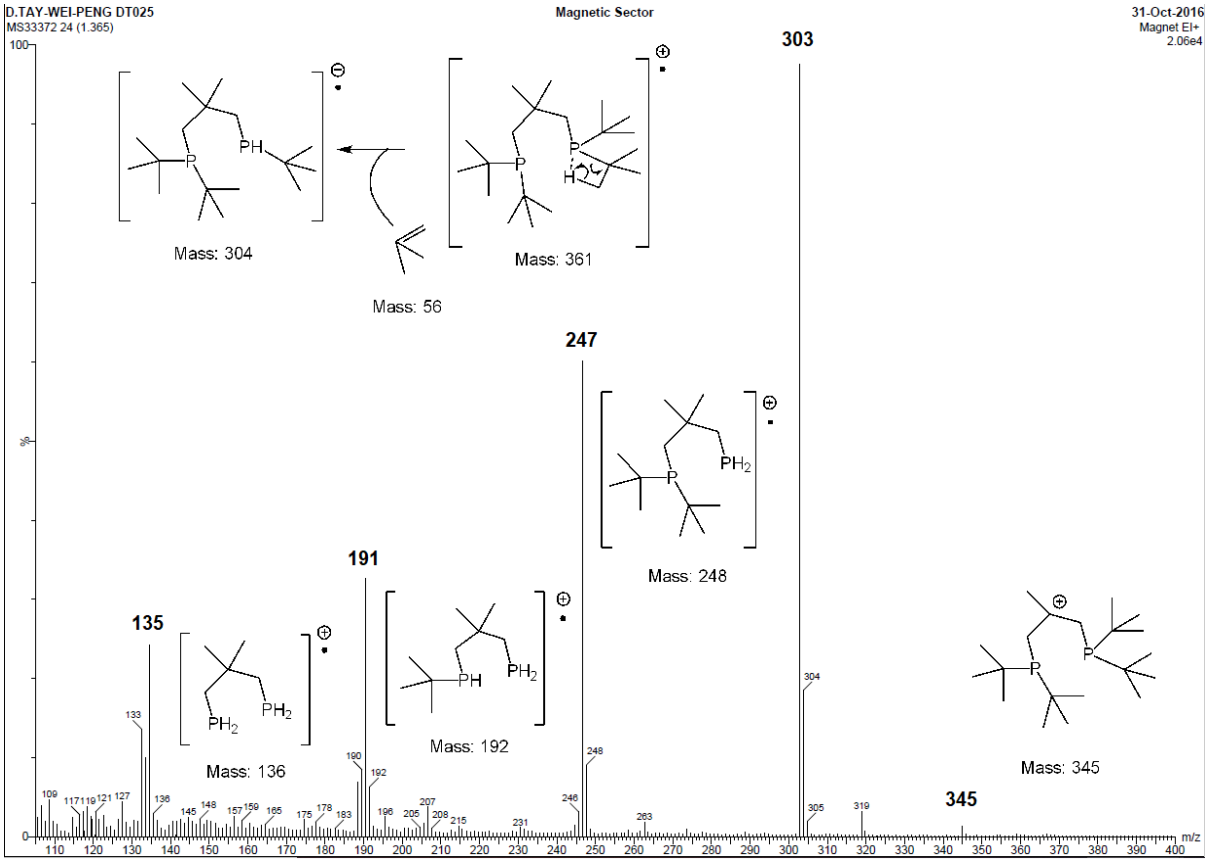

Figure 6.14 MS (+ve EI) spectrum of (2,2-dimethylpropane-1,3-diyl)bis(di-tert-butylphosphane) **(DTBPDMP)** and a proposed fragmentation pattern.

6.2.3 X-Ray Analyses

The X-ray crystal structure of [Pd(DPPDMP)Cl_2]

Crystal data for [Pd(**DPPDMP**)Cl_2]: $C_{29}H_{30}Cl_2P_2Pd$, M = 617.77, monoclinic, $P2_1/c$ (no. 14), a = 11.3082(5), b = 17.6113(11), c = 13.8182(6) Å, β = 92.789(4)°, V = 2748.7(2) Å^3, Z = 4, D_c = 1.493 g cm^{-3}, μ(Mo-Kα) = 1.002 mm^{-1}, T = 173 K, pale yellow needles, Agilent Xcalibur 3 E diffractometer; 5490 independent measured reflections (R_{int} = 0.0305), F^2 refinement,[1-2] R_1(obs) = 0.0377, wR_2(all) = 0.0821, 4410 independent observed absorption-corrected reflections [$|F_o| > 4\sigma(|F_o|)$, completeness to θ_{full}(25.2°) = 98.8%], 310 parameters. CCDC 1936380.

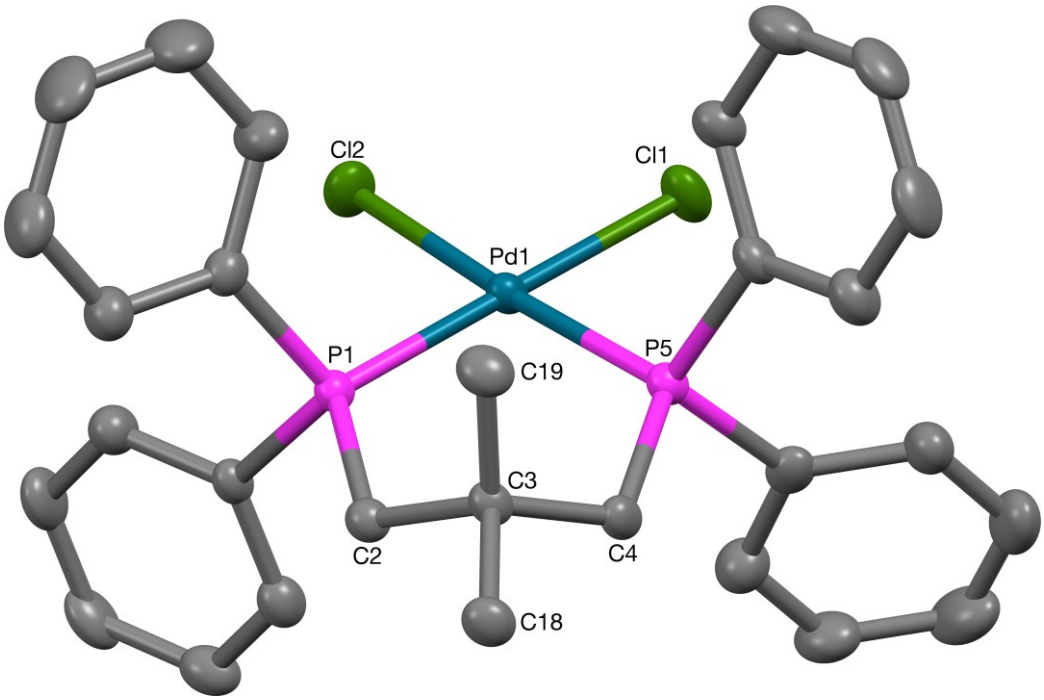

Figure 6.15 The crystal structure of [Pd(**DPPDMP**)Cl_2] (50% probability ellipsoids).

Table 6.2 Bond lengths [Å] and angles [°] for [Pd(**DPPDMP**)Cl_2].

Pd(1)-P(5)	2.2371(9)	C(9)-C(10)	1.377(6)
Pd(1)-P(1)	2.2423(9)	C(10)-C(11)	1.385(5)
Pd(1)-Cl(1)	2.3391(9)	C(12)-C(13)	1.387(4)
Pd(1)-Cl(2)	2.3570(9)	C(12)-C(17)	1.389(5)
P(1)-C(6)	1.808(3)	C(13)-C(14)	1.382(5)
P(1)-C(12)	1.818(3)	C(14)-C(15)	1.376(5)
P(1)-C(2)	1.832(3)	C(15)-C(16)	1.369(5)
C(2)-C(3)	1.538(4)	C(16)-C(17)	1.387(5)
C(3)-C(19)	1.530(4)	C(20)-C(21)	1.391(5)
C(3)-C(18)	1.535(4)	C(20)-C(25)	1.395(5)
C(3)-C(4)	1.536(4)	C(21)-C(22)	1.373(5)
C(4)-P(5)	1.820(3)	C(22)-C(23)	1.378(6)
P(5)-C(20)	1.815(4)	C(23)-C(24)	1.379(6)
P(5)-C(26)	1.823(3)	C(24)-C(25)	1.384(5)
C(6)-C(7)	1.394(5)	C(26)-C(31)	1.384(5)
C(6)-C(11)	1.395(5)	C(26)-C(27)	1.394(5)
C(7)-C(8)	1.390(5)	C(27)-C(28)	1.385(5)
C(8)-C(9)	1.367(6)	C(28)-C(29)	1.374(5)

C(29)-C(30)	1.371(5)
C(30)-C(31)	1.395(5)

P(5)-Pd(1)-P(1)	95.84(3)
P(5)-Pd(1)-Cl(1)	84.49(3)
P(1)-Pd(1)-Cl(1)	179.02(3)
P(5)-Pd(1)-Cl(2)	176.05(3)
P(1)-Pd(1)-Cl(2)	88.09(3)
Cl(1)-Pd(1)-Cl(2)	91.59(3)
C(6)-P(1)-C(12)	107.45(15)
C(6)-P(1)-C(2)	104.72(15)
C(12)-P(1)-C(2)	102.34(14)
C(6)-P(1)-Pd(1)	112.92(11)
C(12)-P(1)-Pd(1)	108.96(11)
C(2)-P(1)-Pd(1)	119.43(11)
C(3)-C(2)-P(1)	118.7(2)
C(19)-C(3)-C(18)	109.5(3)
C(19)-C(3)-C(4)	112.3(3)
C(18)-C(3)-C(4)	106.2(3)
C(19)-C(3)-C(2)	111.7(3)
C(18)-C(3)-C(2)	106.7(3)
C(4)-C(3)-C(2)	110.1(3)
C(3)-C(4)-P(5)	118.9(2)
C(20)-P(5)-C(4)	100.71(15)
C(20)-P(5)-C(26)	108.43(16)
C(4)-P(5)-C(26)	105.40(15)
C(20)-P(5)-Pd(1)	110.33(12)
C(4)-P(5)-Pd(1)	118.27(11)
C(26)-P(5)-Pd(1)	112.74(11)
C(7)-C(6)-C(11)	118.9(3)
C(7)-C(6)-P(1)	120.2(3)
C(11)-C(6)-P(1)	120.8(2)
C(8)-C(7)-C(6)	119.6(3)
C(9)-C(8)-C(7)	120.7(4)
C(8)-C(9)-C(10)	120.5(4)
C(9)-C(10)-C(11)	119.5(4)
C(10)-C(11)-C(6)	120.7(3)
C(13)-C(12)-C(17)	119.0(3)
C(13)-C(12)-P(1)	122.0(3)
C(17)-C(12)-P(1)	118.8(2)
C(14)-C(13)-C(12)	119.8(3)
C(15)-C(14)-C(13)	120.8(4)
C(16)-C(15)-C(14)	120.0(3)
C(15)-C(16)-C(17)	119.8(4)
C(16)-C(17)-C(12)	120.6(3)
C(21)-C(20)-C(25)	118.5(3)
C(21)-C(20)-P(5)	117.2(3)
C(25)-C(20)-P(5)	124.3(3)
C(22)-C(21)-C(20)	121.4(4)
C(21)-C(22)-C(23)	119.5(4)
C(22)-C(23)-C(24)	120.4(4)
C(23)-C(24)-C(25)	120.2(4)
C(24)-C(25)-C(20)	120.1(4)
C(31)-C(26)-C(27)	118.6(3)
C(31)-C(26)-P(5)	120.0(3)
C(27)-C(26)-P(5)	121.3(3)
C(28)-C(27)-C(26)	120.6(4)
C(29)-C(28)-C(27)	120.1(4)
C(30)-C(29)-C(28)	120.2(3)
C(29)-C(30)-C(31)	120.1(3)
C(26)-C(31)-C(30)	120.4(3)

The X-ray crystal structure of [Pd(DPPIPIPP)Cl_2]

Crystal data for [Pd(**DPPIPIPP**)Cl_2]: $C_{35}H_{42}Cl_2P_2Pd{\cdot}CH_2Cl_2$, M = 786.85, orthorhombic, *Pbca* (no. 61), a = 21.8565(6), b = 14.7082(4), c = 22.7524(6) Å, V = 7314.2(3) Å^3, Z = 8, D_c = 1.429 g cm^{-3}, μ(Mo-Kα) = 0.911 mm^{-1}, T = 173 K, colourless platy needles, Agilent Xcalibur 3 E diffractometer; 7280 independent measured reflections (R_{int} = 0.0269), F^2 refinement, [1-2] R_1(obs) = 0.0469, wR_2(all) = 0.1192, 5500 independent observed absorption-corrected reflections [$|F_o| > 4\sigma(|F_o|)$, completeness to θ_{full}(25.2°) = 99.0%], 418 parameters. CCDC 1936381.

The included dichloromethane solvent molecule in the structure of [Pd(**DPPIPIPP**)Cl_2] was found to be disordered. Four orientations were identified of *ca*. 36, 29, 19 and 16% occupancy, their geometries were optimised, the thermal parameters of adjacent atoms were restrained to be similar, and all of the atoms were refined isotropically.

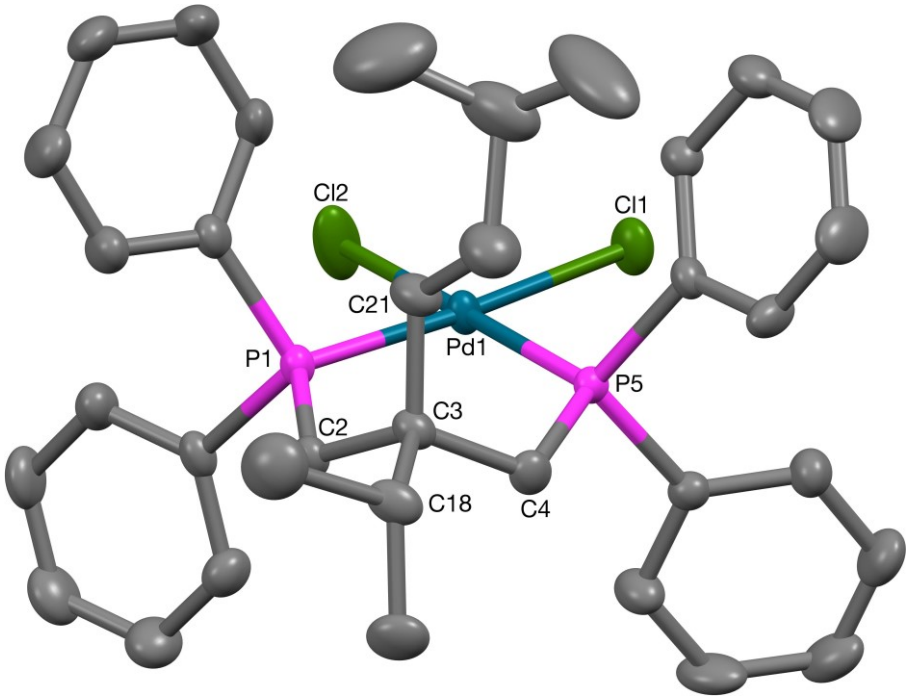

Figure 6.16 The crystal structure of [Pd(**DPPIPIPP**)Cl_2] (50% probability ellipsoids).

Table 6.3 Bond lengths [Å] and angles [°] for [Pd(**DPPIPIPP**)Cl_2].

Pd(1)-P(5)	2.2449(11)	P(1)-C(2)	1.832(4)
Pd(1)-P(1)	2.2452(11)	C(2)-C(3)	1.545(5)
Pd(1)-Cl(2)	2.3381(12)	C(3)-C(4)	1.538(6)
Pd(1)-Cl(1)	2.3480(10)	C(3)-C(21)	1.549(6)
P(1)-C(6)	1.817(4)	C(3)-C(18)	1.576(6)
P(1)-C(12)	1.822(4)	C(4)-P(5)	1.834(4)

P(5)-C(32)	1.820(4)	C(40)-Cl(41)	1.785(13)
P(5)-C(26)	1.820(4)	C(40)-Cl(42)	1.836(14)
C(6)-C(7)	1.385(6)	C(45)-Cl(46)	1.794(15)
C(6)-C(11)	1.393(6)	C(45)-Cl(47)	1.826(15)
C(7)-C(8)	1.378(7)	C(50)-Cl(52)	1.798(17)
C(8)-C(9)	1.370(7)	C(50)-Cl(51)	1.817(16)
C(9)-C(10)	1.376(7)	C(55)-Cl(56)	1.815(17)
C(10)-C(11)	1.386(7)	C(55)-Cl(57)	1.828(17)
C(12)-C(17)	1.386(6)		
C(12)-C(13)	1.394(6)	P(5)-Pd(1)-P(1)	96.29(4)
C(13)-C(14)	1.386(6)	P(5)-Pd(1)-Cl(2)	176.95(5)
C(14)-C(15)	1.375(7)	P(1)-Pd(1)-Cl(2)	85.59(4)
C(15)-C(16)	1.371(7)	P(5)-Pd(1)-Cl(1)	86.37(4)
C(16)-C(17)	1.377(7)	P(1)-Pd(1)-Cl(1)	176.56(4)
C(18)-C(20)	1.528(6)	Cl(2)-Pd(1)-Cl(1)	91.85(4)
C(18)-C(19)	1.572(7)	C(6)-P(1)-C(12)	106.45(19)
C(21)-C(22)	1.477(7)	C(6)-P(1)-C(2)	104.75(19)
C(22)-C(23)	1.566(8)	C(12)-P(1)-C(2)	101.76(19)
C(23)-C(25)	1.461(10)	C(6)-P(1)-Pd(1)	111.45(14)
C(23)-C(24)	1.502(9)	C(12)-P(1)-Pd(1)	112.85(13)
C(26)-C(27)	1.387(6)	C(2)-P(1)-Pd(1)	118.46(13)
C(26)-C(31)	1.387(6)	C(3)-C(2)-P(1)	117.7(3)
C(27)-C(28)	1.388(6)	C(4)-C(3)-C(2)	108.2(3)
C(28)-C(29)	1.373(7)	C(4)-C(3)-C(21)	112.7(3)
C(29)-C(30)	1.357(7)	C(2)-C(3)-C(21)	109.9(3)
C(30)-C(31)	1.400(6)	C(4)-C(3)-C(18)	107.9(3)
C(32)-C(37)	1.387(6)	C(2)-C(3)-C(18)	108.6(3)
C(32)-C(33)	1.395(6)	C(21)-C(3)-C(18)	109.5(3)
C(33)-C(34)	1.379(6)	C(3)-C(4)-P(5)	117.8(3)
C(34)-C(35)	1.382(7)	C(32)-P(5)-C(26)	105.61(19)
C(35)-C(36)	1.371(7)	C(32)-P(5)-C(4)	104.51(19)
C(36)-C(37)	1.389(6)	C(26)-P(5)-C(4)	102.54(19)

C(32)-P(5)-Pd(1)	116.18(14)	C(30)-C(29)-C(28)	119.6(4)
C(26)-P(5)-Pd(1)	108.54(14)	C(29)-C(30)-C(31)	120.7(5)
C(4)-P(5)-Pd(1)	118.01(14)	C(26)-C(31)-C(30)	120.0(4)
C(7)-C(6)-C(11)	118.6(4)	C(37)-C(32)-C(33)	119.1(4)
C(7)-C(6)-P(1)	120.8(3)	C(37)-C(32)-P(5)	121.4(3)
C(11)-C(6)-P(1)	120.6(3)	C(33)-C(32)-P(5)	119.5(3)
C(8)-C(7)-C(6)	120.4(4)	C(34)-C(33)-C(32)	119.9(4)
C(9)-C(8)-C(7)	120.9(4)	C(33)-C(34)-C(35)	120.5(5)
C(8)-C(9)-C(10)	119.5(5)	C(36)-C(35)-C(34)	119.9(5)
C(9)-C(10)-C(11)	120.3(5)	C(35)-C(36)-C(37)	120.2(4)
C(10)-C(11)-C(6)	120.3(4)	C(32)-C(37)-C(36)	120.3(4)
C(17)-C(12)-C(13)	119.1(4)	Cl(41)-C(40)-Cl(42)	105.0(8)
C(17)-C(12)-P(1)	119.1(3)	Cl(46)-C(45)-Cl(47)	103.8(11)
C(13)-C(12)-P(1)	121.8(3)	Cl(52)-C(50)-Cl(51)	105.0(12)
C(14)-C(13)-C(12)	119.6(4)	Cl(56)-C(55)-Cl(57)	101.3(13)
C(15)-C(14)-C(13)	120.5(5)		
C(16)-C(15)-C(14)	120.1(5)		
C(15)-C(16)-C(17)	120.1(5)		
C(16)-C(17)-C(12)	120.6(4)		
C(20)-C(18)-C(19)	109.2(4)		
C(20)-C(18)-C(3)	114.6(3)		
C(19)-C(18)-C(3)	110.9(4)		
C(22)-C(21)-C(3)	120.1(4)		
C(21)-C(22)-C(23)	114.7(5)		
C(25)-C(23)-C(24)	113.6(6)		
C(25)-C(23)-C(22)	110.4(6)		
C(24)-C(23)-C(22)	110.1(6)		
C(27)-C(26)-C(31)	118.8(4)		
C(27)-C(26)-P(5)	118.6(3)		
C(31)-C(26)-P(5)	122.6(3)		
C(26)-C(27)-C(28)	120.0(4)		
C(29)-C(28)-C(27)	120.9(5)		

The X-ray crystal structure of [Pd(DPPDIPP)Cl_2]

Crystal data for [Pd(**DPPDIPP**)Cl_2]: $C_{33}H_{38}Cl_2P_2Pd$, M = 673.87, monoclinic, $P2_1/n$ (no. 14), a = 11.2984(5), b = 20.6157(8), c = 14.1400(6) Å, β = 110.081(5)°, V = 3093.3(2) Å^3, Z = 4, D_c = 1.447 g cm^{-3}, μ(Mo-Kα) = 0.897 mm^{-1}, T = 293 K, colourless needle, Rigaku Oxford Diffraction SuperNova diffractometer; 7841 independent measured reflections (R_{int} = 0.0235), F^2 refinement,[1-2] R_1(obs) = 0.0352, wR_2(all) = 0.0829, 5960 independent observed absorption-corrected reflections [$|F_o| > 4\sigma(|F_o|)$, completeness to θ_{full}(25.2°) = 99.6%], 347 parameters. CCDC 1936382.

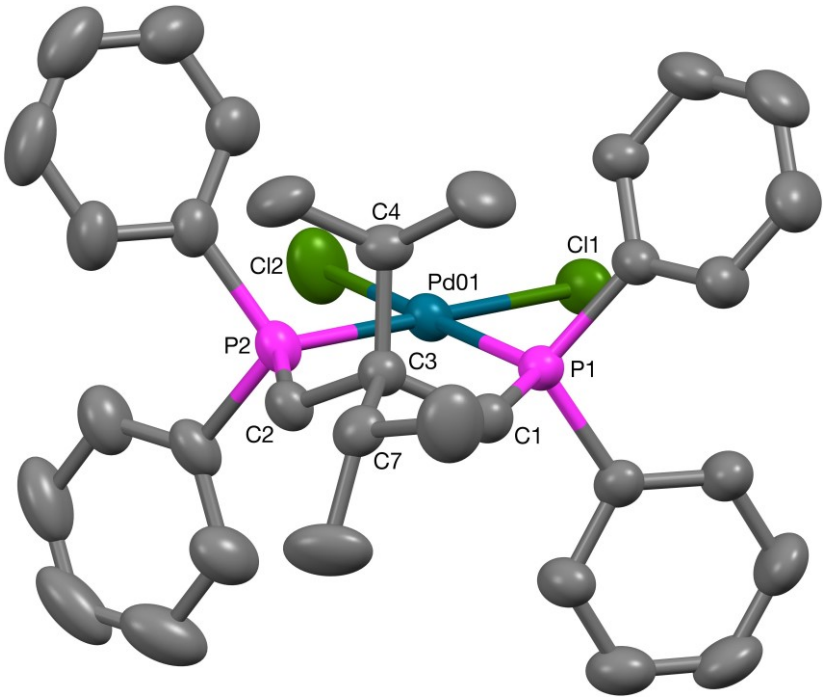

Figure 6.17 The crystal structure of [Pd(**DPPDIPP**)Cl_2] (50% probability ellipsoids).

Table 6.4 Bond lengths [Å] and angles [°] for [Pd(**DPPDIPP**)Cl_2].

Pd01	P1	2.2433(6)	C15	C14	1.383(4)
Pd01	Cl1	2.3586(7)	C28	C33	1.390(4)
Pd01	P2	2.2386(7)	C28	C29	1.386(4)
Pd01	Cl2	2.3435(7)	C16	C17	1.373(4)
P1	C1	1.841(2)	C16	C21	1.387(4)
P1	C22	1.817(2)	C4	C6	1.534(4)
P1	C10	1.820(3)	C4	C5	1.535(4)
P2	C2	1.837(2)	C14	C13	1.370(4)
P2	C28	1.816(3)	C11	C12	1.380(4)
P2	C16	1.827(2)	C17	C18	1.392(4)

C1	C3	1.547(3)	C23	C24	1.381(4)
C2	C3	1.554(3)	C33	C32	1.388(4)
C3	C7	1.578(3)	C13	C12	1.381(4)
C3	C4	1.557(3)	C29	C30	1.387(4)
C22	C27	1.386(3)	C24	C25	1.372(4)
C22	C23	1.388(3)	C26	C25	1.380(4)
C27	C26	1.386(4)	C21	C20	1.390(4)
C10	C15	1.395(3)	C32	C31	1.371(5)
C10	C11	1.380(4)	C31	C30	1.374(5)
C7	C8	1.524(4)	C18	C19	1.366(5)
C7	C9	1.526(3)	C19	C20	1.360(5)

P1	Pd01	Cl1	86.66(2)	C11	C10	C15	118.5(2)
P1	Pd01	Cl2	177.46(3)	C8	C7	C3	115.5(2)
P2	Pd01	P1	94.69(2)	C8	C7	C9	107.5(2)
P2	Pd01	Cl1	178.52(2)	C9	C7	C3	114.5(2)
P2	Pd01	Cl2	87.69(3)	C14	C15	C10	120.7(3)
Cl2	Pd01	Cl1	90.95(3)	C33	C28	P2	120.6(2)
C1	P1	Pd01	120.85(8)	C29	C28	P2	120.6(2)
C22	P1	Pd01	112.46(8)	C29	C28	C33	118.7(3)
C22	P1	C1	104.88(11)	C17	C16	P2	119.7(2)
C22	P1	C10	107.65(11)	C17	C16	C21	118.5(3)
C10	P1	Pd01	108.40(8)	C21	C16	P2	121.8(2)
C10	P1	C1	101.51(11)	C6	C4	C3	113.1(2)
C2	P2	Pd01	119.22(8)	C5	C4	C3	116.9(2)
C28	P2	Pd01	113.70(9)	C5	C4	C6	108.1(2)
C28	P2	C2	105.56(12)	C13	C14	C15	119.7(3)
C28	P2	C16	106.38(12)	C10	C11	C12	120.9(3)
C16	P2	Pd01	109.64(9)	C16	C17	C18	121.5(3)
C16	P2	C2	100.96(11)	C24	C23	C22	121.3(3)
C3	C1	P1	120.62(16)	C32	C33	C28	120.4(3)
C3	C2	P2	121.36(16)	C14	C13	C12	120.4(3)
C1	C3	C2	107.27(19)	C28	C29	C30	120.5(3)

C1	C3	C7	108.29(19)	C25	C24	C23	119.3(3)
C1	C3	C4	112.4(2)	C25	C26	C27	119.9(3)
C2	C3	C7	107.03(19)	C16	C21	C20	119.8(3)
C2	C3	C4	109.83(19)	C11	C12	C13	119.8(3)
C4	C3	C7	111.74(19)	C31	C32	C33	120.1(3)
C27	C22	P1	120.02(19)	C32	C31	C30	120.2(3)
C27	C22	C23	118.6(2)	C19	C18	C17	119.1(3)
C23	C22	P1	121.34(19)	C20	C19	C18	120.5(3)
C22	C27	C26	120.3(3)	C24	C25	C26	120.6(3)
C15	C10	P1	118.7(2)	C31	C30	C29	120.0(3)
C11	C10	P1	122.71(19)	C19	C20	C21	120.7(3)

The X-ray crystal structure of [Pd(DPPP)$_2$](CF$_3$CO$_2$)$_2$

Crystal data for [Pd(**DPPP**)$_2$](CF$_3$CO$_2$)$_2$: [C$_{54}$H$_{52}$P$_4$Pd](C$_2$F$_3$O$_2$)$_2$, M = 1157.27, monoclinic, $P2_1/n$ (no. 14), a = 11.0969(3), b = 18.3586(5), c = 12.3866(3) Å, β = 94.460(2)°, V = 2515.79(11) Å$_3$, Z = 2 [C$_i$ symmetry], D_c = 1.528 g cm^{-3}, μ(Mo-Kα) = 0.567 mm^{-1}, T = 173 K, pale yellow blocks, Agilent Xcalibur 3 E diffractometer; 5026 independent measured reflections (R_{int} = 0.0163), F^2 refinement,[1-2] R_1(obs) = 0.0291, wR_2(all) = 0.0694, 4263 independent observed absorption-corrected reflections [$|F_o| > 4\sigma(|F_o|)$, completeness to θ_{full}(25.2°) = 98.6%], 331 parameters. CCDC 1953466.

The palladium atom in the structure of [Pd(**DPPP**)$_2$](CF$_3$CO$_2$)$_2$ was found to sit on a centre of symmetry.

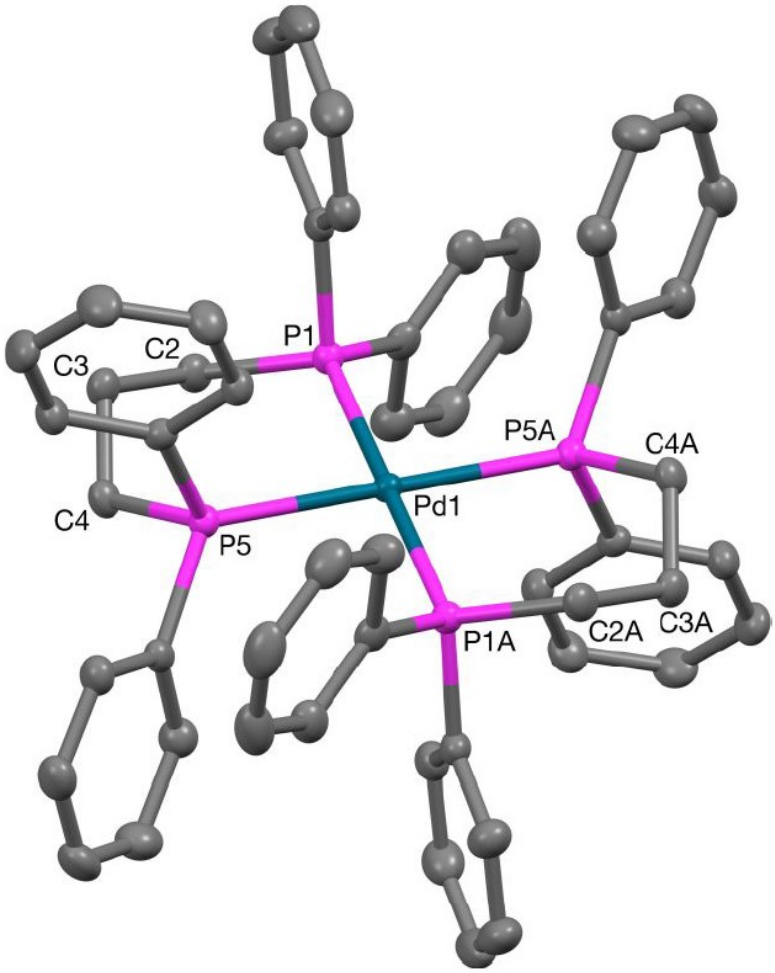

Figure 6.18 The structure of the Cis-symmetric di-cationic complex present in the crystal of [Pd(**DPPP**)$_2$](CF$_3$CO$_2$)$_2$ (50% probability ellipsoids).

Table 6.5 Bond lengths [Å] and angles [°] for [Pd(**DPPP**)$_2$](CF$_3$CO$_2$)$_2$.

P(1)-C(6)	1.816(2)	C(6)-C(7)	1.385(3)
P(1)-C(12)	1.830(2)	C(6)-C(11)	1.403(3)
P(1)-C(2)	1.835(2)	C(7)-C(8)	1.389(3)
P(1)-Pd(1)	2.4082(5)	C(8)-C(9)	1.377(4)
Pd(1)-P(5)	2.4000(5)	C(9)-C(10)	1.381(4)
Pd(1)-P(5)#1	2.4000(5)	C(10)-C(11)	1.378(3)
Pd(1)-P(1)#1	2.4082(5)	C(12)-C(13)	1.389(3)
C(2)-C(3)	1.519(3)	C(12)-C(17)	1.401(3)
C(3)-C(4)	1.519(3)	C(13)-C(14)	1.391(3)
C(4)-P(5)	1.827(2)	C(14)-C(15)	1.375(4)
P(5)-C(24)	1.814(2)	C(15)-C(16)	1.371(4)
P(5)-C(18)	1.828(2)	C(16)-C(17)	1.386(3)

C(18)-C(19)	1.392(3)
C(18)-C(23)	1.394(3)
C(19)-C(20)	1.390(3)
C(20)-C(21)	1.384(3)
C(21)-C(22)	1.377(3)
C(22)-C(23)	1.388(3)
C(24)-C(29)	1.389(3)
C(24)-C(25)	1.404(3)
C(25)-C(26)	1.381(3)
C(26)-C(27)	1.381(3)
C(27)-C(28)	1.380(3)
C(28)-C(29)	1.382(3)
C(30)-O(31)	1.232(3)
C(30)-O(32)	1.237(3)
C(30)-C(33)	1.537(3)
C(33)-F(34)	1.325(3)
C(33)-F(35)	1.328(3)
C(33)-F(36)	1.349(3)

C(6)-P(1)-C(12)	106.89(10)
C(6)-P(1)-C(2)	102.09(10)
C(12)-P(1)-C(2)	97.76(10)
C(6)-P(1)-Pd(1)	110.18(7)
C(12)-P(1)-Pd(1)	119.35(7)
C(2)-P(1)-Pd(1)	118.54(7)
P(5)-Pd(1)-P(5)#1	180.0
P(5)-Pd(1)-P(1)	88.765(18)
P(5)#1-Pd(1)-P(1)	91.235(18)
P(5)-Pd(1)-P(1)#1	91.237(18)
P(5)#1-Pd(1)-P(1)#1	88.764(18)
P(1)-Pd(1)-P(1)#1	180.0
C(3)-C(2)-P(1)	115.60(15)
C(4)-C(3)-C(2)	110.80(18)
C(3)-C(4)-P(5)	115.35(15)
C(24)-P(5)-C(4)	103.98(10)
C(24)-P(5)-C(18)	106.69(10)
C(4)-P(5)-C(18)	96.31(9)
C(24)-P(5)-Pd(1)	110.23(7)
C(4)-P(5)-Pd(1)	117.18(7)
C(18)-P(5)-Pd(1)	120.51(7)
C(7)-C(6)-C(11)	118.6(2)
C(7)-C(6)-P(1)	120.30(16)
C(11)-C(6)-P(1)	121.05(17)
C(6)-C(7)-C(8)	120.5(2)
C(9)-C(8)-C(7)	120.3(2)
C(8)-C(9)-C(10)	119.8(2)
C(11)-C(10)-C(9)	120.4(2)
C(10)-C(11)-C(6)	120.4(2)
C(13)-C(12)-C(17)	119.0(2)
C(13)-C(12)-P(1)	122.87(17)
C(17)-C(12)-P(1)	118.13(17)
C(12)-C(13)-C(14)	119.8(2)
C(15)-C(14)-C(13)	120.7(2)
C(16)-C(15)-C(14)	120.1(2)
C(15)-C(16)-C(17)	120.2(2)
C(16)-C(17)-C(12)	120.2(2)
C(19)-C(18)-C(23)	119.3(2)
C(19)-C(18)-P(5)	118.32(16)
C(23)-C(18)-P(5)	121.96(17)
C(20)-C(19)-C(18)	119.9(2)
C(21)-C(20)-C(19)	120.6(2)
C(22)-C(21)-C(20)	119.4(2)
C(21)-C(22)-C(23)	120.7(2)
C(22)-C(23)-C(18)	120.0(2)

C(29)-C(24)-C(25)	118.9(2)	O(31)-C(30)-C(33)	114.6(2)
C(29)-C(24)-P(5)	119.59(16)	O(32)-C(30)-C(33)	113.9(2)
C(25)-C(24)-P(5)	121.55(16)	F(34)-C(33)-F(35)	106.4(2)
C(26)-C(25)-C(24)	119.7(2)	F(34)-C(33)-F(36)	107.4(2)
C(27)-C(26)-C(25)	120.7(2)	F(35)-C(33)-F(36)	105.3(2)
C(28)-C(27)-C(26)	120.0(2)	F(34)-C(33)-C(30)	114.4(2)
C(27)-C(28)-C(29)	119.9(2)	F(35)-C(33)-C(30)	113.6(2)
C(28)-C(29)-C(24)	120.9(2)	F(36)-C(33)-C(30)	109.1(2)
O(31)-C(30)-O(32)	131.3(2)		

6.2.4 Cartesian Coordinates from Geometry Optimisation

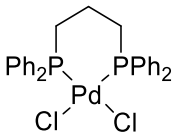

P	1.61060000	-0.16670000	-0.60430000
C	1.25620000	-0.07080000	-2.40590000
C	-0.07200000	0.55000000	-2.83840000
C	-1.30990000	-0.22180000	-2.38700000
P	-1.64670000	-0.17480000	-0.57960000
C	1.92470000	1.53900000	-0.05410000
C	3.22200000	-1.00070000	-0.64790000
C	-1.89410000	1.58820000	-0.21270000
C	-3.26430000	-0.99200000	-0.51280000
C	2.09390000	1.75740000	1.31780000
C	2.27700000	3.04430000	1.79960000
C	2.27770000	4.12800000	0.92730000
C	2.11400000	3.91730000	-0.43500000
C	1.94550000	2.62760000	-0.92550000
C	3.26460000	-2.39490000	-0.64030000
C	4.47900000	-3.05250000	-0.76510000
C	5.65860000	-2.32450000	-0.88320000
C	5.62060000	-0.93600000	-0.87810000
C	4.40440000	-0.27290000	-0.76350000
C	-1.46920000	2.07890000	1.02340000
C	-1.57660000	3.43220000	1.31260000
C	-2.11080000	4.30700000	0.37520000
C	-2.54860000	3.82460000	-0.85350000
C	-2.44080000	2.47230000	-1.14660000
C	-3.30730000	-2.37820000	-0.67180000
C	-4.52430000	-3.04040000	-0.67970000
C	-5.70750000	-2.32690000	-0.51400000
C	-5.66670000	-0.95040000	-0.33890000
C	-4.44810000	-0.28090000	-0.33950000
Pd	-0.00940000	-0.99560000	0.73820000
Cl	-1.70780000	-1.50040000	2.28370000
Cl	1.68630000	-1.69220000	2.22100000
H	1.31180000	-1.10680000	-2.74720000
H	2.09330000	0.44740000	-2.87620000
H	-0.14150000	1.58030000	-2.49080000
H	-0.07810000	0.59500000	-3.92960000
H	-2.19680000	0.14950000	-2.90070000
H	-1.22430000	-1.27900000	-2.64560000
H	2.07320000	0.91500000	1.99680000
H	2.40850000	3.20120000	2.86160000
H	2.40530000	5.13220000	1.30850000
H	2.11630000	4.75450000	-1.11970000
H	1.82930000	2.48510000	-1.98910000
H	2.35350000	-2.95810000	-0.49810000
H	4.50730000	-4.13330000	-0.74800000
H	6.60600000	-2.83960000	-0.96660000
H	6.53670000	-0.36640000	-0.95690000
H	4.38010000	0.80780000	-0.74880000
H	-1.05500000	1.39710000	1.75210000
H	-1.23410000	3.80120000	2.26910000
H	-2.18660000	5.36240000	0.59940000
H	-2.97060000	4.50100000	-1.58440000
H	-2.78390000	2.11230000	-2.10630000
H	-2.38650000	-2.94040000	-0.75040000
H	-4.54960000	-4.11550000	-0.79400000
H	-6.65620000	-2.84630000	-0.50740000
H	-6.58250000	-0.39380000	-0.19270000
H	-4.42260000	0.78800000	-0.18650000

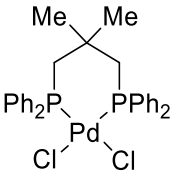

P	1.68590000	0.07800000	0.40360000
C	1.26230000	-0.05850000	2.19110000
C	0.00000000	-0.84550000	2.59020000
C	-1.26230000	-0.05850000	2.19110000
P	-1.68590000	0.07800000	0.40360000
C	2.58530000	-1.46460000	0.05080000
C	2.92140000	1.41040000	0.42950000
C	-2.58530000	-1.46460000	0.05080000
C	-2.92140000	1.41040000	0.42950000
C	2.23620000	-2.23830000	-1.05470000
C	2.88300000	-3.44350000	-1.29660000
C	3.88820000	-3.88160000	-0.44400000
C	4.25230000	-3.10750000	0.65280000
C	3.60330000	-1.90640000	0.89960000
C	4.19360000	1.24590000	-0.11340000
C	5.08990000	2.30670000	-0.12250000
C	4.72170000	3.54050000	0.39830000
C	3.44610000	3.71610000	0.92330000
C	2.55000000	2.65780000	0.93490000
C	-2.23620000	-2.23830000	-1.05470000
C	-2.88300000	-3.44350000	-1.29660000
C	-3.88820000	-3.88160000	-0.44400000
C	-4.25230000	-3.10750000	0.65280000
C	-3.60330000	-1.90640000	0.89960000
C	-2.55000000	2.65780000	0.93490000
C	-3.44610000	3.71610000	0.92330000
C	-4.72170000	3.54050000	0.39830000
C	-5.08990000	2.30670000	-0.12250000
C	-4.19360000	1.24590000	-0.11340000
Pd	0.00000000	0.47030000	-1.03430000
Cl	-1.72540000	0.79930000	-2.61050000
Cl	1.72540000	0.79930000	-2.61050000
C	0.00000000	-0.94560000	4.12390000
C	0.00000000	-2.26170000	2.00600000
H	1.17550000	0.96260000	2.56360000
H	2.13080000	-0.49140000	2.68790000
H	-1.17550000	0.96260000	2.56360000
H	-2.13080000	-0.49140000	2.68790000
H	1.47540000	-1.88260000	-1.73280000
H	2.60440000	-4.03480000	-2.15800000
H	4.39240000	-4.81920000	-0.63550000
H	5.04240000	-3.43730000	1.31380000
H	3.90460000	-1.30860000	1.74890000
H	4.47640000	0.29960000	-0.54790000
H	6.07330000	2.17030000	-0.55110000
H	5.41960000	4.36650000	0.38330000
H	3.14550000	4.67940000	1.31230000
H	1.54900000	2.81560000	1.31480000
H	-1.47540000	-1.88260000	-1.73280000
H	-2.60440000	-4.03480000	-2.15800000
H	-4.39240000	-4.81920000	-0.63550000
H	-5.04240000	-3.43730000	1.31380000
H	-3.90460000	-1.30860000	1.74890000
H	-1.54900000	2.81560000	1.31480000
H	-3.14550000	4.67940000	1.31230000
H	-5.41960000	4.36650000	0.38330000
H	-6.07330000	2.17030000	-0.55110000
H	-4.47640000	0.29960000	-0.54790000
H	-0.88260000	-1.48260000	4.47440000
H	0.88260000	-1.48260000	4.47440000
H	0.00000000	0.04360000	4.58490000
H	0.00000000	-2.26200000	0.91870000
H	0.88420000	-2.80870000	2.33310000
H	-0.88420000	-2.80870000	2.33310000

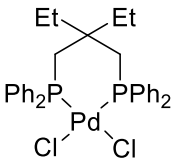

P	1.66290000	-0.13000000	0.23100000
C	1.26650000	0.24230000	1.99540000
C	0.00230000	1.06460000	2.31170000
C	-1.24970000	0.22300000	1.99330000
P	-1.70550000	-0.05380000	0.23070000
C	2.75330000	1.24650000	-0.24100000
C	2.71980000	-1.60200000	0.38360000
C	-2.86500000	-1.44640000	0.36910000
C	-2.69700000	1.41170000	-0.19650000
C	2.39560000	2.09880000	-1.28250000
C	3.18290000	3.20320000	-1.58200000
C	4.33930000	3.45530000	-0.85480000
C	4.71180000	2.59760000	0.17510000
C	3.92050000	1.50060000	0.48300000
C	2.26380000	-2.69710000	1.12050000
C	3.01090000	-3.86430000	1.18500000
C	4.22080000	-3.95250000	0.50640000
C	4.67060000	-2.87350000	-0.24430000
C	3.92270000	-1.70610000	-0.31380000
C	-4.14080000	-1.39890000	-0.18850000
C	-4.97500000	-2.50680000	-0.11630000
C	-4.54070000	-3.67310000	0.50030000
C	-3.26020000	-3.73410000	1.03900000
C	-2.42610000	-2.62840000	0.96950000
C	-3.74440000	1.82230000	0.63170000
C	-4.46350000	2.97180000	0.33750000
C	-4.13970000	3.72520000	-0.78600000

C	-3.10400000	3.31750000	-1.61730000
C	-2.38770000	2.16310000	-1.32830000
Pd	-0.03350000	-0.48770000	-1.20560000
Cl	-1.76980000	-0.86590000	-2.75890000
Cl	1.68030000	-0.90230000	-2.77620000
C	-0.00730000	1.37010000	3.83080000
C	-0.04360000	2.39740000	1.53430000
C	1.03200000	3.42620000	1.87300000
H	2.14520000	0.73740000	2.40790000
H	1.19520000	-0.71890000	2.49890000
H	-2.11970000	0.67210000	2.47340000
H	-1.13890000	-0.76890000	2.42740000
H	1.51450000	1.88230000	-1.86750000
H	2.89660000	3.85930000	-2.39240000
H	4.95390000	4.31270000	-1.09330000
H	5.61700000	2.78290000	0.73730000
H	4.21880000	0.83700000	1.28360000
H	1.31130000	-2.65490000	1.63160000
H	2.64420000	-4.70610000	1.75650000
H	4.80310000	-4.86260000	0.55280000
H	5.60060000	-2.94350000	-0.79180000
H	4.26080000	-0.88640000	-0.92780000
H	-4.47390000	-0.50730000	-0.69670000
H	-5.96190000	-2.46070000	-0.55620000
H	-5.19050000	-4.53620000	0.54900000
H	-2.90720000	-4.64560000	1.50180000
H	-1.41970000	-2.70030000	1.36070000
H	-4.01240000	1.23960000	1.50250000
H	-5.27630000	3.27740000	0.98230000
H	-4.69850000	4.62260000	-1.01490000
H	-2.85650000	3.89210000	-2.49920000
H	-1.60320000	1.82850000	-1.98980000
H	-0.84600000	2.04490000	4.02510000
H	-1.02640000	2.84540000	1.69480000
H	0.00540000	2.18220000	0.46630000
H	2.03720000	3.01910000	1.77960000
H	0.91740000	3.82050000	2.88190000
H	0.96400000	4.26740000	1.18360000
C	-0.09970000	0.17460000	4.77700000
H	-1.02620000	-0.38470000	4.64860000
H	0.73140000	-0.51880000	4.64430000
H	-0.06980000	0.51640000	5.81170000
H	0.89660000	1.93190000	4.06910000

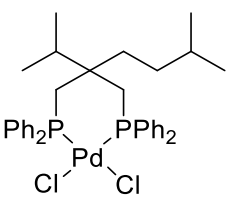

C	-1.29990000	0.34950000	1.79880000
C	1.17310000	-0.05500000	1.88060000
P	-1.79740000	-0.09240000	0.08300000
P	1.48930000	-0.80560000	0.22280000
C	-2.45720000	1.46270000	-0.59630000
C	-2.01670000	1.92660000	-1.83450000
C	-3.35270000	2.23800000	0.14420000
C	-2.44980000	3.15590000	-2.31420000
C	-3.78870000	3.46340000	-0.33950000
C	-3.33160000	3.92770000	-1.56820000
C	-3.21730000	-1.18140000	0.39590000
C	-3.00260000	-2.35770000	1.11730000
C	-4.48340000	-0.91990000	-0.12160000
C	-4.04490000	-3.24370000	1.34300000
C	-5.52630000	-1.80880000	0.10620000
C	-5.31230000	-2.96740000	0.84140000
C	2.84800000	0.20100000	-0.44980000
C	4.02720000	0.36810000	0.28120000
C	2.71260000	0.83740000	-1.68090000
C	5.05090000	1.16420000	-0.21030000
C	3.73590000	1.64110000	-2.16780000
C	4.90410000	1.80620000	-1.43590000
C	2.22240000	-2.40870000	0.67360000
C	1.54790000	-3.24230000	1.56830000
C	3.38320000	-2.87310000	0.05680000
C	2.04040000	-4.50490000	1.86450000
C	3.87650000	-4.13540000	0.35760000
C	3.21100000	-4.95230000	1.26290000
Pd	-0.24050000	-1.08170000	-1.19700000
Cl	1.34680000	-2.12260000	-2.60230000
Cl	-2.01730000	-1.37260000	-2.72220000
C	0.07340000	1.01820000	2.01500000
C	0.13750000	1.58300000	3.47580000
C	0.27490000	2.15640000	0.99380000
C	-0.09680000	0.53250000	4.56690000
C	1.50940000	3.03570000	1.16120000
C	1.69080000	4.03210000	0.00820000
C	0.52690000	5.01960000	-0.09460000
C	3.01970000	4.77170000	0.15270000
H	-2.09270000	0.98400000	2.18970000
H	-1.34760000	-0.58000000	2.36360000
H	2.12710000	0.34380000	2.22430000
H	0.93840000	-0.88800000	2.53680000
H	-1.35010000	1.31540000	-2.42370000
H	-3.71960000	1.88730000	1.09890000
H	-2.09920000	3.50690000	-3.27500000
H	-4.48320000	4.05450000	0.24190000
H	-3.66600000	4.88560000	-1.94310000
H	-2.01150000	-2.60050000	1.47800000
H	-4.65050000	-0.03680000	-0.71890000
H	-3.86570000	-4.15490000	1.89730000
H	-6.50470000	-1.59980000	-0.30450000

H	-6.12480000	-3.66070000	1.01100000
H	4.15470000	-0.13480000	1.23040000
H	1.81810000	0.68180000	-2.26450000
H	5.96180000	1.28260000	0.36060000
H	3.62040000	2.13070000	-3.12490000
H	5.70070000	2.42950000	-1.81880000
H	0.62150000	-2.92030000	2.02520000
H	3.88650000	-2.25910000	-0.67330000
H	1.50620000	-5.14120000	2.55700000
H	4.77620000	-4.48550000	-0.12950000
H	3.59480000	-5.93750000	1.49000000
H	0.30940000	1.71940000	-0.00600000
H	-0.61570000	2.78030000	0.99690000
H	-1.11320000	0.13730000	4.53490000
H	0.03980000	0.98680000	5.54860000
H	0.59430000	-0.30650000	4.50290000
H	1.45790000	3.59760000	2.09760000
H	2.40500000	2.41650000	1.22180000
H	1.72800000	3.45430000	-0.91980000
H	0.70270000	5.74110000	-0.89390000
H	-0.41900000	4.52280000	-0.30690000
H	0.41340000	5.58070000	0.83720000
H	3.18770000	5.44950000	-0.68580000
H	3.85530000	4.07280000	0.19260000
H	3.03340000	5.36810000	1.06870000
C	-0.80300000	2.76860000	3.71420000
H	-0.65200000	3.15970000	4.72080000
H	-0.63620000	3.58530000	3.01580000
H	-1.85140000	2.47520000	3.64080000
H	1.15910000	1.95070000	3.60020000

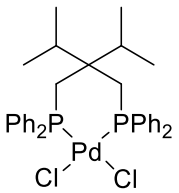

P	-1.65080000	0.16500000	0.15730000
C	-1.22730000	-0.64560000	1.76970000
C	0.03330000	-1.52560000	1.88770000
C	1.26370000	-0.60320000	1.70130000
P	1.68170000	0.09760000	0.04390000
C	-2.39800000	1.73220000	0.69550000
C	-3.00370000	-0.87590000	-0.47020000
C	2.61840000	1.59090000	0.53870000
C	2.89620000	-1.07900000	-0.63790000
C	-1.68650000	2.55420000	1.57290000
C	-2.18230000	3.80000000	1.92770000
C	-3.39180000	4.24150000	1.40250000
C	-4.09260000	3.43730000	0.51260000
C	-3.59680000	2.19130000	0.15210000
C	-2.87700000	-1.55500000	-1.67910000
C	-3.87300000	-2.42880000	-2.09510000
C	-5.00530000	-2.62270000	-1.31440000
C	-5.14410000	-1.93710000	-0.11200000
C	-4.14650000	-1.07000000	0.30970000
C	2.58960000	2.72730000	-0.27180000
C	3.28470000	3.87150000	0.09980000
C	4.01600000	3.89950000	1.27970000
C	4.04970000	2.77400000	2.09470000
C	3.35390000	1.63000000	1.72960000
C	4.14980000	-1.23650000	-0.04690000
C	5.03170000	-2.19910000	-0.51970000
C	4.66840000	-3.01090000	-1.58800000
C	3.42630000	-2.84730000	-2.18890000
C	2.54570000	-1.88210000	-1.72130000
Pd	-0.02690000	0.60310000	-1.33990000
Cl	1.57880000	1.02850000	-3.01860000
Cl	-1.78970000	1.36980000	-2.71060000
C	0.13070000	-2.07140000	3.36140000
C	0.06840000	-2.66150000	0.81540000
C	-0.95340000	-3.07980000	3.75470000
C	1.26820000	-3.60120000	0.96670000
C	0.17650000	-0.97770000	4.43930000
C	-1.19990000	-3.51290000	0.63770000
H	-2.11380000	-1.20680000	2.05330000
H	-1.14180000	0.16840000	2.48410000
H	2.15800000	-1.11090000	2.06060000
H	1.13030000	0.27290000	2.32990000
H	-0.72800000	2.23920000	1.96410000
H	-1.62000000	4.42860000	2.60450000
H	-3.77840000	5.21380000	1.67600000
H	-5.02290000	3.78460000	0.08430000
H	-4.12730000	1.58750000	-0.56740000
H	-2.01010000	-1.38460000	-2.29810000
H	-3.76530000	-2.95110000	-3.03570000
H	-5.78160000	-3.30030000	-1.64310000
H	-6.02830000	-2.07570000	0.49520000
H	-4.26380000	-0.53860000	1.24480000
H	2.03890000	2.70720000	-1.19980000
H	3.25050000	4.74230000	-0.54050000
H	4.55540000	4.79240000	1.56560000
H	4.61560000	2.78510000	3.01660000
H	3.38980000	0.77260000	2.38530000
H	4.45070000	-0.60160000	0.77420000
H	6.00370000	-2.30930000	-0.05830000
H	5.35600000	-3.75950000	-1.95770000
H	3.14530000	-3.46250000	-3.03270000
H	1.59490000	-1.73390000	-2.20980000
H	1.08820000	-2.59540000	3.40840000
H	0.19490000	-2.13160000	-0.13230000
H	-1.95810000	-2.68330000	3.60340000

H	-0.87610000	-4.01170000	3.20530000
H	-0.85940000	-3.31820000	4.81470000
H	1.15910000	-4.23920000	1.84420000
H	2.21740000	-3.07670000	1.04080000
H	1.33380000	-4.25310000	0.09590000
H	0.36520000	-1.43890000	5.40890000
H	0.96160000	-0.24200000	4.27770000
H	-0.77300000	-0.44670000	4.51940000
H	-1.22390000	-3.90280000	-0.37990000
H	-2.12270000	-2.96160000	0.78350000
H	-1.21310000	-4.36950000	1.30710000

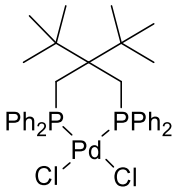

P	1.53760000	-0.18510000	-0.01570000
C	1.03560000	1.00490000	1.30700000
C	-0.00730000	2.14840000	1.16230000
C	-1.40440000	1.55470000	0.81380000
P	-1.67060000	-0.02590000	-0.12730000
C	2.05930000	-1.64030000	0.95500000
C	3.09260000	0.48470000	-0.68390000
C	-2.02110000	-1.30950000	1.12970000
C	-3.28050000	0.36360000	-0.88570000
C	1.34630000	-2.07480000	2.07450000
C	1.70440000	-3.24640000	2.72780000
C	2.77210000	-4.00470000	2.26600000
C	3.47380000	-3.59010000	1.13960000
C	3.11930000	-2.42060000	0.48400000
C	3.20710000	0.86080000	-2.01940000
C	4.37610000	1.45530000	-2.47680000
C	5.44040000	1.66690000	-1.60990000
C	5.33950000	1.27400000	-0.27920000
C	4.17140000	0.68530000	0.18140000
C	-1.76930000	-2.63970000	0.77770000
C	-1.98440000	-3.66250000	1.69000000
C	-2.44920000	-3.37690000	2.96770000
C	-2.72170000	-2.06130000	3.32240000
C	-2.51640000	-1.03690000	2.40680000
C	-4.47800000	0.13370000	-0.21280000
C	-5.68530000	0.52610000	-0.78070000
C	-5.70180000	1.15120000	-2.02010000
C	-4.50800000	1.37250000	-2.69950000
C	-3.30340000	0.97440000	-2.14090000
Pd	-0.04840000	-0.87540000	-1.45400000
Cl	-1.71890000	-1.82740000	-2.81280000
Cl	1.66640000	-1.96790000	-2.65120000
C	-0.15400000	2.76980000	2.66240000
C	0.40880000	3.20530000	0.03020000
C	-0.21660000	1.64860000	3.72780000
C	-0.39640000	4.51700000	0.07230000
C	-1.44600000	3.59230000	2.87430000
C	1.89870000	3.59770000	0.06640000
C	1.02650000	3.66150000	3.08080000
C	0.14170000	2.63400000	-1.37600000
H	1.96470000	1.39680000	1.71440000
H	0.64600000	0.33160000	2.05890000
H	-1.98260000	2.28750000	0.26080000
H	-1.96690000	1.39550000	1.72520000
H	0.48840000	-1.52950000	2.43700000
H	1.13700000	-3.56810000	3.59030000
H	3.04920000	-4.91890000	2.77330000
H	4.29410000	-4.18430000	0.76080000
H	3.64630000	-2.12500000	-0.40960000
H	2.39560000	0.66440000	-2.70190000
H	4.45620000	1.74270000	-3.51610000
H	6.35050000	2.12720000	-1.97030000
H	6.17000000	1.42300000	0.39750000
H	4.10290000	0.37560000	1.21560000
H	-1.40340000	-2.86980000	-0.21260000
H	-1.77520000	-4.68300000	1.40100000
H	-2.60420000	-4.17430000	3.68190000
H	-3.09810000	-1.82930000	4.30960000
H	-2.75800000	-0.02760000	2.70320000
H	-4.47850000	-0.36680000	0.74430000
H	-6.61100000	0.33460000	-0.25510000
H	-6.64150000	1.45120000	-2.46370000
H	-4.51690000	1.83430000	-3.67730000
H	-2.38520000	1.09660000	-2.69520000
H	-0.91900000	0.85640000	3.47760000
H	0.75340000	1.19080000	3.91140000
H	-0.54560000	2.08370000	4.67140000
H	-0.16000000	5.13410000	0.93420000
H	-1.47260000	4.34980000	0.04830000
H	-0.14620000	5.09920000	-0.81510000
H	-2.34480000	2.98040000	2.82260000
H	-1.56430000	4.41270000	2.17940000
H	-1.41670000	4.01870000	3.87760000
H	2.16960000	4.16230000	0.95040000
H	2.56100000	2.74410000	-0.00650000
H	2.10970000	4.23140000	-0.79550000
H	1.98900000	3.17690000	2.92660000
H	1.03670000	4.61620000	2.56360000
H	0.94120000	3.87560000	4.14720000
H	0.61630000	1.67730000	-1.56040000
H	-0.92080000	2.51500000	-1.57620000
H	0.52960000	3.33020000	-2.11910000

6.2.5 Additional Geometry Calculations

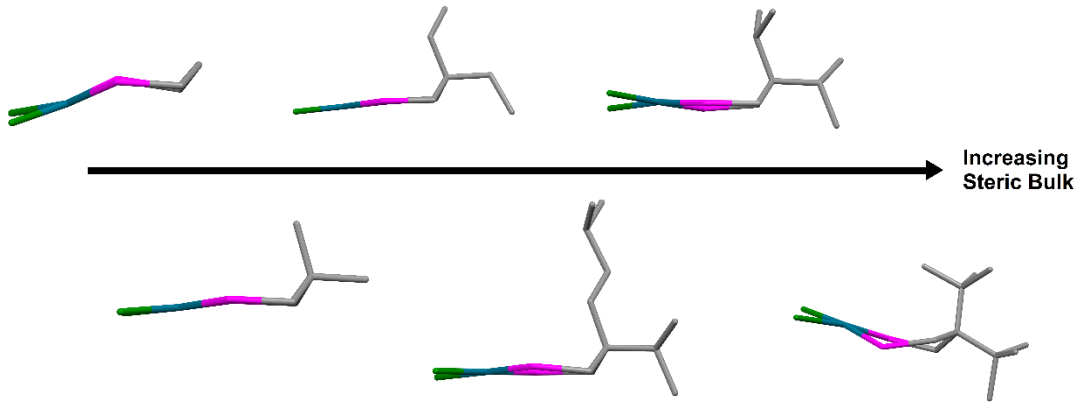

Figure 6.19 [Pd(diphosphine)Cl_2] structures calculated at 150 ˚C and arranged by increasing steric bulk of *gem*-dialkyl substituents showing 6-membered chelate conformations (side view across P-C bonds). Phenyl groups and hydrogen atoms removed for clarity.

6.2.6 Mechanistic Studies

Table 6.6 Data for **Figure 2.28** (Ligand **DPPDMP**), available at: 10.14469/hpc/6231.

	JobID	**ΔG (kcal/mol)**
CO	10059037	***
Propylene	10059040	***
I	10058975	0
II-TS	10059144	+25.7
III	10059180	+12.4
IV-TS	10059315	+14.2
V	10059045	+10.5
VI-TS	10059038	+11.3
VII	10059046	+5.80
VI-TS’	10059029	+27.4
IRC from II-TS (forward)	10059160	***
IRC from II-TS (reverse)	10059159	***

Table 6.7 Data for selected intermediates (**Figure 2.28**) using ligands **DPPDMP**, **DPPP** and **DPPDTBP** (including dispersion, solvent and temperature correction when stated), available at: 10.14469/hpc/6231.

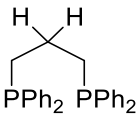

DPPP

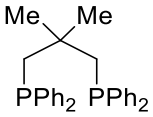

DPPDMP

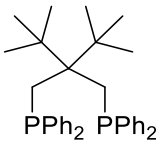

DPPDTBP

For **DPPDMP** (Me, Me)	**JobID**	**ΔG (kcal/mol)**
I	10058975	0
II-TS	10059144	+25.7
VI-TS	10059038	+11.3
VII	10059046	+5.80
For **DPPP** (H, H)		
Ia	10059194	0
IIa-TS	10059176	+25.3
For **DPPDTBP** (^{t}Bu, ^{t}Bu)		
Ib	10059047	0
IIb-TS	10059311	+24.7
VIb-TS	10059134	+12.1
IRC from IIb-TS	10059503	***
Including dispersion (GD3BJ), solvent (cpcm=THF) and temperature (423.15 K) correction		
CO	10059667	***
Propylene	10059668	***
Ia	10059628	0
IIb-TS	10059598	+17.8
VIb-TS	10059597	+8.7

6.2.7 Octane Quantification

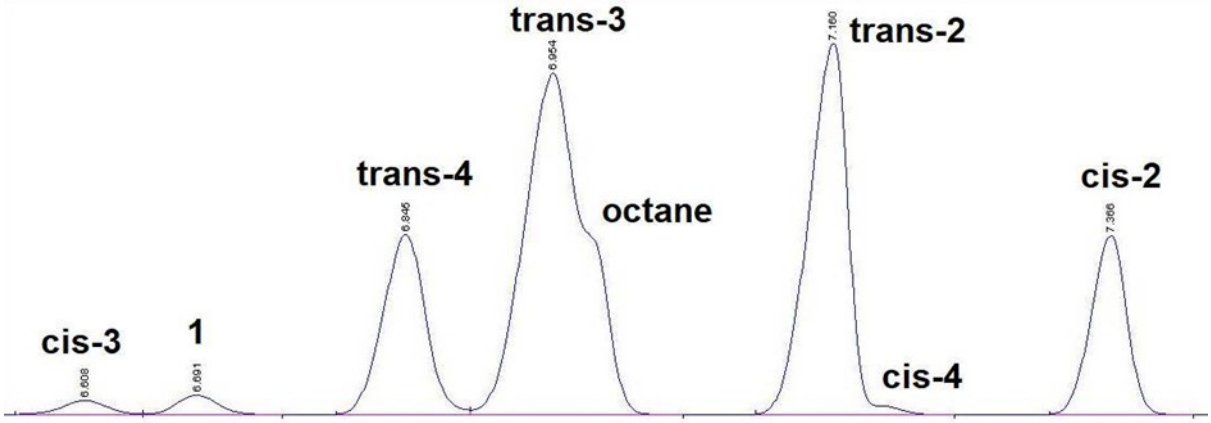

Figure 6.20 GC spectrum of the octene region for run 5 from **Table 2.3**.

Due to incomplete resolution of octane from octene on the GC, post-processing was required to quantify the amount of *trans*-3-octene and octane detected. Both *trans*-3-octene and octane were assumed to follow gaussian distributions which were then integrated using the following formula:

$$\int_{-\infty}^{\infty} ae^{-\frac{x^2}{2\sigma^2}} = a\sigma\sqrt{2\pi}$$

Where,

$$a = height\ of\ bell\ curve$$
$$\sigma = standard\ deviation$$

The ratio of their integrals was then used to apportion the area of the combined *trans*-3-octene/octane peak.

6.3 Supplementary Information for Chapter 3

6.3.1 NMR Spectra

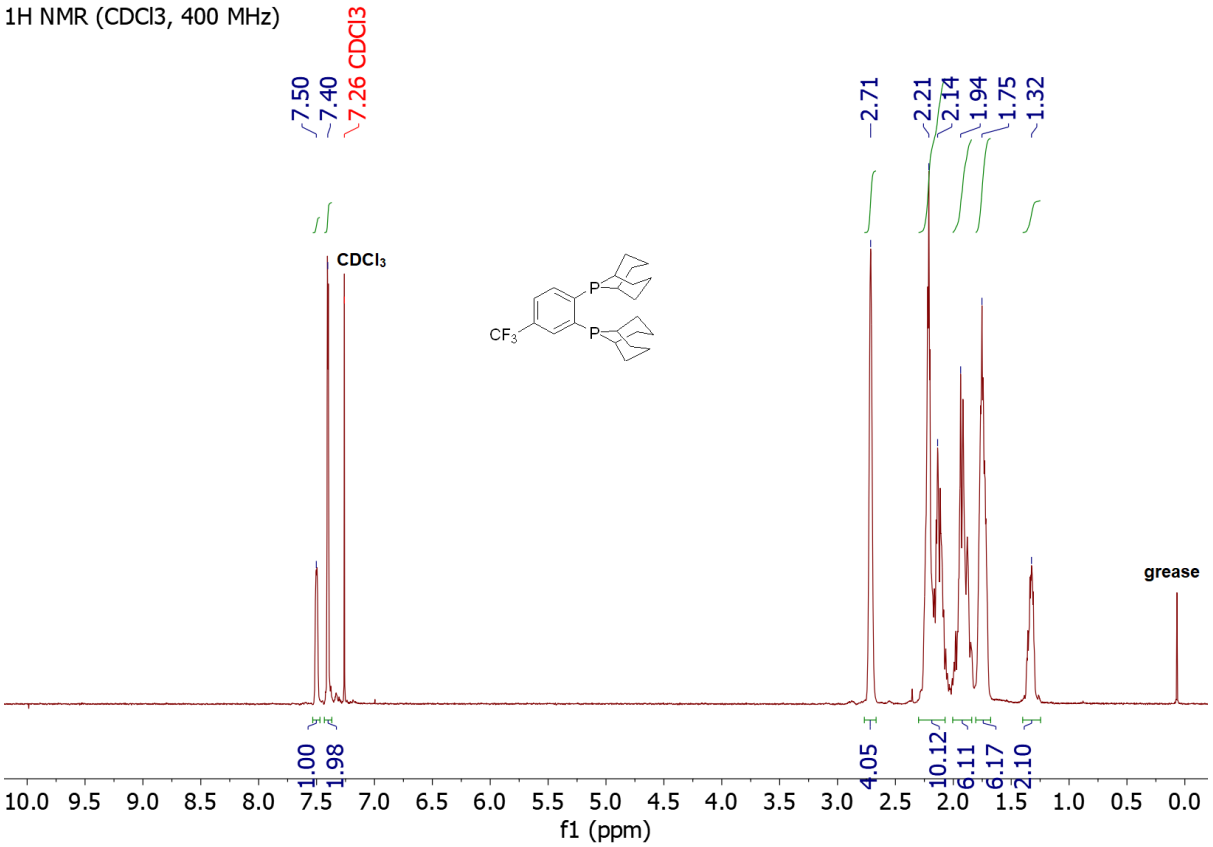

Figure 6.21 ^{1}H NMR (400 MHz, $CDCl_3$, 25 °C) spectrum of 9,9'-(4-(trifluoromethyl)-1,2-phenylene)bis(9-phosphabicyclo[3.3.1]nonane), **BCOPF**.

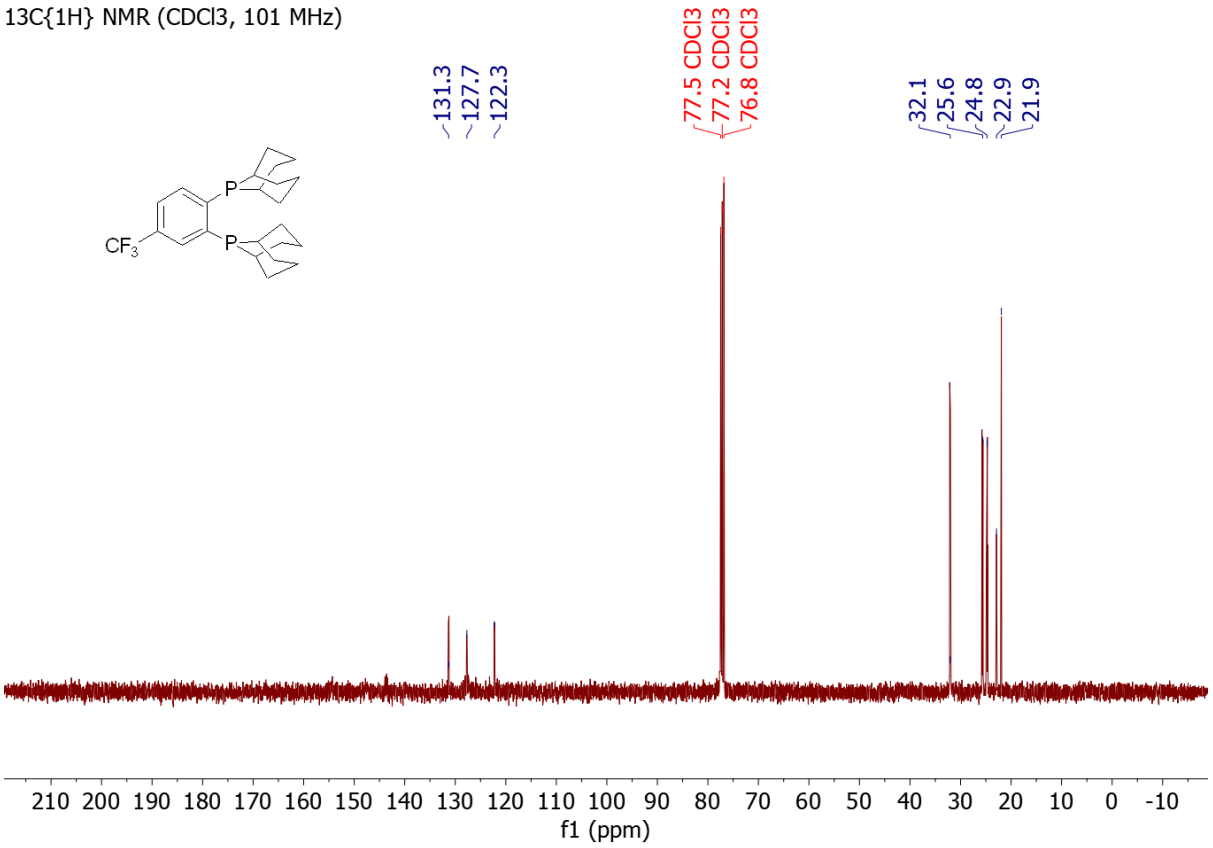

Figure 6.22 $^{13}C\{^{1}H\}$ NMR (101 MHz, $CDCl_3$, 25 °C) spectrum of 9,9'-(4-(trifluoromethyl)-1,2-phenylene)bis(9-phosphabicyclo[3.3.1]nonane), **BCOPF**.

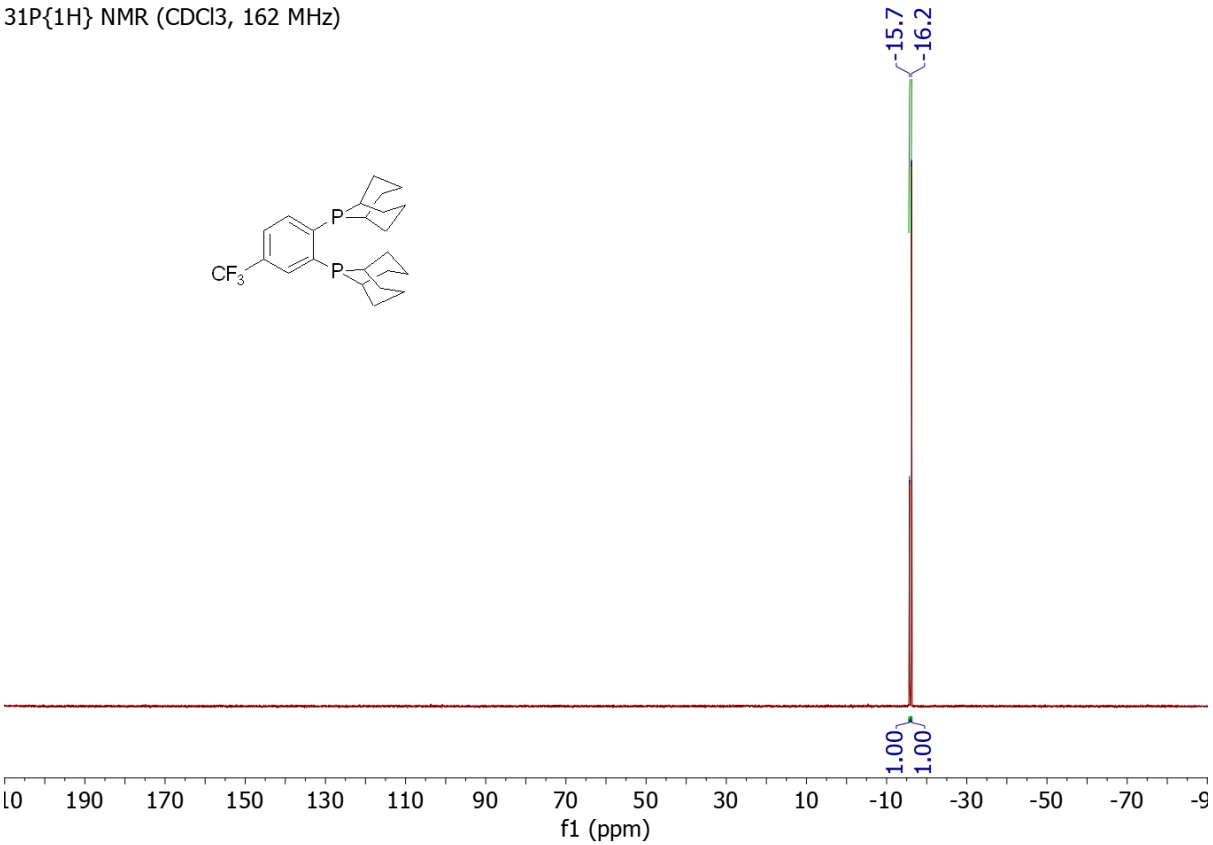

Figure 6.23 $^{31}P\{^{1}H\}$ NMR (162 MHz, $CDCl_3$, 25 °C) spectrum of 9,9'-(4-(trifluoromethyl)-1,2-phenylene)bis(9-phosphabicyclo[3.3.1]nonane), **BCOPF**.

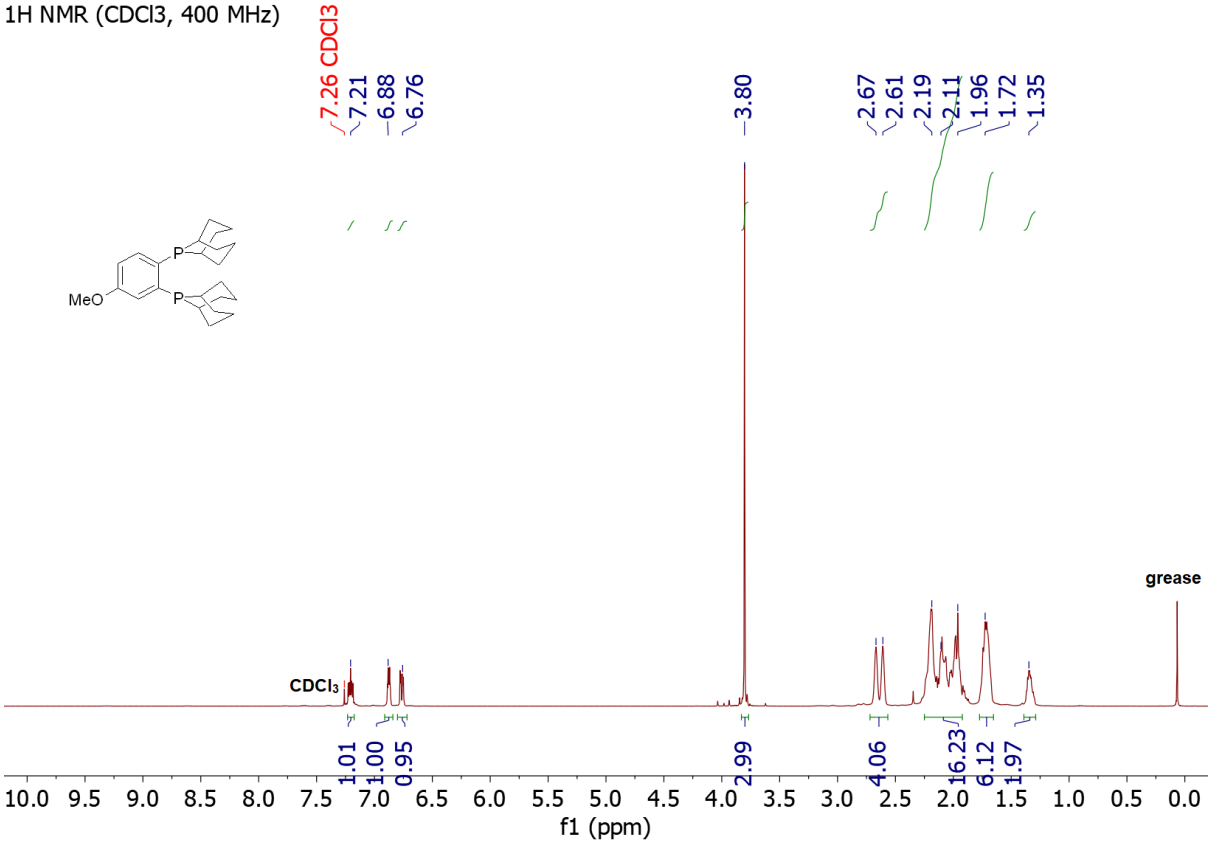

Figure 6.24 ^{1}H NMR (400 MHz, $CDCl_3$, 25 °C) spectrum of 9,9'-(4-methoxy-1,2-phenylene)bis(9-phosphabicyclo[3.3.1]nonane), **BCOPA**.

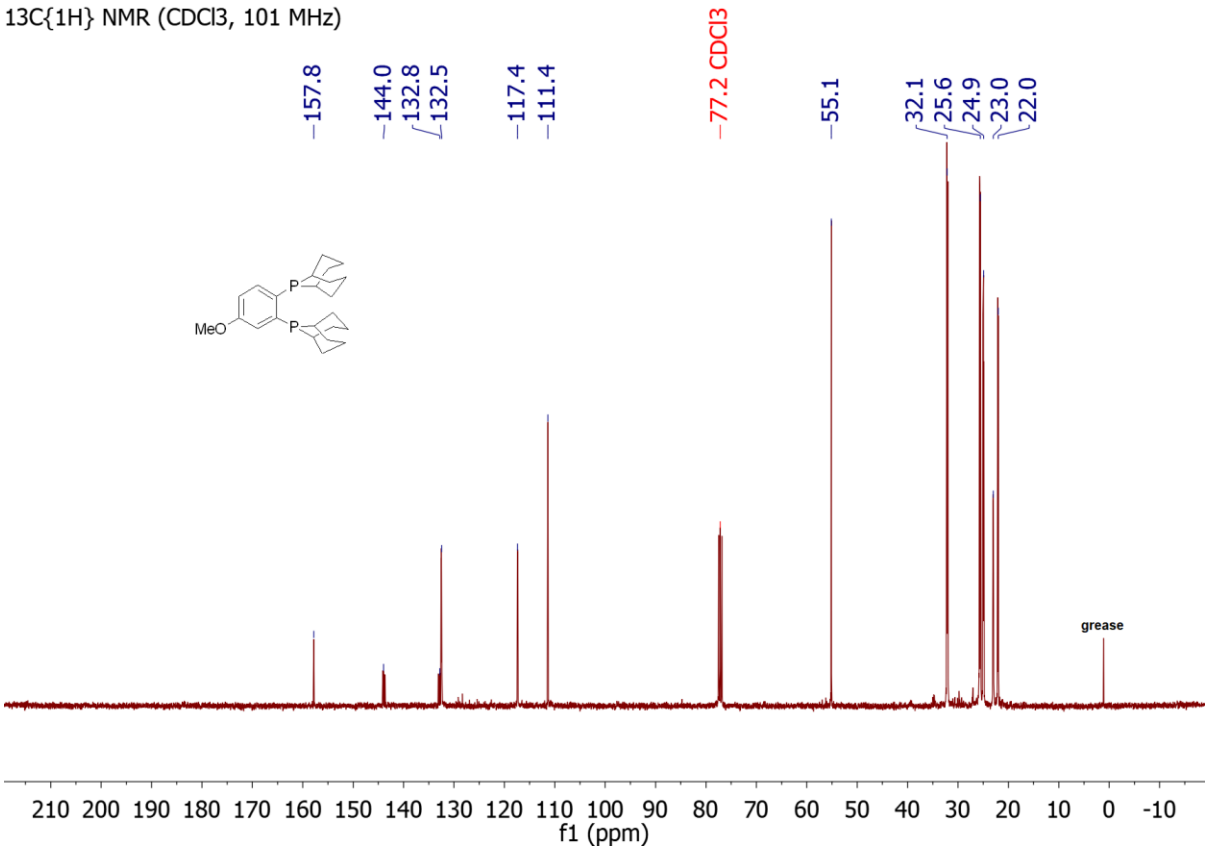

Figure 6.25 $^{13}C\{^{1}H\}$ NMR (101 MHz, $CDCl_3$, 25 °C) spectrum of 9,9'-(4-methoxy-1,2-phenylene)bis(9-phosphabicyclo[3.3.1]nonane), **BCOPA**.

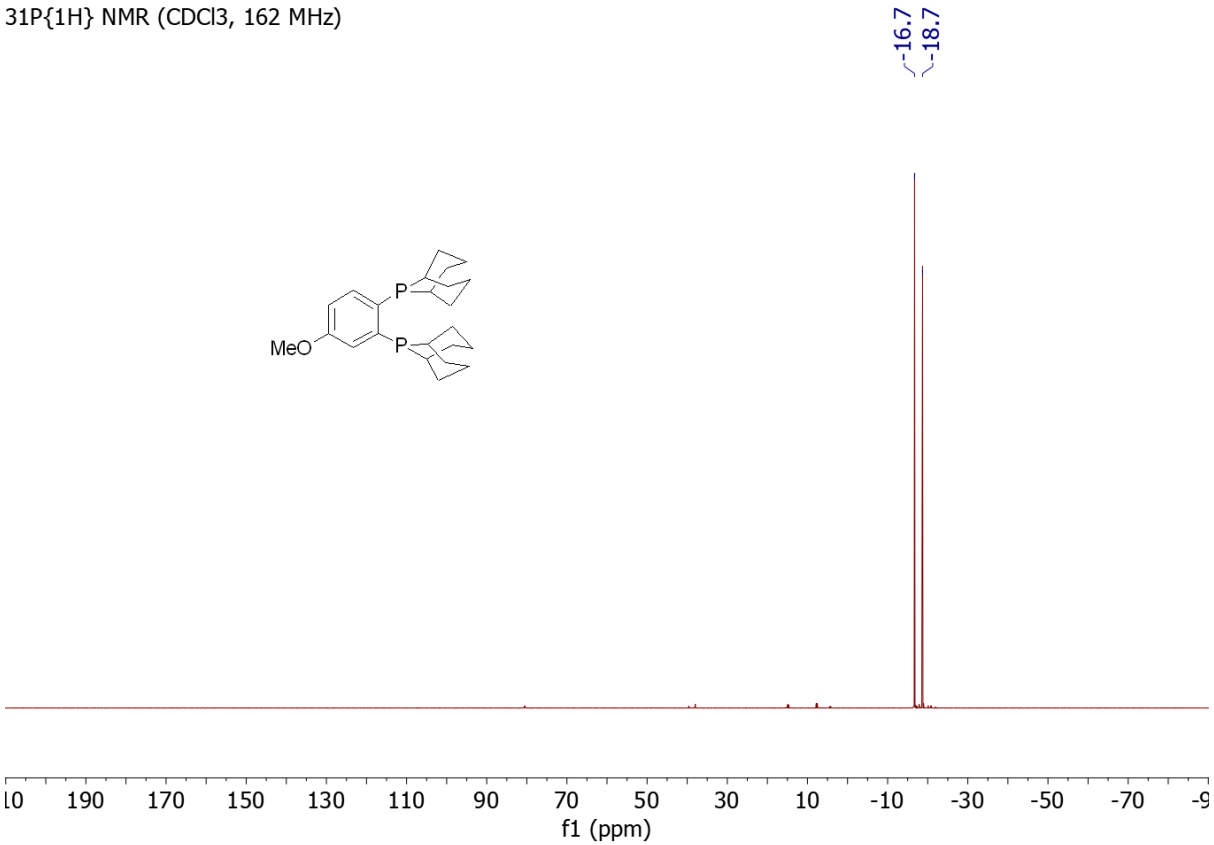

Figure 6.26 $^{31}P\{^{1}H\}$ NMR (162 MHz, $CDCl_3$, 25 °C) spectrum of 9,9'-(4-methoxy-1,2-phenylene)bis(9-phosphabicyclo[3.3.1]nonane), **BCOPA**.

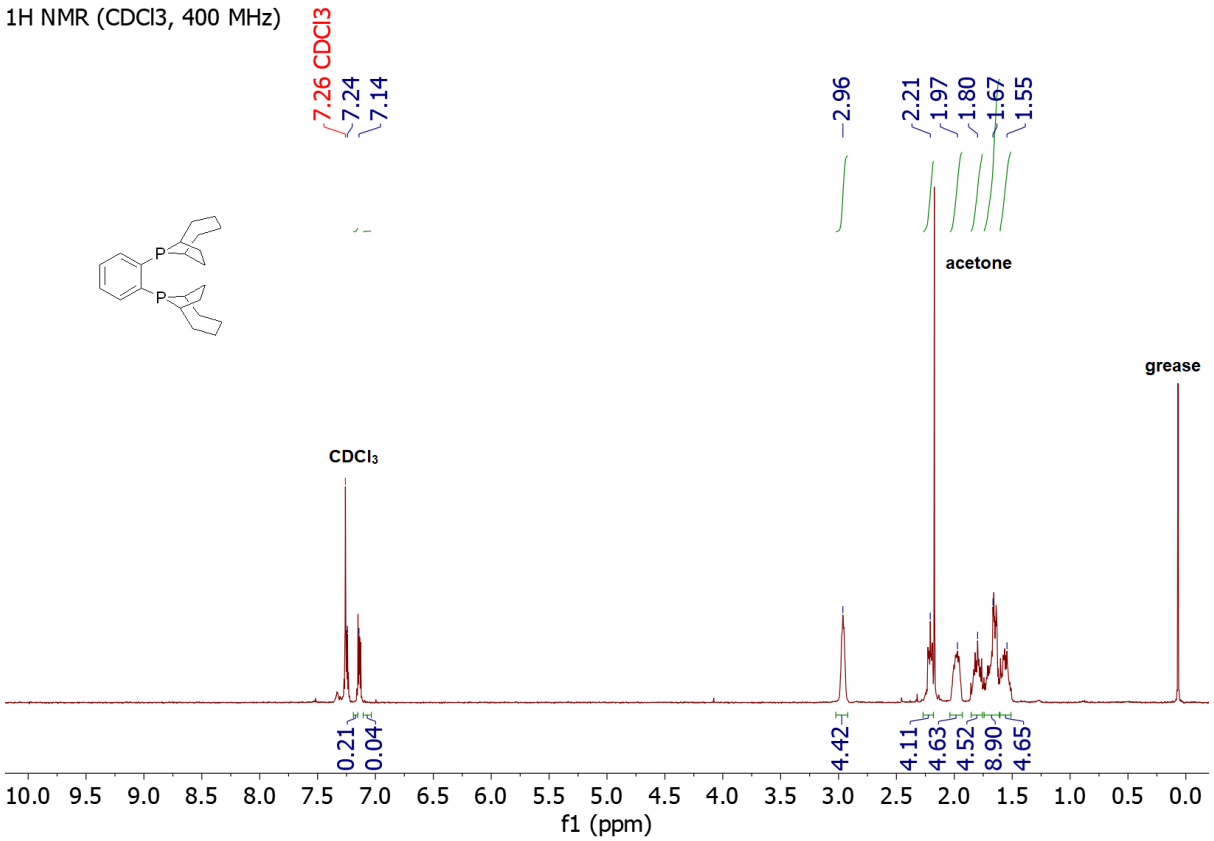

Figure 6.27 ^{1}H NMR (400 MHz, $CDCl_3$, 25 °C) spectrum of 1,2-Di(9-phosphabicyclo[4.2.1]nonan-9-yl)benzene, **a-BCOPP**.

6.3.2 X-Ray Analyses

The X-ray crystal structure of [Pd(BCOPE)Cl_2]

Crystal data for [Pd(**BCOPE**)Cl_2]: $C_{18}H_{32}Cl_2P_2Pd$, M = 487.67, monoclinic, $P2_1/c$ (no. 14), a = 11.7219(2) Å, b = 12.3373(2) Å, c = 13.6858(2) Å, β = 96.2390(10)°, V = 1967.47(5) Å^3, Z = 4, T = 295.79(10) K, μ(CuKα) = 11.605 mm^{-1}, D_c = 1.646 g cm^{-3}, 28422 reflections measured (7.586° ≤ 2Θ ≤ 145.426°), F^2 refinement,[1-2] 3890 unique (R_{int} = 0.0922, R_{sigma} = 0.0373) which were used in all calculations. The final R_1 was 0.0535 (I > 2σ(I)) and wR_2 was 0.1522 (all data).

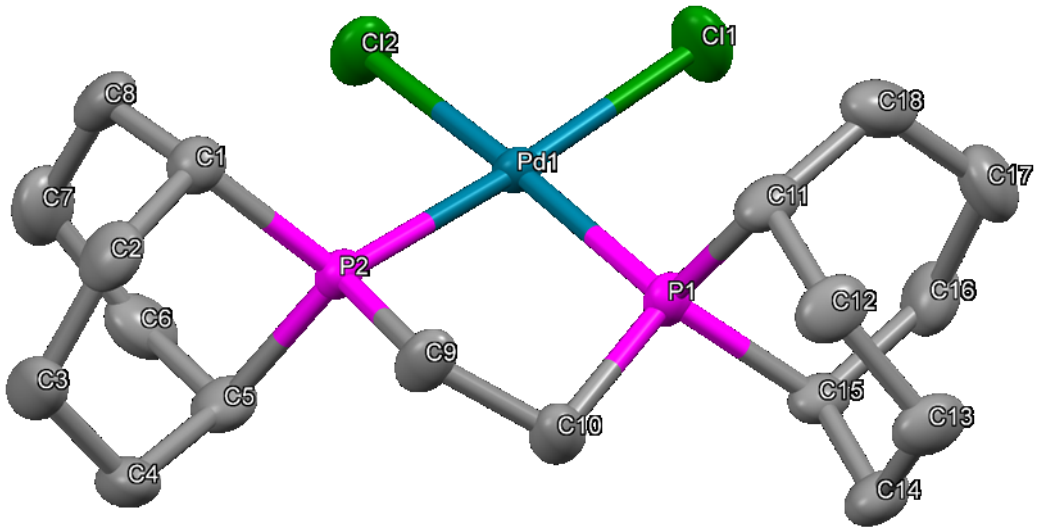

Figure 6.28 The crystal structure of [Pd(**BCOPE**)Cl_2] (50% probability ellipsoids).

Table 6.8 Bond lengths [Å] and angles [°] for [Pd(**BCOPE**)Cl_2].

Pd1	P1	2.2840(15)	C14	C15	1.540(9)		
Pd1	P2	2.2752(15)	C14	C13	1.531(9)		
Pd1	Cl2	2.3673(15)	C15	C16	1.526(10)		
Pd1	Cl1	2.3686(17)	C5	C4	1.554(10)		
P1	C11	1.822(7)	C3	C2	1.526(11)		
P1	C15	1.829(7)	C3	C4	1.531(10)		
P1	C10	1.824(7)	C13	C12	1.531(10)		
P2	C1	1.833(7)	C7	C8	1.532(12)		
P2	C9	1.834(6)	C17	C16	1.521(11)		
P2	C5	1.828(7)					
C11	C18	1.544(11)	P1	Pd1	Cl2	175.34(7)	
C11	C12	1.534(9)	P1	Pd1	Cl1	94.44(6)	
C1	C2	1.537(9)	P2	Pd1	P1	85.48(5)	
C1	C8	1.535(9)	P2	Pd1	Cl2	94.88(6)	
C9	C10	1.500(9)	P2	Pd1	Cl1	174.62(7)	
C6	C5	1.531(10)	Cl2	Pd1	Cl1	85.64(6)	
C6	C7	1.536(12)	C11	P1	Pd1	117.3(2)	
C18	C17	1.535(12)	C11	P1	C15	96.4(3)	
			C11	P1	C10	108.6(3)	

C15	P1	Pd1	122.8(2)	C13	C14	C15	115.7(6)
C10	P1	Pd1	106.0(2)	C14	C15	P1	108.7(5)
C10	P1	C15	104.6(3)	C16	C15	P1	111.2(5)
C1	P2	Pd1	120.0(2)	C16	C15	C14	114.0(6)
C1	P2	C9	105.6(3)	C6	C5	P2	107.7(5)
C9	P2	Pd1	106.1(2)	C6	C5	C4	114.0(6)
C5	P2	Pd1	119.0(2)	C4	C5	P2	110.9(5)
C5	P2	C1	96.6(3)	C2	C3	C4	116.0(6)
C5	P2	C9	108.5(3)	C3	C2	C1	116.5(6)
C18	C11	P1	108.0(5)	C14	C13	C12	116.4(6)
C12	C11	P1	110.0(5)	C8	C7	C6	116.8(6)
C12	C11	C18	113.9(6)	C3	C4	C5	116.9(6)
C2	C1	P2	108.6(5)	C16	C17	C18	116.6(6)
C8	C1	P2	110.0(4)	C13	C12	C11	116.5(6)
C8	C1	C2	113.5(6)	C7	C8	C1	117.3(6)
C10	C9	P2	108.0(4)	C9	C10	P1	107.4(5)
C5	C6	C7	116.0(6)	C17	C16	C15	116.3(6)
C17	C18	C11	117.3(6)				

The X-ray crystal structure of [Pd(BCOPP)Cl_2]

Crystal data for [Pd(**BCOPP**)Cl_2]: $C_{22}H_{32}Cl_2P_2Pd.CH_2Cl_2$, M = 620.64, monoclinic, $P2_1/c$ (no. 14), a = 14.08010(10) Å, b = 13.60620(10) Å, c = 13.7056(2) Å, β = 106.2050(10)°, V = 2521.35(5) Å^3, Z = 4, T = 296.7(3) K, μ(CuKα) = 11.107 mm^{-1}, D_c = 1.635 g cm^{-3}, 12231 reflections measured (9.222° ≤ 2Θ ≤ 145.382°), F^2 refinement,[1-2] 4858 unique (R_{int} = 0.0355, R_{sigma} = 0.0391) which were used in all calculations. The final R_1 was 0.0427 (I > 2σ(I)) and wR_2 was 0.1233 (all data).

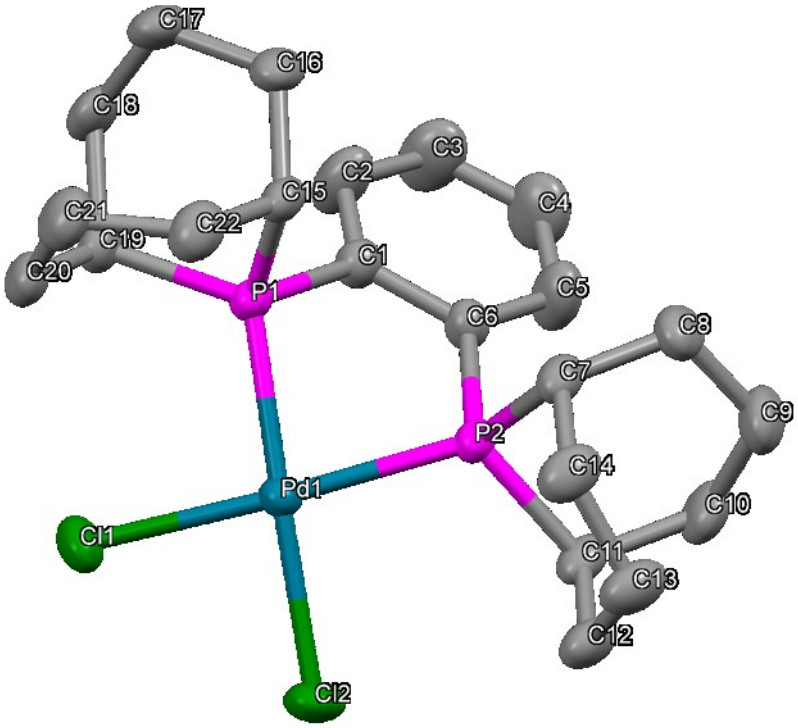

Figure 6.29 The crystal structure of [Pd(**BCOPP**)Cl_2] (50% probability ellipsoids).

Table 6.9 Bond lengths [Å] and angles [°] for [Pd(**BCOPP**)Cl_2].

Pd1	P1	2.2484(8)	C15	C22	1.539(5)
Pd1	Cl1	2.3777(9)	C15	C16	1.543(5)
Pd1	P2	2.2817(8)	C7	C8	1.531(5)
Pd1	Cl2	2.3467(9)	C7	C14	1.538(5)
P1	C1	1.823(4)	C11	C12	1.551(5)
P1	C19	1.833(3)	C11	C10	1.540(5)
P1	C15	1.834(4)	C20	C21	1.522(6)
P2	C6	1.855(3)	C8	C9	1.540(6)
P2	C7	1.835(3)	C22	C21	1.518(5)
P2	C11	1.846(3)	C12	C13	1.514(5)
C1	C6	1.405(5)	C16	C17	1.536(5)
C1	C2	1.396(5)	C10	C9	1.533(6)
C6	C5	1.391(5)	C14	C13	1.518(5)
C19	C20	1.548(5)	C2	C3	1.391(6)
C19	C18	1.546(5)	C4	C5	1.393(6)

C4	C3	1.356(7)
C18	C17	1.537(6)
Cl3	C23	1.743(6)
C23	Cl4	1.736(6)

P1	Pd1	Cl1	94.02(3)
P1	Pd1	P2	82.31(3)
P1	Pd1	Cl2	173.97(4)
P2	Pd1	Cl1	165.85(3)
P2	Pd1	Cl2	96.46(3)
Cl2	Pd1	Cl1	85.76(3)
C1	P1	Pd1	99.93(11)
C1	P1	C19	115.32(16)
C1	P1	C15	106.24(16)
C19	P1	Pd1	117.85(12)
C19	P1	C15	95.95(15)
C15	P1	Pd1	122.00(11)
C6	P2	Pd1	99.59(11)
C7	P2	Pd1	125.91(12)
C7	P2	C6	107.19(16)
C7	P2	C11	95.52(15)
C11	P2	Pd1	115.74(12)
C11	P2	C6	113.28(16)
C6	C1	P1	115.2(2)
C2	C1	P1	125.6(3)
C2	C1	C6	119.3(3)
C1	C6	P2	115.5(2)
C5	C6	P2	125.7(3)
C5	C6	C1	118.8(3)

C20	C19	P1	106.4(2)
C18	C19	P1	113.3(3)
C18	C19	C20	112.0(3)
C22	C15	P1	107.9(3)
C22	C15	C16	115.8(3)
C16	C15	P1	109.3(3)
C8	C7	P2	109.3(3)
C8	C7	C14	114.5(3)
C14	C7	P2	108.8(3)
C12	C11	P2	107.3(2)
C10	C11	P2	113.2(3)
C10	C11	C12	112.0(3)
C21	C20	C19	116.2(3)
C7	C8	C9	118.2(3)
C21	C22	C15	116.6(3)
C13	C12	C11	115.9(3)
C17	C16	C15	117.1(3)
C9	C10	C11	116.9(3)
C13	C14	C7	115.9(3)
C3	C2	C1	120.6(4)
C3	C4	C5	120.3(4)
C22	C21	C20	113.5(3)
C10	C9	C8	118.5(3)
C12	C13	C14	113.9(3)
C17	C18	C19	117.6(3)
C6	C5	C4	120.8(4)
C16	C17	C18	117.3(3)
C4	C3	C2	120.1(4)
Cl4	C23	Cl3	112.0(3)

The X-ray crystal structure of [Pd(*α*-BCOPP)Cl_2]

Crystal data for [Pd(***α*-BCOPP**)Cl_2]: $C_{22}H_{32}Cl_2P_2Pd$, M = 535.71, monoclinic, $P2_1/n$ (no. 14), a = 7.62310(10) Å, b = 19.9191(2) Å, c = 14.50130(10) Å, β = 94.9510(10)°, V = 2193.74(4) Å^3, Z = 4, T = 295.3(3) K, μ(CuKα) = 10.473 mm^{-1}, D_c = 1.622 g cm^{-3}, 21164 reflections measured (7.56° ≤ 2Θ ≤ 148.05°), F^2 refinement,[1-2] 4389 unique (R_{int} = 0.0508, R_{sigma} = 0.0338) which were used in all calculations. The final R_1 was 0.0298 (I > 2σ(I)) and wR_2 was 0.0810 (all data).

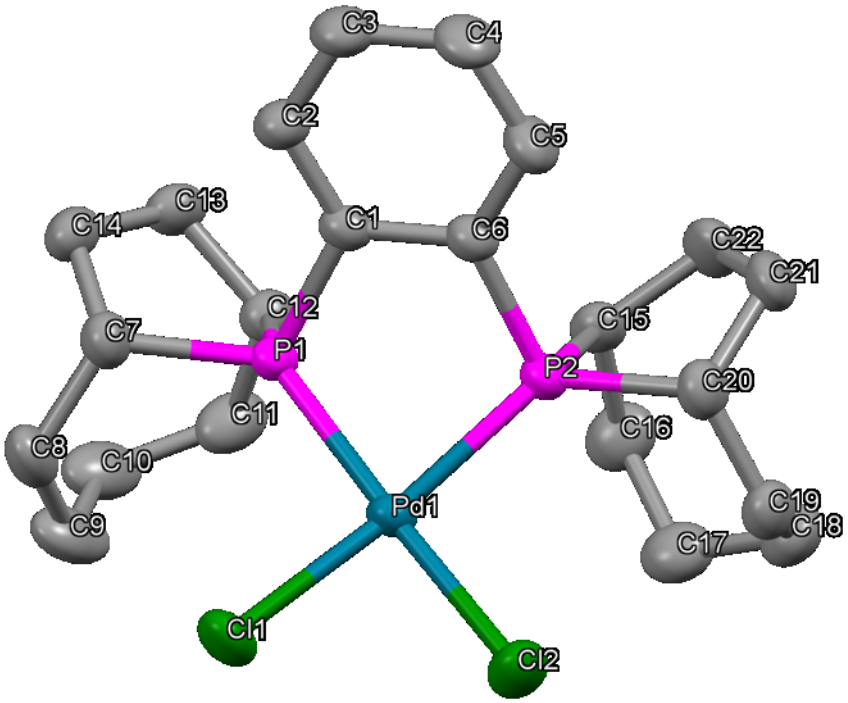

Figure 6.30 The crystal structure of [Pd(***α*-BCOPP**)Cl_2] (50% probability ellipsoids).

Table 6.10 Bond lengths [Å] and angles [°] for [Pd(***α*-BCOPP**)Cl_2].

Pd1	P2	2.2752(6)	P1	C1	1.833(2)
Pd1	P1	2.2661(6)	P1	C12	1.840(3)
Pd1	Cl2	2.3518(6)	P1	C7	1.853(3)
Pd1	Cl1	2.3383(7)	C1	C6	1.402(4)
P2	C6	1.831(3)	C1	C2	1.390(4)
P2	C15	1.841(3)	C12	C13	1.536(4)
P2	C20	1.857(3)	C12	C11	1.535(4)

C6	C5	1.391(3)
C2	C3	1.381(4)
C15	C16	1.535(4)
C15	C22	1.546(4)
C5	C4	1.390(4)
C3	C4	1.378(5)
C20	C19	1.546(4)
C20	C21	1.534(4)
C7	C14	1.556(4)
C7	C8	1.533(4)
C13	C14	1.537(5)
C11	C10	1.515(5)
C19	C18	1.533(5)
C16	C17	1.520(4)
C8	C9	1.526(6)
C21	C22	1.543(5)
C18	C17	1.511(5)
C10	C9	1.531(6)

P2	Pd1	Cl2	96.04(2)
P2	Pd1	Cl1	170.47(3)
P1	Pd1	P2	82.18(2)
P1	Pd1	Cl2	176.26(3)
P1	Pd1	Cl1	95.35(2)
Cl1	Pd1	Cl2	85.88(3)
C6	P2	Pd1	99.95(8)
C6	P2	C15	103.44(12)
C6	P2	C20	109.26(12)
C15	P2	Pd1	124.59(9)
C15	P2	C20	92.64(13)
C20	P2	Pd1	125.20(9)
C1	P1	Pd1	100.81(8)
C1	P1	C12	105.22(12)
C1	P1	C7	106.57(13)
C12	P1	Pd1	122.41(9)
C12	P1	C7	92.74(13)
C7	P1	Pd1	127.12(10)
C6	C1	P1	115.91(19)
C2	C1	P1	124.0(2)
C2	C1	C6	120.1(2)
C13	C12	P1	102.20(19)
C11	C12	P1	113.7(2)
C11	C12	C13	113.8(2)
C1	C6	P2	115.19(18)
C5	C6	P2	126.0(2)
C5	C6	C1	118.8(2)
C3	C2	C1	120.4(3)
C16	C15	P2	112.27(19)
C16	C15	C22	115.7(3)
C22	C15	P2	103.5(2)
C4	C5	C6	120.6(3)
C4	C3	C2	120.0(3)
C19	C20	P2	114.47(19)
C21	C20	P2	103.80(19)
C21	C20	C19	109.5(2)
C14	C7	P1	104.0(2)
C8	C7	P1	114.2(2)
C8	C7	C14	111.4(2)
C12	C13	C14	110.4(2)
C3	C4	C5	120.2(3)

C13	C14	C7	111.7(2)	C21	C22	C15	112.3(2)
C10	C11	C12	117.5(3)	C17	C18	C19	115.2(3)
C18	C19	C20	116.9(2)	C11	C10	C9	115.4(3)
C17	C16	C15	118.3(3)	C8	C9	C10	118.4(3)
C9	C8	C7	118.1(3)	C18	C17	C16	116.1(3)
C20	C21	C22	110.7(2)				

The X-ray crystal structure of [Pd(BCOPE)Cl]$_2$

Crystal data for [Pd(**BCOPE**)Cl]$_2$.(CH_3SO_3H)$_3$(H_3O)(CH_3SO_3): $C_{40}H_{82}Cl_2O_{13}P_4Pd_2S_4$, M = 1306.87, monoclinic, $P2_1/c$ (no. 14), a = 12.15543(14) Å, b = 18.6842(2) Å, c = 23.4183(3) Å, β = 100.2268(11)°, V = 5234.12(11) Å^3, Z = 4, T = 100.1(5) K, μ(MoKα) = 1.129 mm^{-1}, D_c = 1.658 g cm^{-3}, 135799 reflections measured (4.956° ≤ 2Θ ≤ 58.402°), F^2 refinement,[1-2] 12994 unique (R_{int} = 0.0471, R_{sigma} = 0.0256) which were used in all calculations. The final R_1 was 0.0315 (I > 2σ(I)) and wR_2 was 0.0669 (all data).

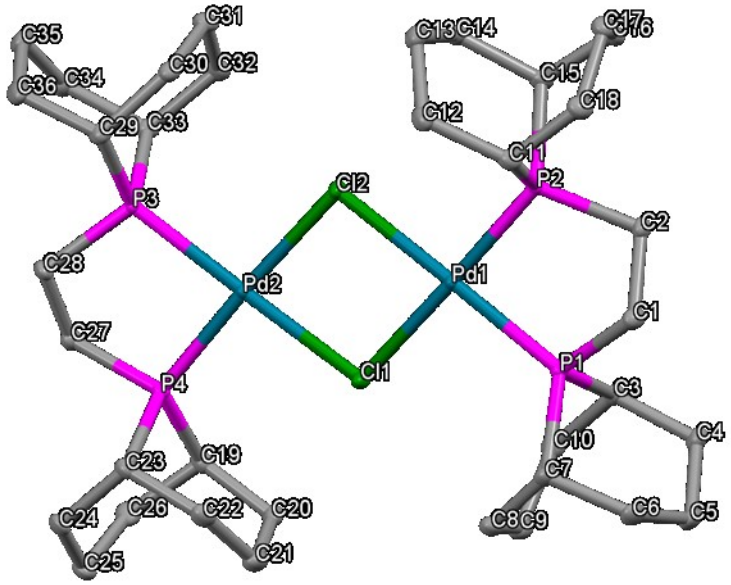

Figure 6.31 The crystal structure of [Pd(**BCOPE**)Cl]$_2$ (50% probability ellipsoids).

Table 6.11 Bond lengths [Å] and angles [°] for [Pd(**BCOPE**)Cl]$_2$.

Pd1	Cl2	2.4139(5)	Pd2	Cl2	2.4230(5)
Pd1	Cl1	2.3969(5)	Pd2	P4	2.2744(6)
Pd1	P1	2.2705(6)	Pd2	Cl1	2.4026(6)
Pd1	P2	2.2630(6)	Pd2	P3	2.2715(6)

P4	C27	1.823(2)	C8	C7	1.540(3)
P4	C19	1.831(2)	C8	C9	1.541(3)
P4	C23	1.827(2)	C32	C31	1.542(3)
P3	C29	1.830(2)	C32	C33	1.548(3)
P3	C28	1.820(2)	C26	C19	1.553(3)
P3	C33	1.828(2)	C26	C25	1.534(3)
S2	O4	1.4385(19)	C2	C1	1.528(3)
S2	O5	1.4441(18)	C21	C22	1.536(4)
S2	O6	1.5055(19)	C21	C20	1.541(4)
S2	C38	1.753(3)	C11	C18	1.545(3)
P1	C7	1.828(2)	C11	C12	1.545(3)
P1	C1	1.823(2)	C27	C28	1.526(3)
P1	C3	1.831(2)	C14	C15	1.542(3)
P2	C2	1.825(2)	C14	C13	1.543(3)
P2	C11	1.824(2)	C18	C17	1.538(3)
P2	C15	1.833(2)	C22	C23	1.541(3)
S4	O12	1.436(2)	C13	C12	1.539(3)
S4	O10	1.4761(19)	C7	C6	1.549(3)
S4	O11	1.4597(19)	C29	C30	1.539(3)
S4	C40	1.760(3)	C29	C36	1.547(3)
S3	O8	1.4474(19)	C19	C20	1.547(3)
S3	O9	1.4791(19)	C23	C24	1.549(3)
S3	O7	1.4475(18)	C31	C30	1.537(3)
S3	C39	1.770(3)	C34	C35	1.536(3)
S1	O1	1.4358(19)	C34	C33	1.543(3)
S1	O3	1.5111(19)	C6	C5	1.537(3)
S1	O2	1.429(2)	C4	C5	1.538(3)
S1	C37	1.755(3)	C4	C3	1.542(3)
C16	C15	1.544(3)	C35	C36	1.540(4)
C16	C17	1.536(3)	C10	C9	1.541(3)

C10	C3		1.548(3)	O4	S2	O6	108.94(12)
C25	C24		1.534(3)	O4	S2	C38	108.67(12)
				O5	S2	O6	110.44(12)
Cl1	Pd1	Cl2	80.939(18)	O5	S2	C38	107.30(13)
P1	Pd1	Cl2	176.92(2)	O6	S2	C38	104.37(13)
P1	Pd1	Cl1	97.12(2)	C7	P1	Pd1	122.68(8)
P2	Pd1	Cl2	97.58(2)	C7	P1	C3	97.39(11)
P2	Pd1	Cl1	178.18(2)	C1	P1	Pd1	107.93(8)
P2	Pd1	P1	84.31(2)	C1	P1	C7	107.90(11)
P4	Pd2	Cl2	177.07(2)	C1	P1	C3	107.70(11)
P4	Pd2	Cl1	96.48(2)	C3	P1	Pd1	112.18(7)
Cl1	Pd2	Cl2	80.639(18)	C2	P2	Pd1	107.67(8)
P3	Pd2	Cl2	97.954(19)	C2	P2	C15	107.78(11)
P3	Pd2	P4	84.94(2)	C11	P2	Pd1	114.50(8)
P3	Pd2	Cl1	178.29(2)	C11	P2	C2	107.69(11)
Pd1	Cl2	Pd2	98.621(19)	C11	P2	C15	97.69(11)
C27	P4	Pd2	108.00(8)	C15	P2	Pd1	120.62(8)
C27	P4	C19	106.99(11)	O12	S4	O10	111.81(11)
C27	P4	C23	109.43(11)	O12	S4	O11	114.76(12)
C19	P4	Pd2	120.60(8)	O12	S4	C40	108.28(13)
C23	P4	Pd2	113.46(8)	O10	S4	C40	105.62(13)
C23	P4	C19	97.68(11)	O11	S4	O10	110.94(11)
Pd1	Cl1	Pd2	99.67(2)	O11	S4	C40	104.74(12)
C29	P3	Pd2	120.61(8)	O8	S3	O9	111.20(12)
C28	P3	Pd2	107.55(8)	O8	S3	O7	114.20(12)
C28	P3	C29	106.63(11)	O8	S3	C39	107.43(12)
C28	P3	C33	109.70(11)	O9	S3	C39	105.79(12)
C33	P3	Pd2	114.03(8)	O7	S3	O9	110.73(12)
C33	P3	C29	97.69(11)	O7	S3	C39	106.99(12)
O4	S2	O5	116.42(11)	O1	S1	O3	110.26(11)

O1	S1	C37	107.44(16)	C20	C19	C26	113.43(19)
O3	S1	C37	103.92(14)	C22	C23	P4	107.72(16)
O2	S1	O1	116.68(13)	C22	C23	C24	114.50(19)
O2	S1	O3	108.57(13)	C24	C23	P4	109.50(16)
O2	S1	C37	109.22(17)	C30	C31	C32	117.39(19)
C17	C16	C15	115.55(19)	C35	C34	C33	116.3(2)
C7	C8	C9	116.36(19)	C16	C17	C18	116.43(19)
C31	C32	C33	117.03(19)	C5	C6	C7	116.97(19)
C25	C26	C19	115.4(2)	C31	C30	C29	117.01(19)
C1	C2	P2	106.33(15)	C2	C1	P1	106.83(15)
C22	C21	C20	117.8(2)	C5	C4	C3	116.16(19)
C18	C11	P2	109.38(16)	C27	C28	P3	108.66(15)
C12	C11	P2	106.85(16)	C21	C20	C19	117.3(2)
C12	C11	C18	116.01(19)	C34	C35	C36	115.2(2)
C28	C27	P4	107.73(16)	C35	C36	C29	116.43(19)
C15	C14	C13	117.21(19)	C9	C10	C3	117.30(19)
C17	C18	C11	116.57(19)	C24	C25	C26	115.27(19)
C16	C15	P2	107.75(16)	C32	C33	P3	107.53(15)
C14	C15	P2	110.96(15)	C34	C33	P3	109.78(16)
C14	C15	C16	113.09(19)	C34	C33	C32	114.35(19)
C21	C22	C23	116.7(2)	C25	C24	C23	116.75(19)
C12	C13	C14	116.98(19)	C13	C12	C11	116.16(19)
C8	C7	P1	110.57(16)	C6	C5	C4	115.73(19)
C8	C7	C6	113.79(19)	C8	C9	C10	116.84(19)
C6	C7	P1	107.80(16)	C4	C3	P1	109.96(16)
C30	C29	P3	110.36(15)	C4	C3	C10	114.52(19)
C30	C29	C36	113.48(19)	C10	C3	P1	107.56(15)
C36	C29	P3	107.74(16)				
C26	C19	P4	107.29(15)				
C20	C19	P4	110.72(16)				

6.3.3 GC Spectra

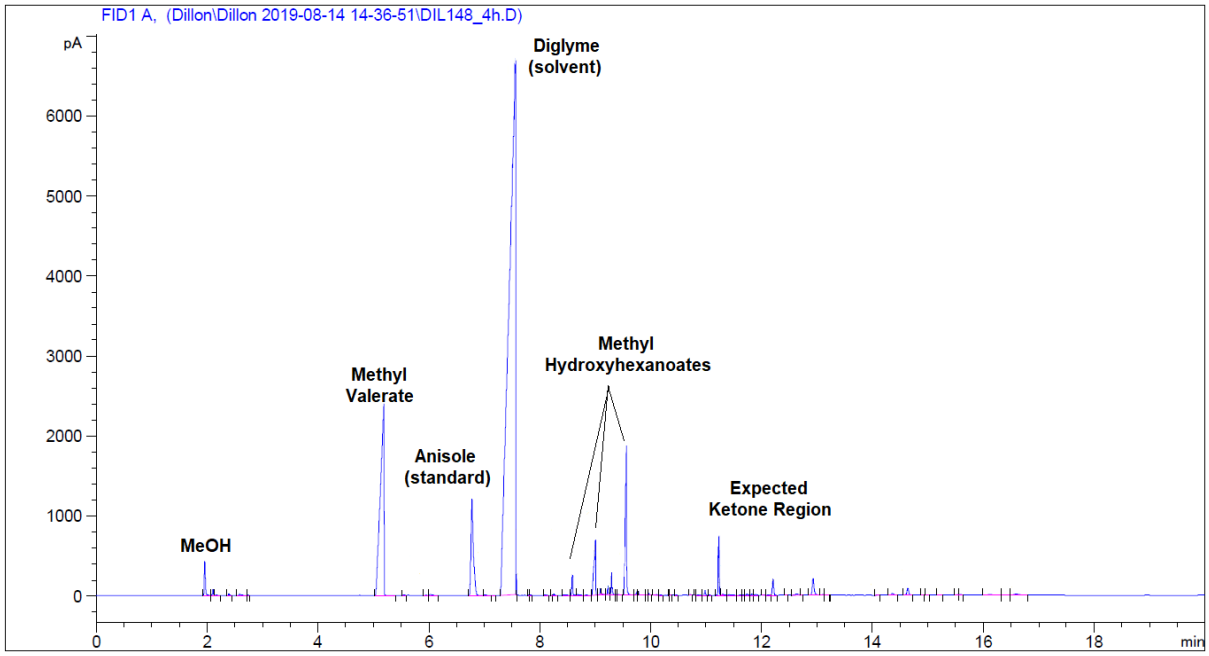

Figure 6.32 GC spectra of palladium catalysed hydroformylation of methyl 4-pentenoate (M4P) using **BCOPE** and MSA (MSA/Pd = 40), run 1 from **Table 3.4**.

6.4 Chapter 6 References

1. *SHELTX v5.1*, Bruker AXS: Madison, WI, 1998.
2. Sheldrick, G., *Acta Crystallographica Section C* **2015,** *71*, 3-8.

Appendix A

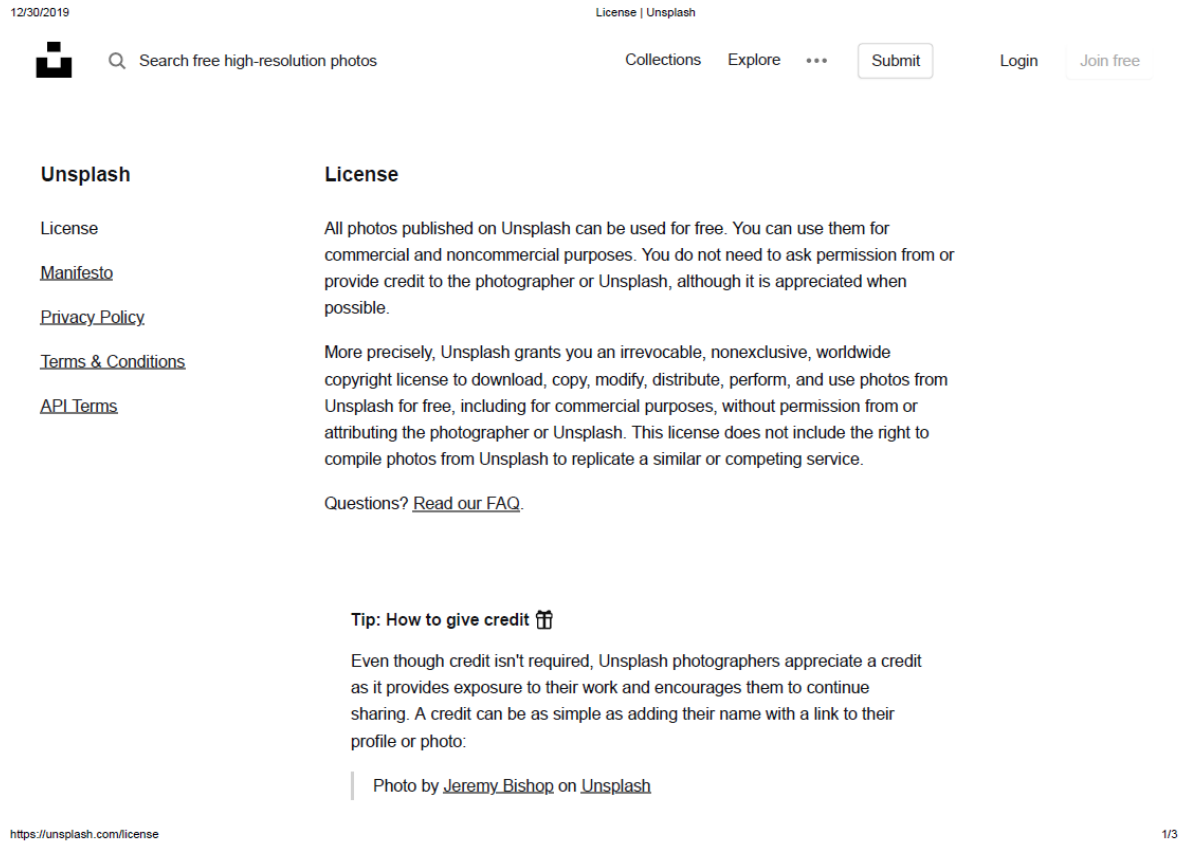

12/30/2019 License | Unsplash

Search free high-resolution photos Collections Explore ••• Submit Login Join free

Unsplash

License

Manifesto

Privacy Policy

Terms & Conditions

API Terms

License

All photos published on Unsplash can be used for free. You can use them for commercial and noncommercial purposes. You do not need to ask permission from or provide credit to the photographer or Unsplash, although it is appreciated when possible.

More precisely, Unsplash grants you an irrevocable, nonexclusive, worldwide copyright license to download, copy, modify, distribute, perform, and use photos from Unsplash for free, including for commercial purposes, without permission from or attributing the photographer or Unsplash. This license does not include the right to compile photos from Unsplash to replicate a similar or competing service.

Questions? Read our FAQ.

Tip: How to give credit

Even though credit isn't required, Unsplash photographers appreciate a credit as it provides exposure to their work and encourages them to continue sharing. A credit can be as simple as adding their name with a link to their profile or photo:

> Photo by Jeremy Bishop on Unsplash

https://unsplash.com/license 1/3

Appendix B

ELSEVIER LICENSE
TERMS AND CONDITIONS

Dec 29, 2019

This Agreement between Mr. Dillon Tay ("You") and Elsevier ("Elsevier") consists of your license details and the terms and conditions provided by Elsevier and Copyright Clearance Center.

License Number	4738490943723
License date	Dec 29, 2019
Licensed Content Publisher	Elsevier
Licensed Content Publication	Journal of Organometallic Chemistry
Licensed Content Title	The oxo-synthesis catalyzed by cationic palladium complexes, selectivity control by neutral ligand and anion
Licensed Content Author	E. Drent,P.H.M. Budzelaar
Licensed Content Date	Jan 15, 2000
Institution name	Imperial College London
Expected presentation date	May 2020
Portions	Fig. 1. Schematic representation of chemoselectivity as a function of ligand and acid properties. found on page 213
Requestor Location	Mr. Dillon Tay 46 Almond Crescent Singapore, 677800 Singapore Attn: Mr. Dillon Tay
Publisher Tax ID	GB 494 6272 12
Total	0.00 GBP

Appendix C

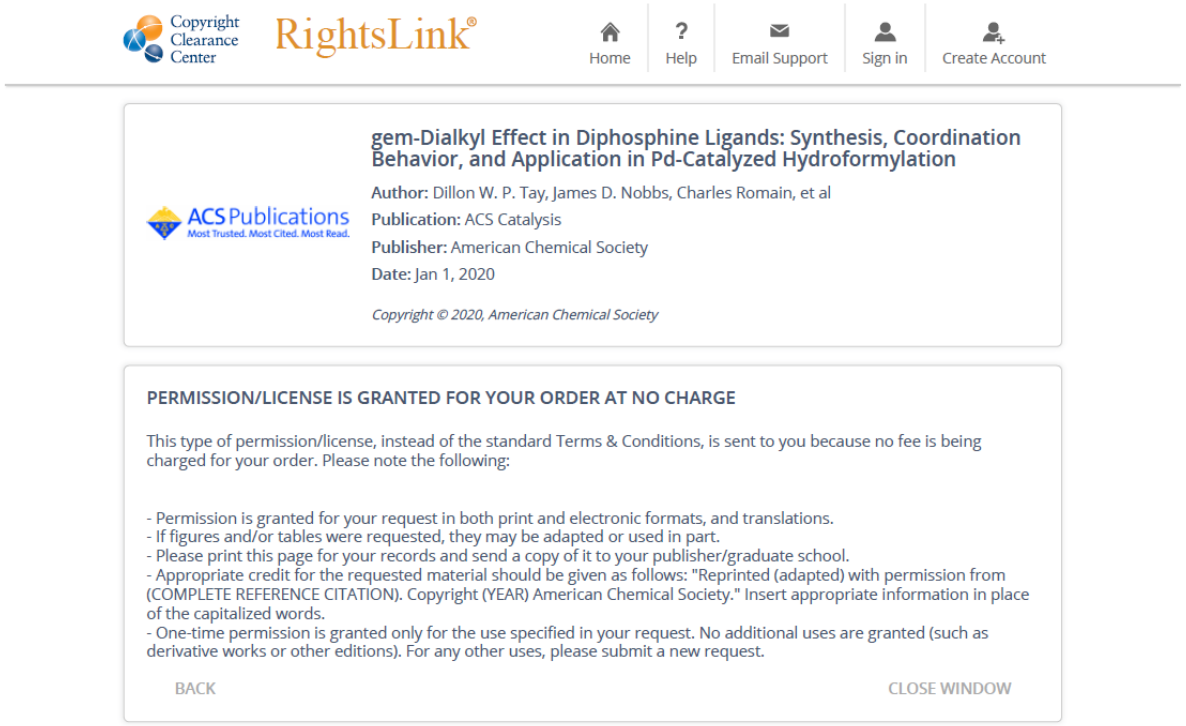
Copyright Clearance Center
RightsLink®
Home
Help
Email Support
Sign in
Create Account
ACS Publications
Most Trusted. Most Cited. Most Read.
gem-Dialkyl Effect in Diphosphine Ligands: Synthesis, Coordination Behavior, and Application in Pd-Catalyzed Hydroformylation
Author: Dillon W. P. Tay, James D. Nobbs, Charles Romain, et al
Publication: ACS Catalysis
Publisher: American Chemical Society
Date: Jan 1, 2020
Copyright © 2020, American Chemical Society
PERMISSION/LICENSE IS GRANTED FOR YOUR ORDER AT NO CHARGE
This type of permission/license, instead of the standard Terms & Conditions, is sent to you because no fee is being charged for your order. Please note the following:
- Permission is granted for your request in both print and electronic formats, and translations.
- If figures and/or tables were requested, they may be adapted or used in part.
- Please print this page for your records and send a copy of it to your publisher/graduate school.
- Appropriate credit for the requested material should be given as follows: "Reprinted (adapted) with permission from (COMPLETE REFERENCE CITATION). Copyright (YEAR) American Chemical Society." Insert appropriate information in place of the capitalized words.
- One-time permission is granted only for the use specified in your request. No additional uses are granted (such as derivative works or other editions). For any other uses, please submit a new request.
BACK
CLOSE WINDOW

Appendix D

JOHN WILEY AND SONS LICENSE
TERMS AND CONDITIONS

Jan 02, 2020

This Agreement between Mr. Dillon Tay ("You") and John Wiley and Sons ("John Wiley and Sons") consists of your license details and the terms and conditions provided by John Wiley and Sons and Copyright Clearance Center.

License Number	4740641443468
License date	Jan 02, 2020
Licensed Content Publisher	John Wiley and Sons
Licensed Content Publication	European Journal of Inorganic Chemistry
Licensed Content Title	In Situ Preparation of Palladium Diphosphane Catalysts
Licensed Content Author	Wilhelmus P. Mul, A. Bart van Oort, Angelica Marson
Licensed Content Date	Oct 14, 2002
Licensed Content Volume	2002
Licensed Content Issue	11
Licensed Content Pages	4
Type of use	Dissertation/Thesis
Requestor type	University/Academic
Format	Print and electronic
Portion	Figure/table
Number of figures/tables	1

Original Wiley figure/table number(s)	Scheme 1. Reactions observed during preparation of some palladium diphosphane catalysts in situ; P-P = dppe (1-4) or dppbz (5,6)
Will you be translating?	No
Title of your thesis / dissertation	Impact of Phosphorous Ligand Modification on Transition Metal Coordination and Homogeneous Carbonylation Catalysis
Expected completion date	May 2020
Expected size (number of pages)	1
Requestor Location	Mr. Dillon Tay 46 Almond Crescent Singapore, 677800 Singapore Attn: Mr. Dillon Tay
Publisher Tax ID	EU826007151
Total	0.00 GBP